Vegan and sustainable hydrogels based on a novel recombinant collagen-like protein for biomedical applications

Zur Erlangung des akademischen Grades eines

Doktors der Naturwissenschaften

(Dr. rer. nat.)

von der KIT-Fakultät für Chemie und Biowissenschaften
des Karlsruher Instituts für Technologie (KIT)

genehmigte

Dissertation

von

M. Sc. Sven Weber

aus

Heidelberg, Deutschland

1. Referentin: Prof. Dr. Ute Schepers
2. Referent: Dr. Zbigniew Lech Pianowski

Tag der mündlichen Prüfung: 25.04.2024

Die vorliegende Arbeit wurde unter der Leitung von Prof. Dr. Ute Schepers vom Juli 2020 bis zum Februar 2024 am Institut für Funktionelle Grenzflächen (IFG) des Karlsruher Instituts für Technologie (KIT, Campus Nord) in Zusammenarbeit mit Evonik Operations GmbH (Darmstadt) angefertigt.

Eidesstattliche Erklärung

Hiermit versichere ich, dass ich die vorliegende Arbeit selbständig angefertigt und keine anderen als die angegebenen Quellen und Hilfsmittel benutzt sowie wörtlich und inhaltlich übernommene Stellen als solche kenntlich gemacht habe. Die Satzung des Karlsruher Instituts für Technologie (KIT) zur Sicherung guter wissenschaftlicher Praxis in der gültigen Fassung wurde beachtet.

Foreword

"Each and every one of us has the power to make a difference in the world - every day and at any time. All we need is to have faith in ourselves and the determination to cultivate our talents and achieve greatness. We should never let the narrow-mindedness of others hold us back, nor never limit others based on your own limited imagination. Instead, we should always seek to collaborate and connect with others to make meaningful progress together."

- Inspired by Jane Goodall, Marie Curie, and Carol W. Greider. -

Acknowledgments

Dear reader,

It is with great pleasure and gratitude that I dedicate this dissertation to my most important supporters and companions. Without their support, encouragement, and inspiration, this work would not have been possible.

First and foremost, special thanks go to my family. For as long as I can remember, you have always been there for me and have supported me on my life's journey. I can always count on you, and you give me more than I could ever give back. Thank you for always having my back and always being there for me.

Second, I would like to thank Maria. Your supportive guidance, the opportunity to develop freely, and our discussions as equals made this work possible in many ways. I have been able to try many new things and have grown with the new tasks and challenges.

Third, I would like to thank my caring and supportive colleagues in and around room 203. Thank you, Camilla, Fabian, Christoph and Erik. You have been with me through the ups and downs and have become very close friends. Your humor and advice helped me get through the bad days.

Fourth, I would like to thank my professor, Ute Schepers. You have given me the freedom to grow and broaden my perspective by always providing innovative food for thought and great ideas. This has enabled me to reach new heights.

I would also like to thank my co-doctoral students, Alisa and Sonja, who were always happy to support me along the way.

Finally, I would like to thank all the other people who supported this dissertation in some way: Alena, Andrea, Anna, Anne, Blerta, Christian, Elisabeth, Eva, Hans-Henning, Jonas, Kathrin, Markus, Melanie, Michael, Moritz, Nadine, Stefan, Steffen, Thomas, Tim, Tobias, Yunxiao and the many others, thank you very much.

Without you the work would not have become what it is today.

Kurzfassung

Nachhaltigkeit wird in der heutigen Gesellschaft immer wichtiger, um zu einer "grüneren" Zukunft beizutragen.[1] In der Materialwissenschaft sind Kollagene die am häufigsten vorkommende, kommerziell genutzte Proteinfamilie auf dem globalen Bioprinting-Markt.[2] Mehrere Nachteile tierischer Kollagene erfordern die Suche nach nachhaltigen Alternativen.[3] In dieser Arbeit wurde ein neues, veganes rekombinantes kollagenähnliches Protein (rCol) für die Erforschung verschiedener biomedizinischer Anwendungen charakterisiert, um einen Beitrag zur wachsenden Nachfrage nach neuartigen Therapien in der regenerativen Medizin zu leisten. Der Schwerpunkt lag dabei auf Implantaten, Medizinprodukten und dem 3D-Druck von künstlichen Geweben und Organen. Um diesen Anwendungen gerecht zu werden, konzentrierte sich die Arbeit auf die Entwicklung neuartiger Hydrogelsysteme. Zu Beginn wurde rCol charakterisiert und die Grenzen des Materials identifiziert. Die im Vergleich zu Säugetierkollagenen hohe Löslichkeit (bis zu 200 mg/ml) in einem weiten pH-Bereich, die hohe Biokompatibilität und die vergleichsweise niedrige Viskosität gewährleisten eine einfache Handhabung bei Konservierung der triplehelikalen Struktur. Aufgrund des geringen Molekulargewichts musste rCol für die Hydrogelbildung chemisch vernetzt werden. Nach einer ersten Bewertung verschiedener Vernetzungsmethoden wurden zwei Vernetzer ausgewählt und detaillierter untersucht. Der Vernetzer DMTMM synthetisierte feste Hydrogele ab 10 mg/ml rCol mit einem breiten Festigkeitsbereich (1,5 - ≥42 kPa) und hoher Porosität, die ein hohes Quellverhalten ermöglichen, um ein flexibles "Weichgewebepflaster" für die Verabreichung von Medikamenten zu schaffen. Durch die Einbettung Meloxicam-beladener Mikropartikel konnte eine anhaltende Wirkstofffreisetzung gezeigt werden. Als Wirkstoffdepot bietet das Pflaster einen interessanten Ansatz, für z. B. die Krebstherapie oder Wundheilung, um einen oder mehrere Wirkstoffe simultan oder mit verschiedenen Freisetzungsprofilen abzugeben. Hybride mit bioinerten Polyethylenglykol ergaben Hydrogel mit mindestens 5 mg/ml rCol mit zellabweisenden Eigenschaften. Zusammen mit der formulierungsabhängigen biologischen Abbaubarkeit ist diese Formulierung sehr attraktiv als Barrieremembran in der Chirurgie, um das Einwachsen von Weichteilgewebe nach einer Operation zu verhindern, ohne dass eine anschließende, manuelle Entfernung erforderlich ist. Darüber hinaus wurden injizierbare Formulierungen für minimalinvasive Anwendungen und für Hautinjektionen im kosmetischen Bereich erforscht. Zusätzlich wurde rCol separat mit Norborneneinheiten (rColN) und mit primären Thiolen (rColS) für die Photopolymerisation mittels Thiol-En-Chemie chemisch modifiziert. Es wurde ein hoher Funktionalisierungsgrad (15-98%) unter Beibehaltung der Triplehelix und einer hervorragenden Biokompatibilität (83-110% Zellviabilität) erreicht. Alle Derivatisierungsschritte wurden ohne organische

Lösungsmittel in einer einstufigen Reaktion bei Raumtemperatur durchgeführt und zeigten hohe Reproduzierbarkeit und hohe Ausbeuten (82-99%). Die resultierende Zweikomponententinte aus rColN und rColS zeigte eine Hydrogelbildung ab 2,5 mg/ml rColNS, einer niedrigen Photoinitiatorkonzentration (0,3 mg/ml Lithium-Phenyl-2,4,6-trimethylbenzoylphosphinat (LAP)) und Belichtungszeiten von wenigen Millisekunden. Im Vergleich zur radikalischen Kettenwachstumspolymerisation von rColN benötigte rColNS dreimal weniger Photoinitiator und viermal weniger Kollagen, um ein Hydrogel zu bilden, was mit der hohen Umsatzrate der Photopolymerisation (86-96%) assoziiert wurde. Insbesondere die schnelle Gelbildung bei sehr niedrigen und biokompatiblen Konzentrationen an Photoinitiator macht diese Technologie für Zellverkapselungsstudien sehr attraktiv. Ein weiteres Highlight war die unerwartete breite Festigkeit (G' von 0,5 bis ≥57 kPa), die nach aktuellem Wissen bisher für kein Kollagenhydrogel veröffentlicht wurde und den nächstliegenden Stand der Technik (16 kPa) um das 3,5-fache übertraf. Dieser breite Bereich könnte sowohl für die Entwicklung von Weichgewebe als auch für steifere Implantate von Interesse sein. Darüber hinaus konnte in 2D- und 3D-Experimenten eine ausgezeichnete Biokompatibilität mit menschlichen Zellen sowie eine formulierungsabhängige und damit einstellbare biologische Abbaubarkeit nachgewiesen werden. In 3D-Zellverkapselungsexperimenten konnte die Streckung von menschlichen Fibroblasten innerhalb eines Tages und eine hohe Zellviabilität in Langzeitkulturen nachgewiesen werden. rColS war außerdem in der Lage, temperatursensitive Hydrogele zu bilden, die hinsichtlich ihrer Reversibilität und möglicher Anwendungen untersucht wurden. Während normale, hochviskose Kollagene auf den 3D-Druck durch Extrusion beschränkt sind, zeigte rColNS hervorragende Eigenschaften für niederviskose Drucktechnologien wie Stereolithografie und Jetting. Die niedrige Viskosität von rColNS gewährleistet eine einfache Handhabung bei der Verarbeitung bei Raumtemperatur, um hochtransparente Hydrogele zu synthetisieren. Soweit bekannt, wurden bisher noch keine 3D-Druckversuche mit Stereolithografie oder Jetting unter Verwendung der Thiol-En-Chemie mit einem rekombinanten Kollagen veröffentlicht die zum Druck stabiler zylindrischer Strukturen führten. Die Verarbeitung der rColNS-Biotinte mit Zellen über Drop-on-Demand beeinträchtigte die Zellviabilität nicht. Darüber hinaus wurde gezeigt, dass der Hybriddruck mit RESOMER® die mechanische Festigkeit weiter erhöhen konnte, um so den Anwendungsbereich zu erweitern. Zusammenfassend lässt sich sagen, dass diese Arbeit das neuartige rCol charakterisiert und verschiedene Vernetzungsoptionen für verschiedene biomedizinische Anwendungen evaluiert hat. Insbesondere die entwickelte rColNS-Formulierung zeigte eine ausgezeichnete Biokompatibilität und ein breites Anwendungsspektrum und wird voraussichtlich einen wichtigen Beitrag als hochwirksame, rekombinante und vegane Kollagenalternative leisten, die den 3D-Bioprinting-Markt in eine nachhaltigere Zukunft revolutionieren könnte.

Abstract

Sustainability is becoming increasingly important in today's society to contribute to a "greener" future.[1] In material science, collagens represent the most abundant, commercially used protein family in the global bioprinting market.[2] Several drawbacks of standard animal-derived sourcing require the need for sustainable alternatives.[3] In this thesis, a new, vegan recombinant collagen-like protein (rCol) was characterized for research and evaluation of various biomedical applications to contribute to the growing demand for novel therapies in regenerative medicine (improvement of patient well-being and product efficiency). The focus was placed on implants, medical devices and 3D printing of artificial tissues and organs. To do justice to these applications, the work concentrated on the development of new types of hydrogel systems. At the beginning, rCol was characterized and material limitations were identified (e.g. structural analyses, temperature effects on the protein structure, solubility, viscosity and biocompatibility). Compared to mammalian collagens, the high solubility (up to 200 mg/ml) in a broad pH range, the high biocompatibility and its comparably low viscosity ensures convenient material handling while ensuring a triple-helical conformation. Due to the low molecular weight, rCol required chemical crosslinking for hydrogel formation. After initial evaluation of various crosslinking methods, two crosslinkers were selected and investigated separately. The crosslinker DMTMM synthesized solid hydrogels starting from 10 mg/ml rCol with a wide range of storage moduli (1.5 - ≥42 kPa) and high porosities allowing high swelling ratios to craft a flexible "soft tissue patch" for drug delivery. By embedding meloxicam-loaded microparticles, a sustained drug release was demonstrated. As a drug depot, the patch offers an interesting approach, e.g. for cancer therapy or wound healing, to transport one or more active ingredients in one dosage form (with or without different release profiles). Hybrids of the naturally bioinert polyethylene glycol (PEG) with at least 5 mg/ml rCol, resulted in a hydrogel with cell-repellent properties. Together with formulation-dependent biodegradability, this formulation is very attractive for biodegradable barrier membranes in surgery to prevent soft tissue ingrowth after operation without the need for subsequent manual removal. Furthermore, injectable formulations thereof in isotonic solutions were explored for minimally invasive applications and as for skin injections in the cosmetic sector. Furthermore, rCol was chemically modified by thiol-ene chemistry to enable photopolymerization. rCol was modified separately with norbornene units (rColN) and with primary thiols (rColS). High levels of functionalization were achieved (15-98%) while maintaining the triple helix and excellent biocompatibility (83-110% cell viability). All derivatization steps were performed without organic solvents in one-step reactions at RT and showed high reproducibility and high yields (82-99%). The resulting two-component ink of rColN and rColS showed

hydrogel formation at low collagen concentrations from 2.5 mg/ml rColNS, a low photoinitiator concentration (0.3 mg/ml Lithium phenyl(2,4,6-trimethylbenzoyl)phosphinate (LAP)) and exposure times of a few milliseconds. In contrast to radical chain growth polymerization of rColN, rColNS required three times less photoinitiator and four times less collagen to form a hydrogel which was associated with the high turnover rate of the photopolymerization (86-96%). In particular, the rapid gelation at very low and highly biocompatible photoinitiator concentrations made this technology very attractive for cell encapsulation studies. Another highlight was the unexpectedly wide range of stiffness (storage moduli (G') from 0.5 to ≥57 kPa), which has not been published for any collagen hydrogel and which surpassed the closest state of the art (16 kPa) 3.5 times. This wide range could be of interest for both soft tissue development and stiffer implants. Next, excellent biocompatibility with human cells (HeLa, NIH3T3, HFF and SW1353 cells) as well as formulation-dependent and thus adjustable biodegradability could be demonstrated in 2D and 3D experiments. 3D cell encapsulation experiments demonstrated cellular stretching of human fibroblasts within one day and great cell viability in long-term cultures. rColS was also able to form temperature-sensitive hydrogels which were explored regarding reversibility and potential applications. While normal collagens are highly viscous and therefore often limited to 3D printing by extrusion, the rColNS showed excellent properties for low-viscosity printing technologies such as stereolithography and drop-on-demand. The low viscosity of rColNS ensures easy handling (increased formulation homogeneity, avoidance of bubble entry) while handling at room temperature to synthesize highly transparent hydrogels. As far as known, 3D printing trials with stereolithographic processing and drop-on-demand printing have not yet been published yet using thiol-ene chemistry and a recombinant collagen which led to the printing of stable cylindric structures. Processing rColNS bioink with cells *via* Drop-on-Demand did not interfere with the cell viability. Additionally, hybrid prints with RESOMER® were demonstrated to further increase mechanical strength and extend the range of applications. In summary, this work characterized the novel rCol and evaluated different crosslinking options for diverse biomedical applications. In particular, the developed rColNS formulation showed excellent biocompatibility and a wide range of applications and is expected to make an important contribution as highly effective, recombinant and vegan collagen alternative which could revolutionize the 3D bioprinting market into a more sustainable future.

Table of Content

List of Abbreviations

1×PBS	Phosphate-buffered saline (PBS)
4PEG-SG, 4Arm-PEG-SG, PEG-SG	4-Arm-PEG-Succinimidyl Glutarate ester
4-Arm-PEG-SH	4-Arm-PEG-Thiol
AcHCT	*N*-Acetyl homocysteine thiolactone
AM	Additive Manufacturing
API	Active pharmaceutical ingredient
ASTM	American Society for Testing and Materials
bCol	bovine collagen
BMP2	Bone morphogenic protein 2
CAGR	Compound annual growth rate
CD	Circular dichroism
CIJ	Continuous-inkjet jetting
rCol	recombinant collagen-like protein
rtColMA	rat tail Collagen methacrylate
DBB	Droplet-based Bioprinting
DDS	Drug Delivery System
DLP	Digital Light Processing
DMEM	Dulbecco's Modified Eagle Medium
DMTMM	(4-(4,6-dimethoxy-1,3,5-triazin-2-yl)-4-methyl-morpholinium chloride)
DNA	Desoxyribonucleic acid
DoD	Drop-on-Demand
DPBS	Dulbecco's (Phosphate) Balanced Salt Solution
DTBP	3,30-dithio-bis-propionimidate
EDC*HCl	1-Ethyl-3-(3-dimethylaminopropyl) carbodiimide-hydrochloride
f.l.t.r.	from left to right
FBS / FCS	Foetal bovine serum / Foetal calf serum
GelMA	Gelatine methacrylate
HA	Hyaluronic acid
HDC	Hexamethylene diisocyanate
HER2	Human epidermal growth factor receptor 2
HFF / HDF /HDFB	Human foreskin fibroblasts / human dermal fibroblasts
IEP, pI	Isoelectric point
IUPAC	International Union of Pure and Applied Chemistry
NCA	5-Norbornene-2-carboxylic Acid

NCA-NHS	5-Norbornene-2-carboxylic Acid *N*-Hydroxysuccinimide
NHS	*N*-Hydroxysuccinimide
NMPA	National Medical Products Administration
MP	Microparticles
PEG	Polyethylene glycol
PEGDA	Polyethylene glycol diacrylate
PI	Photo initiator
PoC	Proof of Concept
rCGP	radical chain growth polymerization
rColN	recombinant norbornene-modified collagen
rColS	recombinant thiolated collagen
RNA	Ribonucleic acid
RT	Room temperature (21 °C – 25 °C)
rtCol	rat tail collagen
SEM	Scanning Electron Microscope
SGP	Step-Growth Polymerization
SL / SLA	Stereolithography
T_m	Melting temperature
XL	Crosslinker

1 Introduction

1.1 Biomaterials

1.1.1 Definitions

Biomaterials are defined by the International Union of Pure and Applied Chemistry (IUPAC) as materials used in contact with living tissues, organisms, or microorganisms[4] and can be derived from organisms (animals, plants, or microorganisms) or synthetic origin. Biomaterials have a wide range of properties. While synthetic biomaterials are often characterized by high mechanical stability and inertness, biologically derived biomaterials are often characterized by high biocompatibility, low immunogenicity, good biodegradability, and good bioresorption.[5] Since the first documented use of biomaterials in ancient Egypt as sutures made from animal tendons, biomaterials have increased in variety and applications.[6] Biomaterials are specifically designed to interact with biological systems to replace or support body parts for therapeutic or diagnostic purposes. The development and research of biomaterials is referred to as biomaterials science or biomaterial engineering. The term biomaterial should not be confused with the term biomacromolecule, which is limited to biologically derived macromolecules such as proteins, nucleic acids, or polysaccharides, and the term biopolymer. The term biopolymer describes a biomacromolecule with a repeating unit called a monomer throughout the structure, which is not mandatory for macromolecules *per se*. The ability of a material to elicit an appropriate host response in a specific application or to avoid an adverse effect when in contact with a living system is referred to as biocompatibility. In contact with living cells, the ability of a substance to elicit a specific response from a living material (e.g. collagen triggers blood clotting when exposed to platelet cells in the blood[7,8]) is referred to as bioactivity or biological activity (verb: bioactive). When a macromolecule is subjected to an enzymatic degradation process that reduces its molar mass, this is called biodegradation and the macromolecule is described as biodegradable. The degradation of a polymer by water without any contribution from living elements is not called biodegradation but is called hydrolysis. *In vivo*, the correct term for a biologically initiated degradation process is biodegradation. When exposed to cells, bioadhesion or bioattachment may occur. Both terms describe the adhesion of cells or tissues to the surface of a material. Cell adhesion is usually followed by proliferation as a biofilm or tissue. In addition, bioresorption describes the biochemical or biophysical resorption of the biomaterial, which may include catabolic and anabolic processes. When manufacturing cellular matrices, the term scaffold is often used. Scaffolds

generally describe porous matrices with communicating pores for the purpose of culturing cells and forming neo-tissues for implantation and integration into a living organism. Scaffold formation can be triggered by several effects, including molecular self-assembly, which involves the spontaneous, thermodynamically induced aggregation of particles without the influence of an external force (e.g. micelle aggregation or collagen triple helix formation).[4]

1.1.2 Diversity of biomaterials

Biomaterials can be divided into synthetic and natural biomaterials. While synthetic biomaterials include materials such as metals, ceramics, and synthetic polymers, natural biomaterials include biomacromolecules such as proteins, nucleic acids, and polysaccharides that were originally formed by living matter.[9] An overview is given in Figure 1-1, and their subtopics are discussed in more detail below.

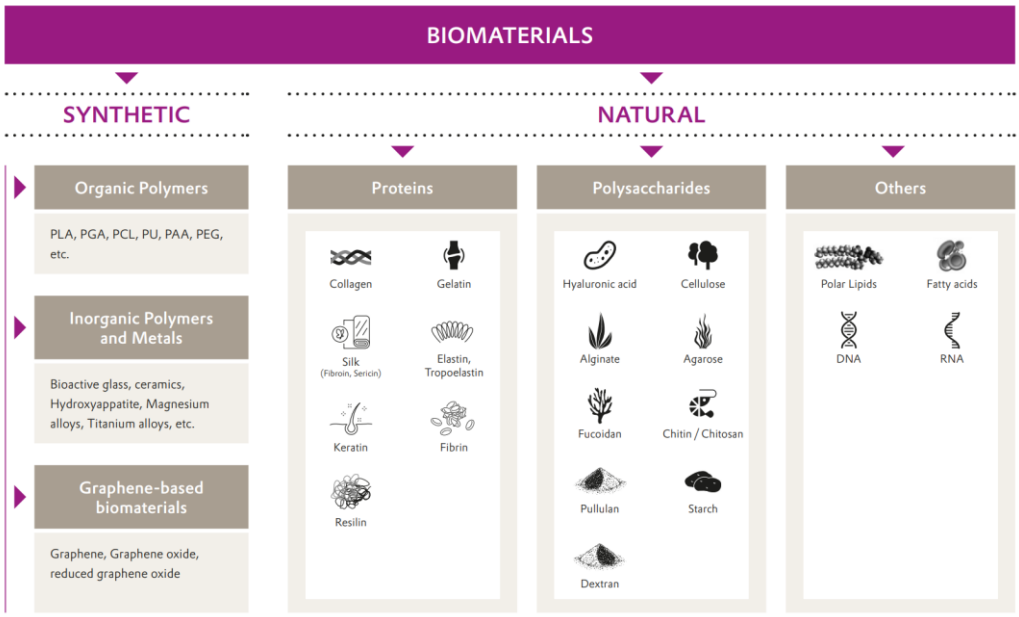

Figure 1-1: Overview of various biomaterials of natural or synthetic origin.

1.1.2.1 Polysaccharide-based biomaterials

Polysaccharide-based biomaterials are made from polysaccharides such as alginate, chitosan and hyaluronic acid. Depending on the polysaccharide, these materials can be biocompatible, biodegradable and non-toxic, making them ideal for a wide range of applications. In addition, these materials can be tailored for a wide range of properties, including mechanical strength, hydrophilicity, and biodegradability, making them customizable for specific applications.[10] These biomaterials can be used in a variety of biomedical applications to create three-

dimensional scaffolds for skin, cartilage, and bone repair, to provide structural support for cells, and to enable tissue engineering and the development of artificial organs.[11] In the field of drug delivery, polysaccharide-based biomaterials can be used to deliver drugs to specific cells or tissues in the body, which can increase efficacy and reduce side effects.[12,13] Polysaccharide-based biomaterials are also attractive as wound healing materials for various dressings to promote healing and prevent infection, and as coatings for biomedical implants to promote biocompatibility. In addition, polysaccharide-based materials can be used as biosensors (for e.g. the anchoring of enzymatic or non-enzymatic detection elements to the electrode surface[14]) and play an important role in the food industry (starch, pectin and carrageenan as thickeners, stabilizers and emulsifiers) and in water treatment to remove heavy metals and other contaminants.[10,15]

1.1.2.2 Protein-based biomaterials

Protein-based biomaterials are derived from proteins like collagen, elastin, fibrin, laminin, vitronectin, fibronectin and many more. These so-called structural proteins are the main component of the extracellular matrix and they form a network that holds tissues and organs together to give them stability and strength. They are therefore of crucial importance for the structure and function of the body.[16] Because they are biocompatible, biodegradable and non-toxic, protein-based biomaterials are ideal for a wide range of applications in e.g. medicine, biotechnology and materials science.[17] They can also be engineered for specific properties such as mechanical strength and biodegradability, allowing them to be tailored for specific applications like scaffolds for tissue engineering[17], bioadhesion[18] or drug delivery[19]. In addition and in contrast to polysaccharide-based biomaterials, peptides and proteins have several advantages, including more interaction sites with other molecules or cells (cell attachment, protein binding, ...) or targeted genetic engineering for application-specific primary sequence designs.[20] The most famous recognition pattern in proteins is the peptide RGD (arginine, glycine and aspartic acid) which acts as integrin binding pattern for cell adhesion. Another example is the platelet binding domain for collagen to induce blood clotting.[21] In addition, post-translational folding and modifications create additional unique properties.[22-24] Depending on the type of tissue, different material compositions allow tissue specific properties. As an example, the extra cellular matrix (ECM) of bones consists mainly out of collagen and minerals to form a stiff and rigid structure, while the ECM of the lung consists mainly of elastin and fibrillin to enable stretchability and elasticity of the tissue. In summary, proteins typically have a longer development phase but are more functional for biological interactions.

In the field of tissue engineering, proteins such as collagen and fibrin can be used to create three-dimensional scaffolds for skin grafting, cartilage repair and nerve regeneration due to their cellular interaction properties to rebuild tissue *in vivo*.[25] In medical devices, biomedical implants can be coated with fibrin, fibroin or collagen to promote cell adhesion and tissue integration. In the food industry, amino acid polymers such as casein and whey are used as emulsifiers, thickeners and gelling agents, or are sold as raw materials for the bodybuilding industry. Overall, protein-based biomaterials offer great potential for use in various fields due to their biocompatibility, biodegradability, and ability to be engineered to meet specific needs.[5,24]

1.1.2.3 Nucleic acid-based biomaterials

Nucleic acid-based biomaterials are synthetic or biologically derived biomaterials composed of nucleic acids. While most applications are based on specific deoxynucleic acid (DNA) or ribonucleic acid (RNA) molecules for transfections and genetic alterations, they can also be used as biomaterials and are separated in specific applications and biomaterial building blocks. RNA has recently experienced a boom for temporary transfection during the COVID pandemic.[26] Other gene therapies include cellular delivery of siRNA, plasmids, or viral vectors for the treatment of genetic disorders or cancer[27] or targeted drug delivery with DNA or RNA-based aptamers to reduce side effects of systemic drug administration.[28] Nucleic acid-based biomaterials can also be used in diagnostics for microarrays or biosensors.[29] Like polysaccharides or proteins, nucleic acids can also be used as scaffolds for tissue engineering applications.[30] Ongoing research in nanotechnology (DNA origami) evaluates nanoscale structures for drug delivery, sensing, electronics, and other applications.[31] In the field of synthetic biology, nucleic acid-based biomaterials, such as DNA circuits and synthetic gene networks, are explored to create novel biological systems for research and biotechnology applications. Overall, the versatility of nucleic acid-based biomaterials makes them a promising area of research with a wide range of potential applications in medicine, biotechnology, and materials science.[32]

1.2 Collagen

1.2.1 General information

The term "collagen" comes from the Greek word "κόλλα" (kólla), meaning "glue", combined with the suffix "-γέν, -gen", meaning "to make". It was originally used to refer to a glue made by boiling animal hides and bones.[33] Collagens are the most abundant protein family in

mammals, accounting for 25-35% of total protein mass/body weight. They have a unique triple-helical structure (see Figure 1-2) and function in many physiological and pathological processes, including cell adhesion, embryonic development, and tissue regeneration. They are also the major class of structural proteins in the extracellular matrix (ECM) where they provide structure, strength, and elasticity.[34] In 2007, Schweizer *et al.* discovered fossilized bones of a 68-million-year-old *Tyrannosaurus rex* with intact collagen, highlighting the long history of this protein family.[35] Naturally, the body's production of collagen decreases with age, but excessive sun exposure, smoking, alcohol consumption, and lack of exercise and sleep are major contributors as well.[36-38]

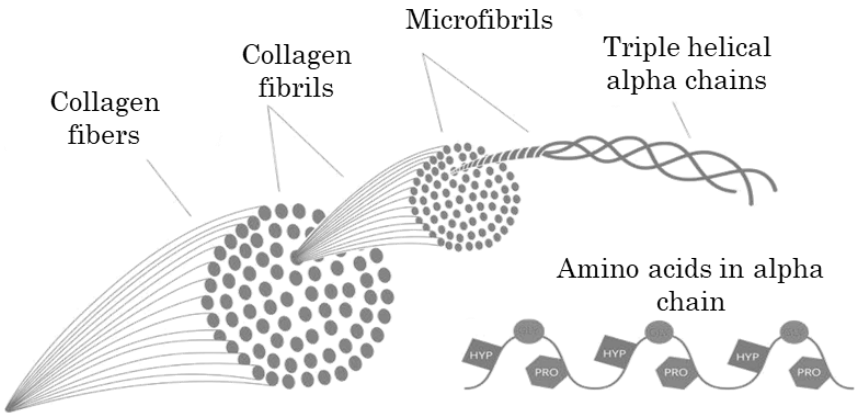

Figure 1-2: Collagen structure and its strand alignment into triple helix, to form fibrils and fibers.

1.2.2 Proteinogenic functions

Some tissue-specific benefits of collagens include the flexibility, support, and movement of cartilage or the encapsulation and protection of delicate organs such as the kidneys or spleen; they fill the sclera of the eye and provide the matrix of teeth that are made as a mineral composite.[39,40] Collagens surround vascular cells and play an important role in blood clotting. When exposed to platelet cells after vessel damaging collagen induces platelet aggregation and fibrin clot formation.[8] In addition, collagens have cell guiding functions for cell migration, differentiation, and proliferation and they are critical for embryonic development and regeneration.[41]

1.2.3 Collagen types and structure

To date, more than 29 different types (designated by Roman numerals) have been identified in humans, forming connective tissue, skin, bones, ligaments, cartilage, and tendons.[39,42] Collagens are also abundant in corneas, blood vessels, intestines, intervertebral discs, and dentin (teeth). Type I collagen is the most abundant type in humans (forming skin, tendons, blood vessels, and bones) with more than 90% total share[43,44], followed by types II (cartilage), III (reticular), IV (basal lamina), and V (cell surfaces, hair, placenta). Type II collagen accounts for approximately 5% to 10% of the total collagen in the body. It is primarily found in cartilage and is responsible for providing structure and resistance to compression.[45] With a share of ~1-5%, collagen type III is found in skin, blood vessels, and internal organs.[46] Depending on the degree of mineralization, collagen tissues can be rigid (bone), compliant (tendon), or both (cartilage).[47-49]

Collagens have a unique structure that can be defined by three features. First, the quaternary structure of collagens consists of three left-handed polyproline type II peptide chains twisted into a right-handed triple α-helix. This is stabilized by intramolecular hydrogen bonds. Second, the tight, supercoiled triple α-helix structure is atypical for proteins, and it is only possible because of the repetitive amino acid motif $(Gly\text{-}Xaa\text{-}Yaa)_n$ in which every third amino acid (aa) is glycine, the smallest known aa that fits sterically without altering the triple helical conformation. Third, Xaa and Yaa are often occupied by proline (Pro) or hydroxyproline (Hyp) due to post-translational modifications. In the most abundant collagen type I 10% proline and 10% hydroxyproline is present which sums up to an initial proline content of ~20% prior to post translational modifications.[49,50] According to Pfang *et al.*, the initial proline content can also reach 25%.[51] The triple helix formed can be composed of identical collagen chains (known as homotrimers, such as collagen II, II, VII, VIII, X) or different chains (known as heterotrimers, such as collagen types I, IV, V, VI, IX, and XI).[42,52] The percentage of triple helical conformation within a collagen sequence ranges from 96% (collagen type I) to less than 10% (collagen type XII).[39]

Based on their structure and supramolecular organization, different collagen subclasses can be identified. These are fibrillar and network collagens, membrane-associated collagens with interrupted triple helices (MACITs), fibril-associated collagens with interrupted triple helices (FACITs), and multiple triple helix domains and interruptions (MULTIPLEXINs).[53,54] To better understand structural differences, the primary sequences of selected collagen genes were assembled based on Ricard-Blum (Figure 1-2).[39]

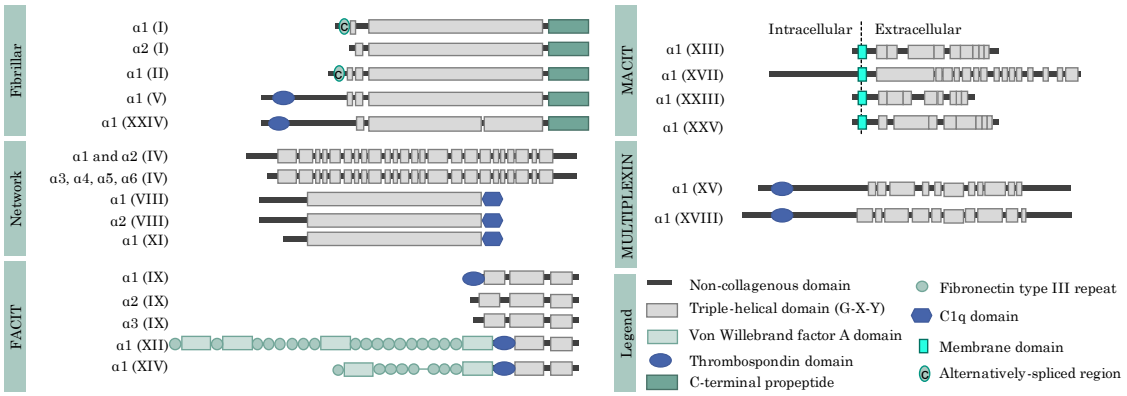

Figure 1-3: Structural organization of collagens in regards to their domain composition modified from Ricard-Blum.[39]

Collagen type I belongs to the fibrillar subclass and will be defined in more detail due to its high abundance. It is composed of >1,000 aa, resulting in the longest triple-helical collagen structure (~300 kDa, 280 µm in length and <2 nm in diameter). Through helical assembly (fibrillogenesis), collagen type I triple helices can form elongated fibrils (>500 µm in span, 500 nm in diameter, and >10^7 molecules).[54] This assembly is dependent on temperature, pH, and ionic strength.[49] Collagens not only contain triple helical areas but also terminal and internal non-triple helical regions which extent their functional capacities.[55] Collagen type I synthesis and degradation are regulated by a variety of factors, including growth factors, cytokines, and mechanical stress. Dysregulation, structural changes, and degradation of collagen production have been implicated in several pathological conditions, including osteogenesis imperfecta, osteoarthritis, skin aging, and cancer.[55]

Table 1-1: Overview of different collagen types, their chain structure, class, and tissue distribution. The table was adapted from Sorushanova *et al.*[49] and Ghomi *et al.*[56] Fibrillar collagens are highlighted in green and bold.

Type	Chains	Class	Tissue distribution
I	[α1(I)]$_2$α2(I)]	**Fibrillar**	Abundant, Dermis, tendon, ligament, cornea, dura mater, bone, tumor
II	[α1(II)]$_3$	**Fibrillar**	Cartilage, vitreous, tendon, intervertebral disc
III	[α1(III)]$_3$	**Fibrillar**	Skin, aorta, uterus, tendon, intestine, blood vessels, liver
IV	multiple	MACIT	Basement membranes of cell membranes
V	multiple	**Fibrillar**	Embryonic tissue, dermis, bone, cornea, hair
VI	multiple	Network	Uterus, dermis, cartilage, muscle
VII	[α1(VII)]$_3$	**Fibrillar**	Skin, amniotic membrane, cornea, mucosal epithelium
VIII	[α1(VIII)]$_2$ α2(VIII)	Network	Descemet's membrane, endothelial cells
IX	[α1(IX) α 2(IX) αα3(IX)]	FACIT	Cartilage, tendon
X	[α1(X)]$_3$	Network	Calcifying cartilage (including parts of tendons)
XI	[α1(XI) α 2(XI) *αα*3(XI)]	**Fibrillar**	Cartilage, intervertebral disc
XII	[α 1(XII)]$_3$	FACIT	Dermis, tendon, cartilage
XIII	[α1(XIII)]$_3$	MACIT	Endothelial cells, epidermis
XIV	[α1(XIV)]$_3$	FACIT	Dermis, tendon, cartilage
XV	[α1(XV)]$_3$	MULTIPLEXIN	Placenta, kidney, heart, ovary, testis
XVI	[α1(XVI)]$_3$	FACIT	Heart, kidney, muscle
XVII	[α1 (XVII)]$_3$	MACIT	Hemidesmosomes (skin), specialized epithelia
XVIII	[α1(XVIII)]$_3$	MULTIPLEXIN	Kidney, liver
XIX	[α1(XIX)]$_3$	FACIT	embryonic development, interneurons and formation of hippocampal synapses, basement membranes, muscle cell, rhabdomyosarcoma
XX	[α1(XX)]$_3$	FACIT	Corneal epithelium, skin, sternal cartilage, tendon
XXI	[α1(XXI)]$_3$	FACIT	Blood vessel walls
XXII	[α1(XXII)]$_3$	FACIT	Tissue junctions
XXIII	[α1(XXIII)]$_3$	MACIT	Tumors (prostate)
XXIV	[α1(XXIV)]$_3$	**Fibrillar**	Regulation of type I fibrillogenesis, osteoblast differentiation marker
XXV	[α1(XXV)]$_3$	MACIT	Interaction with ß-amyloid plaques in Alzheimer's disease
XXVI	[α1(XXVI)]$_3$	FACIT	Ovary and testis
XXVII	[α1(XXVII)]$_3$	**Fibrillar**	Hypertrophic cartilage
XXVIII	[α1(XXVIII)]$_3$	Beaded filament	Schwann cells, peripheral nervous system
XXIX	[α1(XXIX)]$_3$	Nonfibrillar	Epidermis, lung, small intestine, colon and testis

1.2.4 Collagen biosynthesis

Collagen is mainly produced by fibroblasts, but chondroblasts, osteoblasts and odontoblasts are also capable of synthesizing collagen for their respective extracellular matrix (ECM). Collagen synthesis is controlled at multiple levels by growth factors such as transforming growth factor beta (TGF-ß), platelet derived growth factor (PDGF), fibroblast growth factor (FGF) or insulin-like growth factor (IGF) or cytokines/lymphokines such as interleukin-1 alpha or beta (IL-1 α,ß) or interferon gamma (INF-γ).[57] Collagen synthesis requires several steps, which will be discussed in more detail in the following.

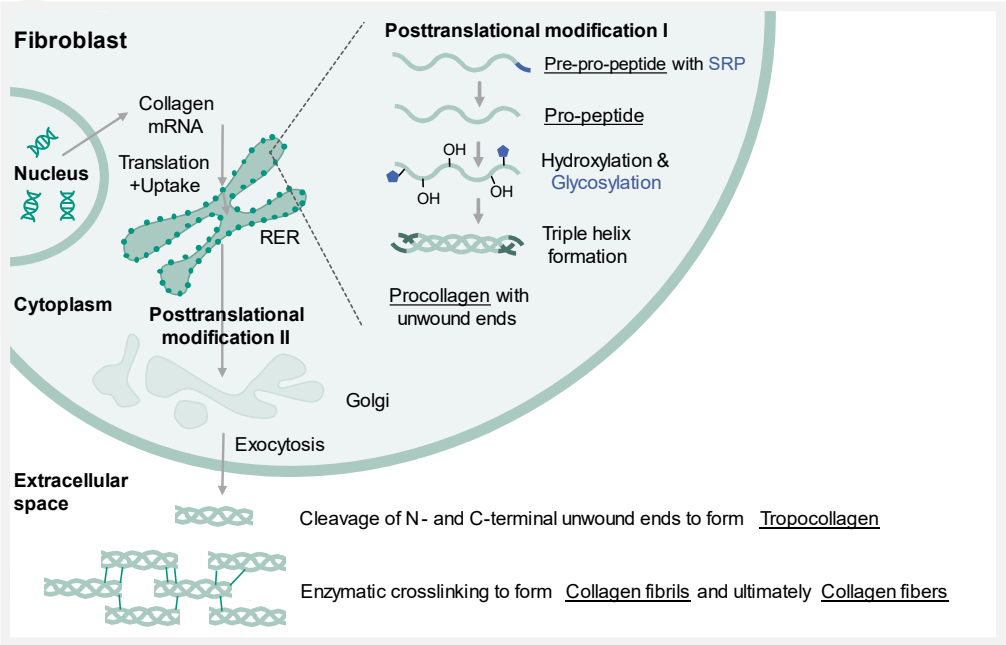

Figure 1-4: Fibrillar collagen biosynthesis.

Transcription and translation: Genes for pro-α1, pro-α2 or pro-α3 (containing a central collagen peptide flanked by pro-peptides and an *N*-terminal signal peptide) are transcribed (in nucleus) and translated (in cytoplasm - ribosomes) to form the pre-pro-peptide (α-chain). The *N*-terminal signal sequence is recognized by a signal recognition particle (SRP) on the rough endoplasmic reticulum (RER), which causes uptake into its lumen.[58]

Post-translational modifications I: Inside the RER lumen, the signal peptide is cleaved to form the pro-peptide (pro-α-chain). Next, the lysine and proline side chains are hydroxylated by lysyl hydroxylase and procollagen-proline dioxygenase (P4H; uses vitamin C as a cofactor, oxygen and iron ions) to form hydroxylysine and hydroxyproline. Glucose or galactose monomers are exclusively conjugated to the hydroxylated lysines (not to the

hydroxyprolines). The twisting of three modified pro-α-chains into a triple helix forms procollagen. Procollagen still has unwound ends that are later truncated.[58]

Post-translational modifications II: Procollagen is translocated to the Golgi apparatus where additional glycosylation occurs, followed by extracellular secretion. Extracellular membrane-bound collagen peptidases remove "loose ends" to form tropocollagen. Tropocollagen molecules self-assemble into collagen microfibrils, which are ultimately crosslinked by lysyl oxidases (extracellular, copper-dependent oxidases) by introducing aldehyde groups onto lysine hydroxylysine side chains, which undergo intramolecular and intermolecular aldol condensation to link tropocollagen units to form collagen fibrils. Multiple collagen fibrils can then assemble into collagen fibers.[58]

1.2.5 Recombinant collagens

Animal-derived collagens are widely used in many medical applications. To date, animals remain the primary source (>50,000 metric tons of collagen and gelatin per year).[59] According to a recent market report, the global collagen market was valued at 9.12 billion in 2022 and is expected to reach $23.1 billion by 2030 (Compound annual growth rate (CAGR) of 10.8%). The growth is driven by the increasing demand for collagen-based products in the food and beverage industry (~ 60%), driven by consumers' health awareness and preference for natural and organic ingredients.[60] In addition, collagen is expected to gain significant market share in the medical and cosmetics sector (~38%) due to expanding applications, changing consumer preferences and lifestyles, higher disposable incomes and increased awareness of health and personal care.[61] Although animal-derived collagens are well established materials, accumulating concerns like source availability, stability, quality issues (batch-to-batch variability, non-sustainability, difficult purification), and the potential of disease transmission arises the need for recombinant alternatives.[62] In addition, ethical and religious concerns as well as a global shift towards a vegan diets favor the development of non-animal-derived alternatives.[3,63,64] So far, recombinant versions from mammalian and insect cells have been tested but have been found to be too costly for mass production.[65,66] Thus, cheaper hosts (yeast and bacteria) are highly attractive and gain in importance. In addition to lower production costs, which is one of the key drivers, recombinant collagens have advantages due to their sustainable origin, scalability of the production system and ease of customization.[62] Molecular engineering allows the biosynthesis of even rare proteins in large quantities in a sustainable and efficient production process.[17] As a result, numerous commercially available recombinant collagens have been developed over the years, e.g. Cellnest (Fujifilm Manufacturing Europe B.V.), recombinant human Type I collagen (rhCollagen) from tobacco plants

(CollPlant Biotechnologies); HumaColl21® (vegan human type XXI collagen) or Collume® (marine inspired vegan collagen) (Geltor Inc.) and VECOLLAN® (Evonik Operations GmbH). Due to the improved properties, recombinant collagens are investigated for biomedical engineering, such as skin repair, tendinopathy, corneal and cardiac repair therapies.[3,67-69]

1.2.6 Comparison of collagen and gelatin

Most of the animal derived collagen is converted to gelatin as the slaughterhouse waste is hydrolyzed with acid or base to release gelatin from bones, skin and cartilage. This process first denatures the collagen fibrils and degrades the long collagen strands in smaller polypeptides which changes the material properties by keeping the amino acid sequence (Figure 1-5). Because the 3D structure of collagen does not need to be preserved, harsh and comparably cheap extraction conditions can be applied which ensure a cheap process and a comparably low price. Compared to collagen, gelatin is water-soluble and is often used as gelation agent, stabilizer or binder for food applications like gummy bears. Collagen, on the other hand, is insoluble in water and forms a strong, fiber-like network that holds tissues and organs together and gives them stability and strength.[70,71] Collagen also degrades more slowly than gelatin.[72] Furthermore, both materials behave differently to temperature. While low temperatures keep collagen liquid, temperature decrease causes gelatin to form a solid hydrogel. Hydrogels will be introduced in the next chapters. By increasing the temperature, both materials behave *vice versa* causing gelatin to melt and collagens can form solid hydrogels triggered by pH adaptations.[73,74] Depending on the application, one material can be preferred over the other. One example is the production of gummy bears where gelatin is highly preferred due to the cheaper material cost. Another example is 3D bioprinting. While very fast gelation due to temperature reduction makes gelatin the easier choice for 3D printing, collagen might outrun gelatin in the biological performance in the long term due to the closer material properties to native tissues. Although both materials are biocompatible and support cell growth and tissue regeneration, collagen is closer to the ECM and has higher mechanical strength and stiffness compared to gelatin. In summary, both materials have their benefits that justify their use depending on the application.

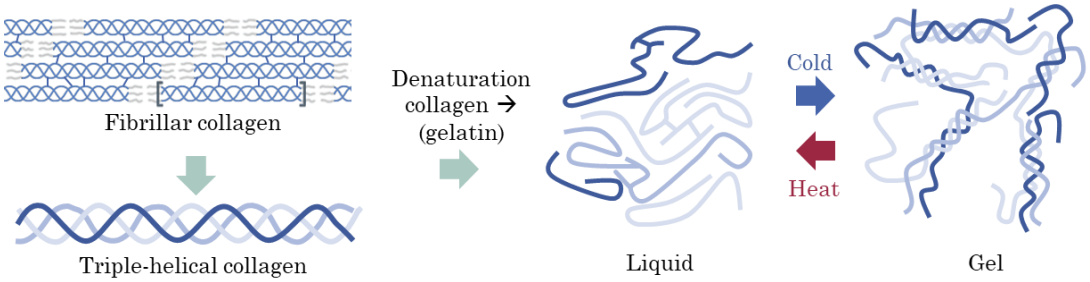

Figure 1-5: Gelatin production and subsequent gelation thereof.

1.3 Hydrogels

1.3.1 Introduction

Hydrogels first appeared in the literature in 1894, describing a variety of hydrophilic polymer networks with water as the dispersing medium.[75,76] They bind high amounts of water (>90% possible) and their 3D shape is held together by physical effects or chemical crosslinking, preventing the gel from dissolving during swelling. Physical stabilizing effects include hydrogen bonding, hydrophobic or ionic interactions, and chain entanglement. Chemical methods rely on covalent bonds.[77] Hydrogels can be made from natural or synthetic materials. Naturally derived hydrogels have better cell interaction, but often have material-derived problems such as batch-to-batch variation, limited tunability, or disease transfer. Synthetic hydrogels on the other hand do not have these downsides, but they often lack biofunctionality. Therefore, hybrid gels are particularly interesting for tissue engineering and additive tissue manufacturing.[78] Furthermore, as degradable matrices, hydrogels are considered as perfect starting point for neo-tissue growth which can allow minimal invasive transplantation *via* injections.[79,80] Hydrogels have a wide range of mechanical properties that make them attractive for many applications. By varying the polymer or crosslinker concentration, different rheological properties, expressed by storage moduli, can be measured (10 Pa to 3 MPa).[81] This adjustable range of mechanical stiffness together with excellent biocompatibility makes hydrogels an interesting approach for biomedical applications to mechanically adapt to the surrounding tissue. In addition, high water absorption and great biodegradability contributes to the attractiveness of hydrogels. Hydrogels' properties can be tailored using different crosslinking approaches and some are even stimuli responsive (so called smart hydrogels) which makes them responsible to environmental changes like pH, temperature, compound concentrations, osmotic pressure, light expose and the exposure to specific molecules like glucose or antigens.[77,82] By choosing the material, the crosslinking strategy, the addition of additional

substances, material concentrations and other parameters, different product properties like mechanical strength, porosity, biocompatibility, and degradability can be adjusted which opens the field for different applications. [77,80] For example, hydrogels used in tissue engineering should mimic the mechanical properties of natural tissues to support cell growth and differentiation, while drug delivery hydrogels should have a controlled release rate to achieve optimal therapeutic efficacy.[82,83] In summary, hydrogels are versatile, highly tunable and responding scaffold materials which can be used in different applications while maintaining great biocompatibility.

Table 1-2: Important general hydrogel characteristics (not limited to collagen) and their definitions.

Bioactive properties: Hydrogels can be engineered to incorporate specific bioactive molecules, such as growth factors or cytokines, that can promote cell proliferation, differentiation, and tissue regeneration.
Biocompatibility: Hydrogels can be engineered to be biocompatible and support cell growth, making them useful in multiple biomedical applications used for tissue engineering, wound healing and drug delivery.
Degradation rate: Hydrogels can be designed to degrade at a controlled rate, which can be important for applications such as drug delivery or tissue engineering. Degradation rate can be controlled by adjusting crosslink density, collagen concentration or by incorporating degradable components.
Mechanical properties: Stiffness, elasticity, and toughness can be engineered to make hydrogels suitable for various applications. These mechanical properties of hydrogels can be controlled by adjusting e.g. the material composition or the crosslinking density.
Porosity: Hydrogels can be synthesized with varying degrees of porosity, allowing them to be used for different applications such as drug delivery to serve as a matrix for drug encapsulation and release.
Self-healing: Some hydrogels can self-heal, meaning that they can repair themselves after being damaged. This property can be useful in applications with repeated mechanical stress.
Stimuli-responsive behavior: Hydrogels can respond to external stimuli such as temperature, pH and light, allowing control over their properties and behavior. For example, pH-responsive hydrogels can be used to deliver drugs to specific areas of the body where the pH is different.
Structural Similarity: Structure-dependent functionality can be accessed by using the respective materials which also naturally occur at the site of action with preserved 3D structures to initialize the desired reaction *in vivo* like cell attachment, cell migration and support for tissue regeneration.
Swelling behavior: Hydrogels can absorb and retain large amounts of water, resulting in significant swelling. The degree of swelling can be tuned by adjusting the chemical composition and crosslinking density.

1.3.2 The role of rheology in tissue engineering

1.3.2.1 Literature review

In tissues, cells are subjected to various mechanical forces, including hydrostatic pressure, shear, compression, and tension. According to Newton's Third Law, for every action there is an equal opposite reaction. Adapted to tissues, cell matrices will respond to environmental changes by adjusting their internal tension through reciprocal actomyosin- and cytoskeleton-dependent counterforces (scientific term: mechanoreciprocity).[84,85] This force adjustment influences the ECM, resulting in changing mechanical matrix properties over time. Force plays an important role in guiding stem cell fate and controlling embryonic development. Force is necessary for normal tissue-specific development by controlling organization and function as well as cell growth, survival, and migration. Its loss can lead to the progression of diseases such as liver fibrosis, atherosclerosis and cancer.[84]

1.3.2.2 Quantities and units

When a force (F) is applied to an area (A_0), deformation can occur. The quotient of the two units is called stress (σ) and is measured in Newtons per square meter (N/m^2), Pascals (Pa), or pounds per square inch (psi). Strain (ϵ) describes the quotient of deformation by the change in length ($\Delta L = L - L_0$) and the original length (L_0) to which stress is applied. The quotient of stress (σ) and strain (ϵ) is called elastic modulus δ (see equation 1-1), which characterizes the resistance of an object or material to elastic deformation and is used to quantify the mechanical properties of materials.[86]

$$\textbf{elastic modulus } \delta = \frac{\textbf{stress } (\sigma)}{\textbf{strain } (\epsilon)} = \frac{\frac{\textbf{force } (F)}{\textbf{area } (A_0)}}{\frac{\textbf{change in length } (\Delta L)}{\textbf{original length } (L_0)}} \qquad \textbf{1-1}$$

Depending on the direction of the applied force, different subcategories of the elastic modulus can be measured (see Table 1-3) and which were visualized in Figure 1-6.

Table 1-3: Overview of different elastic moduli.

Name & description	Definition
Young's modulus (E): material's resistance to deformation under tensile or compressive forces (uniaxial deformation, linear stress)	ratio of stress (force per unit area) to strain (change in length per unit length) in the linear elastic region of the stress-strain curve.
Shear modulus (G): material's resistance to deformation under shear forces (deformation of shape at constant volume).	ratio of shear stress (force per unit area) to shear strain (change in angle per unit length) in the linear elastic region.
Bulk modulus (K): material's resistance to compression under hydrostatic pressure.	ratio of hydrostatic stress (pressure) to volumetric strain (change in volume per unit volume) in the linear elastic region.
Poisson's ratio (v): material's tendency to expand in one direction when compressed in another one.	negative ratio of lateral strain (change in width per unit width) to axial strain (change in length per unit length) in the linear elastic region.

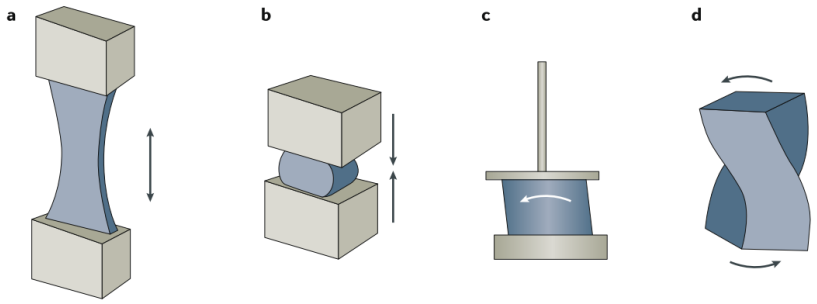

Figure 1-6: Main mechanical deformations representing tensile (a), compressive (b), shear (c) and torsion (d) deformations. The figure was extracted from Gumarães *et al* and reproduced with permission from Springer Nature.[87]

To describe a hydrogels resistance to deformation, the shear modulus (G) is mostly used. When sheared, the material can store some of the applied energy which is described as the elastic component which is expressed by the shear storage modulus (G'). After relaxation, the stored energy triggers reverse deformation to return to the initial conditions. In ideal elastic materials, the energy is released without damaging the material structure, even when multiple cycles of stress and replication are applied. If the structure is irreversibly damaged by the deformation energy, the energy is dissipated, for example, by heat, which represents the viscous part, described as the shear loss modulus (G"). Ideally, viscous materials exhibit an irreversible deformation behavior that changes the material irreversibly after several stress-relaxation cycles. G' and G" are components of the complex modulus (G*), which is describes as the material's response to both elastic and viscous deformation. It connects G' and G" by the imaginary unit i through the equation $G^* = G' + iG''$. An important correlation between G' and G" is tangent delta ($\tan \delta$). This dimensionless quantity describes the ratio of viscous

and elastic shares within a viscoelastic material and is defined as: tan δ = G" / G'. It is often used in dynamic mechanical analysis (DMA) and other rheological techniques to study the mechanical properties of materials. For an ideally elastic behavior, no viscous portion (G") is measured and tan δ is 0 (G' > G"). For an ideally viscous behaviors, no elastic portion (G') is measured, meaning tan δ approaches infinity (G" > G'). When tan δ=1 (during gelation) the so-called sol/gel transition point is reached. Previous studies suggest the following tan δ values for different hydrogel stiffnesses. In case of a weak hydrogel, tan δ is near 1. A medium stiff hydrogel is represented by a tan δ of between > 0.1 and ≤ 0.5 and a strong hydrogel produces a tan δ of ≤ 0.1.[88,89]

1.3.2.3 Correlation of the Young modulus and the shear modulus

The Young modulus (E) can be used to characterize materials, including different tissues (Figure 1-7). Annealing to the stiffness of native tissues, is important for the development of artificial matrices for cellular wellbeing and the integration into surrounding tissues in case of implantation. For softer hydrogel formulations, tensile strength measurements are highly difficult due to low material integrity as well as the required mechanical sample fixation for the measurement. Instead, the shear modulus (G) can be measured even for very soft hydrogel formulations using a plate-plate rheometer. With the help of Poisson's ratio, the modulus of elasticity (E) can be calculated using equation 1-2.[87] For hydrogels, a Poisson's ratio (v) of 0.25 - 0.49 can be estimated[90]

$$G = \frac{E}{2(1+v)}; \qquad G * \big(2(1+v)\big) = E; \qquad E = 2.5G \text{ to } 3G \tag{1-2}$$

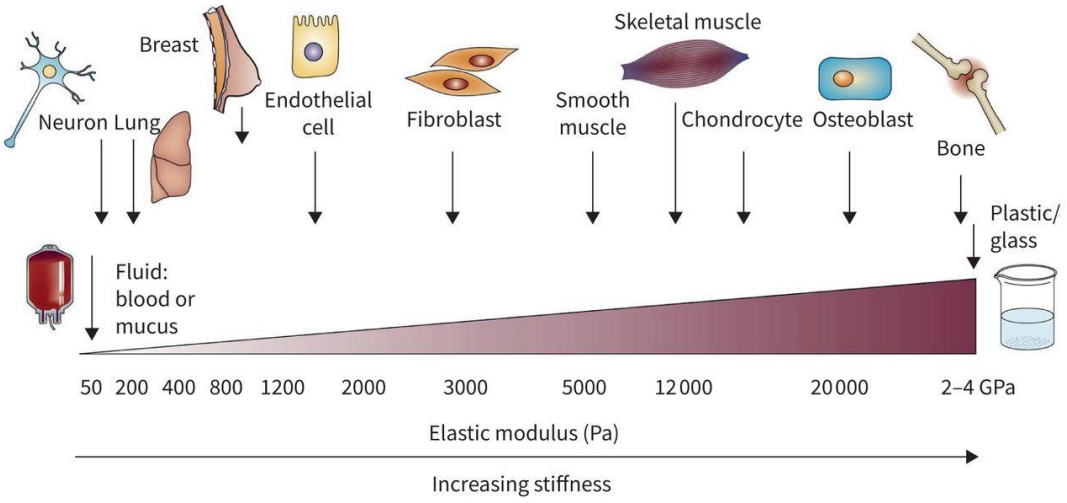

Figure 1-7: Elastic moduli of different tissues. The graphic was reproduced with permission from Springer Nature.[84]

1.3.3 Hydrogel Synthesis

1.3.3.1 Physical crosslinking

Hydrogels can be formed by physical or chemical crosslinking methods.[77] Physical crosslinking is highly structure-dependent and is based on intermolecular non-covalent reversible interactions. They can be based on ionic/electrostatic or hydrophobic/hydrophilic interactions, hydrogen bonding, crystallization, metal coordination, host-guest interactions and others (see Table 1-4). Due to their non-covalent interactions, some hydrogels can respond to external stimuli such as temperature, pH, light or electric fields. These special forms of hydrogels are called "smart" or "stimuli-responsive". Some are even self-healing (breaking bonds under high shear stress and reforming under low stress). Not all physically crosslinked hydrogels are stimuli-responsive like ionotropic gelation of physical entanglement.[77,91] Physically crosslinked hydrogels have several advantages, including high biocompatibility, and ease of synthesis. These properties can be tuned by adjusting the parameters of the crosslinking method. Stimuli-responsiveness can be useful for drug delivery or tissue engineering applications, and some formulations allow adjustable degradability over time and injectability. Disadvantages include inferior mechanical properties compared to chemically crosslinked hydrogels, which makes physically crosslinked hydrogels more prone for breaking or deformation under stress. Physical crosslinking can also lead to instability over time, as network formation can be reversible. It is challenging to create hydrogels with desired properties or network structures due to non-covalent interactions. Physically crosslinked hydrogels may also not respond as efficiently or rapidly to external stimuli compared to selected chemically crosslinked hydrogels, and their weaker mechanical properties may limit their suitability for some applications, including drug delivery or tissue engineering.[75,92] Some example for physically crosslinked hydrogels are alginate which can be crosslinked by divalent cations, like calcium (Ca^{2+})[93], gelatin[94] or agarose[95] which gel and liquify due to temperature changes and ionic interactions happening between the cationic chitosan and the anionic alginate.[96] Animal-derived collagens are normally physically crosslinked when heated by self-assembly to form fibrils (see chapter 1.2.1, Figure 1-2). The process (called fibrillogenesis) is guided by hydrogen bond formations and van der Waals forces. Physically gelated collagen hydrogels are normally quite weak and changes in pH and temperature can alternate the electrostatic interactions and change the properties of formed hydrogels. Thus, chemical crosslinks were explored to achieve more defined structures, a higher overall stiffness and an increased resistance to environmental, physical parameters.[97] The recombinant collagen studied for this thesis (rCol) is not capable of physical gelation which made chemical crosslinking mandatory to craft 3D structures.

Table 1-4: Physical intermolecular interactions for hydrogel formation.

Interaction	Description and Examples
Ionic/electrostatic interactions	Ionic interactions occur between charged molecules of opposite charges (like cations & anions) forming strong bonds. Same charge → repulsion, opposing charge → attraction. Prominent examples: alginate crosslinked by divalent cations (Ca^{2+}, Ba^{2+} or Mg^{2+}) & polycationic chitosan + anionic chondroitin sulfate and alginate, or polylactic acid for electrostatic interactions.
Hydrogen bonds	Most common interaction type; very weak; great stability by multitude of hydrogen bonds; stabilizes biopolymers like DNA or proteins. Other examples: Amides, urea carboxylic acids, pyrrole and carbazole + pyridine or imidazole.
Hydrophobic/ hydrophilic interactions	Polymers with hydrophilic and hydrophobic areas can undergo sol-gel transition at lower critical solution temperatures (LCSTs) or upper critical solution temperatures (UCSTs) or when treated with ultrasonification. Examples: poly(*N*-isopropylacrylamide) (PNIPAAm) for LCST and poly(*N*-acryloyl glycinamide) (PNAGA) for UCST. Fibroin (variance in α-helices and ß-sheets) can be changed by ultrasonification which strongly determines its water solubility.
Crystallization/stereocomplex formation	Polymer chains can align in a regular, repeating pattern, resulting in a more rigid and ordered structure. Stereo complex formation occurs when two different types of polymers with opposite stereochemistry interactions meet, resulting in a more stable and ordered hydrogel structure. The effectiveness depends on factors such as molecular weight, concentration, temperature, and the number of freeze-thaw cycles.
Metal coordination / Chelation	Interactions between functional groups in polymers and metal ions. Bipyridyl-functionalized poly(2-oxazoline)s can be crosslinked with Fe(II), Ni(II), Ru(II) or Co(III) or 3,4-dihydroxyphenylalanine (DOPA) functionalized 4-Arm-Polyethylene glycol (4PEG) molecules complexing Fe(III) ions. Especially the pH is crucial for this kind of interactions.
Host guest interaction	Usually, a host is a molecule with large cavity volume like α-cyclodextrins (CDs) and crown ethers. Guests with complementary shape can also interact (key-lock principle). A good example is a α-CD modified PEGs. They are injectable and can be used for controlled drug release.[77]
π- π stacking	π-π stacking by the overlap of electron clouds surrounding aromatic rings, resulting in attractive van der Waals interactions between the rings. Examples: polyphenylene oxide (PPO), polyethylene glycol (PEG) and polyacrylates. The strength and specificity of the π-π stacking interaction can be influenced by various factors, like the aromatic ring distance, their orientation, size and shape. These factors can be controlled through the design and synthesis of the polymer chains, allowing the synthesis of hydrogels with tailored properties.
Polymerized entanglement	Also known as physical entanglement or physical interpenetration. In polymerized entanglement, the polymer chains are not covalently bonded to each other, but instead become entangled due to their high molecular weight and chain flexibility. When the polymer chains are mixed in a solution and undergo polymerization, they become physically interlocked and entangled, forming a stable and reversible network structure. Influencing factors are the molecular weight of the polymer chains, the degree of polymerization, the crosslinking density, and the presence of additives or surfactants in the solution.

1.3.3.2 Chemical crosslinking (with focus on collagen)

1.3.3.2.1 Introduction

Chemical crosslinking forms strong covalent bonds that are generally more stable than physical interactions and less sensitive to environmental changes such as temperature or pH.[77] Variations in material concentration and functional groups per molecule allow finetuning of material properties such as stiffness, swelling, and degradation. Depending on the functional groups available in the applied biomaterial, different crosslinking approaches are feasible. The following is a detailed description of the different chemical crosslinking options for biomaterials. While some technologies are based on the addition of small molecules or chemical linkers, others require material functionalizations prior to crosslinking. The most used crosslinking methods are based on inexpensive and highly reactive chemicals such as formaldehyde (FA) or glutaraldehyde (GTA). FA reacts with the ε-amino group of lysine and hydroxylysine residues in collagens to form imines, which further react with tyrosine or amide groups of asparagine or glutamine residues. The reaction results in brittle and toxic products, as well as toxic by-products that must be thoroughly removed (in the case of GTA), making it unsuitable for biomedical purposes.[98] As a replacement for GTA, hexamethylene diisocyanate (HDC) has been introduced with fewer toxic side effects in a long-term culture with human skin fibroblasts.[99] Also, 3,3-dithio-bis-propionimidate (DTBP) and dimethyl suberimidate (DMS) have been successfully tested on collagen with lower toxicity than GTA[100] as well as polyepoxy compounds with acceptable cytotoxicity.[101]

1.3.3.2.2 Activation reagents

In addition, carbodiimides (R_1-N=C=N-R_2) are widely described and used in literature. An overview of commonly used carbodiimides is given in Figure 1-8. 1-Ethyl-3-(3-dimethylaminopropyl)carbodiimide (EDC) represents a water-soluble carbodiimide which is often used for biochemical applications such as protein conjugation or protein crosslinking. In combination with *N*-Hydroxysuccinimide (NHS) the yield can be increased. The precise reaction mechanism is depicted in Scheme 1-1. When comparing with previously introduced GTA, HDC or acyl azide, EDC shows the best results in terms of biocompatibility and tissue regeneration.[102] As an activation reagent, carbodiimides initiate the reaction but they are not part of the final linkage.[102] In addition, these reagents are often classified as hazardous, and their byproducts can also be problematic. Therefore, they are not recommended for direct cell contact, but rather for cell-free scaffolds with washing steps prior to cell contact.

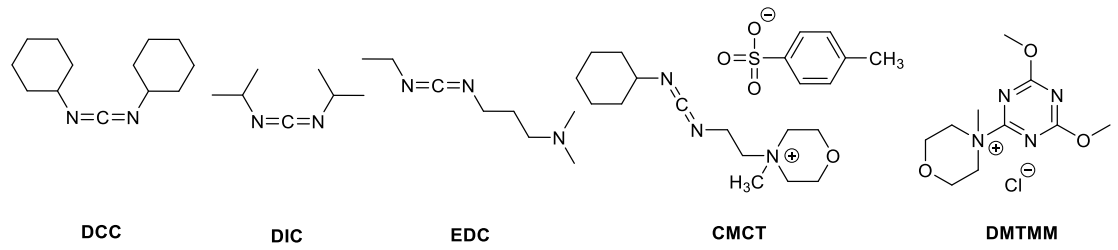

Figure 1-8: Chemical structures of carbodiimide derivatives with *N,N'*-Dicyclohexylcarbodiimide (DCC), Diisopropylcarbodiimide (DIC), 1-Ethyl-3-(3-dimethylaminopropyl) carbodiimide (EDC), *N*-Cyclohexyl-*N'*-(2-morpholino-ethyl)carbodiimid-methyl-p-toluolsulfonat (CMCT) and the triazine derivative 4-(4,6-dimethoxy-1,3,5-triazin-2-yl)-4-methyl-morpholinium chloride (DMTMM).

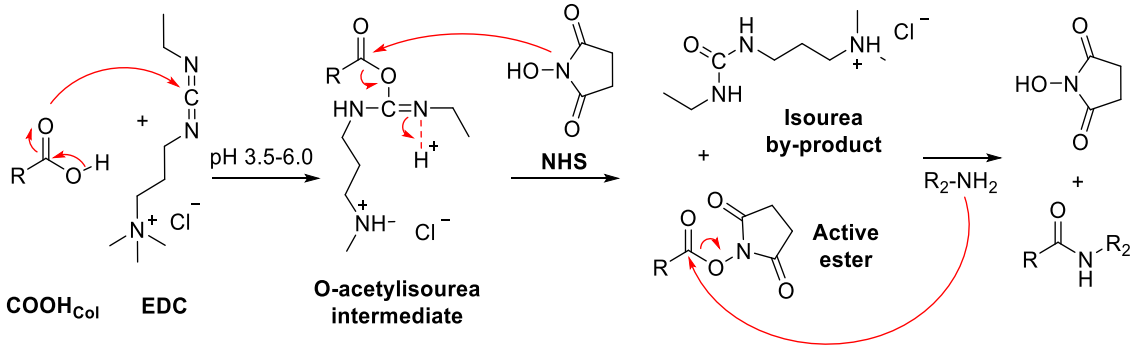

Scheme 1-1: Carbon acid activation followed by primary amine conjugation. An active O-acylisourea intermediate is formed by the reaction of EDC with a carbon acid in collagen. This step is most efficient at an acidic pH around 4.5. This intermediate can react directly with primary amines. The instability of the active ester in aqueous solution allows hydrolysis of the intermediate within a short time. Substitution with NHS forms a water-stable NHS ester that allows conjugation to primary amines at physiological pH. During the formation of the active NHS ester, an isourea by-product (1-(3-dimethylaminopropyl)-3-ethylurea) is formed. During the subsequent substitution of NHS by a primary amine, NHS is released. This reaction step requires a pH 7.0–9.0.[103]

EDC/NHS was compared with 4-(4,6-dimethoxy-1,3,5-triazin-2-yl)-4-methylmorpholinium chloride (DMTMM), another carbon acid activation reagent, which shows higher reaction efficiency even in the absence of pH control, which is essential for EDC conjugation (pH 3.5-4.5)[104] followed by pH increase to slightly alkaline conditions. DMTMM was successfully used between pH 5.0 and 9.0. Only by going ≤3 and ≥10, no crosslinking was observed.[105] In addition, DMTMM is classified as less hazardous than EDC with high yields and low epimerization levels.[106,107] Also bubble formation during gelation was reported with EDC in literature which interrupts a homogenous network formations and favors the usage of DMTMM as crosslinker. It was indicated that traces of ethyl isocyanate (one of the educts in EDC synthesis) could be responsible for the gas formation.[108,109] To avoid bubble formation and due to the described broader pH range, DMTMM was determined as the better choice of crosslinker.

Furthermore, DMTMM can form amide bonds in alcoholic or aqueous media without ester formation. The carboxylate anion reacts with DMTMM to form an active ester, which is attacked by an amine or alcohol to form the corresponding amide or ester (see Scheme 1-2).[107,110]

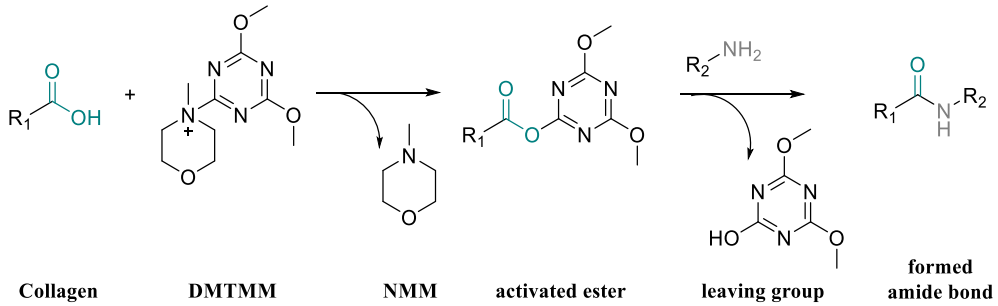

Scheme 1-2: Carbon acid activation by the triazine derivative DMTMM followed by substitution with a primary amine to form an amide bond. NMM = *N*-methylmorpholine. The leaving group within the 2nd step is called 4,6-dimethoxy-1,3,5-triazin-2-ol.

1.3.3.2.3 Bi- and multi-functionalized linker

GTA is one of the best known crosslinkers in protein chemistry, providing two terminal aldehyde functions that can react with primary amines to form Schiff bases. Although the homo-bifunctionalized linker is cheap, it is classified as a hazardous CMR substance. Polyethylene glycol (PEG) instead represents a large group of synthetic molecules with different molecular weights and branches. The terminal alcohols can be derivatized to introduce different side chains that are interesting for different crosslinking approaches. The material is biologically inert and cell adhesion or proliferation is only possible with additional functionalizations.[111] PEG itself is FDA approved and is used in a variety of products ranging from highly engineered bioactive formulations to food additives including the functionalization of proteins, nucleic acids, or hydrophobic drugs to enhance their blood circulation time or to enhance the solubility in water.[112] It exists in different molecular weights and can be designed as linear or branched versions (4-arm, 6-arm and 8-arm derivatives) with different terminal functionalizations (homo- and hetero-functionalized). Various companies such as JenKem Technology USA Inc. or Creative PEGWorks offer a wide range of functionalized PEG derivatives. To enable chemical crosslinking, commercially available 4-fold branched NHS-activated Star-PEG derivatives were tested with rCol based on a previous publication with animal-derived collagen[113] and further results with this chemistry are presented in the experimental part of

the thesis. Terminally modified NHS esters are known for great reaction efficiencies.[103] The underlaying reaction chemistry is depicted in Scheme 1-3.

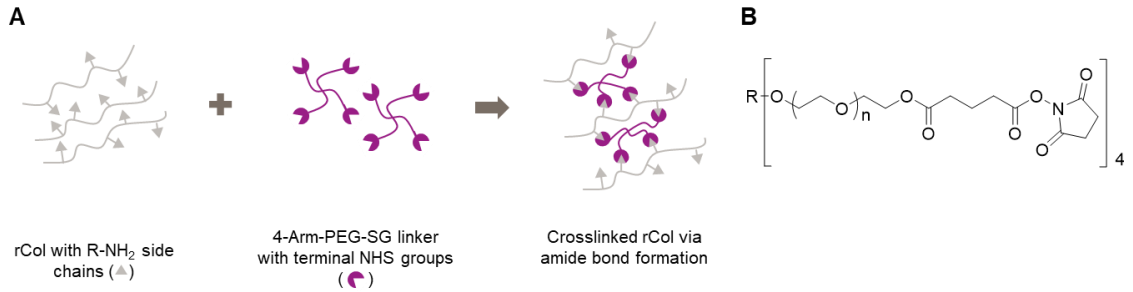

Scheme 1-3: (A) Chemical crosslinking of rCol using the NHS activated 4-Arm-PEG linker which reacts with primary amines present in lysine side chains to form peptide bonds. **(B)** Chemical structure of the 4-Arm-PEG-NHS crosslinker.

1.3.3.2.4 Genipin

Besides synthetic crosslinkers like the Star-PEG compound, more natural crosslinking reagents like genipin are desired. Genipin was first extracted from the fruit of *Gardenia jasminoides*, which describes a small molecule that undergoes a nucleophilic substitution reaction with primary amines and the reactive carbonyl group of genipin. The crosslinking reaction can be controlled by adjusting the pH, temperature, and concentration of genipin. The resulting crosslinked protein structures have improved stability, mechanical strength, and resistance to degradation, making them suitable for various biomedical and industrial applications. Limitations of this chemistry include potential dose-dependent cytotoxicity (limited to 0.5 mM)[114], a long reaction time, and the blue color, which is limiting for some applications. Other interesting natural chemical crosslinkers include nordihydroguaiaretic acid and tannic acid. Nordihydroguaiaretic acid is a natural polyphenolic compound obtained from the creosote bush[115] and contains two reactive ortho-catechol groups. In addition to being a crosslinking agent, it has been shown to have anticancer and antioxidant properties.[116,117]

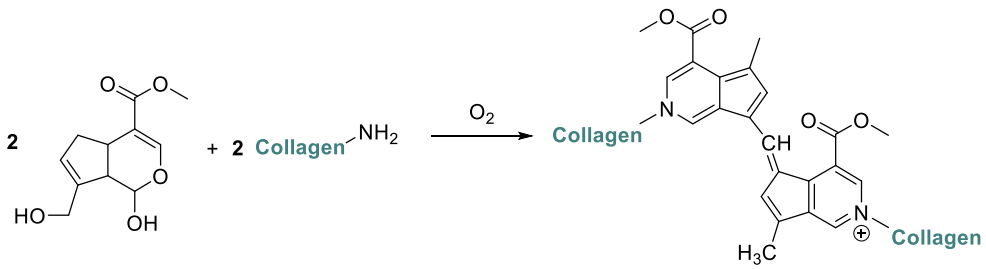

Scheme 1-4: Genipin-based crosslinking of collagen.

1.3.3.2.5 Click chemistry and bioorthogonal click chemistry

Click chemistry, introduced by Sharpless *et al.* in 2001 and awarded with the Nobel Prize in 2022, refers to a set of chemical reactions that are highly efficient, modular and effective.[118] Some of them are listed in Table 1-5. They have fast reaction kinetics, high yields and mild reaction conditions. Click chemistry is widely used in synthetic chemistry, materials science, and drug discovery to create new compounds and materials. Some common examples of reactions are the Huisgen cycloaddition, the copper-catalyzed and strain-promoted azide-alkyne cycloaddition, and the tetrazine click reaction.[119] Bioorthogonal chemistry describes chemical reactions that can occur in living organisms without interfering with native biological processes.[120] They are often used in chemical biology and biochemistry to study and manipulate biological systems. Additionally, to the requirements of click reactions, bioorthogonal reactions have addition requirements which differentiates them from click reactions. They must be non-toxic and their fidelity should not be affected by the plethora of endogenous functionalities present in cellular media.[121] This class of high-yielding chemical reactions allows rapid and selective crosslinking *in vitro* and *in vivo* without affecting endogenous functional groups. The origin of bioorthogonal reactions arose from molecular labeling using Staudinger Ligation in 2000, and the term bioorthogonal was first defined by Bertozzi *et.al.* in 2003.[122,123] Since then, an increase in scientific publications was observed, followed by the Nobel prize in 2022 which was given to Carolyn R. Bertozzi, Morten Meldal and K. Barry Sharpless for their development of Click Chemistry and bioorthogonal chemistry as stated above.[124] Using bioorthogonal reactions, researchers can introduce specific chemical groups into biomolecules (such as proteins, nucleic acids, and lipids) and track their behavior in real time. Bioorthogonal chemistry also allows specific biomolecules to be selectively labeled and modified without affecting the rest of the system. Besides Staudinger ligation more examples are inverse electron demand Diels-Alder reaction (IEDDA), aldehyde/ketone-tetrazine cycloaddition, tetrazine ligation, oxime, and hydrazone ligation.[125] A great paper comparing different bioorthogonal reactions was published in 2019 by Van Hoorick *et. al.*[126] While click chemistry and bioorthogonal chemistry share some similarities (such as their focus on highly selective reactions), they have different goals and applications. Click chemistry is primarily used to create new compounds and materials, while bioorthogonal chemistry is used to study and manipulate biological systems. In addition, not all click chemistry reactions are bioorthogonal, as some may interfere with biological processes (e.g. toxic catalysts or harsh reaction conditions), and not all bioorthogonal reactions are click chemistry, as they may not involve the formation of covalent bonds. For a better overview of different click reactions and their suitability for biological systems, see Table 1-5. In the following chapters, selected bioorthogonal click reactions are described in more detail.

Table 1-5: Summary of different click reactions (CC) and the separation from bioorthogonal (BO).[77,121]

Reaction	Description and/or examples	BO
Aldehyde/ketone-tetrazine cycloaddition	Tetrazine + aldehyde or ketone → stable triazoline intermediate → amide (slower than Tetrazine-click reaction, can require elevated temperatures or catalysts to proceed efficiently)	yes
CuAAC	azide + alkyne → stable triazole, cupper catalyzed	yes
Enzymatic reactions	6 different enzyme classes; mostly ligases; covalently linked, e.g. Tyr + Tyr; Gln + Lys	yes
ieDDA	strained alkene or alkyne + tetrazine → stable cycloadduct	yes
Michael additions	base-catalyzed thiol-vinyl sulfone or base-catalyzed thiol-maleimide coupling	yes
SPAAC	azide + alkyne → stable triazole; strain promoted	yes
Staudinger Ligation	reaction between an azide and a phosphine to form an amide	yes
Tetrazine-click reaction	Tetrazine + strained alkene like trans-cyclooctene → stable 1,2,4,5-tetrazine adduct	yes
Thiol-ene chemistry	photoinitiated thiol-ene photocoupling	yes
Diels-Alder	[4 + 2] cycloaddition; Furan + Maleimide	no
Huisgen cycloaddition	azide + alkyne → stable triazole; 1,3-dipolar cycloaddition, normally organic solvent	no
Schiff base	amine + aldehyde or ketone → conjugated imine	no

1.3.3.2.5.1 Enzyme-based methods

Enzymatic reactions are attractive because they are fast, highly selective, and easy to gelate without toxic by-products. On the other hand, residual enzymes can continue to catalyze unwanted crosslinking with surrounding tissues in the body, while enzyme removal remains challenging. In addition, many enzymes depend on cofactors such as Ca^{2+} or cytotoxic compounds such as H_2O_2. Although small amounts are required, enzymes can be quite expensive compared to small molecule-based crosslinkers. Common enzymes are horse-radish peroxidase (HRP; H_2O_2 dependent) or tyrosinase to crosslink tyrosine side chains, transglutaminases to link lysines to glutamine side chains (Ca^{2+} dependent), or exogenous lysyl oxidase to convert lysine side chains to highly reactive aldehydes that form Schiff bases with other lysine side chains. This third enzymatic reaction is known from collagen maturation.[127] Within this thesis HRP, tyrosinase and transglutaminase were tested and led to hydrogel formation with rCol (data not shown here) but were not pursued further due to the described drawbacks.

1.3.3.2.5.2 Thiol-Michael Addition

Thiol-Michael addition is a chemical reaction in which a thiol (such as cysteine) reacts with a Michael acceptor (such as an α,ß-unsaturated carbonyl compound) to form a carbon-sulfur bond in a nucleophilic addition reaction. The reaction proceeds under mild conditions and is

highly efficient, making it an attractive method for organic synthesis. This chemistry has been used for various applications, including protein labeling, site-specific conjugation, and drug delivery. The reaction has also been used in the development of bioorthogonal imaging and compound sensing applications.

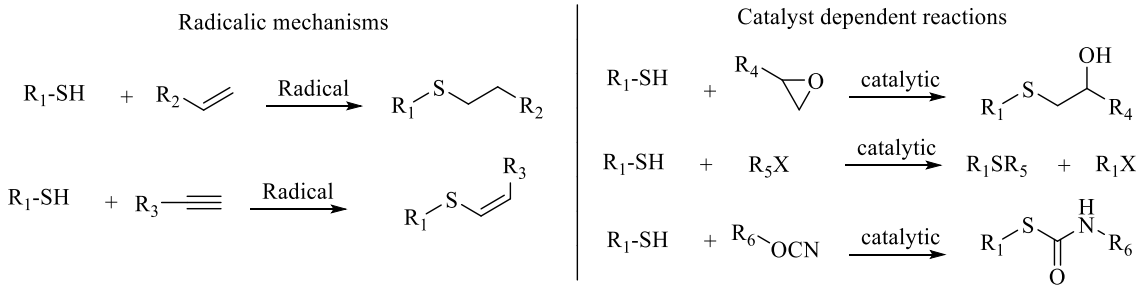

Scheme 1-5: Thiol-Michael addition and its different reaction mechanisms as overview.[128]

1.3.3.2.6 Photopolymerization

1.3.3.2.6.1 General information

Light-induced polymerization occurs significantly faster than chemical crosslinking which is mandatory to avoid layer crumbling during layer-based printing processes. The use of light in 3D bioprinting is well established.[129] Based on a broad range of photo-activated groups, several modifications respond upon a light stimulus to trigger a reaction. Radical polymerizations are widespread in bioprinting due to the stability of radicals in aqueous physiological conditions and their tolerance towards hydrophilic compounds. Also cycloadditions like Diels-Alder or 1,3-dipolar cycloadditions belong to light-induced crosslinking reactions.[130] Photo-activated click reactions are separated from the other introduced reactions above due to the high relevance for this thesis. Benefits of photopolymerization reactions are rapid and light-triggered mechanism which can happen at ambient temperature and under mild conditions. This allows the mixture of all formulation components including cells and subsequent molding thereof followed by the rapid curing upon light exposure which prevents cellular sedimentation. Photopolymerization can happen with two different polymerization mechanisms. One happens by a chain growth polymerization and the other one by a strep-growth polymerization process.[131] Both mechanisms are compared in the following chapter and advantages were highlighted.

1.3.3.2.6.2 Radical chain growth polymerization vs. Step-growth polymerization

Light-induced radical formation initiates the reaction of vinyl monomers which undergo propagation and ultimately termination.[132] Generally, the reactivity decreases starting from acrylate > acrylamide > vinyl ester ≈ vinyl carbonate > methacrylate > methacrylamide.[133] Most frequently used are methacryloyl monomers. Advantages are their relatively simple

execution, their robustness, the diverse array of commercially available monomers and the easy and comparably cheap synthesis using anhydrides.[130] Besides (meth)acrylates also (meth)acrylamides or vinyl esters are common. Material examples are polyethylene glycol diacrylate (PEGDA) or gelatin methacrylate (GelMA) as well as modified polysaccharides like methacrylated alginate or methacrylated hyaluronic acid. Regarding the synthesis with methacrylic anhydride (hazardous substance; GHS05 and GHS07) the formed side product methacrylic acid (toxic and acidic (GHS05 and GHS06) requires thorough purification to ensure material safety. Also, the often-applied high pH could potentially denature or hydrolyze the applied biopolymer and pH tolerance of the biopolymer should be evaluated beforehand. Also, several drawbacks regarding radical chain growth polymerization (rCGP) should be addressed. One is oxygen inhibition (side reaction; propagating radicals and O_2 form unreactive peroxides which interrupt the polymerization reaction).[134,135] Also, radical chain growth polymerizations are defined by diffusion-controlled reaction kinetics. The movement of radical sites within molecules is restricted due to the limited mobility of macroradical chain ends. This results in reaction termination only through propagation reactions, which leaves a significant amount of unreacted double bonds.[136] Both parameters (oxygen inhibition and reaction conversion) are critical for the viability of cells during photopolymerization.[130] Third, the reactivity of radical species is locally driven by diffusion which results in high microstructural heterogeneity which can lead to hydrogel shrinkage which could lead to deformation or mechanical failure.[137,138] Another downside is the creation of hydrogels with extensive crosslinking, which may result in volume shrinkage. This effect is bad for 3D printing where shape and volume-fidelity plays an important role.[139,140] Examples of the step-growth polymerization (SGP) mechanism are the thiol-ene chemistry, thiol-yne chemistry or the thiol-Michael addition, which was described in the previous chapter. Thiol-ene reactions describe the reaction of a thiol with an alkene. The mechanism can occur radical-mediated or base-catalyzed (Michael Addition). In case of the radical procedure, the radical initiator abstracts the thiol radical to form a thiyl radical. Next, an anti-Markovnikov addition to the alkene occurs to create a carbon centered radical which overtakes the radical from near thiol to form another thiyl radical to repeat the cycle. The reaction is faster with more sterically exposed alkenes. Especially with norbornenes, the reaction is very fast due to a ring strain relief effects.[126] In 2019, Van Hoorick *et al.* published a comparison of reaction rates: Norbornene > vinyl ether > propenyl > alkene ~ vinyl ester > *N*-vinyl amides > allyl ether > *N*-vinyl amides > acrylate > acrylonitrile ~ methacrylate > styrene > conjugated dienes.[126]

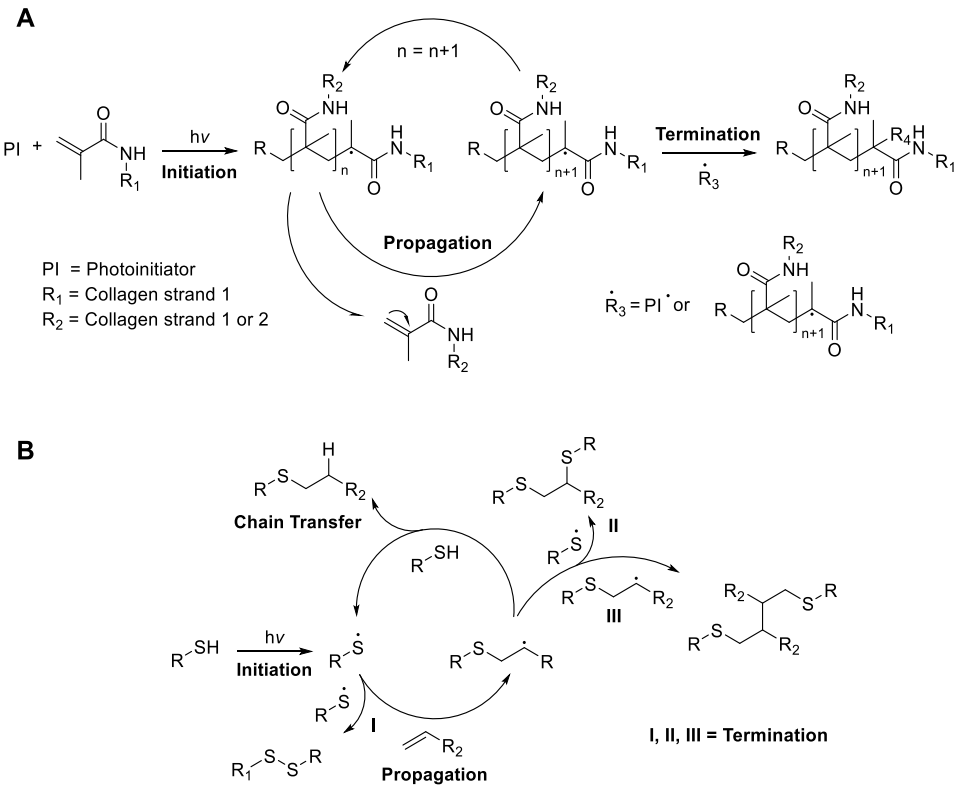

Scheme 1-6: (A) Scheme of photoinitiated rCGP based on methacrylated collagen. **(B)** Scheme of SGP based on thiol-ene click reaction using a terminal alkene. The scheme was taken from Hoorick *et al.* with minor modifications.[126]

1.3.3.2.6.3 Advantages of step growth polymerization

The step-growth reaction mechanism has many advantages compared to the rCGP. First, some alkenes (i.e. norbornenes and vinyl ethers) do not undergo competitive chain-growth homo-polymerization allowing supreme reaction control yielding in a higher conversion rate of functional groups and a homogenous network formation.[141,142] Second, the high reaction selectivity allows less shrinkage during crosslinking and less post polymerization. Third, and in comparison to rCGP, SGP is not prone to oxygen inhibition (rapid radical scavenging by oxygen molecules) as mentioned before which leads to less hydroxy peroxides and alcohol formation which can produce better cell viabilities after printing. Fourth, circumventing the oxygen inhibition consumes less starting material, photoinitiator (PI) and less light intensity. Also, the required irradiation times were lower than for radical chain-polymerizations. Especially higher PI concentrations and more light exposure make radical chain polymerization less attractive for direct cell encapsulation.[126,143] A potential drawback of thiol-ene reactions is the non-bioorthogonal nature of the reaction. Available cysteines on protein surfaces (~1.7%) could interfere within the reaction.[144] Also containing thiols can form disulfide bonds.[145] Nevertheless several cell types were successfully encapsulated using the thiol-ene

mechanism using human dermal fibroblasts[146], fibroblasts and chondrocytes[147], mesenchymal stem cells (MSC cells)[148], insulin secreting cells[149], or adipose tissue-derived stem cells (ASCs)[150].

1.3.3.2.6.4 The choice of photoinitiator

The selection of a good photoinitiator (PI) is critical. Requirements for biological applications are aqueous solubility, low cytotoxicity, high efficiency in radical generation by visible, low intensity light and an excellent monomer reactivity.[130,151] Also the absorption maximum, the response to different wavelengths, the minimal required PI concentration for hydrogel synthesis, the molar extinction coefficient, stability, the GHS classification, the requirement to add additional compounds like co-initiators, price and the toxicity of the PI before and after irradiation is important to consider.[151,152] PIs can be differentiated into single-photon initiators (1PIs) (Norrish Type I and Type II), two photon initiators (2PI) and initiators which undergo photofragmentation. An overview of the different options and the underlaying chemical activation is depicted in Figure 1-9.

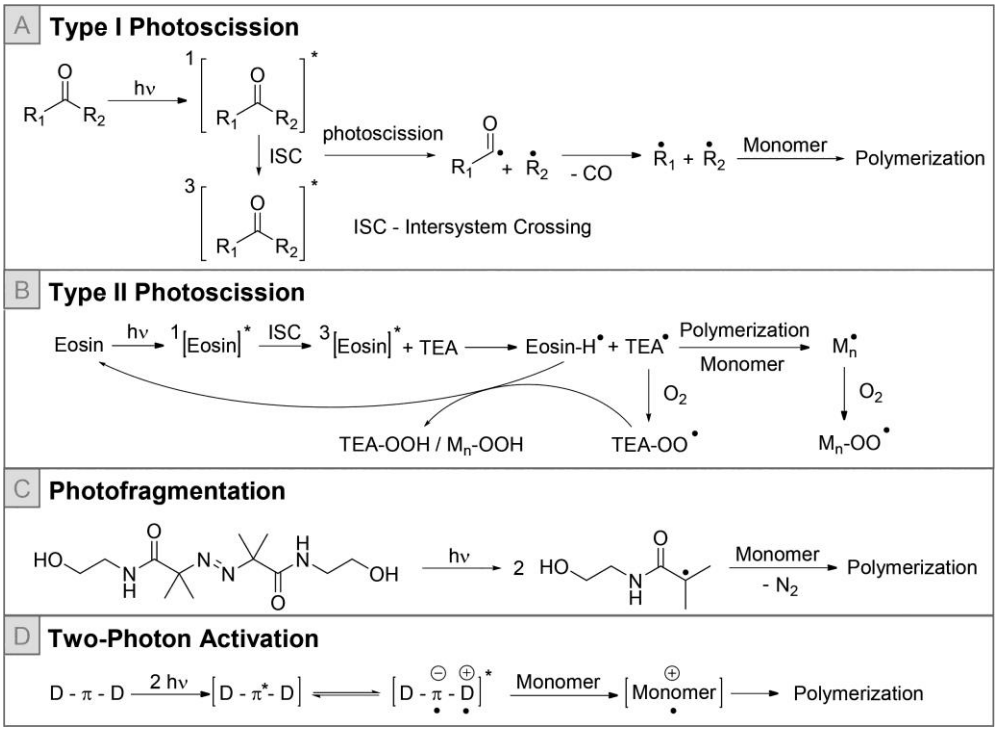

Figure 1-9: Different activation mechanisms of different PI types. Reprinted with permission from the American Chemical Society.[130] Copyright 2023

Table 1-6: PI comparison. The table was made based on Benedikt *et al.*[153], Elkhoury *et al.*[154] and Lee *et al.*[130].

PI	Chemical structure	Water solubility	Key strengths/ Key Drawbacks	λ_{max} (nm)	ε_{max} ($M^{-1}cm^{-1}$)	Ref
I2959 **($C_{12}H_{16}O_4$)** **CAS: 106797-53-9**	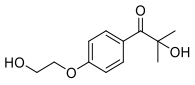	5 g/L	High initiation rate, low cytotoxicity and immunogenicity / Low initiation energy, UV light needed, low water solubility	**328** **365**	296 5	153 155
LAP **($C_{16}H_{16}LiO_3P$)** **CAS: 85073-19-4**	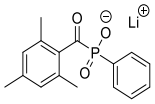	47 g/L	Good water solubility, UV and VIS light can be used / low initiation efficiency especially with VIS light	**365** **380** **405**	218 191 30	153 156
VA-086 **($C_{12}H_{24}N_4O_4$)** **CAS: 61551-69-7**	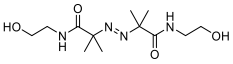	45 g/L	Low toxicity, good water solubility, high initiation rate / Releases N_2 which causes bubble formation	**375**	30	130
Ru(bpy)$_3$/SPS	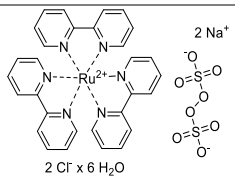	10 g/L	Good water solubility, enhanced penetration depth due to VIS light use, great cell viabilities / sensitivity to air and moisture which can lead to degradation and reduced efficiency.	**450**	14600	157
Eosin Y **CAS: 17372-87-1**	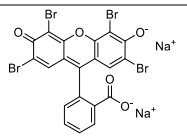	1 g/L	Low cytotoxicity, wide range of absorption in VIS range, works with low light powers / a co-initiator is needed	**515** **516**	69800 86500	158,159
Riboflavin **($C_{17}H_{20}N_4O_6$)** **CAS: 83-88-5**	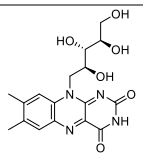	0.06-1.2 g/L	Wide absorption range also in VIS area, non-toxic, beneficial to cells / reactive oxygen species could be formed	**374** **449**	10300 12100	160,161

Single-photon initiators (1PIs) from the Norrish Type I undergo photoscission by homolytic bond cleavage causing direct decay into two primary radicals. They are commonly used due to their excellent biocompatibility and direct availability after irradiation. Examples are acetophenone and phosphine oxides. Some common 1PIs Type I are 1-[4-(2-hydroxyethoxy)-phenyl]-2-hydroxy-2-methyl-1-propane-1-one (short: Irgacure 2959 or I2959) and Lithium phenyl-2,4,6-trimethylbenzoylphosphinate (short: LAP). Single-photon initiators (1PIs) of the Norrish Type II undergo a biomolecular reaction where the excited triplet state of a PI transfers energy to a co-initiator (auxiliary molecule, hydrogen donor) to generate secondary radicals.[162] Examples are benzophenones, thioxanthones, Eosin Y and Riboflavin. Two-photon initiators (2PIs) are based on molecules with a π-conjugated system which absorbs two-photons at the same time which ensures a smaller laser focal volume leading to unprecedented spatiotemporal resolution (see Figure 1-14). During irradiation, two photons are absorbed

simultaneously which allow the use of low energy near-infrared (NIR) light which is less harmful than UV light and allows deep tissue penetration for polymerization under the skin.[163] Photofragmentation happens with selected molecules including azo compounds which result in photofragmentation of the weakest C-N bond by nitrogen molecule release thus forming alkyl radicals which initiate radical polymerization. One example is 2,2'-Azobis[2-methyl-N-(2hydroxyethyl)propionamide] (also known as VA-086).[130] Recently Ru^{II} complexes (metal-catalyzed radical polymerizations) like the water-soluble tris(2,2'-bipyridyl)-ruthenium(II) chloride hexahydrate $[Ru(II)(bpy)3]^{2+}$ reached growing interest due to their activation under visible light (400-450 nm). Together with sulfate anions like sodium persulfate, Ru^{III} species are formed as well as SO_4 radicals which initiate the polymerization.[157,164] A comparison of commonly used PIs is given in Table 1-6.

1.3.3.2.7 The limitations of physically gelated mammalian collagen hydrogels

Collagen products mainly comprise crosslinked structures to provide the needed 3D structure as observed from chapter 1.4.6, Table 1-7. In addition to the described disadvantages of mammalian collagens (see chapter 1.2.5), the properties of physically and chemically crosslinked collagens divergent making chemically crosslinked collagens denser and stronger networks at identical shear stress moduli.[165] The limited stiffness of physically crosslinked collagen hydrogels can be challenging for 3D printing as well as the susceptibility to changes of pH and temperature. By applying chemical crosslinking, researchers identified a reduced degradation rate and the avoidance of cell-mediated scaffold contraction for cartilage repair.[166] Furthermore, the thermally driven self-assembly is more difficult to control and could lead to different product properties. To allow chemical crosslinking on demand, researchers introduced chemical components such as methacrylates for photopolymerization.[167] In summary, mammalian collagens can normally be physically and chemically crosslinked. By using chemical crosslinking, the material is more stable and material properties are easier to adjust the respective application. Therefore, chemically crosslinked collagens are seen as more relevant for future developments regarding collagen products.

1.4 Biomedical applications of (collagen) hydrogels

The wide range of biomaterial applications includes disciplines such as chemistry, biology, medicine, tissue engineering and materials science. In biomedicine, biomaterials are widely used in implants (artificial hips, knees, teeth and heart valves, stents, vascular grafts, nerve conduits, breast implants), prosthetics (artificial replacements for limbs and other parts of the body, artificial ligaments and tendons, bone cement), medical devices (contact lenses, surgical sutures, clips and stables),drug delivery systems (used to deliver drugs in a

controlled manner), gene therapy (RNA transfection), tissue engineering (scaffolds, artificial organs, artificial skin) and biomolecule detection (diagnostic assays, health monitoring).[168] Hydrogels are used in a wide variety of fields, including agriculture, food industry and biomedical applications. Most research is done in the medical field, as scaffolds for tissue engineering, wound healing, wound dressings, smart hydrogels for drug delivery, antibiotic storage compartments or biosensors. Hydrogel applications can be divided into cell-free hydrogel scaffolds and cell-loaded scaffolds (see Figure 1-10).[85] Cell-free scaffolds are interesting for dermal, intraocular or cartilage filler, drug delivery, wound dressings and others (bioimaging, biosensing).[75] Cell-loaded hydrogel scaffolds are used for skin and liver regeneration, cancer vaccines, the therapy of diabetes, disease models, neo-vascularization and many more.[85] An overview of hydrogel applications was depicted in Figure 1-10.

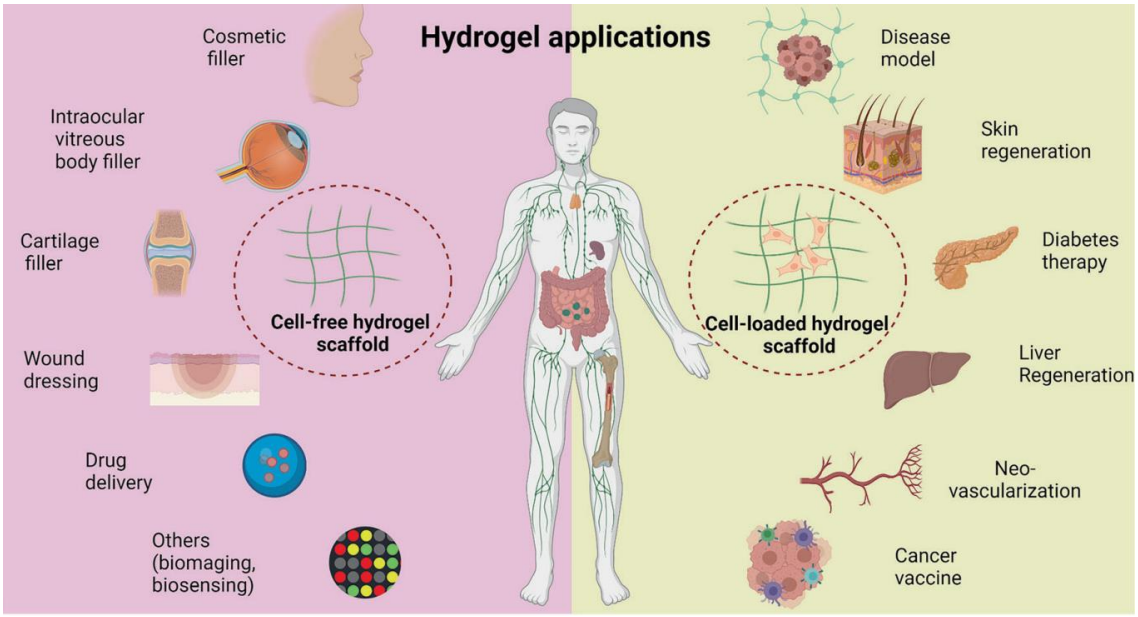

Figure 1-10: Hydrogel application overview. Reprinted with permission from a Cao *et al.*[85]

Different applications will be described further in the following with the focus on collagen as biomaterial. Collagen-based biomaterials are widely used for *in vitro* and *in vivo* applications like food, cosmetics, pharmaceuticals, artificial skin and glue.[169] A low immunological response, biodegradability, low antigenicity, an excellent biocompatibility and cell growth potential predetermine collagens for medical approaches.[170] By using genetic engineering, recombinant alternatives could provide multiple opportunities towards new and innovative material properties enabling a bright and exiting future. Currently, recombinant alternatives are being investigated for mainly medical applications including dermal fillers;[171] wound dressings;[172] microcarriers;[173] drug delivery applications;[98] bone void fillers[174] and for tissue engineering scaffolds.[175,176] Other applications are collagen shields for ophthalmology, dural

grafts, nerve tubes, ophthalmic shields, and lacrimal plugs.[177] According to a query of the National Medical Products Administration (NMPA) database by Liu *et al.*, more than 30 recombinant collagen products have already been approved for market entry in China, with a strong focus on skin wound treatment (more than 50%).[62] To manufacture a collagen product, formulations as powder, hydrogel or sponge are possible. Most of these applications are not produced from unprocessed collagen but require post-synthetic crosslinking into 3D water-insoluble hydrogel structures, which can be further processed into lyophilized sponges, fleeces and sheets. A comprehensive list of collagen applications has been published by Kumar *et al* in 2022[177] and some applications are described in more detail below.

1.4.1 Drug Delivery

As described above, hydrogels have an extraordinary affinity for water and can absorb large amounts of it. Thus, dried scaffolds thereof (sponges) can be swollen in a drug solution for subsequent release at the site of interest over time, reducing the frequency of dosing. Made from water-absorbing polymers, drugs can be encapsulated and released by absorbing fluids from the environment. Stimuli-responsive hydrogels can provide precise control of drug release, especially for drugs with short half-lives or rapid clearance. For example, pH-responsive hydrogels can release drugs in response to changes in acidity, which is useful for delivering drugs to specific regions of the body such as the stomach or intestine. In addition, hydrogels can be used for topical applications (especially ionic drugs, skin penetration by iontophoresis) and mucoadhesive hydrogels for targeted drug delivery. Li *et al.* analyzed different forms of hydrogels (macro-, micro- and nanogels) and their mesh size dependance on the release kinetics based on different release mechanisms. Based on the burst release within 24 h and the half-life of different hydrogel delivery systems, the release was categorized by different release mechanisms. By blotting the data, huge differences were seen showing burst release and fast drug release for diffusion-controlled mechanisms and low burst release and retained drug release for degradation-controlled mechanism (see Figure 1-11).[82] The use of conventional drugs and their high concentrations can cause severe side effects, creating the need for drug delivery systems (DDS) to deliver the drug to its target site of action.[178] DDS made of polymers, nanoparticles, and lipids are known for attaching or encapsulating drugs for long-term sustained release.[179] Hydrogels can be used to e.g. deliver naproxen for antimicrobial properties[180] or NGF-ß for corneal regeneration.[181] Injectable hydrogels were tested for the release of cisplatin for tumor treatment[182] or to deliver growth factors to support wound healing.[183]

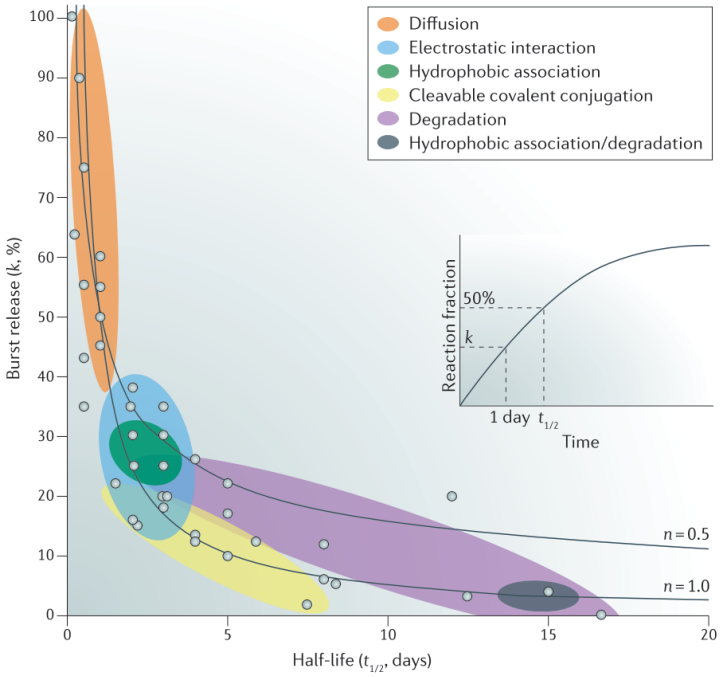

Figure 1-11: Drug release property chart of hydrogels. The figure was taken from Li *et al.* and reproduced with permission from Springer Nature.[82]

Collagens are an attractive option due to their tunable pore size for drug loading, efficient fibrillar network, susceptibility to enzymatic degradation, in vivo stability, biocompatibility, low antigenicity, minimal toxicity, and high safety standards.[184] High abundances of carboxyl, hydroxyl, and primary amines allow for a wide range of material crosslinking strategies. Some applications comprise the delivery of tetracycline[185], growth factors[186] or doxorubicin for cancer treatment.[187] Collagen can be processed as a sponge, (composite) film, as nano- or microgel, as mesh and many more. Collagen microparticles are used for e.g. the delivery of glucocorticosteroids.[188] A table with a variety of applications has been published by Amit Kumar Verma in 2022.[177] Collagens can also be used as a hydrogel formulation for sustained release of liposomes loaded with, e.g. RNA.[189] or for drug delivery in transdermal patches.[190] Collagen delivery systems with controlled release can be achieved by adjusting the configuration of the collagen matrix or by attaching other proteins, such as fibroin.[191] Collagen has garnered significant attention due to its customizable pore size for drug encapsulation, efficient network of fibrils, susceptibility to enzymatic breakdown, in vivo durability, biocompatibility, low antigenicity and minimal toxicity.[184]

1.4.2 Tissue repair and engineering

Hydrogels can be used as "close-to-*in vivo*" structures to support the regeneration of skin, cartilage, bone, nerve, heart, liver, cornea, vascular, dental, muscle, trachea, bladder, tendon and ligament, pancreatic and other tissues. These results can be achieved by incorporating relevant cells and additional compounds, including growth factors and antimicrobial agents. Relevant areas include cancer research, cell therapy, tissue engineering, drug discovery and personalized medicine.[192]Collagen, a major component of various tissues in the body, has an important function in wound healing and tissue regeneration. It can be used in various forms such as dressings, particles and scaffolds to promote wound closure by moisturizing, absorbing wound fluid, inducing biological responses and facilitating collagen degradation by cells such as keratinocytes and fibroblasts. Collagen-based products can be combined with growth factors and antibacterial agents to enhance wound healing.[193] In addition, collagen has been used extensively in orthopedics and sport medicine for bone repair (trauma or disease) where it promotes cell attachment, proliferation, and growth of new bone tissue. Collagen can be incorporated into scaffolds with other biomaterials to improve their mechanical properties and regenerative potential, including bioceramics such as beta-tricalcium phosphate and hydroxyapatite, bioactive glass, and other osteoconductive substances.[194] In cartilage repair, collagen scaffolds are used to mimic native tissue and facilitate hyaline cartilage regeneration, for example, by adjusting pore structure and degradation rates. Collagen is also used in tendon and ligament repair.[195,196] In addition, collagen has been used in studies focused on muscle tissue regeneration, myocardial regeneration, cardiac stem cell therapy, nerve regeneration, corneal regeneration, and vascular research. Injectable collagen hydrogels have shown promise in vascular network formation. Overall, collagen-based materials offer a wide variety of opportunities for regenerative medicine and tissue engineering.[197] As the main structural protein in the ECM of hard and semihard tissue, the development of applications for cartilage or bone tissue engineering was obvious. However, due to the high material strength of bone, combination products are required, like by including nanosized hydroxyapatite (nHA).[198]

1.4.3 Medical devices

Collagens have been investigated for clinical translation in many medical applications. As a component of medical devices, collagens are interesting for wound dressings products or bone void fillers.[62] Applied as dressing or gel with or without antimicrobial agents or growth factors, hydrogels can provide a moist environment to promote healing, absorb wound fluid, reduce infection risks, preventing scar formation and help to debride necrotic and fibrotic

tissue. Hydrogel dressings come in various forms and are particularly useful for wounds that are difficult to bandage. They reduce pain and can be left in place for several days to reduce the frequency of dressing changes & thus promote faster healing.[199] Hydrogel coatings are thin layers of hydrogel material applied to products to enhance their properties or functionality. These coatings improve surface properties such as wettability, adhesion and lubricity, they modify drug release, prevent biofouling, and enhance biocompatibility. Hydrogel coatings are used in medical devices, contact lenses, textiles, and electronic devices. They can also be responsive to specific stimuli, such as changes in pH or temperature, and can be engineered to be biodegradable or degrade over time to minimize environmental impact. Further research is needed to optimize their properties and ensure safety and efficacy in various applications.[200] Collagens' bioactivity plays an important role in physiology and cellular responses from cells especially from connective tissue and can be used as a hydrogel to promote cell adhesion, migration, proliferation and differentiation of relevant cells to promote wound healing.[201] Another type of cell interaction happens with blood platelets which induces hemostasis. Platelets adhere to collagens, aggregate and activate blood clotting. The strength of this interaction is dependent on both the extent of crosslinking in collagen hydrogels and the presence of positively charged groups on their side chains. Blocking carboxylic side chains due to crosslinking eliminates over 98% of the hemostatic activity. Also, the change in conformation strongly influences platelet aggregation. Platelet activation is induced by non-denatured, fibrillar collagen, whereas denatured collagen (gelatin) does not activate platelet aggregation.[198]

1.4.4 Plastic and reconstructive surgery and Cosmetics

The plastic surgery and cosmetic industries have experienced significant growth in recent years, driven by various factors such as the desire to maintain a youthful and attractive appearance. Hydrogels are relevant product formulations due to their high biocompatibility, high water content and low cost. Hydrogel-based beauty masks are claimed to hydrate the skin, restore elasticity, and slow down the aging process.[202] In cosmetics, collagen plays a role due to their ability to metabolize and replace external collagen with body-own versions over a period of months, making them ideal for subcutaneous injection as soft tissue fillers to reduce wrinkles by lifting the skin.[203,204] Subcutaneous injections are also used to treat nasolabial folds and to promote acne scar healing.[70,202] In surgery, collagen containing devices can be used for suture reinforcement, hernia repair, and in the manufacture of acellular dermal substitutes made from decellularized extracellular matrices or collagen scaffolds combined with cells such as keratinocytes and fibroblasts to replace skin defects. They are also used for breast reconstruction.[205,206]

1.4.5 Dental applications

Collagen scaffolds can be used in regenerative dentistry, especially for periodontal (teeth surrounding) tissues. In particular, collagen plugs/sponges as hemostatic, resorbable wound dressings to accelerate healing and collagen barrier membranes to protect epithelial migration and the ingrowth of pluripotent stem cells are highly important. In addition, bone grafts and combination with bioactive compounds are under investigation.[207] In 2022, Binlateh *et al.* published a list of studies on dental collagen applications. They comprise e.g. the use of collagen hydrogel scaffolds combined with the bone morphogenetic protein 2 (BMP2), showing improved reconstruction of periodontal attachment and increased amount of periodontal ligament compared to BMP2 alone in beagle dogs.[208] Another example used collagen sponge scaffolds with injected dental pulp stem cells (DPSCs) to demonstrate an optimal support for bone repair in humans[209] or collagen-based barrier membranes to treat bone defects without showing adverse effects.[210] Using mineralized collagen bone grafts, stimulation of new bone formation around the dental implant was observed in minipigs with excellent clinical performance.[211] In terms of hemostasis and wound healing, collagen plugs have been successfully tested for accelerated soft tissue healing, reduction of postoperative pain, and increased cell proliferation.[212,213] These findings suggest that collagen scaffolds have promising applications in dental medicine and may provide an effective approach to promoting tissue regeneration and restoring dental health.

1.4.6 Biosensors

A relatively new approach is the use of collagen as a biosensor. Biosensors are analytical devices that measure a change in a biological process by converting it into a detectable signal.[214,215] They are classified by the biological component used (enzymes, antibodies, nucleic acids, cells, etc.) or by the type of signal transducer (electrochemical, optical, mass-based or piezoelectric).[216] The applied biomaterial like collagen forms hereby the hydrogel matrix for the biological component and the signal transducer. Hydrogel-based biosensors offer advantages over other types of biosensors, including high biocompatibility, enhanced sensitivity, high flexibility and conformability, good stability and long shelf life, real-time monitoring, low cost, and ease of fabrication and use. They can be used for medical diagnostics, food safety testing and environmental monitoring, and can be integrated with other technologies to create more sophisticated sensing systems.[217,218] Some hydrogel-based applications include glucose sensing for monitoring blood glucose levels in diabetic patients (glucose oxidase immobilized in an electroconductive collagen matrix).[219-221] Another application is the detection of ethanol or lactate (collagen membranes loaded with alcohol dehydrogenase or lactate

dehydrogenase).[222] Similarly, cholesterol biosensors based on hydrogels have also been developed to monitor cholesterol levels, which is important for the management of cardiovascular diseases.[223] Hydrogel biosensors have also been used in environmental monitoring, such as the detection of heavy metals, pesticides, and pathogens in water.[224] Another hydrogel biosensor based on aptamer-functionalized hydrogels was developed for detecting thrombin in human serum.[225] Biosensors can be used as well for antifouling electrode interfaces[226] or for high-performance tyrosinase-sensing transistor-based biosensors to detect tyrosinases.[227] Hydrogel-based biosensors can also be used for cancer detection. An example was published by Wang *et al.* who conjugated anti-HER2 antibodies to the hydrogel for selective sensing of HER2, a breast cancer biomarker.[228] A comprehensive overview of identified products is given in Table 1-7 based on extensive market research. While a few applications are in powder form, primarily for supplements, the primary applications for the biomedical field are based on hydrogels and hydrogel-derived sponges. Sponges are primarily used for medical devices and surgery, where their porosity and 3D structure facilitate cell infiltration and tissue ingrowth, and allow for high water uptake ratios, which can help maintain a moist environment for tissue regeneration.[229,230] Although collagen sponges are the most prevalent product in the market, there is a need for a better understanding of hydrogels, which offer more research potential than sponges due to their complexity and compatibility with additive manufacturing methods such as 3D bioprinting. Collagen hydrogels can mimic the extracellular matrix due to their high water content and are more likely used for soft tissue engineering, such as skin, nerve, or muscle regeneration, as well as in the fields of cosmetics and wound care. They have the advantage of being able to be injected or molded into various shapes, which can be useful for minimally invasive procedures.[17,231,232]

Table 1-7: Examples of some collagen-based products on the market. This list is not exhaustive, and the products have not been specifically selected, but are merely the result of a broad web search.

Application field	Category	Example products	Manufacturer
Supplements	Powder	CollaGEN	Ortho Molecular Products
	Powder	Collagen peptides	Fitmart GmbH & Co. KG
Orthopedics	Sponge	Orthoss® Collagen	Geistlich Biomaterials
	Sponge	Parasorb Resodont®	Resorba Medical GmbH
Dental applications	Sponge	Collacone® or Collafleece®	botiss biomaterials GmbH
	Fleece	Parasorb® Fleece w/ gentamycin	Resorba Medical GmbH
wound care / wound dressing	Hydrogel	Stimulen®	Southwest Technologies Inc.
	Hydrogel	Collasate® w/ or w/o silver oxide	PRN Pharmacal
	Hydrogel	Woun'Dres®	Coloplast Corp.
	Sponge	Simpurity collagen dressing	Safe n Simple
	Sponge	Hemopatch	Baxter International Inc.
	Powder/sponge/gel	DermaCol™ w/ and w/o silver	DermaRite Industries, LLC.
	Sponge	Puracol® Collagen wound dressing	Medline Industries, Inc.
	Sponge	Suprasorb® C	Lohmann & Rauscher
	Sponge	KOLLAGEN resorb™	Resorba Medical GmbH
	Sponge	Fibracol® Plus	Johnson&Johnson
	Collagen particles	Medifil® II Collagen Particles	Human BioSciences, Inc.
Cardio-vascular	Sponge	Omniflow™ II Vascular Prosthesis	LeMaitre Vascular, Inc.
	Sponge	Artegraft® Collagen Vascular Graft	LeMaitre Vascular, Inc.
Surgery	Sponge	Avitene™, Avitene™ Ultrafoam™	BD (Becton, Dickinson and Company)
	Sponge	Hemocollagene	Septodont
	Sponge	Colo Plug	Cologenesis Healthcare Pvt Ltd.
	Sponge	Integra® Helistat® and Helitene®	Integra LifeSciences Corporation
	Sponge	Lyostypt®	B. Braun Conpany
	Sponge	PROMOGRAN®	Systagenix Wound Management Ltd
Cosmetics	Film	High Prime Collagen Film	Dermarssance
	Injectable hydrogel	Bellafill®	Suneva Medical, Inc.
	Injectable hydrogel	Cosmoderm™ and Cosmoplast™	Allergan, Inc.
Tissue engineering	Hydrogel	CollaGel Hydrogel R	Neuromics
	Liquid	PureCol® EZ Gel	Advanced BioMatrix (A BICO company)
	Sponge	SpongeCol®	Advanced BioMatrix (A BICO company)
	Liquid / Bioink	Fibercoll-Flex-A®	Viscofan BioEngineering
	Powder/Liquid/Sponge	AteloCell®	KOKEN CO., LTD.
Ophthalmol-ogy	Film	ABCcolla®	ACRO Biomedical Co., Ltd.
	Sponge	ologen™ Collagen Matrix	Aeon Astron Europe B.V.
	Liquid	ColloRx® Collagen Eye Drops	AlfaMedic Ltd.
Drug Delivery	Sponge	Collatamp® G w/ gentamicin	Syntacoll GmbH
	Sponge	Sulmycin® Implant E	Syntacoll GmbH

1.5 Additive manufacturing

1.5.1 Status Quo and future trends of additive manufacturing

Additive manufacturing (AM, also known as layer manufacturing process, rapid prototyping or 3D printing (short: 3DP)) was defined in 2012 by the American Society for Testing and Materials (ASTM) in the document F2792-12a as the process of joining materials to create objects from 3D model data, typically layer by layer, as opposed to subtractive manufacturing methods.[233] This process can be used to create complex shapes and designs with a high degree of accuracy and precision. Additive manufacturing is used to create customized prototypes, tools, end-use products, and many other items in a resource-efficient manner.[234] In 2014, a global sustainability perspective calculated a total cost reduction of US$170-593 billion due to 3D printed alternatives, as well as a reductions in CO_2 (130.5-525.5 Mt) and energy (2.5-9.3 EJ) by 2025.[235] AM includes technologies such as material jetting, vat photopolymerization, material extrusion, binder jetting, powder bed fusion, sheet lamination, and more. Due to the wide variety of printing technologies, they can also be separated by their material origin. An associated list is shown in Table 1-8.

Table 1-8: Selection of standard printing technologies based on their starting material appearance.

powder-based:	Selective Laser Sintering (SLS), Direct Metal Laser Sintering (DMLS), Selective Laser Melting (SLM) or Electron Beam (Additive) Melting (EB(A)M)
molten material-based:	Fused Filament Fabrication (FFF), which is also called Fuse Deposition Modeling (FDM)
liquid material-based:	Stereolithography (SLA or SL), Digital Light Processing (DLP), Multi Jet Modelling (MJM) or PolyJet Printing, Material Jetting (MJ) or Drop-on-Demand (DoD), Film Transfer Imaging (FTI)
others:	(Laser Metal Deposition (LMD) or Laminated Object Modeling (LOM)

1.5.1.1 Advantages and Disadvantages of AM

Additive manufacturing is not designed to replace traditional manufacturing methods, but it does expand the range of manufacturing choices. There are three major benefits that can be broken down into several aspects. These benefits are time and cost savings and increased manufacturing flexibility. AM can produce complex shapes with fewer materials and less labor.[236] In addition, the increased production speed is of great importance. Having manufacturing systems on-site reduces CO_2 emissions for transportation, eliminates waiting time for delivery of spare parts or their replacement, which reduces costs and ensures lower capacity

utilization, reduces the need for inventory management, and increases flexibility in material design.[237] In addition, AM can use leftover materials to build new parts, which can reduce material waste by 40% compared to traditional methods, and 95%-98% of leftover materials can be recycled.[238] The flexibility to create complex designs, including easy access to changes in material composition and design, is another advantage for creating, for example, devices with more strength in one part and more ductility in another.[239] This rapid change in prototypes and their easy functionalization can allow for rapid alignment with customers according to their needs. Additive manufacturing can produce complex shapes and designs that would be impossible with traditional methods (versatility), allowing items to be customized to individual specifications. Furthermore, AM is much faster than traditional methods and can be used to create items on demand with minimal waste by using only the materials that are actually needed for the product.[236] Despite the benefits, there are several challenges, obstacles and limitations to consider. These include imperfections, cost, production time, material limitations, and size limitations. Imperfections include surface quality and roughness, which are most prevalent in layer-based methods, and the removal of support structures after printing.[240] Cost issues arise from the partially high prices of AM systems, the materials used, and mass production (too time-consuming compared to traditional methods).[241,242] Although many materials are suitable for AM, a few materials, such as magnesium or biodegradable polymers, remain challenging and require further research.[236] Finally, the printing time, the size limitations of the printing machines, and the required energy consumption make AM challenging for major objections compared to traditional methods.[243] In summary, much research is needed to tinker with these limitations, and it is unlikely that AM will displace traditional manufacturing methods from the market. More likely, they will be used in combination to produce complex products.[236]

1.5.1.2 The AM market forecast

A recent global market report analyzes AM market size, shares, and trends by component, printer type, technology, software, application, material, and other criteria, and estimates the global AM market size at US$13.84 billion (in 2021) and is anticipated to grow (CAGR of 20.8%) from 2022-2030, resulting in a revenue forecast of US$76.16 billion in 2030. 2.2 million printer units will be shipped worldwide in 2021 and the number is expected to reach 21.5 million in 2030. The reason for this increase is the growing demand for prototyping, including industries such as healthcare, automotive, aerospace and defense. The key companies mentioned are Stratasys, Ltd; Materialise NV; EnvisionTec, Inc; Autodesk Inc. and others.[244] One year later, the 3D printing market share, size, trends by component (hardware, software, services), by e.g. printer type, technology software and other aspects were again evaluated,

which estimated the global 3D printing market size at US$16.75 billion (in 2022) with a CAGR of 23.3% from 2023-2030, leading to a revenue forecast of US$88.28 billion in 2030. This strong growth is again driven by the increasing demand for prototyping across multiple industries. Unlike the previous report, this one evaluates and compares different technologies and analyzes their growth. Stereolithography dominated the market in 2022 with a revenue share of more than 10%.[245] The data from both market reports show a growing market with an average CAGR of ~22% and an increased expected market revenue within the newer market report.

1.5.1.3 Bioprinting

Bioprinting is a subsegment of AM. Its market size was valued at US$2 billion in 2022 and is expected to grow at a CAGR of 12.5% from 2023 to 2030 to reach revenues of US$5.3 billion in 2030. This market growth is driven by the limited number of organ donors and an increasingly aging population with chronic respiratory diseases. Increasing investments in bioprinting and rapid technological advancements forecast a growing market in the coming years. The inkjet-based segment accounted for the largest revenue share in 2022 (36%), and magnetic levitation is projected to grow at the fastest CAGR of 13.7%, as it is expected to solve more than 80% of 3D bioprinting errors due to advanced features, improved speed, and precision. The medical segment accounts for the largest market share in 2022 (37.6%), with an expected CAGR of ~15% through 2030. This is followed by food and animal products with ~25%, bioinks with ~15%, dental applications, biosensors, and consumer/personal product testing. For bioprinting, Asia Pacific accounted for a revenue share of 26% in 2022 and is expected to continue its dominance over the forecast period, mainly due to Japan and China. North America accounted for a revenue share of 30.9% in 2022 and is expected to lead the market throughout the forecast period. Key players are focusing on R&D to develop technologically advanced applications to gain a competitive edge. Some of the key players are Cellink Global; EnvisionTEC, Inc.; Organovo Holdings, Inc.; Allevi by 3D Systems; Regemat 3D S.L.; Inventia Life Science Pty Ltd. and 3D Bioprinting Solutions. Other university-based companies include Formlabs (from the Massachusetts Institute of Technology); Fluicell (Chalmers University of Technology in Sweden); Poietis (Inserm and the University of Bordeaux); and the Wyss Institute at Harvard University.[246]

1.5.1.4 3D Bioprinting and 3D cell culture

A recent study (September 2022) compared the global market for laboratory animal models, 3D cultures, and organoids, and examined future trends over the next 5 years. The study was

driven by the shift from classical animal models to 3D cell culture-based alternatives. Animal studies are an essential part of drug development and safety testing to explore *in vitro* results in a more complex tissue environment, leading to better predictions of human physiology prior to clinical trials. The use of animals in research is guided by the 3Rs initiative (Replacement, Reduction and Refinement) to reduce the number of tests and ensure comparable data by using inbred strains for highly specific models (genetic homogeneity). The most commonly used animals are mice and rats, as their small size offers an ideal combination of genetic proximity to humans, breeding costs and colony maintenance. Driven by factors such as ethical concerns, the desire to personalize healthcare, the need for faster and cheaper screening, and the ability to enable real-time observation.

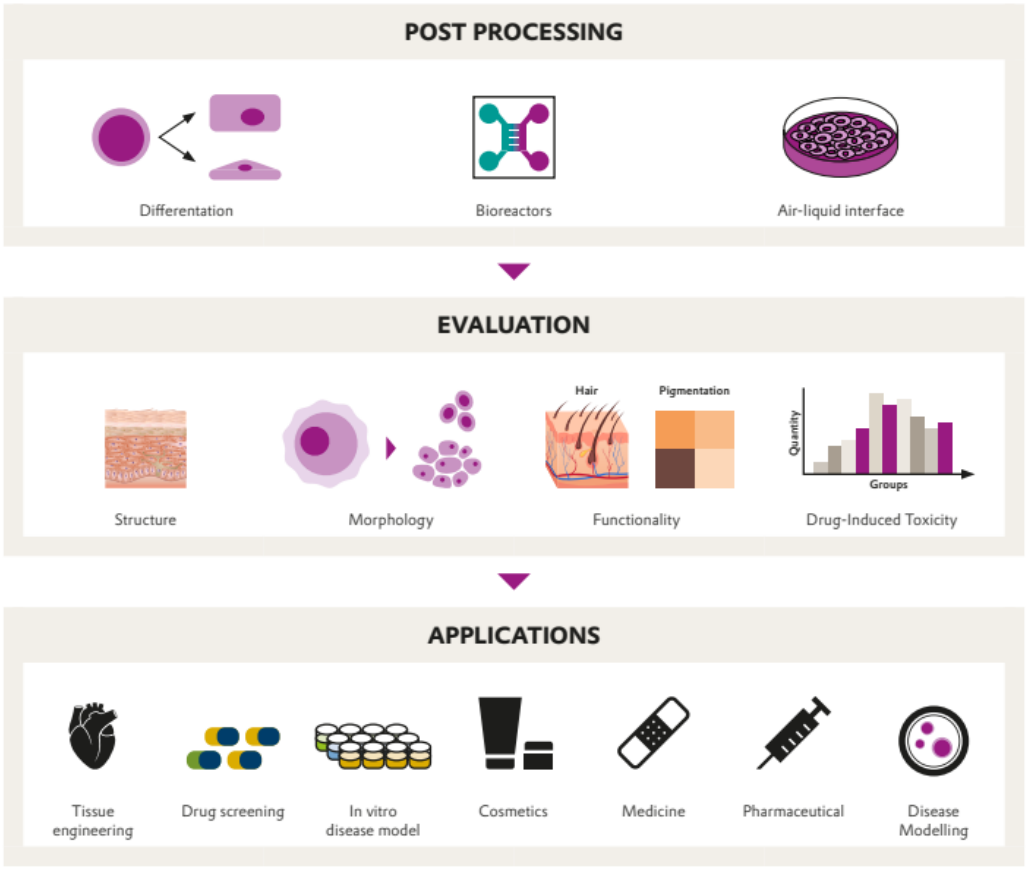

Figure 1-12: Post-printing maturation of bioprinted structures with some test model examples for evaluation followed by application developments using these established models.

3D cell culture alternatives are paving the way. In addition, simplicity of design, scalability, and high relevance to human physiology are contributing to growth. This is particularly relevant in areas where the use of animals becomes too costly or problematic for study design. 3D cell culture-derived organoids can mimic organic function and are gaining acceptance.

Extracted from Figure 1 of the market report reference is the timeline for possible availability of 3D-printed organs and tissues for humans between 2020 and 2026 (timeframe of PhD thesis plus a few additional years), which comprises corneas, vasculature, cartilage tissues, bone tissues, skin, cancer models and adipose tissue. The figure forecasts applications until 2045 with the heart as last position between 2034 and 2045.[247] In Figure 1-12, different applications of 3D bioprinted test systems are depicted with their maturation phase and the evaluation of printed models.

1.5.2 Bioprinting Methods

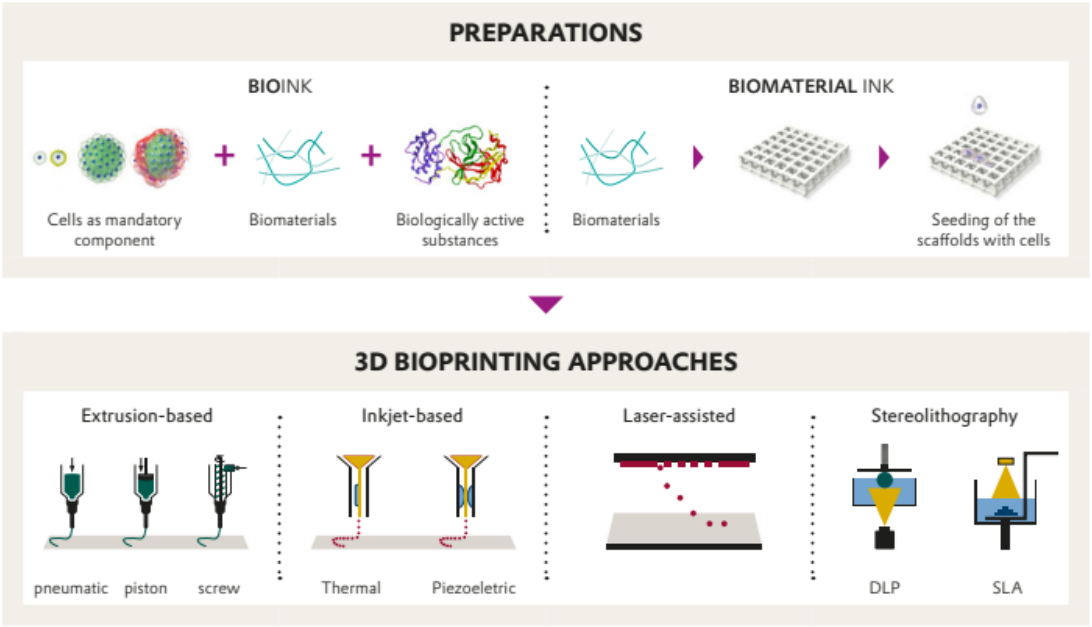

Figure 1-13: Visualization of the difference of bioink and biomaterial inks and the most used technologies for 3D bioprinting.

To craft scaffolds with cells, two approaches need to be separated (bioink printing and biomaterial printing). While bioinks are capable to include cells and bioactive components like growth factors for biofabrication, biomaterial inks are used to create biocompatible 3D structures that can support the growth of cells but do not contain them during the printing process.[248,249] As described earlier, several additive manufacturing methods are known (see chapter 1.5.1, Table 1-8).[250] Only some are useful for 3D bioprinting. The most common technologies are depicted in Figure 1-13 and compared in more detail in Table 1-9.

Table 1-9: Technology comparison for bioprinting based on previous literature.[251-253]

	Bioprinting technology			
Criterium	**Inkjet printing**	**(Micro)extrusion**	**Laser-assisted**	**SLA**
Viscosity	3.5-12 mPa*s[254]	30 to >6×10^7 mPa*s[255]	1-300 mPa*s[256]	5-200 mPa*s
Cell density	Low, <5x10^6 cells/ml	High	Medium, 10^8 cells/ml[256]	Medium
Cell viability[251]	80-95%[257]	40-92%[258,259]	>95%	>85%
Resolution	50 µm[260]	100 µm - mm[261]	10-100 µm	10 µm
Print speed[251,262]	Fast (<1 to >300 pl; 1-10000 drops/s)[263]	Slow (100 µm/s)	Medium (2-1600 mm/s)	Fast
Nozzle size	20-150 µm[254]	20 µm - mm	Nozzle-less	Nozzle-less
Working principle	Non-contact	Contact	Non-contact	Contact
Mechanical integrity	Low	High	Low	/
Vertical structure[251]	Poor	Good	Medium	Good
Cost[251]	Low	Medium	High	Low
Main limitation[253,264]	Only low viscous solutions, weak mechanical integrity, low cell densities	Only viscous liquids, bad cell viability when high extrusion pressure	Metallic residues, costly, time-consuming preparations, thermal damage	Difficult with multiple inks, UV light can damage cells; limited to photo curable inks
Main advantage[253,264,252]	Allows cell gradients, electronic control over drop size and ejection rate, fast, low cost, high resolution	Simple, high cell densities works for vascular tissue constructs	Nozzle-free, high resolution, high resolution, broad viscosity range.	Nozzle-free, high resolution, high cell viability, fast printing time-independent of complexity

1.5.2.1 Extrusion-based bioprinting

Extrusion-based bioprinting is a type of additive manufacturing where a highly viscous material formulation is deposited through a nozzle in a pre-programmed pattern. The technology has a comparably bad resolution but allows a high material throughput and the printing of high cell numbers to create a wide range of tissue types. The most common technologies are pneumatic, piston-based or screw-based methods. An overview of the three most common technologies is given in Figure 1-13. Microextrusion printing (µEP) relies on smaller nozzle diameters which allow higher precision, and which are limited to a slower printing speed mostly used for non-biological applications but can be used for bioinks as well. The technology needs slightly viscous bioinks, creates tissues with high cell densities and can be used to print

vascular structures. On the downside, relatively high shear forces affect cell viability negatively and increasement of print speed is therefore limited. Furthermore, the resolution is bad compared to light triggered technologies.[253,255,265] Liquid Support Bath–Assisted 3D Bioprinting is a relatively new material extrusion printing technology. This technology is based on a liquid, low viscous ink which is displaced into a liquid support bath by smooth nozzle movement while trapping the extruded material for further crosslinking *in situ*.[266] This kind of printing is relevant for soft hydrogels which are generally not self-supporting enough to use direct in-air printing without viscosity enhancers. This technology is interesting because adding extensive viscosity modifiers can lead to unwanted material properties.[267,268] Liquid Support Bath–Assisted 3D Bioprinting can be further divided into two subcategories: embedded 3D printing and support bath-enabled 3D printing. Embedded 3D printing is mainly used to print functional patterns or hollow channels in a bulk structure while support bath-enabled 3D printed is s a promising method to print complex freeform structures.[269-271]

1.5.2.2 Droplet-based Bioprinting (DBB)

Droplet-based bioprinting (or inkjet printing) offers great advantages due to simplicity and precise control of deposition including cells, proteins, genes, drugs and other substances and thus is used in many different scientific fields. The deposit of droplets depends on different technologies which are outlined in the following.[272] The mechanism is based on single droplet placing down to the nanoliter to picoliter range on an acceptor substrate. The technology has a higher resolution than extrusion printing and cell gradients can be printed and growth factors or other proteins can be incorporated. Drop size and ejection rate can be adjusted allowing variable control over the print construct. This technology is comparably cheap and allows rapid printing speed. Disadvantages are the need for low bioink viscosities (especially for picolitre droplets, very low viscosities are needed) and the weak mechanical integrity of printed constructs. Additionally recent clogging can interrupt the printing process.[253] Inkjet printing can be subdivided into three different subcategories: Continuous-inkjet jetting (CIJ), Drop-on-demand inkjet bioprinting (DoD) and Electrohydrodynamic jetting (EHD). For CIJ, the printer head continuously ejects ink through a nozzle by pressure to form a droplet stream. DoD is preferred over CIJ for tissue printing because of the selected droplet positioning when needed by pressure pulses formed by a voltage signal through a thermal, piezoelectric or electrostatic actuator. In the case of thermal inkjet jetting (TIJ) the pressure is generated by an expanding printing liquid by heating[273,274]; piezoelectric inkjet jetting (PIJ) is based on volumetric change of the fluid chamber[273,275] and electrostatic inkjet jetting (EIJ) generates pressure by electrostatic force.[276] While most DoD technologies are based on droplet ejections by an applied pressure through a nozzle, acoustic bioprinting employs a gentle

acoustic field to eject droplets from a reservoir.[277] This nozzle-free technology allows high cell concentrations or even cell spheroid deposition without the risk of clogging. Cell viability of >94% can be achieved, which is higher than current inkjet-based methods (>85%) or extrusion-based methods (40-80%). The device itself is said to be small and flexible with respect to different types of bioinks. Even low-viscosity solutions can be printed with high resolution by gaining a better understanding of the positioning, fluidity, and 3D morphology of individual droplets. In a recent publication (2021), the authors printed a small tumor model to demonstrate a functionality.[278]

1.5.2.3 Vat-polymerization

Vat polymerization (VP) describes the structure printing from a vat of photo-sensitive resin through controlled light exposure.[130] Depending on the type of light, different technologies are formed. Starting with stereolithography (SL, also known as SLA, optical fabrication, photo-solidification, or resin printing) in 1987 as a method to form solid structures from a layer-by-layer printing procedure by a laser beam[279], advanced light exposure techniques emerged such as digital light processing (DLP) and two-photon stereolithography. SL allows precise resin curing and is typically used to create prototypes and final products with a high degree of accuracy and detail. Digital Light Processing (DLP) uses a digital light projector instead of a laser light source. DLP is typically faster than SL, but SL produces resolutions with sharper details and smoother surfaces.[280,281] Two different projection configurations are known. In the bottom-up configuration, the printing stage moves up and photo crosslinking occurs at the bottom of the reservoir. In the top-down configuration, the stage moves down while photopolymerization occurs at the air-liquid interface. Single-photon SL is based on single photons with high energy which requires high-energy light sources such as UV lamps and limits the resolution of the printed structures to ~100 µm. A relatively new technology called continuous liquid interface production (CLIP) where radical-induced crosslinking is inhibited in a “dead zone” created by oxygen where photoexcited photoinitiators or free radicals get quenched and thus avoiding polymerization.[282] Also other types of inhibitors can be used. This method allows for continuous elevation of the printing platform without the need for multistep procedures which increases the printing speed significantly.[130]

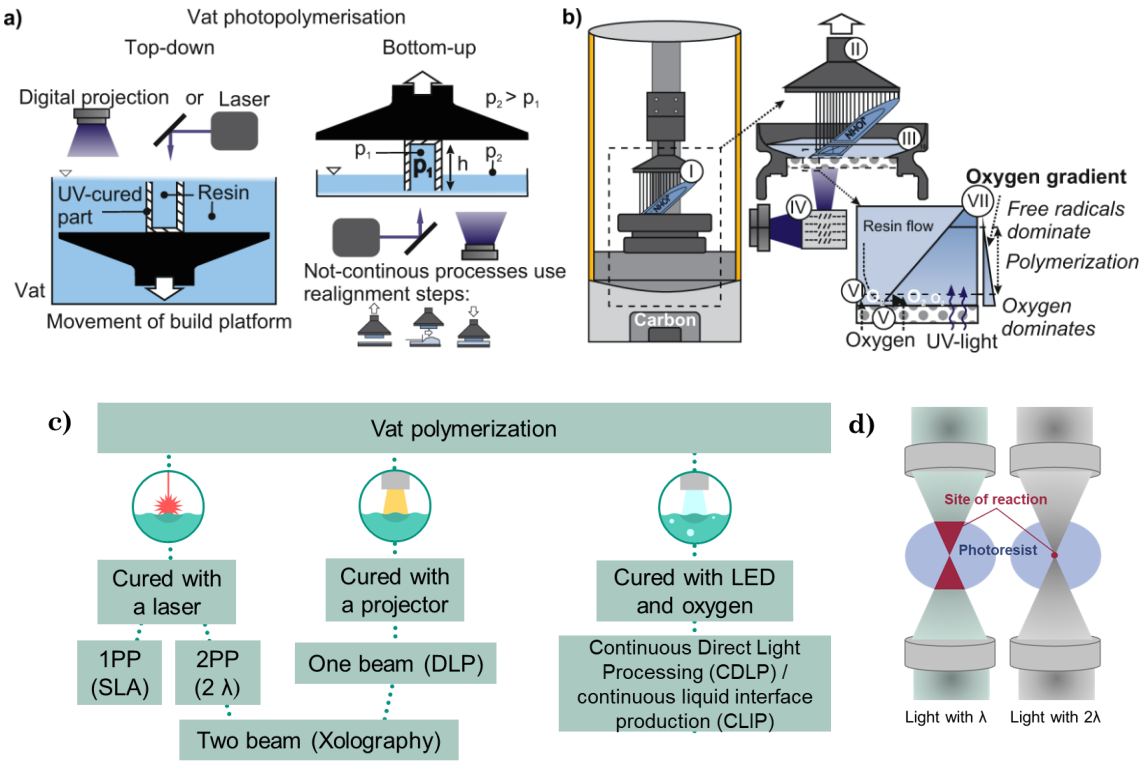

Figure 1-14: a) Top-down vat photopolymerization process (resin is solidified on the resin surface and cavities are naturally filled with resin) and bottom-up vat photopolymerization (resin is solidified at the bottom of the vat). **b)** Graphic depiction of the CLIP: (I) Personalized geometry (II) Constant elevation of the build platform (III) Resin-filled vat (IV) DLP system with micro-mirrors (V) Light and oxygen penetrable window (VI) Zone of no polymerization (VII) UV-cured object. The figure was extracted from Bachmann et al.[283] **c)** Overview of different vat polymerization methods. **d)** Difference between one photon polymerization (1PP; light with λ) and 2PP (light with 2 λ) regarding the reaction side.

A newer and more advanced method uses two-photon polymerization (2PP) (also named two-photon lithography or direct laser writing DLW), which offers tight 3D control over complex structures while allowing sub-micrometer precision due to the non-linear photophysical phenomenon known as two-photon absorption (2PA).[130] The applied femtosecond laser operates in the near-infrared (NIR) and two low energy photons are used for curing. This allows much higher resolutions of a few nanometers. The lower energy photons can also penetrate deeper into tissue or resin for more precise control. On the downside, this technology requires a more powerful laser and is generally more expensive than 1P-SL.[284] One of the main limitations in vat polymerization is the slow speed of printing in the vertical direction. In case of a cell containing ink, this can cause cellular sedimentation and thus inhomogeneity and that's why most cell-laden constructs are more horizontally distributed than vertically.[130] One recently developed technology is volumetric 3D printing (Xolography) which is based on special photoswitchable initiator which requires light of two wavelengths for activation. Xolography uses

a laser-generated light sheet (one wavelength) in combination with orthogonally applied, projected cross-section images with light of another wavelength. Compared to SLA/DLP, Xolography relies on high viscosity materials. This eliminates the need for a support structure and avoids sinking of the build during printing. Advantages of Xolography are high speed (no moving of the printing plate required, and curing does not have to be completed before moving to the next layer), high resolution (known from light-based methods, producing a smooth surface; no subsequent polishing is required), no support structures are required, and material diversity is high, allowing stronger and more durable objects with increased polymer chain length.[285,286]

1.5.2.4 Laser-assisted bioprinting

The most known technology is called Laser-Induced Forward Transfer (LIFT) which transfers a small amount of substance from a donor to a receiving substrate with a pulsed laser. By focusing on the thin donor film, the laser beam induces the formation of a high-pressure bioink bubble by local melting. The bubble is then "shot" onto the substrate layer. Advantages of direct laser writing are the nozzle-free process which avoids clogging, a high resolution (microscale), a high printing speed, compatibility with a wide range of bioink viscosities and single cell droplet printing. Disadvantages are the bioink requirement for fast gelation kinetics and potential contaminations from the absorbing layer in case of metallic surfaces. Also the technology is comparably expensive, time-consuming in preparation and cell positioning remains difficult.[253] Magnetic levitation 3D bioprinting is another type of additive manufacturing that uses a combination of magnetic and optical forces to precisely deposit materials in a pre-programmed pattern by employing biocompatible magnetic nanoparticles. Before printing, cells are incubated with nanoparticles which adhere to the cell membrane *via* electrostatic interactions. Subsequently, these labelled cells are magnetically printed using permanent magnetic fields to print 3D patterns (rings or dots).[287]

1.5.2.5 Others

Other technologies include hybrid bioprinting[288] and 4D printing[289]. While hybrid bioprinting describes the simultaneous use of different material processing methods, 4D (bio)printing refers to 3D printed constructs that can morph into artificial structures after printing due to external stimuli such as a change in pH or light.

1.6 Goal of the thesis

Collagens are the most abundant natural biomaterials for biomedical applications, with widespread use in tissue engineering, wound healing, drug delivery, and other biomedical applications. However, due to their high usage and mostly animal origin, sustainable alternatives such as the recombinant collagen-like protein (rCol) are highly attractive. The overall objective of this work is to investigate the synthesis of novel hydrogels based on a vegan rCol developed by Evonik Operations GmbH and to evaluate their applicability in various biomedical applications.

To achieve this goal, subgoals were defined:

1. rCol characterization to identify performance and handling limitations, such as solubility, 3D structure, viscosity, and biocompatibility.
2. Proof of Concept (PoC) trials for hydrogel synthesis with different crosslinking technologies to target different biomedical application scopes (drug delivery, cell adhesion, cell encapsulation). Generation of case studies for the most promising technologies.
3. Chemical functionalization of rCol to explore photopolymerization by thiol-ene chemistry due to the conjugation with norbornene and thiol units. The reaction products shall be tested for hydrogel synthesis. Resulting hydrogels shall be characterized and tested for 3D (bio)printing.

2 Results and Discussion

2.1 rCol characterization

Collagens belong to an important and abundant group of structural proteins. Together with other proteins like gelatin, keratin, silk, fibroin, sericin, elastin, fibrin, dairy-based proteins (casein, whey proteins) and plant-based proteins (zein), collagens can be used as biopolymers to craft 3D scaffolds. Compared to saccharide-based biopolymers (cellulose, dextran, chitosan, etc.), protein-based polymers often have biological interaction domains for, e.g. cell binding which make them more interesting for biological applications. A very interesting alternative to commonly used animal-derived collagens are recombinant collagen-like proteins. Two of these proteins comprise the collagen-like domains of the Scl1 and Scl2 protein whose genes are expressed naturally by *Staphylococcus pyrogenes*. While the Scl1 gene is known to interact with integrins α2β1 and α11β1 through the sequence GLPGER[290], Scl2.28 does not contain any known binding sites and is therefore reported as "blank slate"[291]. Other Scl2 variants with altered sequences contain binding motifs like GFPGER, and are able to bind to cells even as a composite with cell repellent PEG.[292] Other researchers modified the Scl2.28 protein by implementing heparin-binding, integrin-binding, and hyaluronic-acid binding peptides to induce desired biological responses.[293] Within Evonik Operations GmbH a recombinant variant of the Scl2 protein was expressed in *Corynebacterium glutamicum* as disclosed in WO2023016890A1, WO2023016892A1 and WO2023016895A1 to produce a dried product with a purity of >95% (RP-HPLC) and a triple helical share of >90% (analyzed by SEC). The purified product was the basis for this thesis and is abbreviated as rCol in the following. The goal of this subchapter aimed for a better understanding of rCol. This includes qualification methods like ^{1}H-NMR, Circular dichroism (CD) spectra and material safety. While the NMR spectra will be important for the qualification and quantification of later chemical derivatizations, CD spectra can confirm collagenous triple helical folding. The material safety was evaluated by a standard cytotoxicity assay. Quantification methods based on light absorbance methods were tested. The processability was explored by determining the solubility in common aqueous solutions, the resulting viscosity and the temperature stability. These parameters are important for the subsequent handling and processing of rCol in the following chapters.

2.1.1 Protein structure

2.1.1.1 Primary sequence

The structure of collagen is unique. The self-assembly of three α-helices into a triple helix gives the protein exclusive properties. When heated or exposed to acid or base, collagens denature which cause a reduction in toughness and strength as shown for bone.[294,295] Also while collagens are resistant to most proteinases, denatured collagen (gelatin) is susceptible to most proteinases.[296] For a better understanding of the explored rCol material, its primary sequence was depicted in Figure 2-1 with the respective share of amino acids.

MNHKVHMHHHHHHADEQEEKAKVRTELIQ
ELAQGLGGIEKKNFPTLGDEDLDHTYMTK
LLTYLQEREQAENSWRKRLLKGIQDHALD
LVPRGSPGLPGPRGEQGPTGPTGPAGPRG
LQGLQGLQGERGEQGPTGPAGPRGLQGER
GEQGPTGLAGKAGEAGAKGETGPAGPQGP
RGEQGPQGLPGKDGEAGAQGPAGPMGPAG
ERGEKGEPGTQGAKGDRGETGPVGPRGER
GEAGPAGKDGERGPVGPAGKDGQNGQDGL
PGKDGKDGQNGKDGLPGKDGKDGQNGKDG
LPGKDGKDGQDGKDGLPGKDGKDGLPGKD
GKDGQPGKPGKY

MW = 22840.53 g/mol

Name	3-Letter	1-Letter	Class	Number	Count, %
Glycine	Gly	G	Hydrophilic	80	33.33 %
Proline	Pro	P	Hydrophobic	32	13.33 %
Lysine	Lys	K	Basic	22	9.17 %
Aspartic Acid	Asp	D	Acidic	19	7.92 %
Glutamine	Gln	Q	Hydrophilic	18	7.5 %
Glutamic Acid	Glu	E	Acidic	16	6.67 %
Alanine	Ala	A	Hydrophobic	15	6.25 %
Leucine	Leu	L	Hydrophobic	12	5 %
Arginine	Arg	R	Basic	11	4.58 %
Threonine	Thr	T	Hydrophilic	7	2.92 %
Asparagine	Asn	N	Hydrophilic	3	1.25 %
Valine	Val	V	Hydrophobic	2	0.83 %
Methionine	Met	M	Hydrophobic	1	0.42 %
Serine	Ser	S	Hydrophilic	1	0.42 %
Tyrosine	Tyr	Y	Hydrophobic	1	0.42 %
Cysteine	Cys	C	Hydrophilic	0	0 %
Histidine	His	H	Basic	0	0 %
Isoleucine	Ile	I	Hydrophobic	0	0 %
Phenylalanine	Phe	F	Hydrophobic	0	0 %
Pyrrolysine	Pyl	O	Basic	0	0 %
Selenocysteine	Sec	U	Acidic	0	0 %
Tryptophan	Trp	W	Hydrophobic	0	0 %
			Total:	240	100 %

Total number of negatively charged residues (Asp + Glu): 35
Total number of positively charged residues (Arg + Lys): 33

Figure 2-1: (Left) Primary sequence of rCol with labelled His tag (grey) and a thrombin cleavage (green). After enzymatic hydrolysis, the resulting amino acid sequence is underlined. (Right) Displayed amino acid composition together with the aa share and the number of negatively and positively charged side chains after cleavage (calculated using: https://www.protpi.ch/Calculator/ProteinTool).

2.1.1.2 Tertiary structure

Based on literature, the collagen's triple helical structure can be visualized by CD data with a maximum at ~ 220 nm and a minimum at <200 nm. In the single-stranded, denatured form, collagens produce a flat curve which anneals zero at 220 nm as shown in Figure 2-2. When multiple triple helices align to fibrils, a minimum at 210 nm is observed.[297-299] To visualize the triple helical structure, CD spectra of rCol were recorded in cooperation with Dr. Julia Wirmer-Bartoschek (Goethe University Frankfurt) according to chapter 4.2.5.6 w/o and w/

prior denaturation (10 min at 40 °C). Data extraction was done by the author of this thesis showing a triple helical structure of rCol before denaturation and a single strand structure after denaturation. This experiment showed that "only" 10 min at 40 °C denatured rCol. To further investigate the temperature limitations of this material, several CD spectra at different temperatures were overlayed to achieve a melting curve. This topic will be outlined in Figure 2-3.

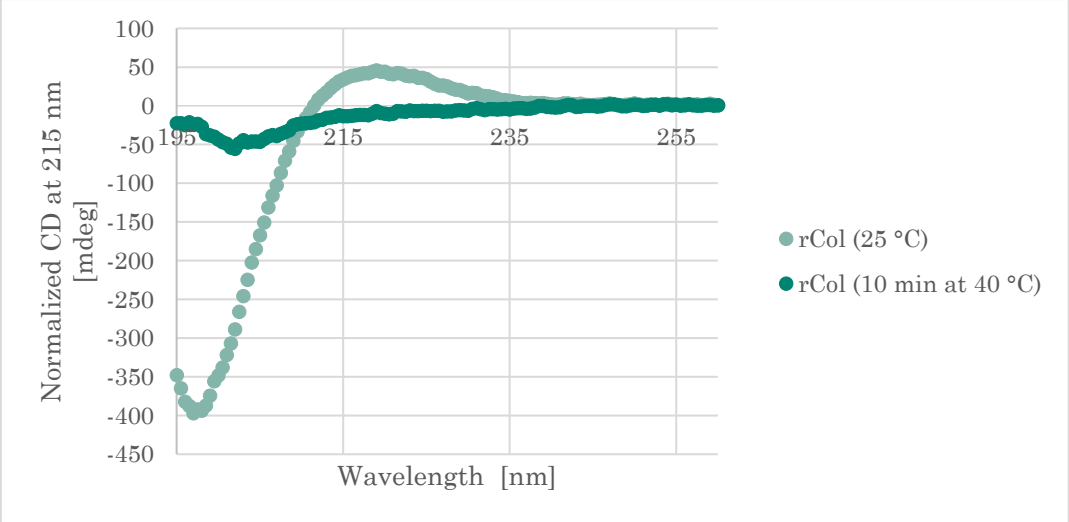

Figure 2-2: Normalized and smoothed CD spectrum of rCol. The sample (0.1 g/kg) was prepared in 50 mM sodium phosphate buffer pH 7.2 with in a thermomixer for one hour at 20 °C. A more detailed description, signal normalization and smoothing was described in chapter 4.2.5.6.

2.1.1.3 Melting temperature

When exposed to temperatures between 30 and 40 °C, most collagens are known to denature (triple helix to single strands; see Figure 2-2) forming gelatin.[300,301] This effect is only partially reversible for animal-derived collagens and is influenced by different factors like incubation time, temperature and chain length.[302-304] The melting temperature (T_m) is defined as the temperature where 50% of the protein triple helix is unfolded into a single strand. This value differs depending on the type and origin of the collagen.[305] While fish-based collagens show a generally low thermal stability (structural changes occur already above 28 °C), some collagens show melting temperatures of above 40 °C.[305] For human collagen type I Leikina *et al.* identified denaturation below body temperature (37 °C). Even 36 °C caused complete unfolding over time. For Collagen type III, a further reduced T_m of 35 °C was determined. This effect is assumed to happen due to the number of posttranslational modifications, especially hydroxyproline, whose increase is associated with an increased thermal stability of triple helix.[306,307]

In a publication from 2022, Fujii *et al.* observed a change in melting temperature of a particular collagen from zebrafish by the exposure of extracted fibroblasts to different temperatures (18 °C to 33 °C). The researchers correlated the formation of hydroxylysine with the exposure temperature which led to 26% hydroxylysine share when cultured at 18 °C and 49-50% when cultured at 33 °C. Additionally, the T_m changed from 34.2 °C to 36.4 °C.[308] To identify the capability of triple helical formation and its unfolding, CD spectroscopy represented an excellent and precise technique. CD spectra of rCol were performed by different temperatures, and overlayed to a melting curve. A detailed procedure is given in chapter 4.2.5.6. While lower temperatures did not affect the protein structure, higher temperatures caused denaturation. A T_m of 33 °C was obtained from the fitting curve for rCol. Therefore, the recommended usage conditions of rCol should not exceed an incubation temperature of 30 °C. Direct usage as a media component for cell culture applications or direct injection within the human body could comprise the biological activity due to triple helical disintegration. In order to maintain the 3D structure at these temperatures, chemical crosslinking was of great interest. Furthermore, follow up experiments in chapter 2.2.2.2.1, Figure 2-14 showed significant changes in hydrogel formation and hydrogel stiffness when the reaction temperature was changed which led to much lower stiffnesses when the triple helix was partially or completely denatured prior to crosslinker addition.

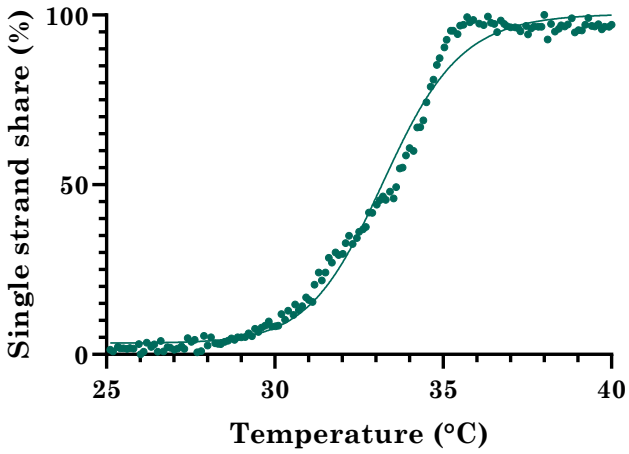

Figure 2-3: CD melting curve of rCol with a sigmoidal curve fitting using GraphPad Prism 9.4.1. From the resulting formula, a melting temperature (T_m) of ~33 °C was calculated.

2.1.1.4 Refolding

Animal-derived collagens are known for their physical gelation due to pH shifts to allow self-assembly by hydrostatic interactions including Van der Waals forces.[304,309] rCol showed no

signs of physical gelation in a wide range of tested parameters including pH, temperature and concentration. It was assumed that the rCol strand was too short to build sufficient hydrogen bonds to stabilize the 3D structure. When heated the material untwined into single strands. To explore refolding properties, denatured rCol was incubated at different temperatures and different concentrations for 20 h. The resulting solutions were analyzed by size exclusion chromatography and the change of area responding for the triple helical conformation in accordance with the remaining peaks was observed over time. After denaturation the formed single strands folded back into their triple helical conformation in a concentration and temperature dependent matter (see Figure 2-4). The higher the concentration the higher the refolding ratio within the same time. While a temperature of 30 °C led to nearly no refolding at any tested concentration, the refolding increased up to 90% of triple helical structure when the temperature was decreased to 4 °C or 10 °C, respectively. This data aligned with the determined melting temperatures *via* CD which indicated denaturation starting from 30 °C. To allow refolding, a temperature between 4 °C and 10 °C can be used for 20 h, maintaining a minimal concentration of 20 mg/ml to yield maximal folding. The refolding behavior observed in this study could be reproduced in subsequent studies (data not shown).

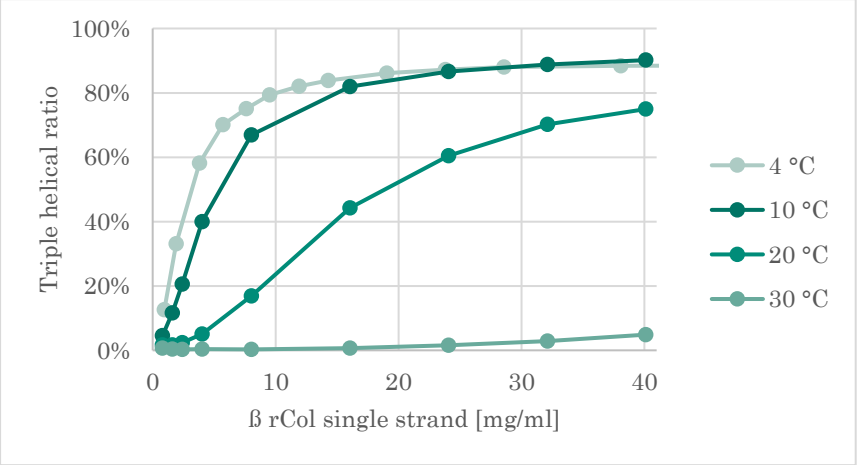

Figure 2-4: Temperature-dependent rCol refolding. This graph was taken from patent WO 2023/016892 A1. The information was reproduced with permission from the authors. A 40 g/L rCol solution was unfolded at 40 °C, split up and further diluted to concentrations from 1-40 mg/ml. The samples were incubated at different temperatures (4-30 °C) for 20 h and analyzed *via* size exclusion chromatography. The relative share of triple helical conformation was calculated based on the peak integrals compared to the remaining peaks (data not shown).

2.1.2 Physicomechanical Characterization

2.1.2.1 Isoelectric point

Solubility describes a critical material property which is important for, e.g. protein crystallization, bioprocess and application development. Proteins are normally dissolved in aqueous solution or in buffer to stabilize the 3D structure. Although proteins often possess great water solubility, this is not always the case. Varying from milligrams per milliliter like serum albumins (>500 mg/ml), also totally non-soluble proteins like crambin are known to literature.[310,311] The solubility itself is influenced by extrinsic and intrinsic factors. Extrinsic factors comprise the pH, ionic strength, temperature, and the presence of additives, whereas intrinsic factors are defined primarily by the protein's secondary structure which defines the protein-solvent interface. Especially with proteins, the three-dimensional structure can change in different solvents resulting in protein denaturation. For aqueous solutions the pH plays a significant role especially for molecules with a zwitterion character. A zwitterion or dipolar ion is per definition a molecule with two or more functional groups which are positively and negatively charged. By having functional basic or acidic groups, amino acids and proteins are good examples for zwitterions. In an aqueous environment, carboxylic side chains (present in glutamic and aspartic acid side chains) tend to deprotonate (dissociation of protons), and amines tend to protonate (present in lysine side chains). At a certain pH, positive and negative charges are even in number resulting in a zero net charge which makes the protein unable to move in an electric field (like using sodium dodecyl sulfate–polyacrylamide gel electrophoresis; short: SDS-PAGE). This pH is called the isoelectric point (IEP, pI). Knowing the isoelectric point for a protein provided a first understanding of the pH-dependent solubility in an aqueous environment and helped to identify an appropriate pH range. Matching the pI of a protein results in protein precipitation due to zero net electronical charge. The pI can be determined experimentally by isoelectric focusing or by calculation. Here, different online tools were applied to calculate the pI of rCol which led to similar values, which were listed in the following. One calculated example curve was depicted in Figure 2-5.

- https://web.expasy.org/compute_pi/: 5.49
- http://isoelectric.org/calculate.php: 5.41
- https://www.protpi.ch/Calculator/ProteinTool: 5.50

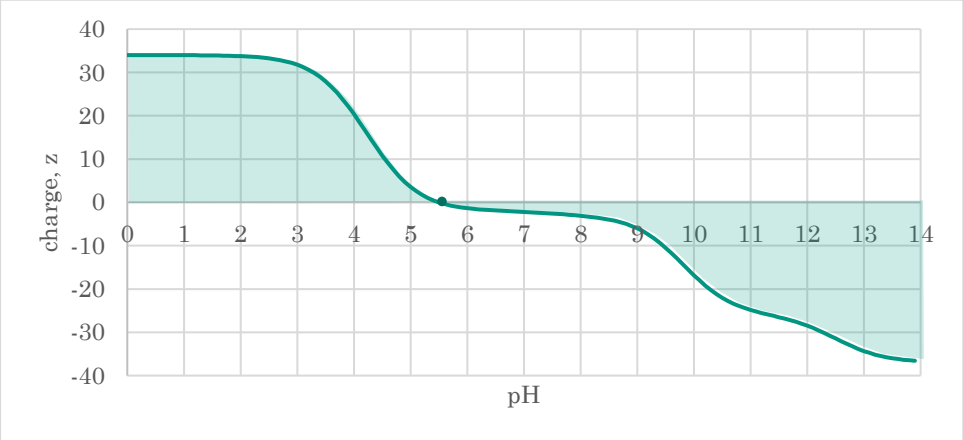

Figure 2-5: rCol titration curve calculated with Prot pi I Protein Tool. The tool calculates a pI of 5.5 and a slightly negative net charge at a pH of 7.4 with z = -2.5.

2.1.2.2 Solubility

Laboratory experiments (not published here) have demonstrated the usage of rCol in different aqueous buffer systems with a broad pH range around pH 7.0. To further define the solubility, an adaptation of the procedure described by Wu *et al.* was applied.[312] A 200 mg/ml stock solution was prepared in three different dilutants at RT (ddH_2O, phosphate-buffered saline (1×PBS) pH 7.4 and HEPES $buffer_{(aq)}$ pH 8.0). The UV absorbance of the solution was measured before and after centrifugation (see Figure 2-6). No visible pellet was observed after 30 minutes of centrifugation at 21,300 rcf and no UV signal loss was measured. This indicated that all three buffer systems can dissolve properly rCol at 200 mg/ml.

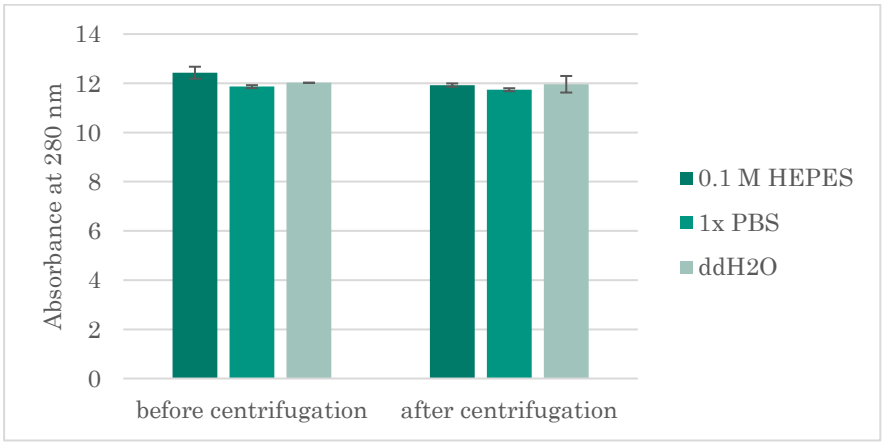

Figure 2-6: rCol quantification before and after centrifugation. A 200 mg/ml rCol solution was prepared in different aqueous solutions followed by centrifugation (21,300 rcf; 30 min). The absorbance before and after centrifugation of the supernatant was measured at UV (λ=280nm) *via* nano drop.

2.1.2.3 Viscosity

Common animal-derived collagens like rat-tail collagen (rtCol) or bovine collagen (bCol) often have high viscosities which hampers material handling and its homogenization with additional compounds. In their application note No. 376, Eppendorf states that a fluid with ≤200 mPa*s can be still transferred using a classic air-cushion pipette.[313] Special pipetting tips and transfer techniques (reverse pipetting) are mandatory to avoid material loss and bubble entry for higher viscosities which produces additional cost. Regarding applications like bioprinting, bubble entry can harm encapsulated cells, hinder homogenous network formation and limits microscopy by light refraction. To analyze the viscosity of animal-derived collagens, a rat-tail collagen (Advanced BioMatrix; PhotoCol®) was tested as reference and a flow curve was recorded by using a plate cone setup within an AntonPaar rheometer as described in chapter 4.2.6.3.1 leading to Figure 2-7 (chapter 2.1.2.2). To identify the linear range of the viscosity/shear rate, several measurements at different shear rates were needed. All concentrations showed a shear-thinning effect which didn't end up in a constant horizontal viscosity value. According to literature, animal-derived collagens show the characteristics of non-newton fluids which is caused by an increase in collagen macromolecule interactions, leading to the increase in the entanglement of the chains.[314] Finally, the linear range could be identified (Figure 2-7; A1), enabling the extraction of the final viscosity value for each of the concentrations tested (Figure 2-7; A2). For comparison, the measurement was repeated with rCol dilutions in ddH_2O from a 100 mg/ml stock solution. While both collagens (animal and non-animal) showed an exponential, concentration-dependent increase in viscosity, the animal-derived collagen rapidly exceeded the value of 200 mPa*s at a concentration of 4 mg/ml rtCol. The threshold of 200 mPa*s is defined as a suitable viscosity for standard pipetting tips according to Eppendorf Application Note 376.[313] rCol, on the other hand, showed a more than 350× lower viscosity at the highest tested concentration of 100 mg/ml rCol in comparison to rtCol. These values are very beneficial as they allow an easy handling of the rCol solution at higher concentration (100 mg/ml, <70 mPa*s), and thus enabling efficient crosslinking due to an improved diffusion of reactants. It was assumed that the aberration in viscosity relied on the reduced molecular weight of rCol (~23 kDa for rCol and ~300 kDa for rtCol). While rtCol formed sufficient electrostatic interactions for physical gelation, rCol lacked this property, which may be conditioned by the shorter chain length and molecular weight. The lack of post-translational hydroxylation and the resulting absence of stabilizing hydrogen bonds by hydroxyprolines was not associated with a change in viscosity but rather is expected to alternate the stability of the protein and to change parameters like the melting temperature.

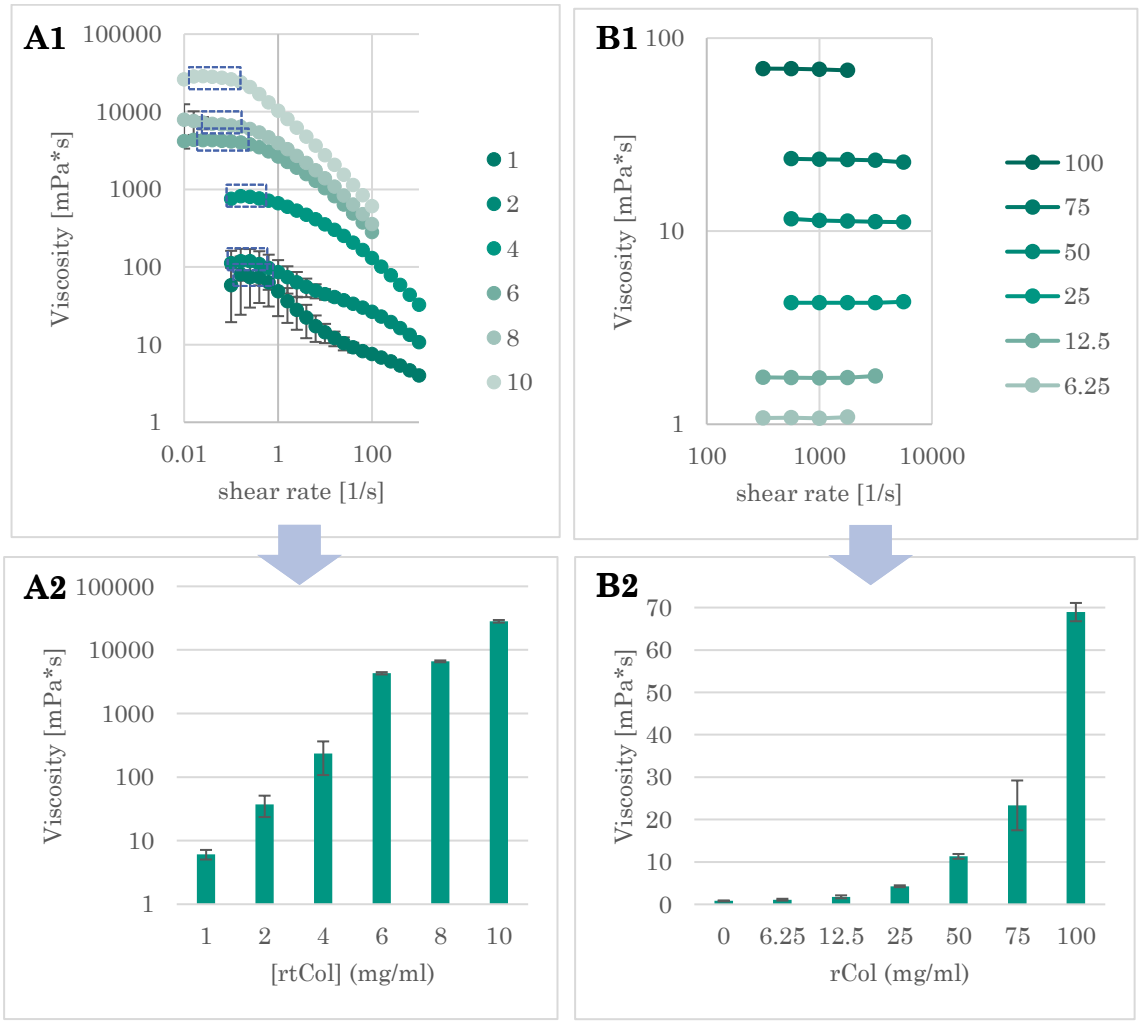

Figure 2-7: Viscosity determinations of different rCol and rtCol formulations. The viscosity was extracted from the linear range of recorded flow curves which were recorded with an Anton Paar MCR 502 WESP system with plate-cone set-up (N = 3). **(A1)** Flow curves of different rtCol formulations (1-10 mg/ml in 20 mM acetic acid). Blue dotted boxes indicate the extracted linear range for figure A2. **(A2)** Blotted linear range with the standard deviation from at least 3 neighboring data points (N = 3). **(B1)** Recorded flow curves of different rCol formulations (6.25-100 mg/ml dissolved in ddH_2O) and the average viscosities of five neighboring data points within the linear range (N = 3). **(B2)** Flow curves were recorded at 4 °C for rtCol and at 20 °C for rCol. All data was normally distributed.

2.1.3 Protein quantification

2.1.3.1 UV/VIS detection by absorbance measurements

Nuclear magnetic resonance (NMR) and mass spectrometry (MS) are effective methods for structure elucidation and compound quantification, but they require expensive equipment and may not be accessible to everyone. UV/VIS absorption spectra are commonly used to

quantify deoxyribonucleic acid (DNA), ribonucleic acid (RNA), and proteins. DNA has an absorption maximum at 260 nm, while RNA and proteins can be detected at 280 nm due to the absorbance maxima for the amino acids tryptophan and tyrosine.[315,316] Here, different concentrations of rCol were prepared at RT and the absorbance at 280 nm was measured at RT using a NanoDrop™ device to reduce the sample volume in comparison to a multiplate reader. A linear signal-concentration correlation was detected for rCol concentrations up to 100 mg/ml. The limit of detection for this technology was determined at ≤2 mg/ml which most probably resided in the rare appearance of tyrosine per molecule (1 Tyr/molecule).

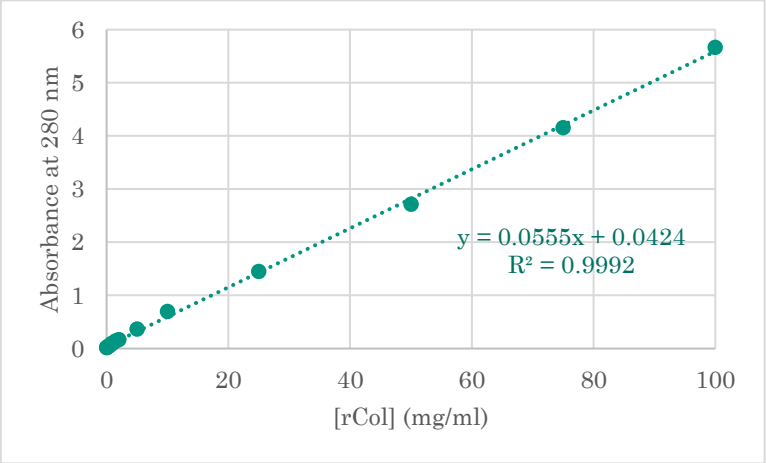

Figure 2-8: Absorbance spectra of different rCol concentrations in ddH_2O between 0.01 mg/ml and 100 mg/ml. The absorbance was measured using a NanoDrop™ One/One^C (Thermo Scientific™) with 2 µl per sample. ddH_2O was used as solvent and as background control.

2.1.3.2 Colorimetric assays

To reduce the limit of detection, two more sensitive, colorimetric assays were tested. (Bradford and BCA assay). Bovine serum albumin (BSA) was used as sample reference. While both assays demonstrated signal-concentration correlations for BSA, only the BCA assay worked for rCol in the tested concentration range. Also, the general sensitivity was higher for the BCA assay. For rCol, the Bradford assay did not show a signal increase compared to the background up to concentrations of 10 mg/ml and thus was neglected. The BCA assay allowed rCol quantification down to 20 µg/ml and was used as complement assay to UV absorption to cover the rCol range between 0.025-2 mg/ml. By increasing the rCol concentration further the Bradford assay might show an extractable signal but exploration thereof was neglected due to the faster and cheaper UV measurement demonstrated above.

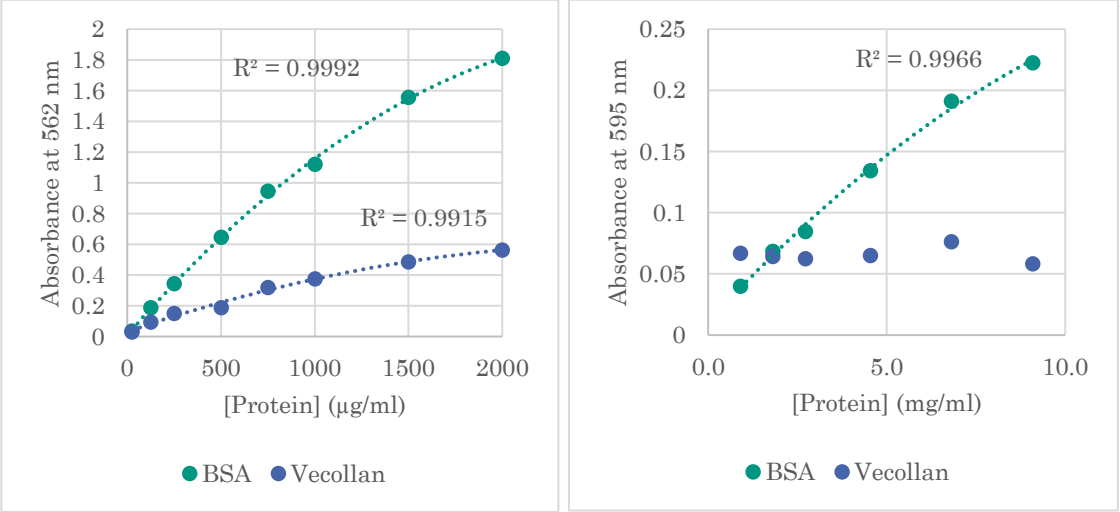

Figure 2-9: Colorimetric rCol quantification by using the BCA Assay (left) and the Bradford Assay (right). BSA was used as a reference. ddH_2O was used as solvent and as background control. A polynomial fit was performed where possible.

2.1.4 Biocompatibility

To determine potential toxic effects of rCol, an assay to measure the metabolic activity of cells was performed (see Figure 2-10). With increased rCol concentration the viscosity of the test solution increased. To avoid viscosity-based effects on the cell viability like a potentially reduced diffusion of nutrition, a max. concentration of 40 mg/ml was used. A correlation between an increase in rCol concentration and a decrease in viability was detected. Still, very good viability values with respect to the control group were detected (87% - 103%). The experiment could be repeated with higher rCol concentrations to determine the LC_{50} value. This was neglected due to the concentration-dependent increase in viscosity which was associated with a slowed down diffusion and a reduced viability. According to the ISO Norm 10993-5, the threshold for materials safety equaled a min. of 70% viability which was exceeded within this experiment for all sample groups. Resulting, the LD_{50} value was >40 mg/ml rCol. In summary, this chapter showed the protein sequence's ability to form a triple helix, and the material was evaluated as non-toxic and usable for the direct contact with living cells. In summary rCol is a novel, recombinant, bacterial-derived collagen which was evaluated as interesting alternative for animal-derived collagens which are currently used as collagen standard. In Table 2 1, major differences to standard mammalian collages were listed. Major differences were found in the hydroxyproline content, the molecular weight, the rheological behavior and the solubility.

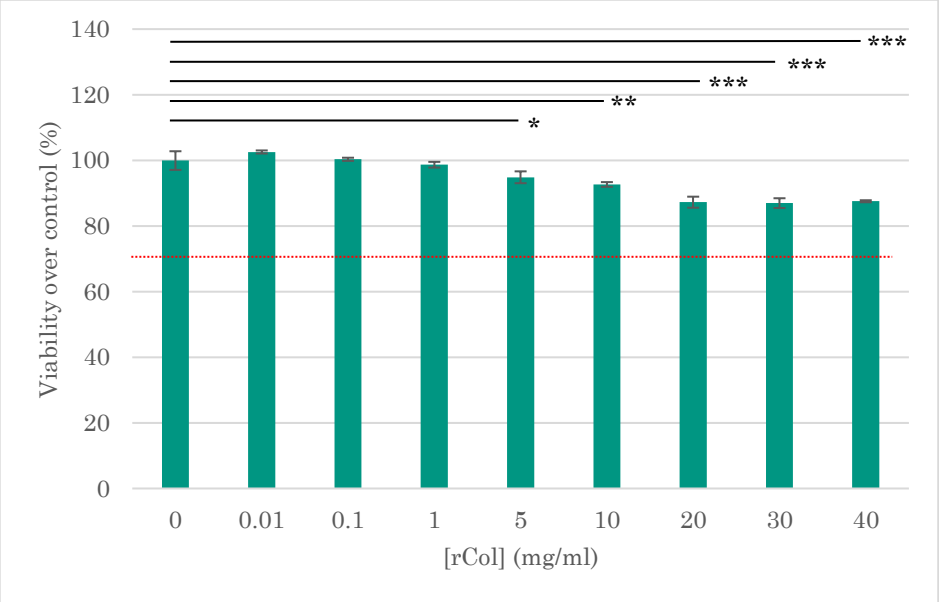

Figure 2-10: Cytotoxicity determination of rCol *via* CellTiter-Glo® assay with HeLa cells. The assay was performed according to the manufacturer's protocol (see chapter 4.2.3.1.2). Untreated HeLa were used as control (100% viability). The defined threshold for safe medical devices by ISO Norm 10993-5 of 70% was depicted by a red dotted line (N=3). All data was normally distributed. A homoscedastic two-sided Student's t-test was performed (*, **, *** represent $\alpha < 0.05$, 0.01, and 0.001, respectively).

Table 2-1: Comparison table for mammalian collagens like rtCol from Cellink and bacterial collagens like rCol. Advantages were highlighted (**green**).

Criterium	Mammalian collagens	rCol
Hydroxyproline	Yes	No
Triple helix	Yes	Yes
Thermal stability	T_m = ~30-35 °C[317]	T_m = ~33-35 °C
Refolding possible?	Yes[317] but partially	**Yes**
Average molecular weight	300 kDa	23 kDa
Solution	non-Newtonian fluid	**Newtonian fluid**
Needed pH for solubility	3.0-3.8 (0.02 M acetic acid)	**6-8 in 1xPBS**
Solubility limit	Up to 20 mg/ml	**Up to 200 mg/ml**
Viscosity (10 mg/ml)	>25,000 mPa*s	**~ 1.5 mPa*s**
Toxicology	safe	safe
Price	Expensive	**Cheaper**
Disease transmittance	Possible	**No**

2.2 rCol crosslinking

2.2.1 Introduction

2.2.1.1 The need for chemical crosslinking

In the previous chapter, the high solubility, low viscosity and processability were highlighted of rCol along with the solubility at neutral pH while maintaining the triple helical structure with its reversibility after denaturation. Identified disadvantages were the temperature sensitivity and lack of physical gelation known for animal-derived collagen when heated to 37 °C. Instead of physical crosslinking, the rCol solution denatured into single strands. Therefore, to craft 3D structures, chemical crosslinking was mandatory.

2.2.1.2 Technology evaluation

To enable chemical crosslinking, relevant functional side chains within the material must be identified and quantified. According to the introduction of this thesis, the most accessible and commonly used side chains in proteins are carboxylic acid groups, primary amines and primary thiols. These functional groups are present in aspartic acid (Asp), glutamic acid (Glu), lysines (Lys) and cysteines (Cys). Other functional groups, such as alcohols, are much more difficult to access and may require more reactive compounds. Due to the lack of cysteines within the sequence, natural crosslinking *via* thiols is not an option. Within chapter 2.3.2.1 high abundance of lysine (9.17%) was quantified *via* ^{1}H-NMR spectra (Figure 2-38). Furthermore, the high number of carboxylic acid side chains (14.6%), made amide bond formation a very attractive crosslinking attempt for a theoretically high variance of network densities. Different crosslinking technologies were established in the beginning of this thesis (Table 2-2). Although all technologies resulted in hydrogel formation, most technologies were excluded from further investigations. As described in chapter 1.3.3, Glutaraldehyde has several downsides which limits its usage. To still connect only primary amines, a PEG-based active ester was tested further based on a previous publication with animal-derived collagen.[113] PEG represents a bioinert, FDA approved material which is commonly used in a wide field from cosmetics to medicine[112] and can be exchanged theoretically by another spacer polymer to generate application-specific rCol copolymers (see chapter 1.3.3.2.3, Scheme 1-3). When comparing EDC/NHS and DMTMM, which work similar, DMTMM was chosen as a target linker due to the described problems with EDC/NHS (see chapter 1.3.3). Another reason for this choice was the observed gas bubble development during gelation using EDC/NHS (data not shown) which were associated in literature with an EDC side product which disrupted a

homogenous hydrogel formation as described in chapter 1.3.3.2.2.[108,109] Both technologies have the unique feature of being no direct crosslinker but rather an activation reagent for carboxylic acids which theoretically allows a crosslinker-free hydrogel product in case of complete turnover. Enzymatic reactions are commonly considered as fast and environmentally friendly. To name some advantages, they do not require chemical solvents and allow reactions at reduced temperatures. Nevertheless, enzymes are difficult to remove after the hydrogel synthesis, and they do not lose their chemical activity due to their role as catalysts. This could lead to unwanted, additional crosslinking within a biological system and could compromise homogenous hydrogel network formation. Although enzymes like transglutaminase were successfully tested, the described issues with enzymatic removal and the elevated prices for enzymes shifted the focus to other technologies. In summary, the DMTMM and the 4PEG-SG crosslinker were selected for further characterization including but not limited to the physical limitations of formed hydrogels and their biological performance.

Table 2-2: Successfully tested crosslinking approaches for rCol.

Technology	Covalent linkage formed	Needed functional groups
Glutaraldehyde	Schiff Base	2x Lys (R-NH_2)
4PEG-SG	Amide bond	2x Lys (R-NH_2)
EDC/NHS	Amide bond	1x Lys (R-NH_2) + 1x R-COOH
DMTMM	Amide bond	1x Lys (R-NH_2) + 1x R-COOH
Transglutaminase	Amide bond	Gln (R-$CONH_2$) + Lys (R-NH_2)

2.2.2 DMTMM induced crosslinking

2.2.2.1 The formulation optimization

The applied molar ratio (MR) of rCol to crosslinker (XL) was based on the molar ratio of the functional side chains of each compound. For the DMTMM crosslinking, the carbon acid side chains in rCol were activated and reacted with the primary amines in rCol (see chapter 1.3.3.2.2, Scheme 1-2). For this crosslinking chemistry, the absolute number of acidic side chains in one mol of rCol was compared to the number of functional side chains within one mol of DMTMM. While one molecule of rCol contains 35 acidic side chains + one terminal COOH group, DMTMM contains only one reactive center per molecule. To achieve an equimolar ratio (1:1), one molecule of rCol was added to 36 molecules of DMTMM. In the following the MR of different formulation is always depicted in the following format: MR of functional side chains in rCol to functional side chains in crosslinker (1:X).

2.2.2.1.1 The gelation range

To identify the minimal, required concentrations of rCol and DMTMM for hydrogel synthesis, different combinations thereof were tested (2.5 – 50 mg/ml rCol; MR range of 1:0.1 – 1:3). For this crosslinking chemistry, a broad reaction efficacy without the need for specific buffer systems was described in literature[106] to allow chemical crosslinking at e.g. at neutral pH (7.0-7.5).[318] If not stated otherwise ddH_2O was used as solvent for the reaction. In an upside-down vial test different formulations were prepared in 2 ml HPLC vials according to chapter 4.2.4. Constant turning of the sealed vials at RT showed gelation within 24 h for most cases. Insufficiently gelated samples moved according to gravity during turning of the vials. An example of the assay was given in Figure 2-11, A and the resulting evaluation of the screening in depicted in B. The reaction kinetics were evaluated as slow due to gelation within the minutes to hour range. This allowed the application of higher rCol concentrations including thorough homogenization prior to hydrogel formation. To keep the water content high and to reduce material cost, a rCol concentration range of 10 - 40 mg/ml was recommended for further experiments.

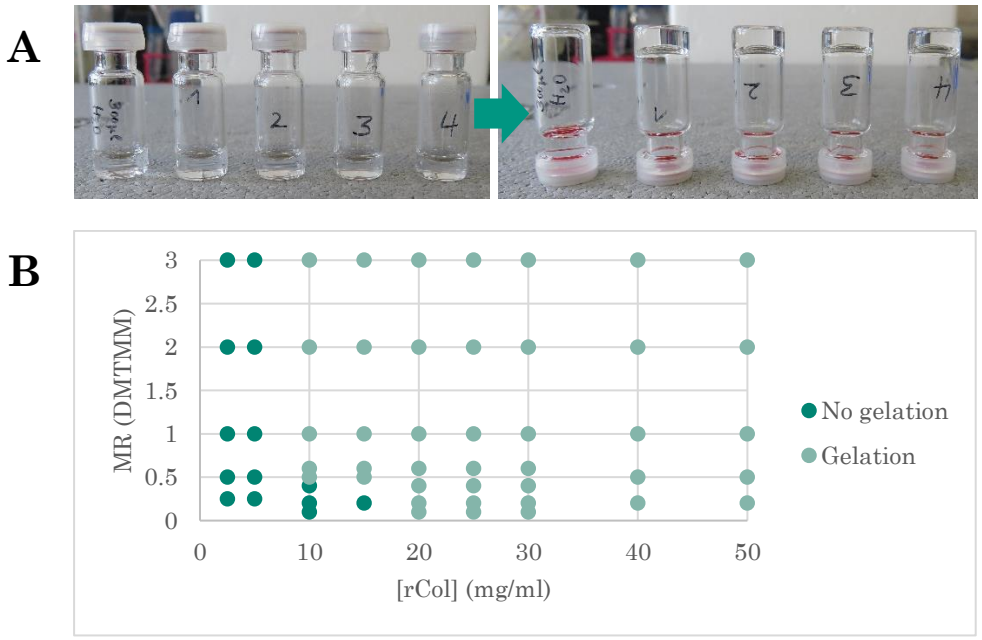

Figure 2-11: (A) Examples for the upside-down vial test with 300 µl formulation each in a sealed 2 ml vial. Gelation was visualized by the immobilization of the formulation when turned upside-down. **(B)** Results of up-side down vial test with selected formulation of rCol and DMTMM. Sample vials were incubated at RT for 24 h with 300 µl formulation each. Gelation and no sufficient gelation were visualized with different colors.

2.2.2.1.2 Biocompatible MRs of DMTMM

DMTMM is a hazardous substance like most chemical linker (LD_{50} 1.091 mg/kg in rats).[319] High equivalents thereof might be counterproductive for the direct contact with tissues and might require washing steps in between. By directly implementing the drug of interest within the patch during crosslinking could lead to drug release during subsequent washing steps, which makes washing undesirable for the application of a tissue patch for drug delivery. To determine the recommended molar ratio (MR) of DMTMM, a leachable experiment was performed. Identical samples were prepared according to chapter 4.2.4.3 and further processed according to chapter 4.2.3.2. Briefly, fully gelated hydrogels were washed thrice with cell culture medium and pre-seeded fibroblasts were exposed to the washing solutions within a cell viability assay. Data showed formulation-dependent, cytotoxic effects of the first extraction solution. Higher concentrations of rCol and DMTMM resulted in a lower viability. The measured viability increased by exposure to subsequent washing solutions (2nd and 3rd wash). Exposed to the 1st washing solution, human foreskin fibroblasts (HFF) showed exceptionally low viabilities of <20% for hydrogels made of 40 mg/ml rCol and a MR of 1:3. By decreasing the MR of DMTMM, the cell viability increased (80% for 1:1 ratio and 87% for 1:0.5 ratio). For formulations made from 20 mg/ml rCol, the detected cytotoxic effect of all washing solutions was lower. Also, single washing was sufficient to result in normalized cell viability values of >80% for all tested formulations which surpassed the threshold of 70%, which was required to evaluate a medical device as safe according to the ISO Norm 10993-5. To reduce the cytotoxic potential, a maximal MR of DMTMM of 1:1 was recommended for further development steps.

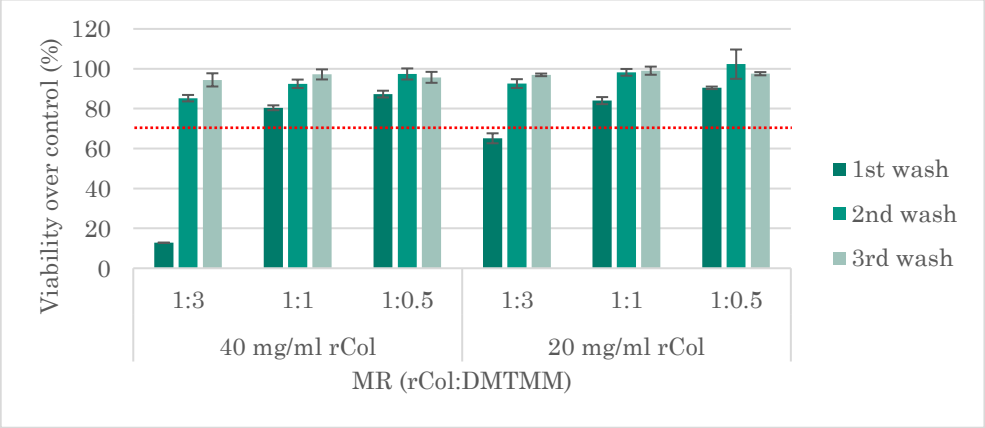

Figure 2-12: MTS cytotoxicity assay of washing solution of different hydrogel formulations exposed to HFF cells. 220 µl hydrogel was washed 1 h at 37 °C with 440 µl culture medium. Seeded HFF cells were exposed to washing solutions for 24 h each. The threshold defined by ISO Norm 10993-5 was indicated by a dotted red line at 70% normalized cell viability (N=3). All data was normally distributed.

The results obtained in this study indicated differences in the cytotoxicity profile of the hydrogels, due to the safety nature of the crosslinker used. Nevertheless, the study indicated that after a proper manufacturing process safe material can be produced. To finally confirm the non-cytotoxicity of those hydrogels, additional testing might be necessary, like a leachable/extractable assay according to the ISO-10993-12/18. This assay is used to evaluate the cytotoxicity of medical device products mimicking final usage conditions, such as exposure time and extraction media of the medical device.

2.2.2.2 Mechanical characterization

2.2.2.2.1 Rheology

Rheological properties are critical to potential applications. Due to the unknown gelation kinetics of different formulations, simple endpoint measurements are not target-oriented. To measure the reaction time required for maximum conversion, the reaction kinetics was observed by shear modulus measurements using the ElastoSens Bio™ instrument as described in chapter 4.2.6.3.2. The measured shear storage modulus (G') and shear loss modulus (G") were shown in Figure 2-13 (A) for three example formulations. The final stiffness, resulted from the max. turnover of the reaction, was extracted from the y-value of the linear portion of the G' curve. The corresponding x-value described the required incubation time according to the applied reaction temperature of 25 °C.

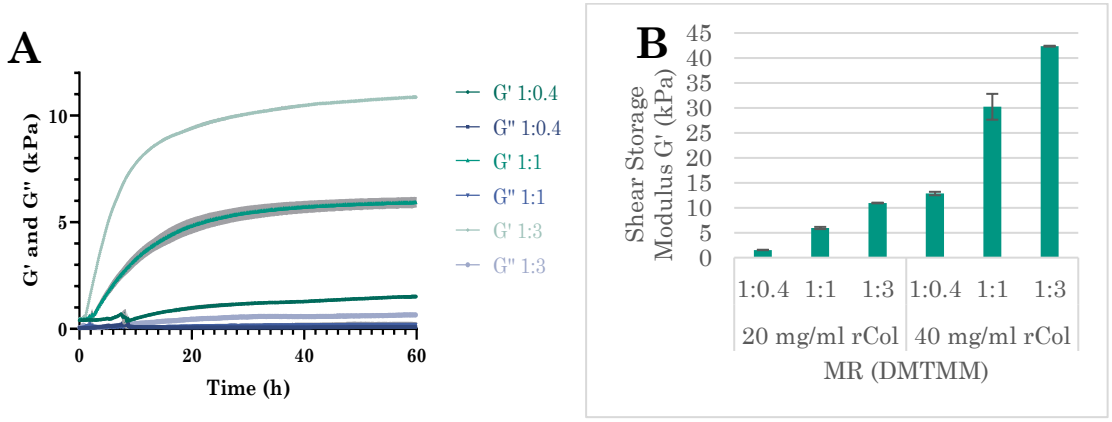

Figure 2-13: (A) Gelation kinetics expressed by shear storage moduli (G') and shear loss moduli (G") of 20 mg/ml rCol crosslinked with different MR of DMTMM. **(B)** Shear Storage Moduli (G') of fully gelated rCol hydrogel formulations extracted from the plateau phase of the online kinetic measurements using the ElastoSens Bio™ instrument by using DMTMM activation reagent (N=2). All data was normally distributed.

As described in the introduction, the triple helical structure is crucial for the material strength. Based on chapter 2.1.1, Figure 2-3, rCol started to denature starting from 30 °C. To determine the change in gelation and final stiffness, a selected formulation (40 mg/ml rCol; DMTMM; MR 1:1) was crosslinked at different temperatures (see Figure 2-14). To ensure a max. degree of folding, the used rCol stock solution was incubated for 24 h at 4 °C (in alignment with chapter 2.1.1.4, Figure 2-4). Prior to adding DMTMM, the mixture of ddH_2O and rCol was incubated for 15 min at the respective reaction temperature to initialize triple helical change. 15 min was chosen due to the successful usage of that timeframe in chapter 2.1.1.2, Figure 2-2 to denature rCol. The change in rheology was monitored by the ElastoSens™ Bio at the desired reaction temperature. By increasing the reaction temperature, the mechanical strength increased from 15 °C up to 25 °C reaction temperature. The increase in stiffness was hypothesized to be the results of different reaction kinetics. The duration until the final stiffness was reached lasted longer at 15 °C. DMTMM is known to hydrolyze over time which might have competed with the crosslinking reaction which might have led to lower stiffnesses. To validate this hypothesis, staining experiments with ninhydrin were performed later in this thesis (see chapter 2.2.2.2.2). Further temperature increase led to a reduced final stiffness starting from 30 °C and let to no hydrogel formation at 37 °C. These findings correlated with the measured melting curves of the triple helix (chapter 2.1.1, Figure 2-3) which demonstrated small amounts of triple helical unfolding at 30 °C and complete unfolding at 37 °C. It was assumed that the elevated reaction temperatures interfered negatively with the crosslinking reaction by denaturing collagen.

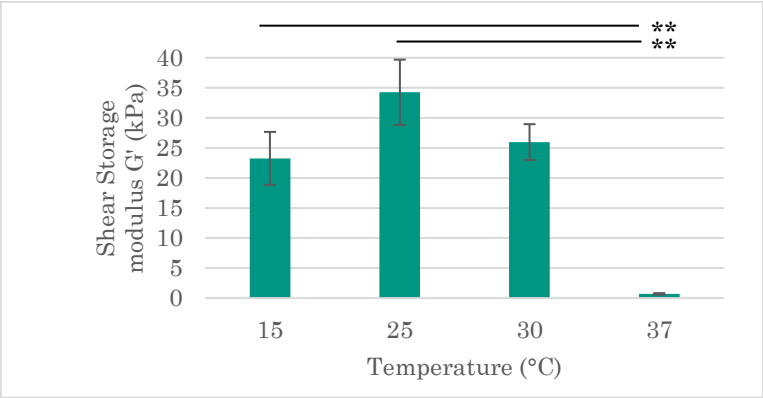

Figure 2-14: (A) Max. measured stiffness at different reaction temperatures for 40 mg/ml rCol crosslinked by a MR of 1:1 DMTMM. Respectively 2 ml sample were used and analyzed with the ElastoSens™ Bio. (N=2). All data was normally distributed. A homoscedastic two-sided Student's t-test was performed (*, **, *** represent $\alpha < 0.05$, 0.01, and 0.001, respectively).

To increase the validity of the temperature-dependent gelation, other established crosslinking technologies were tested like the rCol/PEG composite at different temperatures which also demonstrated a change in rheology with reaction temperatures between 30 °C and 37 °C. In summary, the stiffness of DMTMM crosslinked rCol hydrogels can be adapted in a broad range in alignment with the final applications. By restricting the MR of DMTMM to max. 1:1 and using a collagen concentration of 20-40 mg/ml, a stiffness range of 1.5 kPa – 30 kPa was identified. By further reducing the rCol concentration, even lower stiffnesses were expected. To further understand the correlation of stiffness and the rate of formed crosslinks within the synthesized hydrogel a colorimetric assay was used in the following chapter.

2.2.2.2.2 Network density

The hydrogel stiffness was assumed to correlate with the intramolecular and intermolecular covalent bonds which formed during the synthesis. To better understand the correlation, one rCol concentration (20 mg/ml) was crosslinked with different MRs (1:0.1 – 1:3). By normalizing all data on the absorbance signal of non-crosslinked rCol, a MR dependent share of free NH_2 groups was detected (see Figure 2-15, A).

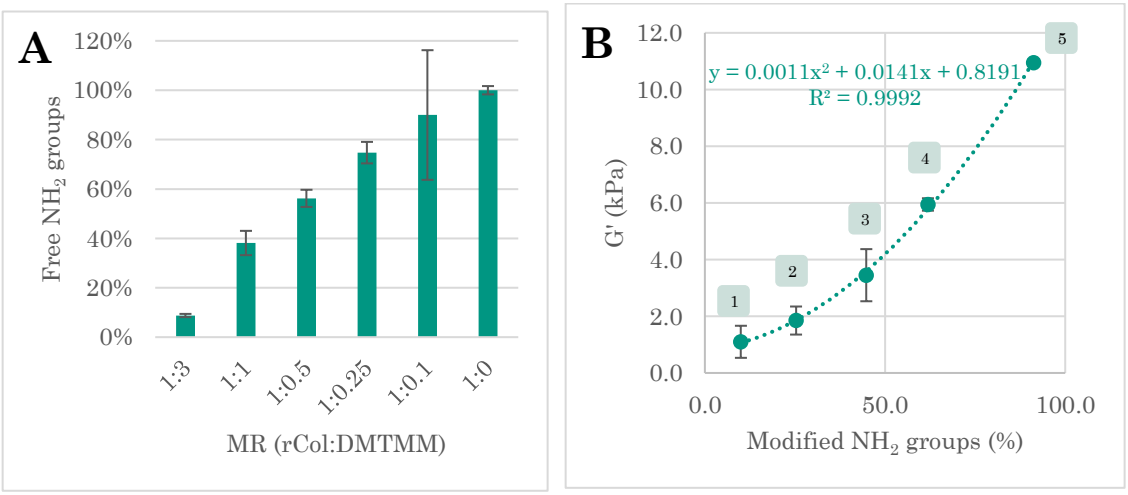

Figure 2-15: (A) Reaction efficiency determination *via* ninhydrin staining using 20 mg/ml rCol in ddH_2O. The experiment was repeated twice. **(B)** Correlation of data from (A) and the measured shear storage modulus G' of the respective formulations. The formulations were indicated by the numbers 1-5 comprising the MRs of rCol to DMTMM of 1:0.1 to 1:3 (N=5) A polynomial fit was added with Excel. All data was normally distributed.

While a 1:0.1 ratio reduced the NH_2 signal by 10% (compete turnover), a 1:0.5 ratio led to 44% signal decrease and a 1:1 ratio a signal decrease of 62%. By increasing the molar ratio to 1:3, a signal decrease of 91% was measured. Next, the rate of modified primary amines was correlated with the final stiffness of the resulting hydrogels demonstrating an

exponential increase in stiffness with increased crosslinks (see Figure 2-15, B). Based on the high ratio of primary amines present in rCol compared to animal-derived collagens (described in the introduction) much higher stiffnesses were expected by chemical crosslinking. In summary, a correlation of hydrogel stiffness and network density was detected.

2.2.2.2.3 Porosity and swelling

In the introduction, a great porosity was correlated with great swelling properties. To visualize internal pores, synthesized hydrogels (according to chapter 4.2.4.3) were freeze-dried (according to chapter 4.2.4.8) and imaged using Scanning Electron Microscopy (SEM) (according to chapter 4.2.6.2). Obtained data gave a first prediction about the swelling capacities as well as the liquid update due to the visualized porosity. As a reference, a commercially available animal-derived collagen sponge was tested (Geistlich BioGride). The animal-derived reference patch showed a fiber like structure with a more closed surface and an undefined inner porosity. Determination of the average pore size was neglected due to the lack of defined pores. The DMTMM crosslinked rCol sample showed a generally hollower structure with more holes in the surface, and a more homogenous pore distribution of similar shape (see Figure 2-16). The diameter of 10 inner pores was measured with the software ImageJ which resulted in an average pore size of ~150 µm with a standard deviation of ~70 µm.

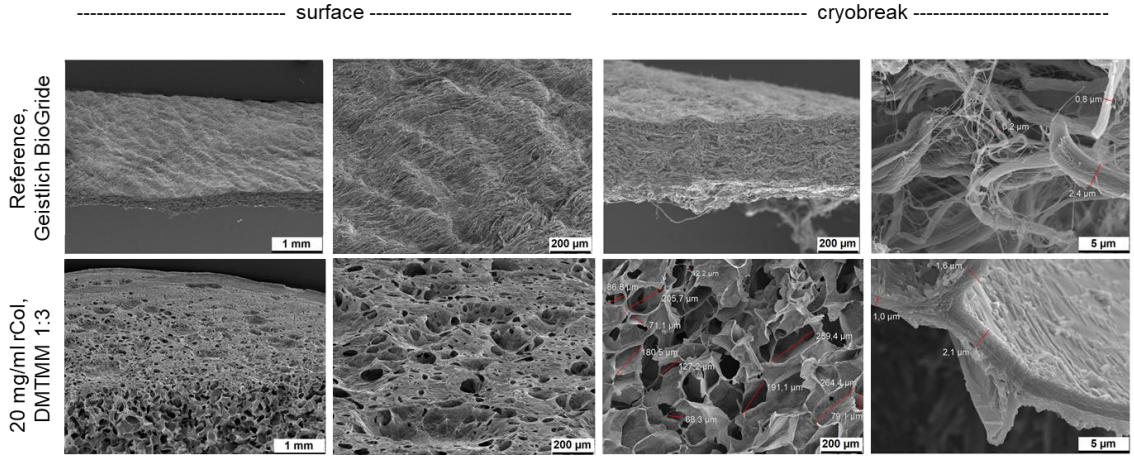

Figure 2-16: SEM pictures a DMTMM crosslinked collagen sponge vs. an animal-derived reference product (Geistlich BioGride).

To further explore aberrations in porosity, different formulations were analyzed ranging from 25 mg/ml – 50 mg/ml rCol with two MR of DMTMM (1:0.4 and 1:0.8). SEM imaging of all samples looked similar by observing the surface and the cross-section (see Figure 2-17, A). To identify differences, the diameters of 25 pores per sample were measured using ImageJ and categorized in different size cluster (see Figure 2-17, B). All formulations showed

comparable pores with diameters of ≤200 µm. A difference was observed in the medium (201-399 µm) and high (400-700 µm) pore size range. While a MR of 1:0.8 led to similar pore diameters for all concentrations of rCol, the tested MR of 1:0.4 resulted in bigger pores by decreasing the rCol concentration (25 mg/ml > 40 mg/ml > 50 mg/ml). The bigger the pores in the sponge microstructure, the bigger was the expected swelling behavior. In summary, all collagen sponges made from rCol showed a comparable macro- and microstructure. The pore size was adjustable by altering the formulation and the number of crosslinks, which showed a bigger pore size by decreasing the MR of DMTMM and the rCol concentration.

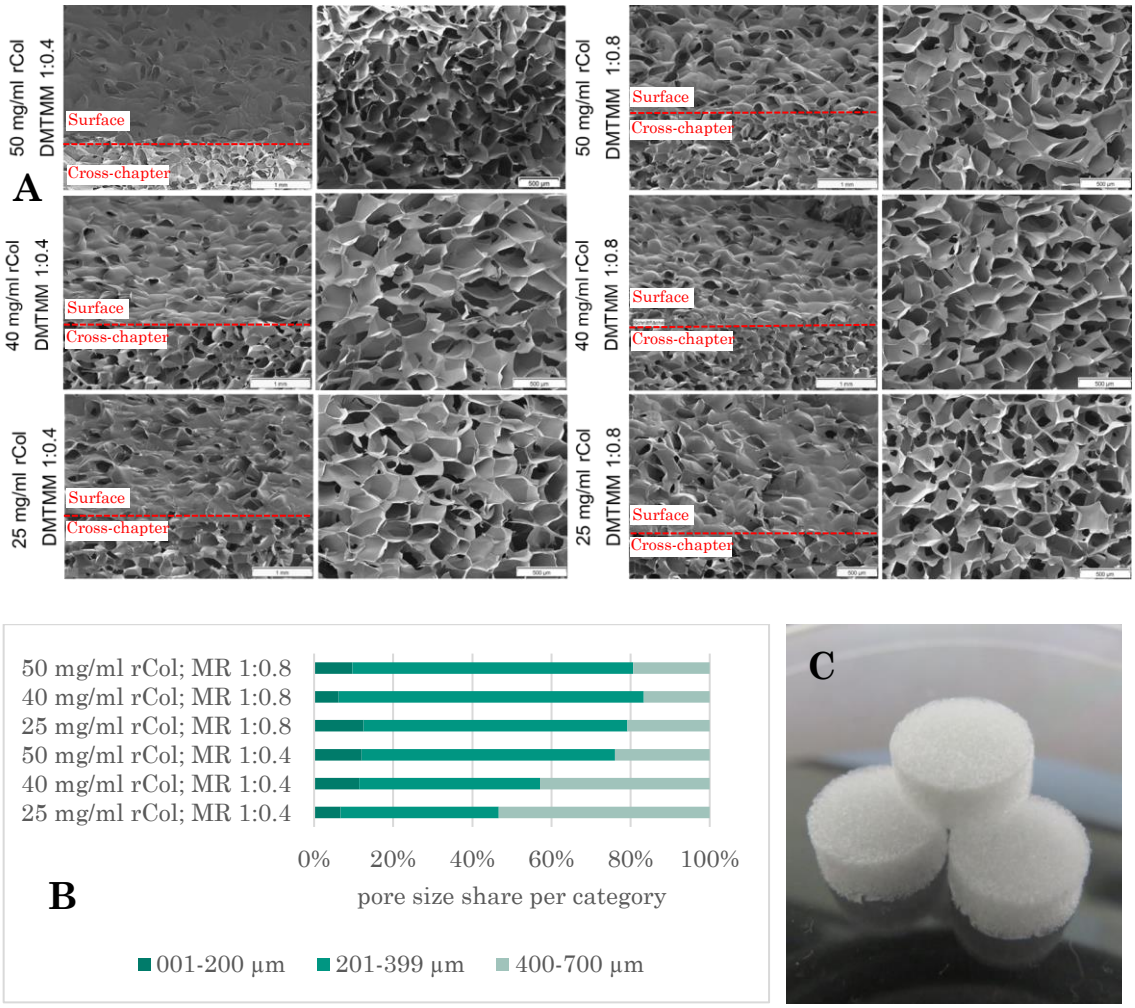

Figure 2-17: (A) SEM imaging of the interfaces between surface and cross-section (1 mm scale bar) and the cross-section (500 µm scale bar). **(B)** Pore size share within the different tested formulations (N=2). 25 pores were analyzed per sponge with the software ImageJ. **(C)** Representative DMTMM crosslinked rCol sponges made from 25 mg/ml rCol and a MR of 1:0.8.

Swelling properties were important for collagen patches or sponges because they can affect the performance of the product. Regarding wound healing, a high swelling can help to

maintain a moist environment for wound healing. This can also help to control bleeding and exudate in the wound area. Also the mechanical properties are highly effected such as their strength and elasticity. This can impact how well the product fits into the wound site and how it interacts with surrounding tissues. Furthermore, the swelling properties of collagen sponges or patches can affect their drug delivery capabilities. If the sponge or patch swells too quickly or too much, it may release incorporated substances like drugs too quickly in case of diffusion-based release mechanism and impaired swelling might not release the drug effectively. Therefore, a good understanding and controlling the swelling properties was important for optimizing their performance for the developed drug delivery patch. To test the swelling capacities sample specimen were prepared based on different formulations as described in chapter 4.2.4.8. Subsequent swelling in 1×PBS at 37 °C showed differences in the resulting wet weight (see Figure 2-18). A high equilibrium swelling ratio (720%-2280%) compared to literature (~650%)[320] was measured within the first 30 min which remained constant for at least two days. A formulation dependent difference in swelling was observed with a clear trend. The higher the MR and the rCol concentration the lower was the resulting water uptake. Here, only two rCol concentrations (20 and 40 mg/ml) and three MR (1:3, 1:1 and 1:0.5) were tested. By extending the formulation range even broader equilibrium swelling ratios were expected and can be explored in future attempts for product specific applications. By blending in other materials like chitosan (25% collagen and 75% chitosan) swelling ratios of 2348% [321] or even 4036%[322] were published. With NaCl as porogen, a recombinant human-like collagen expressed in *E.coli* (crosslinked with transglutaminase) demonstrated a swelling ratio of ~ 3250%.[323] Blending rCol with these materials (especially hyaluronic acid (HA)) or applying pore forming agents could be interesting to increase the swelling capacity of the product further. The high swelling ratio makes DMTMM crosslinked sponges interesting for products with a high fluid absorption capacity. Increased swelling by using less DMTMM could also simplify regulatory approval. By correlating this data with the measured pore size in the previous chapter showed a correlation of increased swelling with bigger pores.

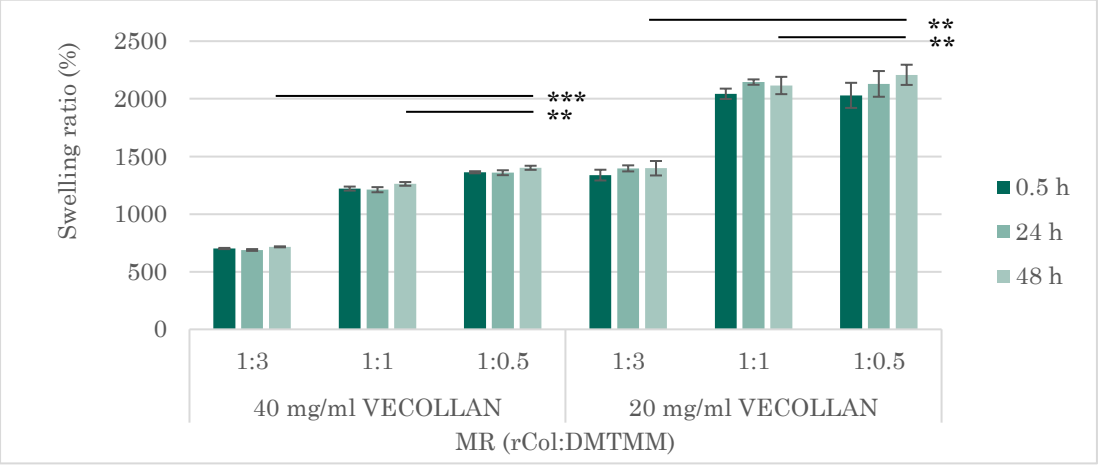

Figure 2-18: Swelling ratio of rCol sponges crosslinked with DMTMM after submersion in 37 °C 1×PBS. Gentamycin was added to avoid bacterial growth (N=3). All data was normally distributed. A homoscedastic two-sided Student's t-test was performed (*, **, *** represent $\alpha < 0.05$, 0.01, and 0.001, respectively).

2.2.2.2.4 Degradation

The time-dependent degradation of rCol hydrogels is an important parameter to estimate the long-term stability of the product as well as the biodegradation *in vivo*. Especially for tissue remodelling, a tissue-specific degradation pattern is highly desired to build up body-own matrices while the incorporated matrix is degraded. Two different degradation experiments were performed for this thesis: hydrolysis and enzymatic degradation. Test specimen were prepared according to chapter 4.2.6.6.1 and freeze-dried according to chapter 4.2.4.8 followed by exposure to 1×PBS buffer at 37 °C for two weeks. The dry weight before wetting was compared to the re-dried hydrogel sponge after different timepoints. Generated data for hydrolysis were depicted in Figure 2-19 (A). After one day of incubation, an initial weight loss was documented for all test specimen, which increased slightly with higher rCol concentrations and strongly with a higher initially applied molar ratio of DMTMM. It was assumed that remaining DMMTM and its side products were washed out of the hydrogel after synthesis. Most cases demonstrated a stable remaining weight without further weight loss for the remaining incubation time. The reason for the increasing weight gain with 20 mg/ml rCol samples by reducing the MR of DMTMM remained unclear. In summary, all samples showed hydrolytic resistance within two weeks test time. Enzymatic degradation is important for *in vivo* applications. Here a mixture of enzymes (secreted by *C. histolyticum)* was applied with a strong enzymatic activity.[324] The enzymatic mixture was chosen instead of a human collagenase due to the common usage[325,326] and the comparable kinetics to matrix metalloproteinases.[327] The two main enzymes are collagenase and clostripain.[328] Different types of collagen are natural substrates for collagenases. Here collagen hydrogel sponges with identical

hydrogel shapes were pre-swollen in reaction buffer (50 mM $CaCl_2$ in 0.1 M TRIS-HCl pH 7.4) and exposed to the enzyme mixture at 37 °C. The decrease in wet weight was documented over time (see Figure 2-19, B). The used samples showed no weight loss over an incubation time of 24 h except for one formulation (40 mg/ml rCol, MR of DMTMM of 1:0.5) which led to the assumption, that the produced samples were resistance to the exposed enzymes. For future experiments, other metalloproteinases should be tested as well to get a broader understanding of the material degradation. Not all MMPs recognize identical aa patterns thus, enzymatic degradation might occur with other enzymes. Additionally, longer incubation times could be tested to intensity effects. In summary, DMTMM crosslinked rCol samples didn't show hydrolytic or enzymatic degradation under the tested conditions. Further investigations are recommended to verify this effect. The stability of these products makes them an interesting approach for implants or other applications which benefits from a strong material integrity over time.

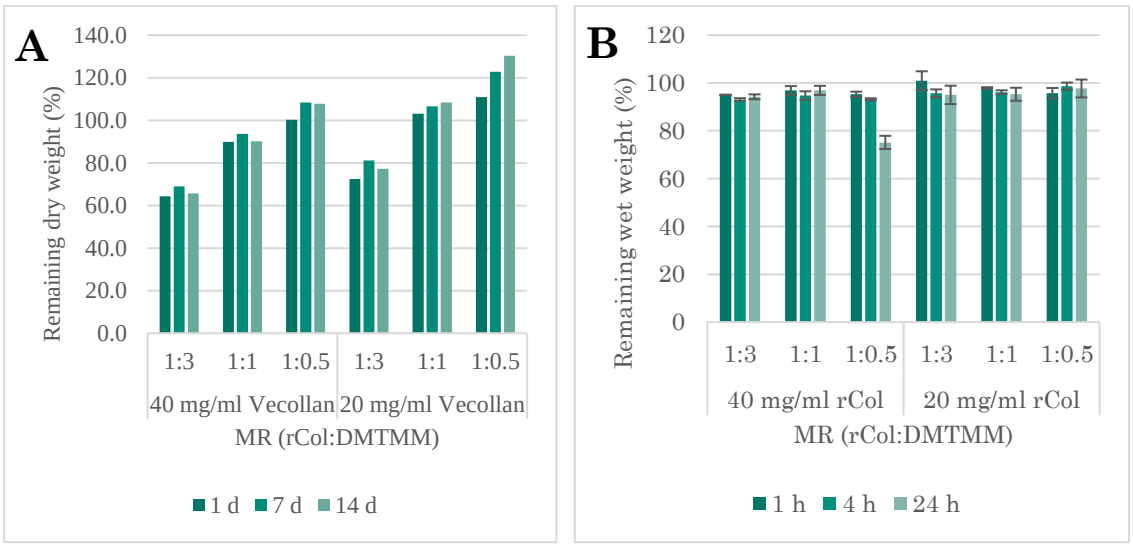

Figure 2-19: (A) Hydrolysis over two weeks (N=1). **(B) Enzymatic hydrolysis** *via* Collagenase (from *Clostridium histolyticum*) over 72 h incubation time at 37 °C. Freeze dried hydrogels with identical, initial hydrogel volume were swollen in Collagenase buffer for 24 h followed by fluid replacement by buffer with enzyme (N=3). Sample groups with missing data at different timepoints mean complete hydrolysis. The sample description describes the applied concentration of rCol followed by the molar ratio of functional groups within one mole of rCol compared with the ratio of functional groups in one mole crosslinker or activation reagent (N=3). All data was normally distributed.

2.2.3 rCol/PEG composite

2.2.3.1 Background

One of the main benefits of hydrogels is the high-water content which is associated with a great biocompatibility. Made by a collagen-like protein (rCol) and a bioinert PEG-linker the product was expected to achieve bioinert and biodegradable hydrogel properties which could be used as a pure material or in combination with a stronger organic polymer product like PLGA or PLA for hernia meshes. Also, the combination thereof could be used for implants to improve cellular colonialization in comparison to implants made purely from organic polymers. Within this chapter, the rCol combination with a PEG polymer linker was tested for hydrogel synthesis. The biocompatibility of the composite, the fabrication thereof and the application for injectability applications and for hydrogel-based membranes was evaluated.

2.2.3.2 The formulation optimization

The described molar ratio (MR) of rCol to crosslinker (XL) was based on number of primary amines per molecule rCol and the four NHS moieties per molecule of 4PEG-SG (see Scheme 1-3). rCol contains 22 lysines and one terminal NH_2 group. As result, an equimolar ratio (1:1), described one mol of rCol vs. 5.75 mol of 4PEG-SG. In the following, the applied MR of different formulation was depicted in the following format: MR of functional side chains in rCol to NHS groups in 4PEG-SG (1:X).

2.2.3.2.1 The gelation range

For NHS-based active esters like 4PEG-SG a pH of 7.2 - 9 was recommended by literature.[329] Therefore, a 0.1 M HEPES buffer with pH 8 was investigated. To identify the mimical concentration for hydrogel formation a concentration range of 2.5 – 30 mg/ml rCol and a MR range of rCol to 4PEG-SG of 1:0.1 – 1:1.6 was tested for the 4PEG-SG crosslinker. Gelation was achieved within seconds to hours. Hydrogel formation was possible starting from 5 mg/ml rCol but limited the recommended rCol concentration range of maximal 20 mg/ml. An overview of tested formulations and the differentiation of gelated and non-gelated formulations was depicted in Figure 2-20. Higher concentrations of rCol caused gelation within seconds which made material processing highly challenging and required very short homogenization and fast molding times. When the PEG-linker was applied in excess, turbidity was observed. The higher the applied rCol concentration, the lower the required MR of 4PEG-SG to cause turbidity (data not shown here). In a summary, recommended formulations comprised concentrations between 5 - 20 mg/ml of rCol and a MR of rCol to 4PEG-SG of 1:0.1 – 1:0.8.

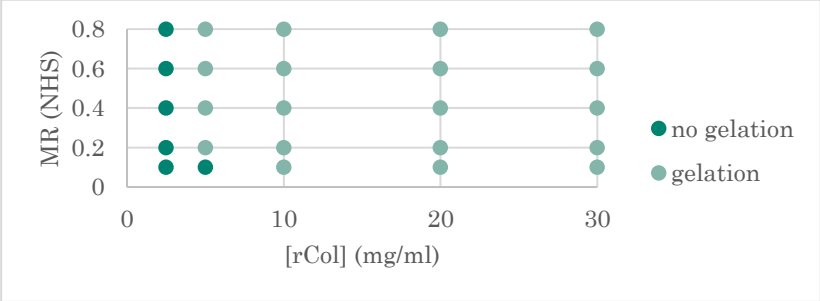

Figure 2-20: Results of up-side down vial test with selected formulation of rCol and 4PEG-SG. Sample vials were incubated at RT for 24 h with 300 µl formulation each. Gelation and no sufficient gelation were visualized with different colors.

2.2.3.2.2 The influence of pH

As described in the previous chapter, NHS-based coupling reactions are pH-dependent. To explore the effect of pH on the gelation speed, three different buffer systems around the neutral point were tested (0.1 M MES pH 6.0, 1x PBS pH 7.4 and 0.1 M HEPES pH 8.0) within the recommended formulation range of (5 - 20 mg/ml rCol and a MR of 4PEG-SG of 1:0.2 - 1:0.8). Gelation was performed at RT for 24 h in closed HPLC vials. The gelation time was determined *via* "up-side down vial assay" as shown above. Fastest gelation kinetics were recorded at pH 8.0 (see Table 2-3). For this reason, a pH of 8.0 was used as standard pH for further experiments. Nevertheless, gelation with 1×PBS (pH 7.4) was possible as well, which could be highly relevant for cellular applications. Due to slowed gelation kinetics with 1×PBS, also higher rCol concentrations were possible which led to even stiffer hydrogels.

Table 2-3: Gelation time observation for 4PEG-SG reaction products in three different buffer systems (0.1 M MES pH 6.0, 1x PBS pH 7.4 and 0.1 M HEPES pH 8.0). Samples with no gelation within 24 h incubation time at RT were labelled with '*' as well as successful (✓) and insufficient gelation (✗).

rCol (mg/ml)	MR (XL)	Gelation (yes/no)			Gelation time (min)		
		pH 6.0	pH 7.4	pH 8.0	pH 6.0	pH 7.4	pH 8.0
5	1:0.2	✗	✓	✓	*	67	20
5	1:0.4	✗	✓	✓	*	45	10
5	1:0.8	✗	✓	✓	*	56	12
10	1:0.2	✓	✓	✓	>120	20	3
10	1:0.4	✓	✓	✓	>120	22	2
10	1:0.8	✓	✓	✓	>120	28	2
20	1:0.2	✓	✓	✓	>50	11	1
20	1:0.4	✓	✓	✓	>50	12	<1
20	1:0.8	✓	✓	✓	>50	16	<1

2.2.3.2.3 Reaction efficiency

The network density was expected to correlate with the final stiffness of the synthesized hydrogel. To visualize the network density within the formed hydrogel, one rCol concentration was selected (20 mg/ml), crosslinked by different MR of 4PEG-SG and colorized by ninhydrin staining according to chapter 4.2.5.2 to detect unreacted primary amines. Resulting data was shown in Figure 2-21. Resulting signals were normalized on the pure rCol signal. By adding increasing MRs of crosslinker, the number of free NH_2 groups continuously decreased. By using a MR of 1:1 (highest tested ratio), 35% free primary amines remained. In comparison with the DMTMM crosslinker (see chapter 2.2.2.2.2; Figure 2-15):, a divergent reaction efficiency was determined (see Figure 2-21, B). While a 1:1 ratio and a 1:0.1 ratio led to similar shares of crosslinked primary amines, MRs in between showed a higher crosslinked share of primary amines with the DMTMM crosslinker. Interestingly, the used exponential fitting curves expected a higher reaction efficiency for the 4PEG-SG crosslinker compared to the logarithmic curve behavior for the DMTMM crosslinker. This could be explained by the hydrolytic nature of DMTMM and the longer reaction time which competes with each other. In summary, data demonstrated an exponential correlation of rCol and 4PEG-SG. By using higher MR than shown, a complete turnover could be achieved by a MR of ~1:1.2.

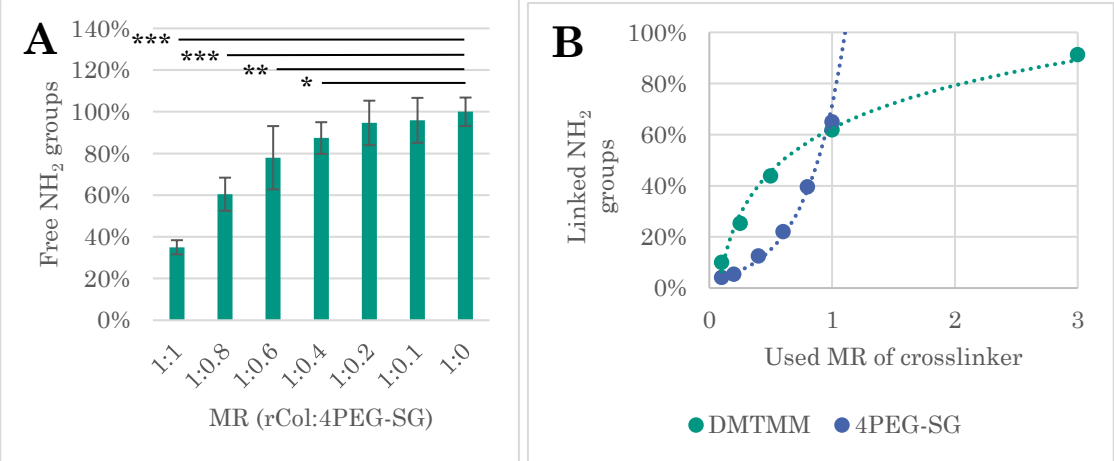

Figure 2-21: (A) Reaction efficiency determination *via* ninhydrin staining using 20 mg/ml rCol in ddH_2O. The experiment was repeated twice with N=2 each. **(B)** Crosslinker comparison (DMTMM vs. 4PEG-SG) regarding the reaction efficiency (N=4). An exponential trendline for 4PEG-SG linker and a logarithmic trendline for DMTMM reagent was calculated. All data was normally distributed. A homoscedastic two-sided Student's t-test was performed with Excel *, **, *** represent $\alpha < 0.05$, 0.01, and 0.001, respectively.

2.2.3.2.4 Leachables

As a part of the manufacturing process of hydrogels, washing steps were included to evaluate the effect on the biological safety of by-products which were generated during the crosslinking reaction. The high standard salt concentration of 0.1 M HEPES buffer is not isotonic and will form a hypertonic osmotic pressure that might damage exposed tissue cells. To avoid this effect, cell compatible HEPES concentrations were extracted from literature (10-25 mM)[330] which led to an application concentration of 20 mM HEPES buffer for this experiment. Hydrogels formed within the normal time frame and were processed according to the description in chapter 4.2.3.2. Considering the assay conditions, no toxic effect was determined with the first washing solution (see Figure 2-22). No additional washing was needed with the applied cell compatible buffer concentration of 20 mM HEPES buffer pH 8.0. The great viability made the rCol/PEG composite interesting for cell encapsulation trials. The increase of viability to >100% within the 3rd washing fraction for some formulations remained unclear. The results obtained in this study indicated no cytotoxic effect of by-product (*N*-Hydroxysuccinimide) and unreacted crosslinker for the tested formulations. To finally confirm the non-cytotoxicity, additional tests might be necessary, such as a leachable/extractable assay according to the ISO-10993-12/18.

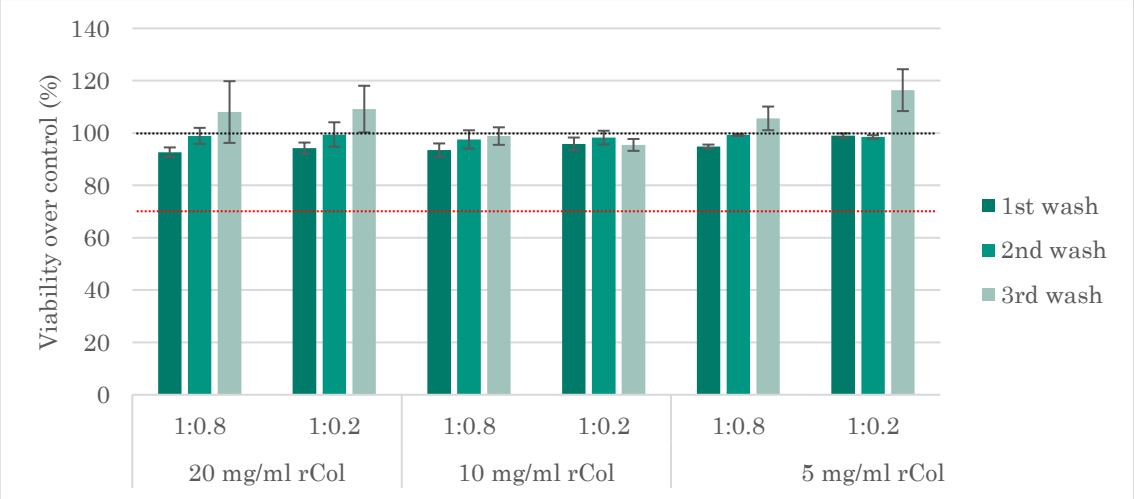

Figure 2-22: MTS cytotoxicity assay. Successive washing solutions of different hydrogel formulations were exposed to pre-seeded HFF for 24 h each. 220 µl hydrogel samples were washed 1 h at 37 °C with 440 µl culture medium. The measured viability of the control group was displayed by a black dotted line and the defined threshold for safe medical devices by ISO Norm 10993-5 of 70% in red (N=3). All data is normally distributed.

2.2.3.3 Mechanical characterization

2.2.3.3.1 Rheology

In analogy to chapter 2.2.2.2.1, the rheological properties were measured using the ElastoSens™ Bio device. In Figure 2-23, the measured shear storage moduli were blotted. Within the tested rCol concentration range of 0.5-20 mg/ml in combination with different MR of 4PEG-SG (1:0.2 and 1:0.8), shear storage moduli between 0.4 and 14.2 kPa were measured. Next, the influence of the reaction temperature was explored as previously done in chapter 2.2.2.2.1 for the DMTMM crosslinked reaction products. With DMTMM as crosslinker, data showed a decrease in stiffness by applying increasing reaction temperature between 25 °C and 30 °C (see Figure 2-14). At a reaction temperature of 37 °C, no hydrogel formation was observed at all. To validate the temperature effect, the experiment was repeated with the 4PEG-SG crosslinker. Data showed a comparable stiffness between 15 and 33 °C. 33 °C was defined in chapter 2.1.1.3, Figure 2-3 as the melting temperature of rCol. By applying higher reaction temperatures (37 °C and 45 °C), lower and comparable values were generated and hydrogels formation was observed. In summary, generated data validated the influence of the reaction temperature on the resulting hydrogel stiffness. To avoid changes in stiffness, material handling below 33 °C was recommended. Data showed the importance of the triple helix during gelation for hydrogel formation.

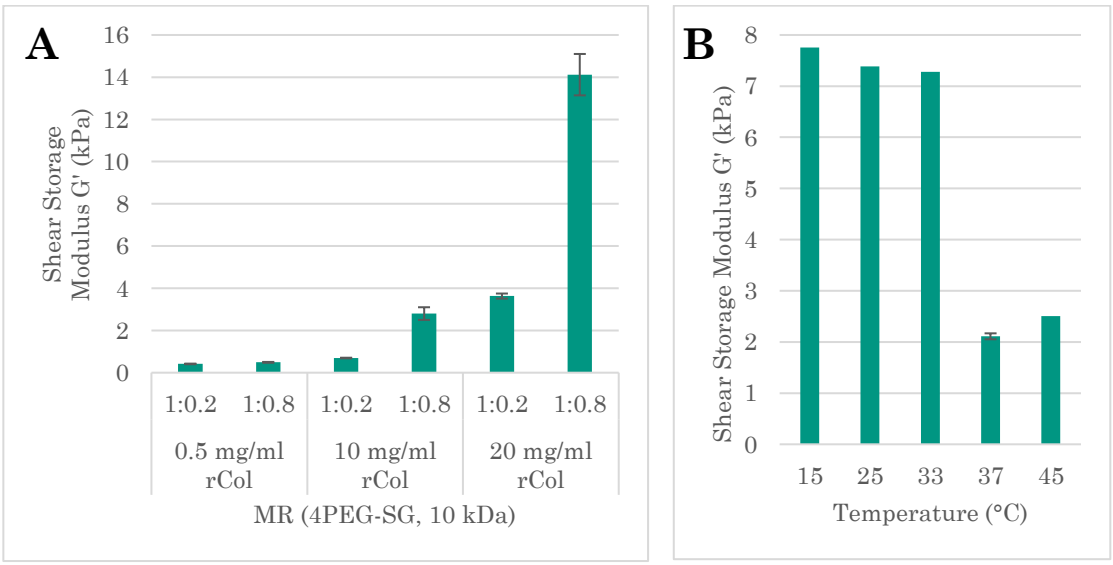

Figure 2-23: (A) Shear Storage Moduli (G') of fully gelated rCol hydrogels extracted from the plateau phase of the online kinetic measurements using the ElastoSens Bio™ using 4PEG-SG crosslinker for hydrogel synthesis (N=2). **(B)** 30 mg/ml rCol with 4PEG-SG and a MR of 1:0.2 at different temp. The solution w/o crosslinker was incubated 15 min at the respective temp. to denature the rCol. The 37 °C sample was tested in duplicate. All data was normally distributed.

2.2.3.3.2 Porosity and swelling

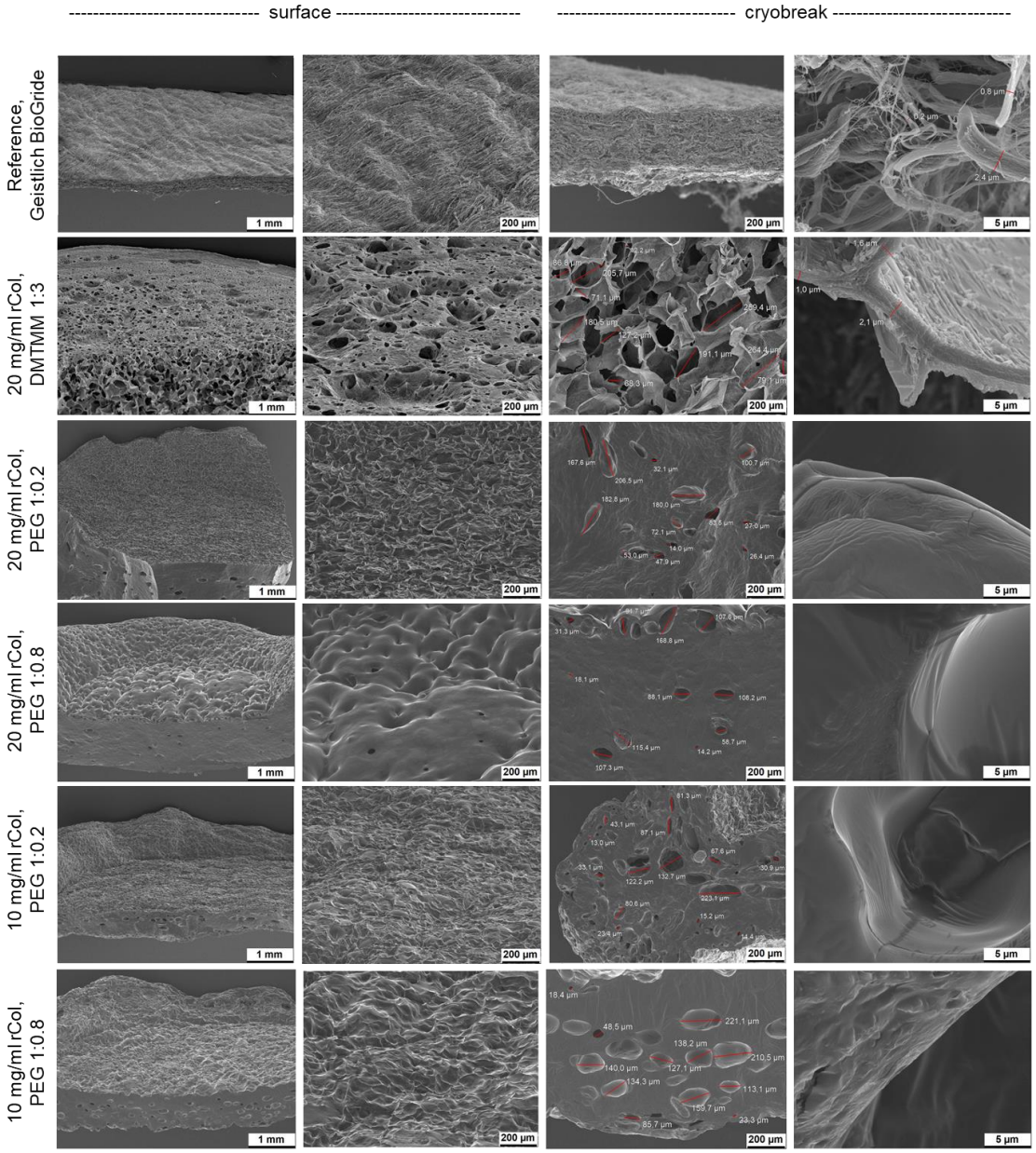

Figure 2-24: SEM pictures of rCol sponges crosslinked with DMTMM or 4PEG-SG including an animal-derived reference product (Geistlich BioGride).

In accordance with chapter 2.2.2.2.3 porosity and swelling were analyzed. As reference, a commercially available animal-derived collagen sponge was tested (Geistlich BioGride). Hydrogels and sponges were prepared according to chapter 4.2.4.4 and chapter 4.2.4.8. Experimental data of this study showed a strong difference between the commercially available, animal-derived reference patch (BioGride) and rCol samples crosslinked by DMTMM (see Figure 2-24). Both showed a rather good porosity compared to all rCol/PEG composites. The

rCol/PEG composites demonstrated a closed open porosity and a bad pore formation within the sample. Differences within the 4PEG-SG crosslinked samples were identified. The higher the rCol concentration, the less pores were detected. In summary, rCol/PEG composites demonstrated less porosity and were expected to swell significantly less compared to the DMTMM crosslinked rCol samples. To quantify swelling, the experimental procedure for Figure 2-18 (chapter 2.2.2.2.3) was repeated with selected rCol/PEG composites. As expected, a low swelling ratio was documented (~400-800%) compared to the reaction products with DMTMM (see chapter 2.2.2.2.3; Figure 2-18). Also longer swelling times were required to achieve stable values. Sample made from 5 mg/ml rCol and a MR of 1:0.2 showed sample disintegration between 24 h and 48 h after starting the experiment. It was assumed that the PEG composite has higher sensibility to hydrolysis compared to the DMTMM crosslinked reaction products which was quantified in chapter 2.2.2.2.4 and chapter 2.2.3.3.1. In summary, rCol/PEG composites were interesting for drug delivery by matrix swelling and for surface coatings to avoid cellular ingrowth. The potential for matrix injections was tested in a later chapter (see chapter 2.2.4.1).

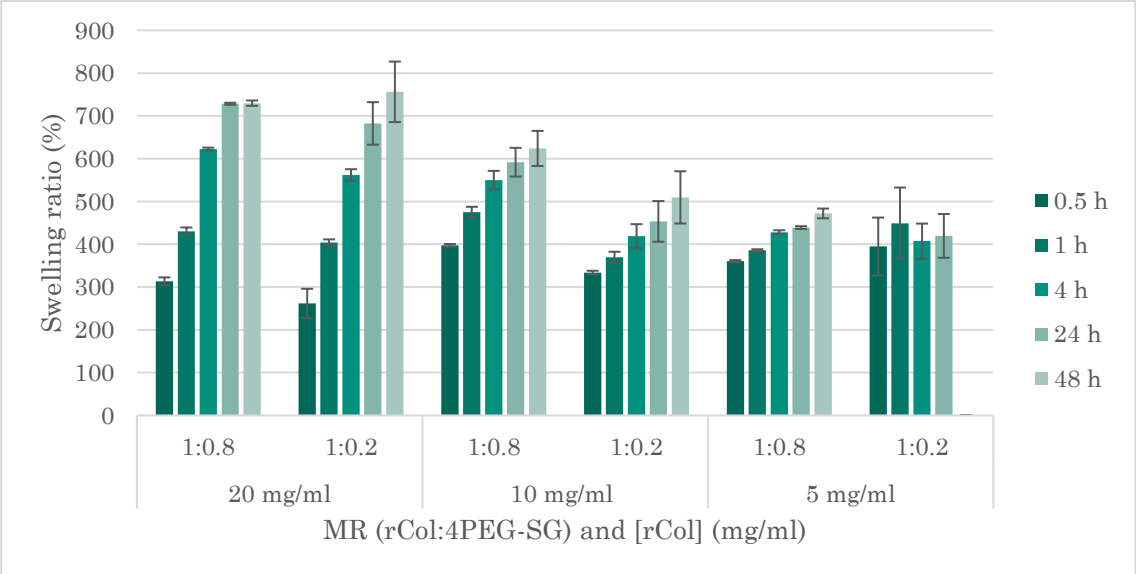

Figure 2-25: Swelling ratio of rCol sponges crosslinked with 4PEG-SG after submersion in 37 °C 1×PBS. Gentamycin was added to avoid bacterial growth (N=3). All data was normally distributed.

2.2.3.3.1 Degradation

The degradation was determined as described in chapter 2.2.2.2.4. Hydrolysis data (Figure 2-26 (A)) demonstrated an initial weight loss within one day of incubation for all samples. The loss in weight was stronger for low rCol concentrations and less applied crosslinker. Samples were prepared with 100 mM HEPES buffer each. It was assumed that washed out

HEPES salts and partially not crosslinked collagen strands caused the change in weight. As a result, the value after one day was evaluated as the better reference und residual values were normalized anew in Figure 2-26 (B). Within one week of incubation all samples crosslinked with a MR of 1:0.8 lost 1-9% of their weight while samples crosslinked with a MR of 1:0.2 dissolved completely except for the highest tested rCol concentration (20 mg/ml). After two weeks of incubation, all tested formulations with less 4PEG-SG crosslinker were disintegrated while all samples with high crosslinker concentration (1:0.8) remained with 4-18% weight loss compared to the value after one day of incubation. Data demonstrated a formulation dependent, adjustable hydrolysis profile which can be influenced by the used rCol concentration and the MR of applied crosslinker.

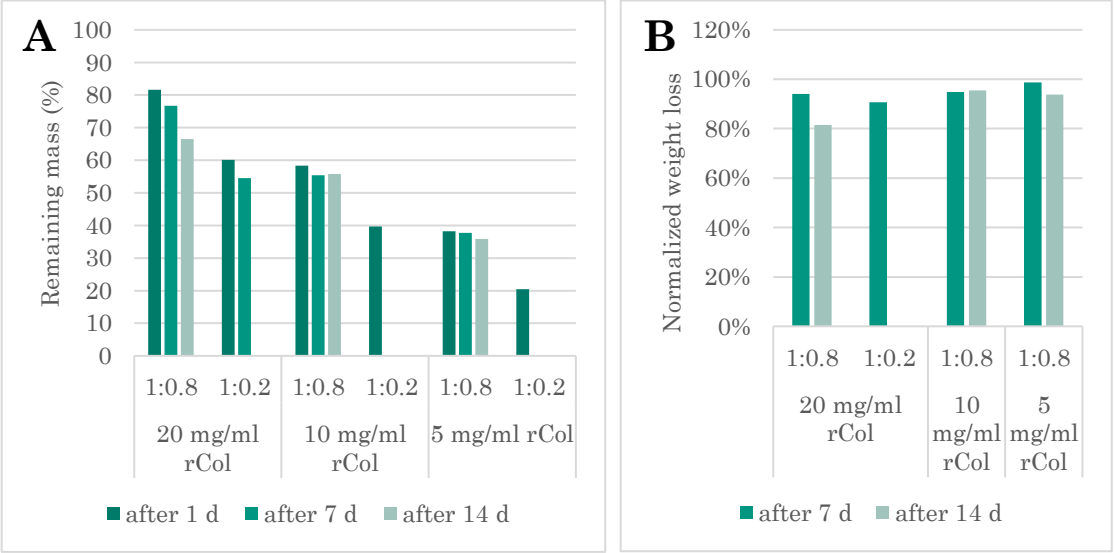

Figure 2-26: Hydrolysis over two weeks (N=1) in (A) absolute values and (B) normalized on the remaining mass after one day of incubation.

Enzymatic degradation was performed identically to chapter 2.2.2.2.4. The applied rCol/PEG test specimens reacted differently to the enzyme mixture (see Figure 2-27). After one hour, no loss in weight was observed. Comparably to the hydrolysis data, a stronger difference was observed by a change of the crosslinker ratio than by a change in rCol concentration. With a high MR of crosslinker (1:0.8), only the lowest rCol concentration (5 mg/ml) demonstrated full degradation within 48 h (maximal incubation time). With a lower MR (1:0.2) degradation effects were strongly rCol concentration dependent as well. While 20 mg/ml rCol samples demonstrated 24% weight loss after 8 h, 10 mg/ml rCol sample lost 70% in weight and the 5 mg/ml rCol sample disinterested completely already within 4 h. In summary, PEG composites showed an adjustable, formulation-dependent degradation behavior which could be interesting for applications which require a matrix degradation within a certain time window

for e.g. the release of an immobilized drug or non-permanent filler material that needs to be remodeled and replaced over time for the body's own tissues and ECM.

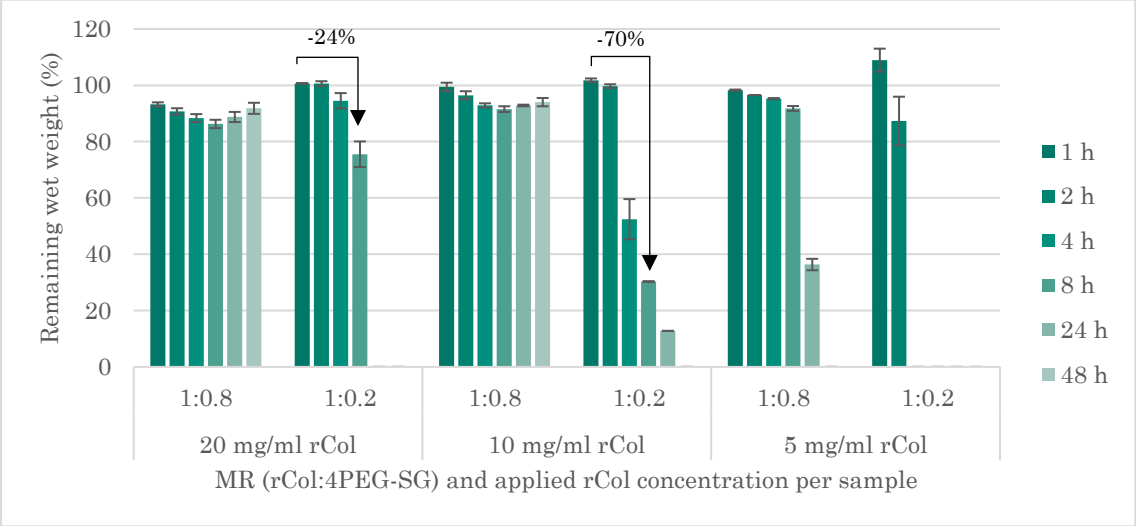

Figure 2-27: Enzymatic hydrolysis via Collagenase (from *Clostridium histolyticum*) over time at 37 °C. Freeze dried hydrogels with identical, initial hydrogel volume were swollen in Collagenase buffer for 24 h followed by fluid replacement by buffer with enzyme (N=3). Sample groups with missing data at different timepoints meant complete hydrolysis. All data was normally distributed.

2.2.3.4 Biological Evaluation

2.2.3.4.1 Cell adhesion

In the introduction of this chapter a change in cellular adhesion was hypothesized due to the natural cell-repellent PEG properties within the rCol/PEG composites.[331,332] To determine the effect of different PEG shares, different molecular weights of the 4PEG-SG linker were tested using standard 10 kDa and 40 kDa. As reference, DMTMM crosslinked rCol samples were tested and rat tail collagen (rtCol) which was chemically gelated with identical MRs and physically according to the manufacturers protocol with a shift of pH and temperature. To better compare the results with rat tail collagen, collagen concentrations were applied using 4 mg/ml for all rtCol and rCol/PEG formulations. Except for the physically gelated rtCol a MR of 4PEG-SG of 1:0.8 was used for all samples. For the DMTMM control, 4 mg/ml didn't result in a stable hydrogel. Therefore, a higher concentration of 20 mg/ml rCol was applied (MR of DMTMM). To achieve a broader understanding, several cell types were tested. The detailed experimental procedure was described in chapter 4.2.3.3. Briefly, thin rCol hydrogels were prepared in a 48-well-plate format. After gelation (humid atmosphere, 25 °C, overnight), hydrogels were washed (3x, with RNAse free, sterile ddH_2O, 220 µl each, 1 h

washing time per washing step on an orbital shaker, 200 rpm). To ensure sterility, samples were irradiated for 30 min with the UV light from a cell culture bench. Finally, hydrogels were washed once with full cell culture media (300 µl each; 1 h) to avoid osmotic pressure effects hydrogels were topped by $3x10^4$ cells/well. Cellular attachment was observed on the positive controls (plasma-treated cell culture plate and physically crosslinked rtCol). This was expected due to the great cell adhesive properties of both materials. rtCol/PEG composites showed a reduced cell adhesion compared to the physically gelated rtCol samples. No significant differences were detected in regards to the applied molecular weight of PEG linker. This first observation demonstrated a slight change in cell adhesion by implementing PEG units (see Figure 2-28). rCol/PEG composites showed cell repellent properties for all tested cell types. Similar results (lack in cell adhesion) were achieved with both tested molecular weights of PEG. Instead of cell-matrix interactions, cells attached to each other and started spheroid formation by cell-cell interactions. The effect was stronger for tested fibroblasts (murine and human foreskin) than with tested epithelial cells (HeLa; epithelial cell-line derived from cervical cancer) and bone cells (Cal72; osteosarcoma cell-line). Additionally, to 4 mg/ml rCol, the experiment was repeated with 10 mg/ml rCol concentration which showed the same effect. rCol hydrogels crosslinked with DMTMM showed different results for different rCol batches which demonstrated cell adhesion with a strongly different number of attached cells (see Figure 2-29). Repetition of the experiment showed issues with reproducibility (data not shown here). In conclusion, cell adhesion on DMTMM crosslinked rCol hydrogels was demonstrated as being possible, but the high variability in adhesion led to the conclusion that it is not usable for cell adhesive purposes, due to the fluctuating effect. Lack of cell adhesion of Scl2/PEG composites was already reported by Cosgriff-Hernandez *et al.* in 2010 by modifying Scl2 with 3.4 kDa Poly(ethylene glycol)-acrylate-*N*-Hydroxysuccinimide followed by photopolymerization. Thus, a lack of cell adhesion was not surprising.[333] In summary, positive controls demonstrated cell adhesion (cell culture plate surface and physically gelated rtCol). Chemically crosslinking rtCol, showed reduction in cell adhesion. Replacing rtCol by rCol led to loss of cell adhesion after crosslinking with 4PEG-SG. With DMTMM as crosslinker, resulting hydrogels showed cell adhesion. The rCol/PEG composite could be used for the spheroid or organoid production. To optimize cell adhesion, the topic was further addressed in chapter 2.3.4.6 with an alternative gelation approach using photopolymerization.

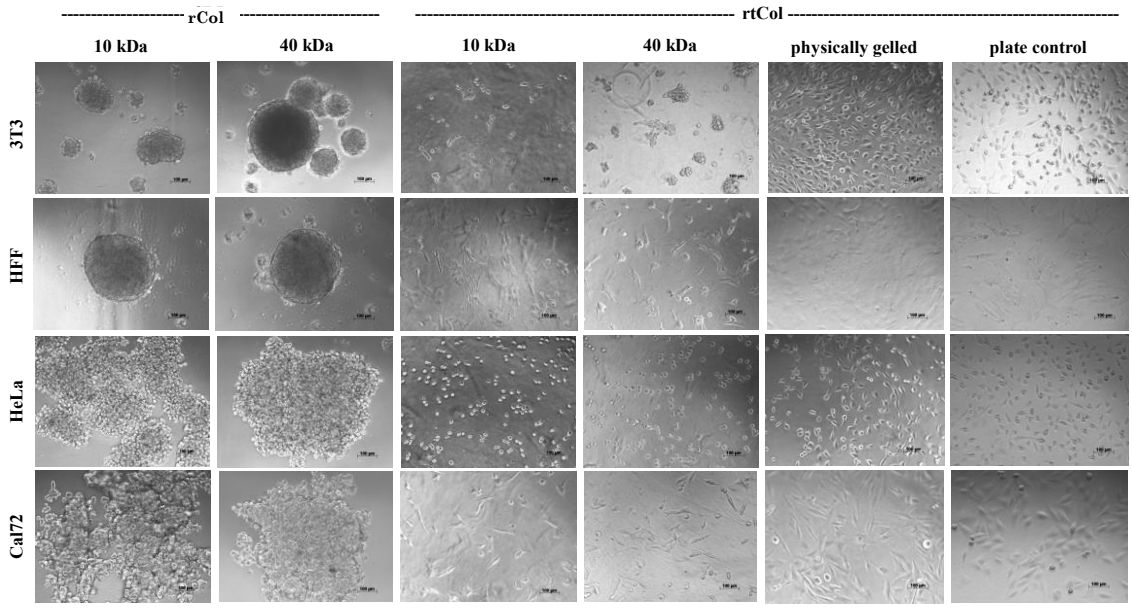

Figure 2-28: Cell adhesion on rCol/PEG and rtCol/PEG hydrogel surfaces with different cell types. All formulations were prepared with 4 mg/ml rCol, a MR of crosslinker of 1:0.8 and different molecular weights (10 kDa and 40 kDa). Rat tail collagen (rtCol) was crosslinked with the same MR. As control, plasma treated cell culture surface were used. The assay was performed as described in chapter 4.2.3.3. Cells were incubated for 24 h under cell culture conditions.

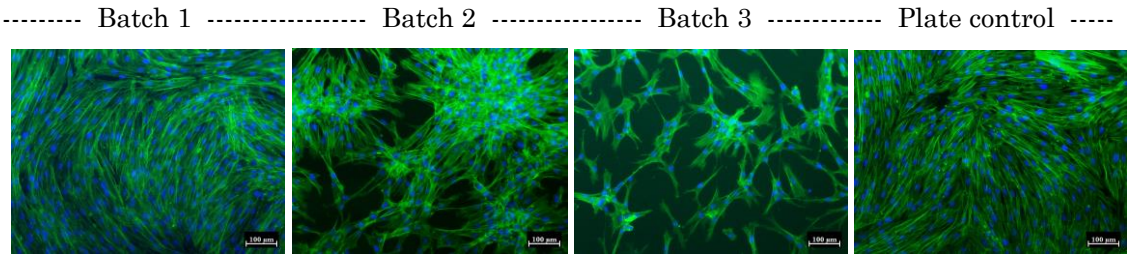

Figure 2-29: HFF adhesion on 20 mg/ml rCol hydrogels crosslinked with DMTMM (MR 1:3) (3 batches) and on a plasma-treated cell culture plate surface (plate control). Cells were incubated for 3 d. The experiment was performed several times. The depicted data was generated by a colleague (M. Liefke; Evonik Operations GmbH) and displayed with her consent. Cells were additionally stained with Phalloidin and Hoechst 33342.

2.2.3.4.2 Cell encapsulation trials

To evaluate the potential of DMTMM crosslinked rCol and the rCol/PEG composite for cell encapsulation, screening experiments were performed. Due to the slow gelation kinetics of the DMTMM reaction, high rCol concentrations were used to speed up the gelation prior to cellular precipitation. Due to these limitations the DMTMM crosslinker was not expected to be suitable. To reduce cytotoxic effects of DMTMM, it was used with low MRs which led to the following formulation test range: 20-60 mg/ml rCol (MRs of 0.4 - 1:1). Contrary to the

performed gelation tests with DMTMM as crosslinker where all tested formulations with 20 mg/ml rCol caused gelation (see chapter 2.2.2.1.1, Figure 2-11), lack of gelation was observed when cells were added to the formulation. It was assumed that side reactions with the cell surfaces increased the required concentration of DMTMM to form sufficient crosslinks for hydrogel formation. While cellular precipitation remained an issue (even higher rCol concentrations), cell stretching was only observed by chance in formulations with a low MR of DMTMM and a rCol concentration close to the gelation limit (see Figure 2-30). The experiment was repeated several times which showed no reproducible results. Furthermore, low viabilities were observed during cultivation, which decreased significantly with higher rCol concentrations and higher DMTMM ratios. Therefore, rCol crosslinking by DMTMM were not considered suitable for direct cell encapsulation.

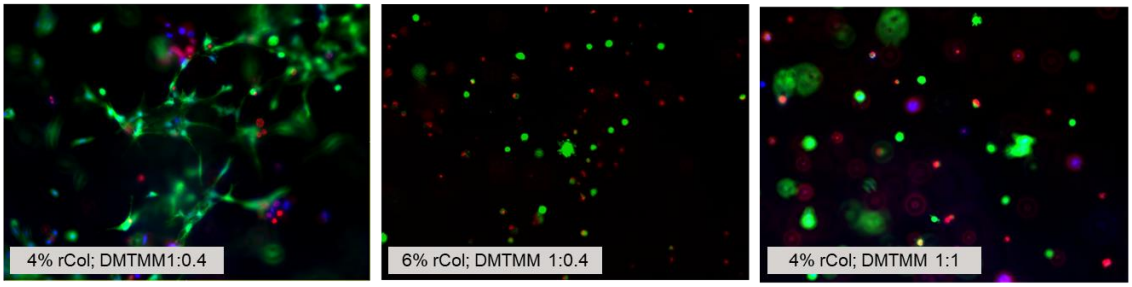

Figure 2-30: LIVE/DEAD/Hoechst 33342 staining of NIH3T3 cells after 7 d of culture. Cells were cultivated in 48 well plate format.

Next, the rCol/PEG composite was screened for cell encapsulation. Based on the results with DMTMM as crosslinker, cell stretching was preferred with low MRs thereof. For this screening a rCol concertation range of 20-40 mg/ml was used in combination with a MR range of 4PEG-SG of 1:0.1 – 1:0:3 according to chapter 4.2.4.3 (hydrogel synthesis) and chapter 4.2.3.7 (cell encapsulation conditions). No formulation showed cell stretching within 14 d. Cells remained round shaped with low viability determined by subsequent LIVE/DEAD staining (data not shown). In alignment with the data on porosity which showed a dense network formation (see chapter 2.2.3.3.2) and the lack of cell adhesion (see chapter 2.2.3.3.1), the rCol/PEG composite was evaluated as being unsuitable for cell encapsulation as well. To allow cell encapsulation while maintaining a great rheology, porosity and cell compatibility another technology (Photopolymerization) was introduced in in chapter 2.3 including cell encapsulation experiments in chapter 2.3.4.7.

2.2.4 Case studies

2.2.4.1 Drug Delivery Patch

2.2.4.1.1 Background

Collagen patches are used for the delivery of antibiotics. Here an alternative approach was pursued to deliver drugs to the site of action by incorporation thereof in a collagen patch. For crosslinking, the DMTMM crosslinker was selected due to affordable chemicals, observed porous networks (see chapter 2.2.2.2.3), capability wit a broad pH range, gentle production conditions compared to other technologies like the dehydrothermal method which requires vacuum and high temperatures, a wide range of interconnectivity due to high abundance carboxylic and aminic side chains, which enable a wide range of stiffness (see chapter 2.2.2.2.1; Figure 2-13) and a "pure" rCol product due to the function as activation reagent. No bridging spacers remain except for byproducts of the reaction. Collected data from chapter 2.2.2 identified rCol concentrations of 10-40 mg/ml in combination with MRs of DMTMM of max. 1:1 to obtain a safe product. The rheology of the resulting hydrogels was tunable and varied in a wide range up to 30 kPa (see 2.2.2.2.1, Figure 2-13). Additionally, the pore size was adjustable, and thus the swelling behavior. Crafted sponges were all porous, and the data obtained showed no hydrolytic effects over the test period of two weeks and no enzymatic degradation. Based on the generated findings, a tissue patch was explored in the next chapters that is flexible and allows sustained release of a model drug component over time. To develop a collagen patch for drug delivery, several criteria were defined like the ideal formulation, patch thickness, product flexibility (for minimally invasive administration and adaption to body movements without tearing), biocompatibility and biodegradability. A porous structure shall ensure strong swelling for a sustained drug delivery profile and to fully cover the implantation site. In the following these parameters were explored.

2.2.4.1.2 Patch Formulation

The formulation of the patch has a significant influence on the stiffness of the product. Different formulations were tested (10-80 mg/ml rCol + three different MRs of DMTMM (1:0.25, 1:0.5 and 1:1). Based on the literature research within the introduction (see chapter 1.4.6; Table 1-7) collagen patches comprise sponges made by freeze-drying. This is also beneficial to avoid hydrolytic effects within the network and can reduce drug leakage. Thus, crosslinked collagen hydrogels were freeze dried to achieve sponge-like collagen patches. 4x4 cm^2 PLA molds with Teflon-coatings were applied with 2 mm hydrogel height by adding 3.2 ml of formulation per mold. While 10 mg/ml rCol with a DMTMM MR of 1:0.25 didn't form a hydrogel (aligned with data from Figure 2-20), all other formulation did (see Figure 2-31). All

formulations were removable from the molds after freeze drying. Obtained patches were evaluated for its flexibility by bending them with the hand and evaluating the breaking angle (see Table 2-4). Most formulations broke when bended for max. 180° except for the 10 mg/ml rCol formulation with a MR of 1:0.5 and 1:1 of DMTMM, which demonstrated to be very flexible in dry state as well the formulation made from 20 mg/ml rCol with a MR of DMTMM of 1:0.25 after rehydration in water. Formulations with 80 mg/ml were brittle in the dry and wet state and were evaluated as not suitable for this application.

Table 2-4: Physical evaluation of the breaking angle of dry and wet rCol crosslinked sponges. Wetting was done by submersion in ddH_2O for 5 min.

rCol	MR	<30°	<45°	<90°	<180°	Rollable (>360°)
10	0.25	----------no sufficient gelation----------				
	0.5					dry / wet
	1					dry / wet
20	0.25			dry		wet
	0.5		dry			wet
	1	dry				
40	0.25			dry		wet
	0.5	dry				wet
	1	dry				
80	0.25	dry				
	0.5	dry				
	1	dry				

In summary, lower concentrations of rCol and DMTMM significantly increased the flexibility of the patch. The lower the rCol concentration, the higher the applicable DMTMM ratio to preserve patch flexibility. Most formulations with a DMTMM ratio of 1:1 broke. Therefore, lower MRs were desired. Formulations up to 40 mg/ml rCol were evaluated as feasible for a hydrogel height of 2 mm to allow bendability in a wet state. Within this trial 20 mg/ml rCol patches with a MR of 1:0.25 and 10 mg/ml rCol with a MR of 1:0.5 and 1:1 showed the best material properties. To include the affordability aspect, lower rCol concentrations were desired. Also, the formulation 10 mg/ml rCol, MR 1:0.5 formed a hydrogel and patch but the mechanical resistance remained low. Thus, the formulation with 10 mg/ml rCol with a MR of DMTMM of 1:1 was evaluated as interesting option.

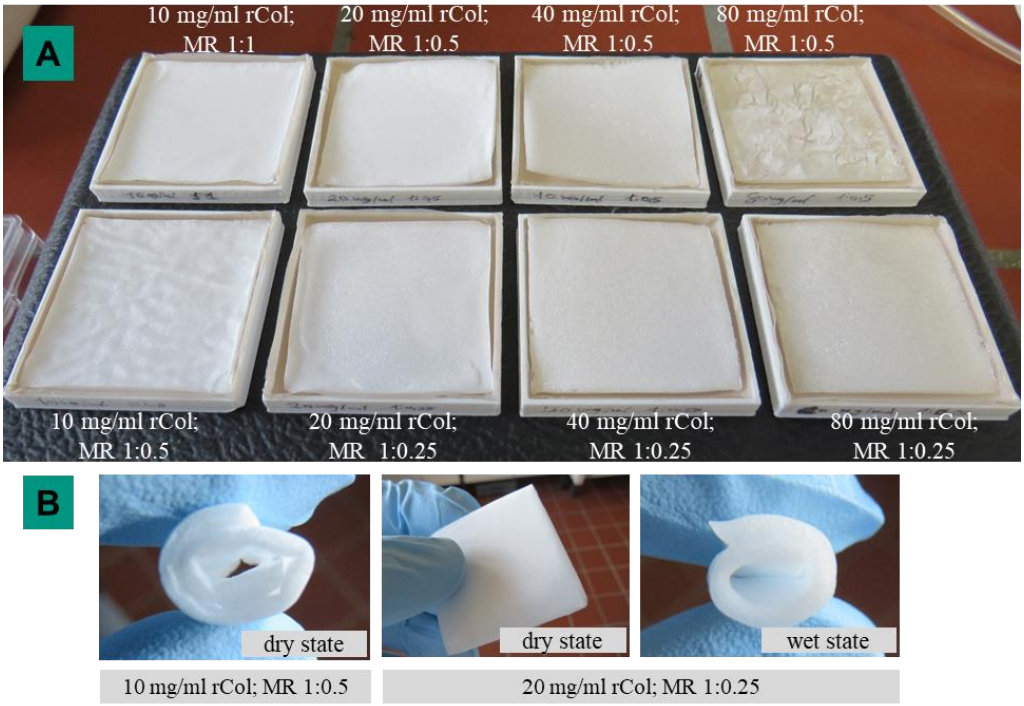

Figure 2-31: Formulation evaluation of rCol hydrogel patches after freeze drying. Wetting was done by submersion in ddH_2O for 5 min.

2.2.4.1.1 Layer thickness

Additionally, to the formulation optimization above, the layer thickness was evaluated in this chapter. Based on the optimized formulation with 10 mg/ml rCol, MR 1:1, different hydrogel heights were tested (2-8 mm; see Figure 2-32). After gelation and freeze-drying, prepared patches were removed from the molds and bent. At a thickness of 2 mm, the patch did not break when bent by 180° (dry and wet). Using 4 mm and 8 mm hydrogel layer thickness led to the breaking of the patches. Another observation was the general loss in height by freeze-drying. While the 2 mm patch lost 25%, the 4 mm patch lost 38%, and the 8 mm hydrogel patch lost 35% of its original height. Based on these results, a 2 mm hydrogel height was evaluated as best option for further developments.

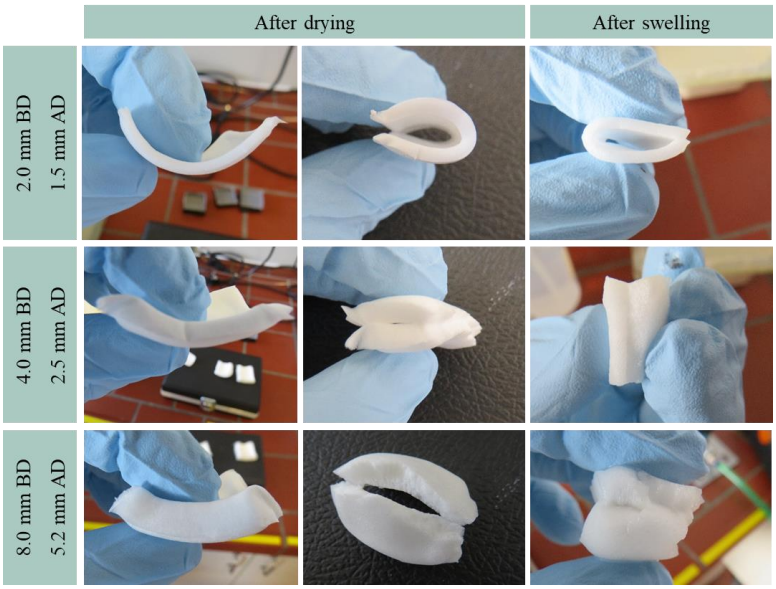

Figure 2-32: Hydrogel sponges before and after swelling (5 min in ddH_2O) made from 10 mg/ml rCol crosslinked with DMTMM with a MR of 1:1. Patches were bent for 180° in dry and wet state. Also, the layer thickness was measured before drying (BD) and after freeze drying (AD) as well as the lost in height.

2.2.4.1.2 Drug release performance

2.2.4.1.2.1 Caffeine release by diffusion

Drug delivery patches might have different requirements on the release profile of the API according to the final application. This might be considered during the development of such a product. In some cases and to match the desired release profile, the usage of a drug carrier (such as microparticles) could be useful. As hydrophilic systems especially hydrophilic APIs such as antibodies or growth factors might be of high interest. As PoC, two drugs were selected and tested (caffeine and meloxicam) due to their high usage and their convenient quantification by light absorbance. Caffeine is cheap and a controlled release thereof could help to reduce unwanted side effects such as nervousness and sleep disturbances that can occur with a rapid release of caffeine.[334] In addition, a sustained-release patch could provide a convenient and discreet way to consume caffeine without the need to regularly drink coffee or other caffeinated beverages. Meloxicam is a nonsteroidal anti-inflammatory drug (NSAID) that is used to relieve pain and inflammation caused by conditions such as osteoarthritis, rheumatoid arthritis, and ankylosing spondylitis. Meloxicam works by reducing the production of prostaglandins, which are chemicals that cause pain and inflammation in the body.[335] In the following, calibration curves of caffeine (see Figure 2-33; A) and meloxicam (see Figure 2-33; C) were recorded and the linear range was identified. Due to the lack of carboxyl groups and primary amines, caffeine could not react with the crosslinker or activated carboxyl group

within rCol and thus was added directly during hydrogel synthesis. To facilitate the experimental set up, the caffeine release was directly tested from the crosslinked hydrogel by submersion in 37 °C water bath according to chapter 4.2.5.7. Absorbance detection showed >90% (w/w) caffeine release within the first hour for different formulations (10 and 30 mg/ml rCol; MR of DMTMM of 1:0.25 and 1:2). No drug retention was observed. Therefore, another system needs to be explored. Internally, the technology for the manufacturing of meloxicam loaded microparticles made from PLGA was known. Based on this knowledge, caffeine was replaced by meloxicam and PLGA particles loaded with meloxicam were tested in comparison to PLGA placebo particles in the next chapter.

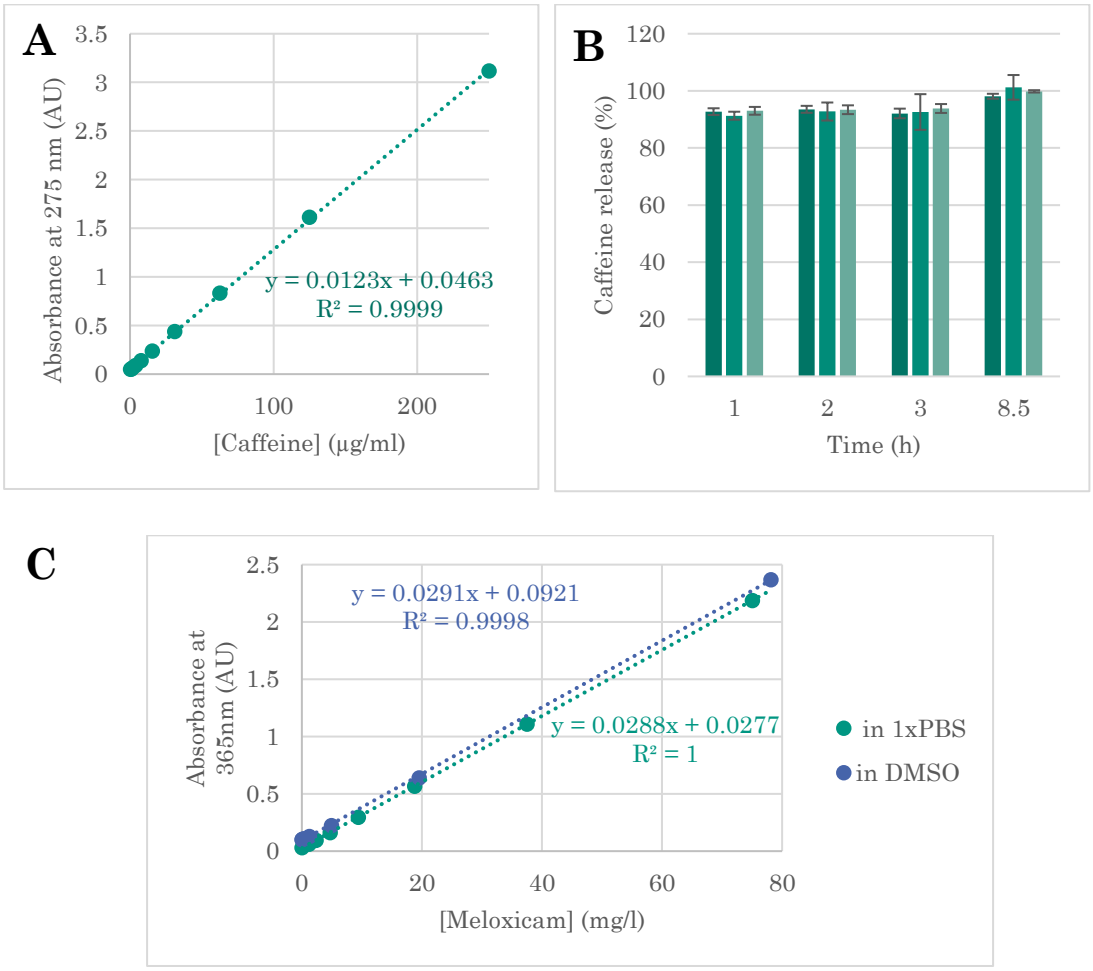

Figure 2-33: (A) Absorbance measurements of different caffeine concentrations in 1×PBS. The measurement was performed with a multi well plate reader (Tecan Reader) using a sample volume of 200 µl/well. **(B)** Caffeine release from DMTMM crosslinked rCol hydrogels (N=3). All data was normally distributed. **(C)** Absorbance measurements of different meloxicam concentrations in 1×PBS or DMSO. The measurement was performed with a multi well plate reader (Tecan Reader) using a sample volume of 200 µl/well.

2.2.4.1.2.2 Meloxicam release from PLGA microparticles

To prolong drug release, the meloxicam loaded PLGA microparticles were tested. Ideally, the rCol hydrogel immobilized the particles and allowed meloxicam release either by diffusion or particle degradation. Particles were provided by a colleague (Dr. M. C. Operti, Evonik Operations GmbH) made from 20% PLGA as placebo and meloxicam-loaded version (96.6% ± 0.9 mg meloxicam per gram g of PLGA and the particles had a diameter (D_{50}) of 87.6 µm and a span of 1.2). The particle analysis was done by Dr. M. C. Operti (method not described). To determine the release profile, several steps were performed prior to the release experiment.

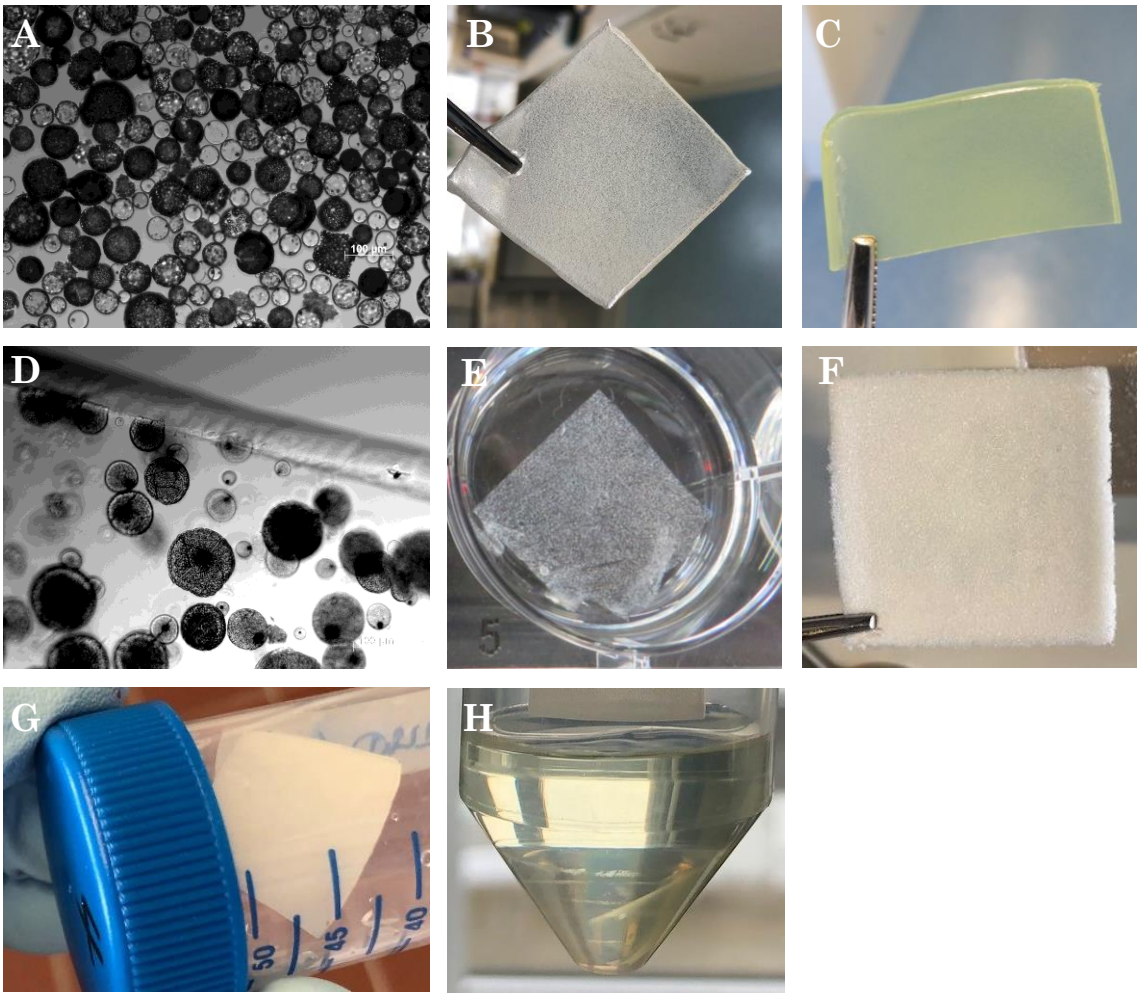

Figure 2-34: (A) Meloxicam-loaded microparticles made from PLGA. **(B)** Homogenously distributed PLGA placebo particles within a rCol hydrogel (particles were added once the formulation started to gelate). **(C)** Air-dried rCol patch with encapsulated PLGA particles containing meloxicam in the mold and separated thereof. **(D)** rCol hydrogel from B under the microscope and **(E)** within 1×PBS. **(F)** Freeze-dried rCol patch with embedded PLGA placebo microparticles. **(G)** Incubated rCol patch containing meloxicam loaded PLGA particles after 240 h of incubation and **(H)** after subsequent replacement of 1×PBS by 5 ml DMSO and 3 h additional incubation at RT.

First, the particle load per patch was adjusted. Different drying studies (data not shown) demonstrated issues with too many particles during drying. A good distribution was identified in Figure 2-34 (D). The number of particles can vary depending on factors like the particle size and the number of layers in which the particles were immobilized. Second, the patch size was adjusted to a total meloxicam concentration within the linear range of the calibration curve (Figure 2-33). To ensure a quantifiable signal in case of 100% meloxicam release, the signal would remain quantifiable. Regarding the extraction volume (40 ml 1×PBS pH 7.4), a meloxicam concentration of 50 mg/l was chosen. Third, the background signal of PLGA in DMSO was explored at the absorption maximum of meloxicam (λ=365 nm) and it was evaluated as not interfering. Background was the complete dissolution of meloxicam in DMSO at the end of the extraction trial to quantify the remaining meloxicam within the patch. Fourth, the degree of drying was selected. Instead of freeze drying, hydrogels were only partially dried in a heat oven to allow microscopic imaging during the release experiment and to determine particle immobilization. In case of complete drying, the collagen patch would turn white which would make microscopic imaging impossible. While PLGA particles had a white color, the yellow color came from the meloxicam. Yellowish staining of the extraction solution correlated with released meloxicam. For the trial, particles and particle containing patches were submersed in 40 ml 37 °C warm 1×PBS buffer and incubated under orbital shaking for up to 10 days. The drug released was monitored by the absorbance signal of the extraction solution (see Figure 2-35). As an internal control, 50 mg/ml meloxicam in 1×PBS was used as reference to evaluate the meloxicam stability during the incubation time. As negative control, placebo particles made from PLGA with similar diameters were tested. The extraction fluid was analyzed until no more significant increase in signal was measured. Then, the 1×PBS was replaced by DMSO to dissolve remaining PLGA and meloxicam within the patch. The 50 mg/ml Meloxicam control in 1×PBS showed no signal change for the tested incubation time of 10 d. Therefore, not subsequent corrections needed to be done regarding the extraction data. Also, the placebo particles showed no relevant background within the 10 d extraction time. For the meloxicam loaded MPs, with and without immobilization in the rCol patch, the extraction solution turned more and more yellowish. After 240 h incubation time, no strong signal was measured any more for the meloxicam particle samples (see Figure 2-35). Next, 1×PBS extraction medium was replaced by 5 ml DMSO. Within the next 3 h, the rCol patch turned transparent and the solution turned yellow (see Figure 2-34, H). To ensure complete meloxicam release another sample was taken after 24 h. No signal difference was quantified. Absorbance measurements showed ~20% additional meloxicam release from the patch (see Figure 2-35).

Independently whether the particles were exposed directly to the medium or they were prior encapsulated in the patch, similar release profiles were observed (see Figure 2-35). Data indicated that the release is not dependent on the patch but solely relied on the MPs. Different particles loaded with different bioactive compounds could be tested in one patch and the difference in release could be explored. If successful, rCol patches could be used for drug depots to deliver one or multiple bioactive components to treat diseases in a long-term perspective with a long-lasting effect. Here the flexibility and great biocompatibility of rCol made this depot matrix an interesting formulation for implants and other biomedical applications.

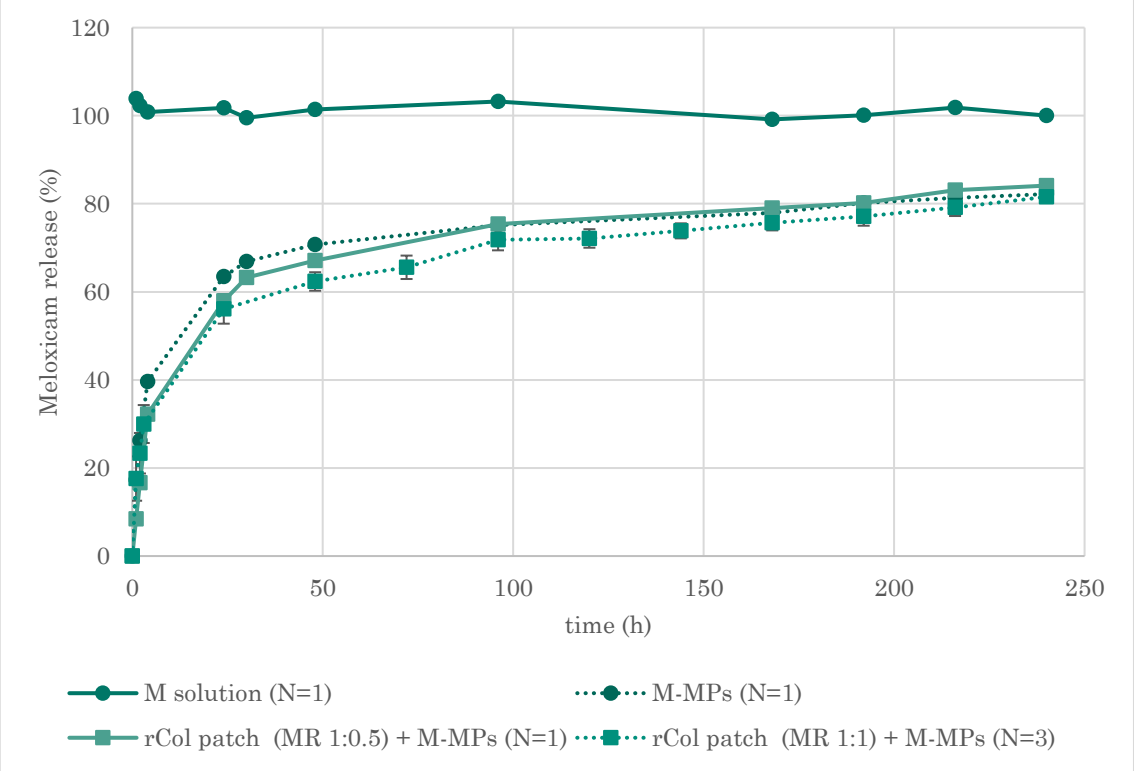

Figure 2-35: Meloxicam release from a Meloxicam (M) solution, from PLGA microparticles (MPs) containing Meloxicam, or DMTMM crosslinked 10 mg/ml rCol patches with embedded MPs loaded with Meloxicam. Samples were incubated in 1xPBS over time at 37°C under orbital shaking (85 rpm) (N=3).

2.2.4.1 Injectables

In the field of cosmetics, hydrogel-based injections are interesting for dermal filler for wrinkle treatment due to their great biocompatibility and adjustable degradation pattern. Injectable, cell repellent hydrogels could be also relevant for minimal invasive surgery. Compared to open surgery, minimal invasive surgery benefits from parameters like smaller incisions, reduced pain, shorter hospital stays, a quicker recovery and a reduced risk of complications

such as infection, bleeding, and other surgical complications.[336] During surgery, postoperative adhesions between tissues and organs happen in 67-97% of all cases.[337] Long term side effects from (abdominal) adhesion can be infertility, chronic and intestinal pain.[338] To avoid cellular adhesion, the cell repellent rCol/PEG formulation could be injected to separate tissues during surgery. With the rCol/PEG composite, good biocompatibility was demonstrated (see chapter 2.2.3.2.4) as well as adjustable degradation (see chapter 2.2.3.3.1). Due to the fast gelation kinetics of the composite, *in situ* mixture followed by injections might be an excellent approach. Also, partially pre-gelated formulations to increase the viscosity might be of interest. Therefore, the rCol/PEG composite was tested as injectable. For subcutaneous injections, a needle size of G25 - G27 was recommended.[339] One formulation (20 mg/ml rCol, MR of 4PEG-SG of 1:0.2 in 1×PBS) was evaluated as PoC. The low ratio of crosslinker (1:0.2) was chosen due to less NHS side product, less potentially side effects on tissue and a softer hydrogel rheology compared to high MRs. First gelation was documented with ~8 min. Data aligned with the identified crosslinking time in chapter 2.2.3.2.2 (Table 2-3) of 11 min. Between 10-15 min after mixing the components, the viscosity increased strongly. Injectability was possible until ~17 min after mixing using needle sizes down to G27. Smaller needle sizes were not tested so far. A similar gelation behavior was observed with 0.9% NaCl as solvent. The prepared formulation was injected into a gelatin hydrogel layer (Figure 2-36 (A)) and between two gelatin blocks from the top into the interspace (Figure 2-36 (B)). The formulation expanded homogenously as desired between both layers. In summary, the low viscous rCol material represents an interesting approach for injections by even very thin needle diameters. To further evaluate the formulation, shear thinning experiments could be performed. By adding a non-hazardous crosslinker like 4PEG-SG, an adjustable gelation time (chapter 2.2.3.2.2, Table 2-3) together with a good biocompatibility (chapter 2.2.3.2.4, Figure 2-22) and an adjustable stiffness (chapter 2.2.3.3.1, Figure 2-23) and degradation rate (chapter 2.2.3.3.1, Figure 2-26 and Figure 2-27) makes the rCol/PEG formulation an interesting approach as injectable. Depending on desired viscosities, the formulation can also be adapted, and slight pH changes can speed up or slow down the reaction time.

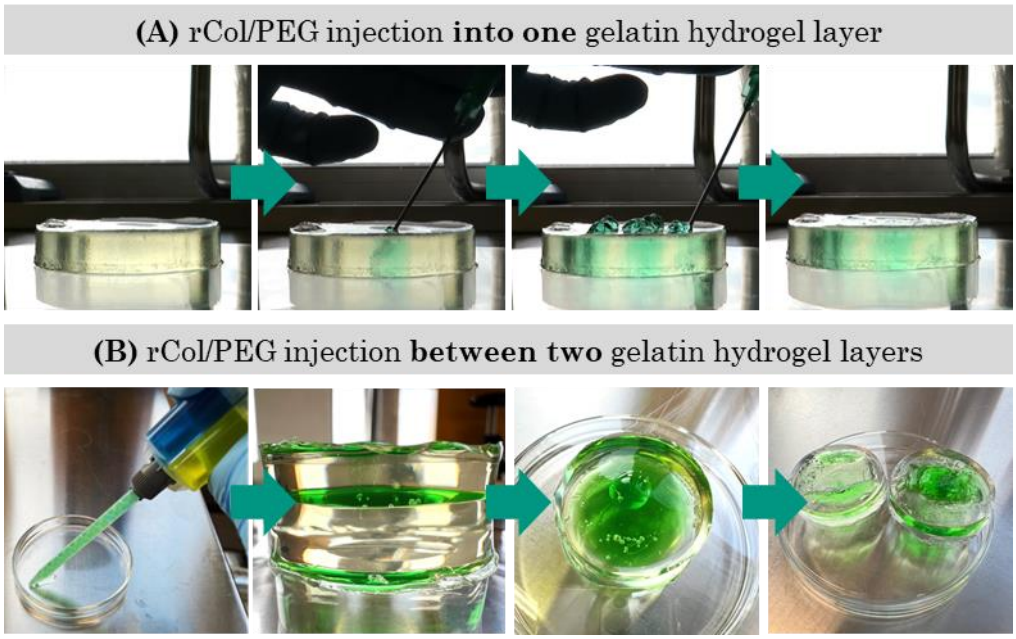

Figure 2-36: Injection test of 20 mg/ml rCol crosslinked with a MR of Col to 4PEG-SG of 1:0.2 in 1×PBS using green food dye as colorant. The formulation was mixed with a two-chamber syringe and static mixing unit. The formulation was ejected **(A)** into a 10% (w/w) gelatin block by a G21 needle or **(B)** injected between two topped gelatin blocks with a G27 needle.

2.2.4.2 Barrier membrane

Medical devices can be made of different materials for desired properties. Hernia meshes for examples are normally made from synthetic materials such as polypropylene.[340] These materials have a great strength, and durability. Occasionally they are coated with ECM materials such as collagen to improve their biocompatibility and reduce the risk of complications.[341] Combining these strong materials with hydrogels can not only improve the biocompatibility to reduce the risk of inflammation and rejection of the implant by the body's immune system, but also enhance lubrication to reduce friction between the implant and surrounding tissues, which can improve the implant's performance and longevity.[342] Also as explored in previous chapters, hydrogels can be designed to release drugs or other therapeutic agents in a controlled manner, which can improve the effectiveness of the implant and reduce the need for additional treatments. Hydrogels furthermore can reduce the risk of infection by releasing antimicrobial agents that can help prevent infections around the implant.[343] Here two experiments were performed. First the rCol/PEG formulation was molded into a patch and the flexibility thereof was explored. The 1 mm patch was flexible but tore easily. Formulation alternations or the implementation of elastic materials like elastin might increase the tensile strength of the product. As described in the introduction, the tensile

strength describes the resistance against an uniaxial deformation caused by stretching or compression. Another approach is the combination with a polymeric mesh. Here a common mesh made from polyester (200 µm pore size) was embedded between two rCol/PEG hydrogel layers. After gelation the patch remained bendable and stretchable. To improve the hydrogels resistance, the patch was dried (16 h at RT and 5 60 °C) (see Figure 2-37)The dried patch remained flexible and stabilized the hydrogel component against external mechanical stimuli. Also, the patch could be easily cut. In chapter 2.2.3.4.1, the cell repellent properties of rCol/PEG hydrogels were explored. To ensure the preservation of this effect with the dried hydrogel composite, further cell adhesion trials were needed. To ensure product sterility of the product, different sterilization methods could be explored as well. Also, the biological performance *in vivo* needs to be evaluated regarding the additional manufacturing cost to evaluate the market potential of the composite.

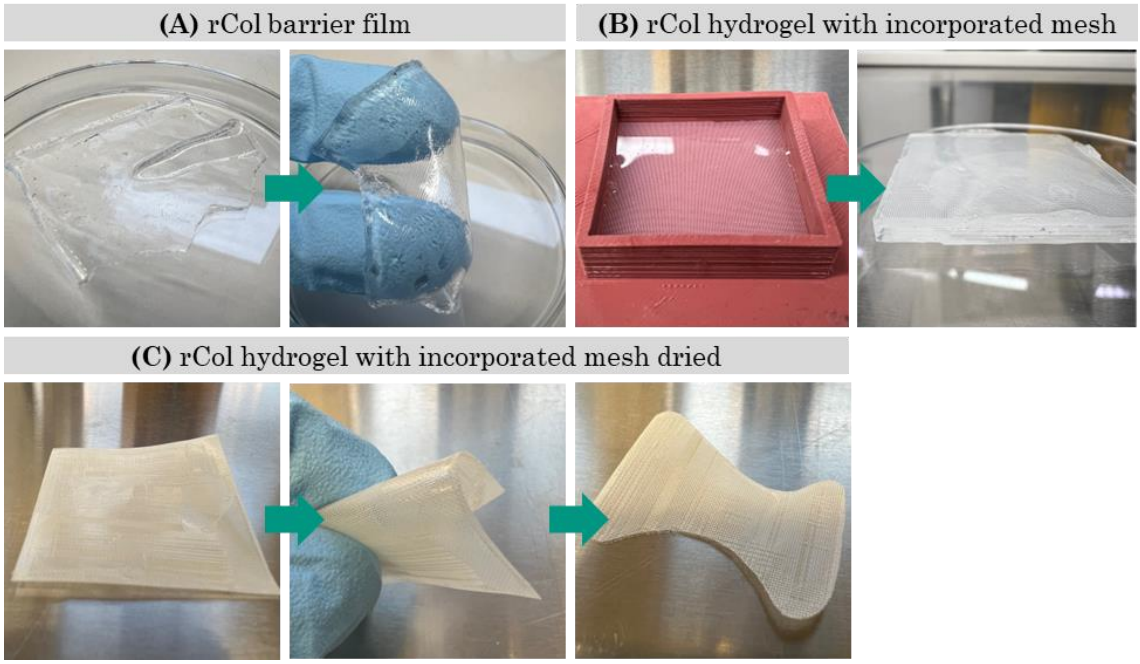

Figure 2-37: 20 mg/ml rCol crosslinked with 4PEG-SG (MR of 1:0.2). **(A)** Molded 1 mm hydrogel film and manual film stretching. **(B)** Hydrogel with embedded polyester mesh. Each hydrogel layer had a height of 1.5 mm. **(C)** Dried patch from (B) by exposure to RT overnight followed by 5 h drying at 60 °C. The mesh was bendable and cuttable after drying.

2.3 Modified rCol for Photopolymerization

2.3.1 Introduction

Photopolymerization represents a great feature for novel biomaterials to generate 3D structures. Rapid curing on demand would be an excellent feature for the low viscous Col solution to immobilize cells or particles on demand. This feature is of high interest for biofabrication (including bioprinting) which describes a growing field in tissue engineering and regenerative medicine allowing customized construction of complex 3D scaffolds while accurately controlling cellular behavior. The enhanced complexity of tissue models made from biofabrication can resemble living tissues better, which makes them more valuable for *in vitro* test systems. The low viscous rCol material enables alternative printing procedures including jetting and SLA, which are not possible or highly challenging with highly viscous fluids including mammalian collagens. In a previous publication from 2021, collagen type I was modified with norbornene units and photopolymerized with HS-PEG-SH for 3D cell encapsulation trials leading to high viability and cellular stretching within seven days after extrusion-based bioprinting.[146] In 2020, Tytgat *et al*. modified a recombinant collagen-like protein (Cellnest from FUJIFILM Manufacturing Europe B.V.) leading to great ASC encapsulation (immortalized human adipose tissue−derived stem cell line) by two-photon polymerization (2PP) as well as proliferation inside of the printed structures.[175] Based on the promising literature data, norbornene and thiol groups were conjugated with rCol. To my knowledge, this has not been reported with rCol so far. Additionally, the produced material composition of norbornene-modified and thiolated rCol was tested for drop-on demand printing and stereolithography. Testing these two technologies with a mixture of norbornene and thiol-modified rCol was also new to science and wasn't published according to the author's knowledge in the past. This chapter comprises the implementation of the functionalization chemistry, the subsequent analytics, the synthesis of hydrogels synthesis *via* Photopolymerization, the identification of formulation limitations, the mechanical and biological characterization of formed hydrogels and ultimately the printing trials.

2.3.2 Chemical functionalization

2.3.2.1 Norbornene-modified rCol (rColN)

Norbornene-modified rCol (rColN) was synthesized by derivatization. Two major synthesis routes were described in literature: Anhydride-based (5-Norbornene-2,3-dicarboxylic anhydride)[146] and acid-based (5-Norbornene-2-carboxylic acid).[175] In both cases, the norbornene

was conjugated to primary amines present in lysine side chains. In the following, the two methods from Scheme 2-1 and Scheme 2-2 were compared.

2.3.2.1.1 Synthesis *via* anhydride

Advantages of the anhydride-based functionalization were an accelerated reaction kinetic (one-step reaction) and cheaper chemicals. Disadvantages comprised the high reactivity of the anhydride which could also initiate modification of other nucleophiles like primary alcohols present in tyrosine, serin or threonine side chains. This effect was observed in several experiments using methacrylic anhydride to methacrylate rCol especially when high DoF were reached (proven *via* ^{1}H-NMR; data not shown). Another disadvantage is the introduction of an additional carboxylic group by each conjugation and the simultaneous elimination of primary amines. Resulting, less NH_2 groups are available which can be protonated. As a result, the altered net charge could influence the pI leading to altered solubility properties (especially in the acidic pH) and an altered 3D structure. In the worst case, repelling forces could inhibit the strand annealing into the triple helical structure which is required for collagen.

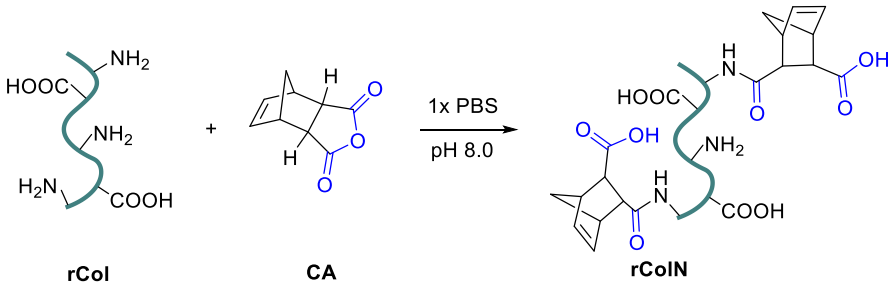

Scheme 2-1: Reaction scheme for the conjugation of cis-5-Norbornene-endo-2,3-dicarboxylic anhydride (CA) to rCol.

2.3.2.1.2 Synthesis *via* norbornene acid as one-pot reaction

The functionalization of gelatin *via* 5-norbornene-2-carboxylic acid (NCA) has been described in the literature as a two-step reaction involving pre-activation of the carboxylic acid followed by subsequent conjugation.[344] The highly water-soluble carbodiimide 1-ethyl-3-(3-dimethylaminopropyl) carbodiimide (EDC)[175] was used to activate the carboxylic acids (see Scheme 2-1). Although this reaction is more complex, it was preferred over the anhydride version and was tested with rCol instead of gelatin according to Scheme 2-2.

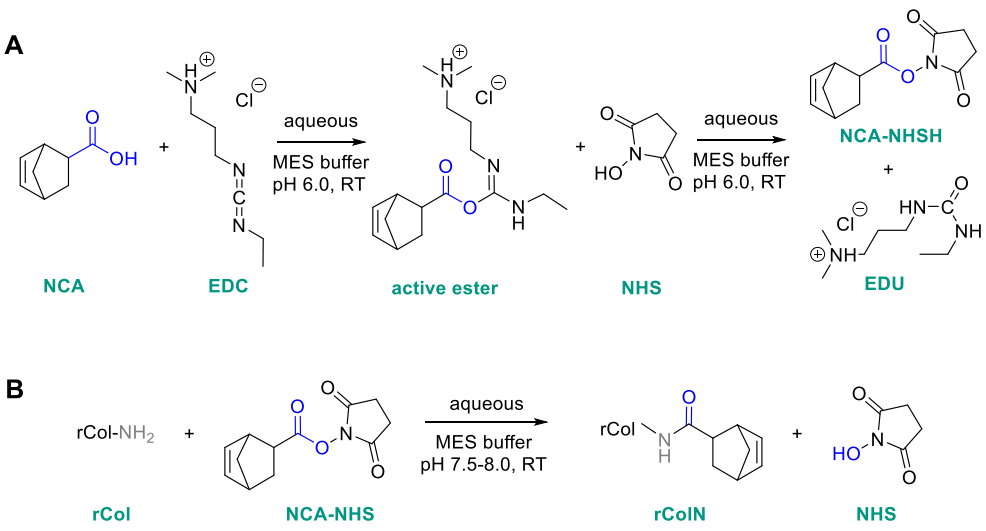

Scheme 2-2: (A) Activation of norbornene carboxylic acid (NCA) with EDC/NHS and **(B)** subsequent conjugation with rCol in a substitution reaction. The reaction conditions were extracted from Gockler *et al.*[344] and adapted to rCol.

As a PoC, the process published by Gockler *et al.* was applied on rCol with a reduced reaction temperature (RT instead of 50 °C) due to the heat sensitivity of the material. Identical compound masses were used due to unknown conversion rates. Recalculation of the molar ratios from animal gelatin to rCol resulted in a 4-fold increase in the occurrence of lysine side chains within the same mass of material (Table 4-12). The synthesis was carried out and the product purified according to chapter 4.2.4.1.1. To quantify the DoF of the product, ^{1}H-NMR spectra were recorded and peaks of the unmodified rCol were assigned using ^{1}H-NMR spectra of gelatin[344] together with published chemical shifts for different amino acids from analyzed tetrapeptides.[345] rCol contains one single aromatic amino acid (tyrosine) which can be used for signal quantification (2,6 H at 7.15 ppm and 3,5 H at 6.86 ppm). Lysins were modified during the reaction, so the change of signal (εCH$_2$ signal at 3.02 ppm) can be used to determine the degree of functionalization (DoF). Each collagen strand contains one tyrosine side chain and 23 primary amines (22 lysine side chains and one terminal -NH$_2$). Introduced norbornene units can be identified by their C=C double bond character, which produces signals between 5.83 to 5.98 ppm and 6.10 to 6.28 ppm. To calculate the DoF, equation 2-1 was used. A DoF of 100% described a total conjugation of all primary amines within a rCol molecule with norbornene units.

$$\boldsymbol{DoF}\ (\%) = \frac{\boldsymbol{A(Norbornene\ signal)/2}}{\boldsymbol{A\ (Tyrosine\ signal)/4}} * \frac{\mathbf{1}}{\mathbf{23}} * \mathbf{100} \qquad \textbf{2-1}$$

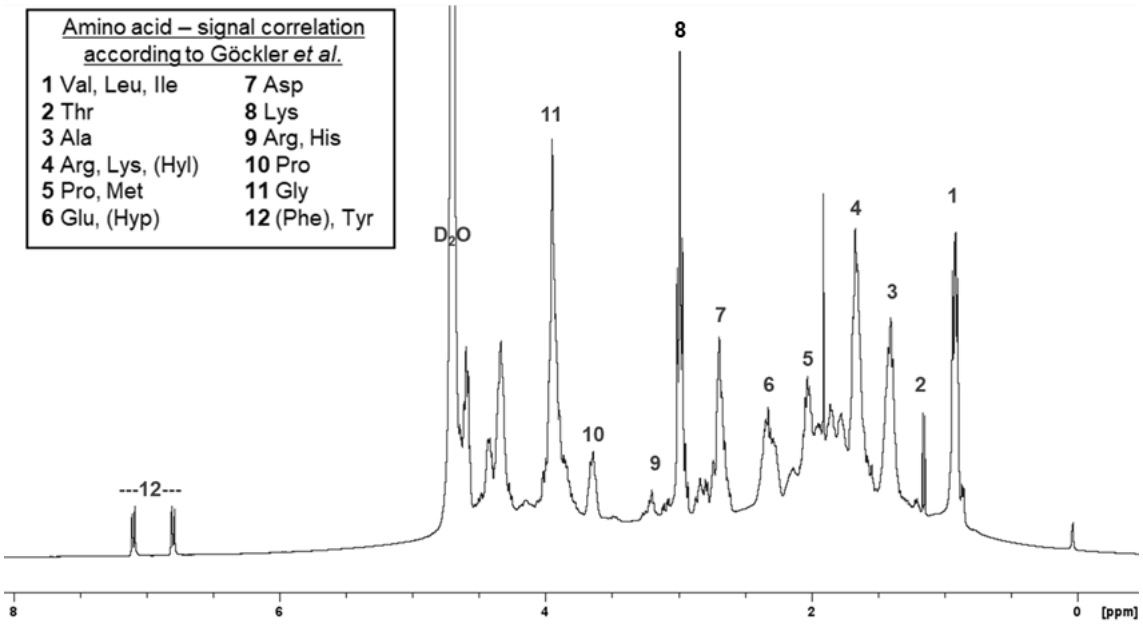

Figure 2-38: ^{1}H-NMR rCol spectrum (50 mg in 1 ml D_2O).

By comparing the two ^{1}H-NMR spectra from Figure 2-39, a degree of functionalization of ~49% was calculated based on equation 2-1. Due to the calculated applied MR of 1:0.5 of NCA, a DoF of 0.49 represented a conversion rate of nearly 100% (0.49/0.5 = 98%). The DoF is an important parameter which contributed to final hydrogel properties like pore size and material stiffness.

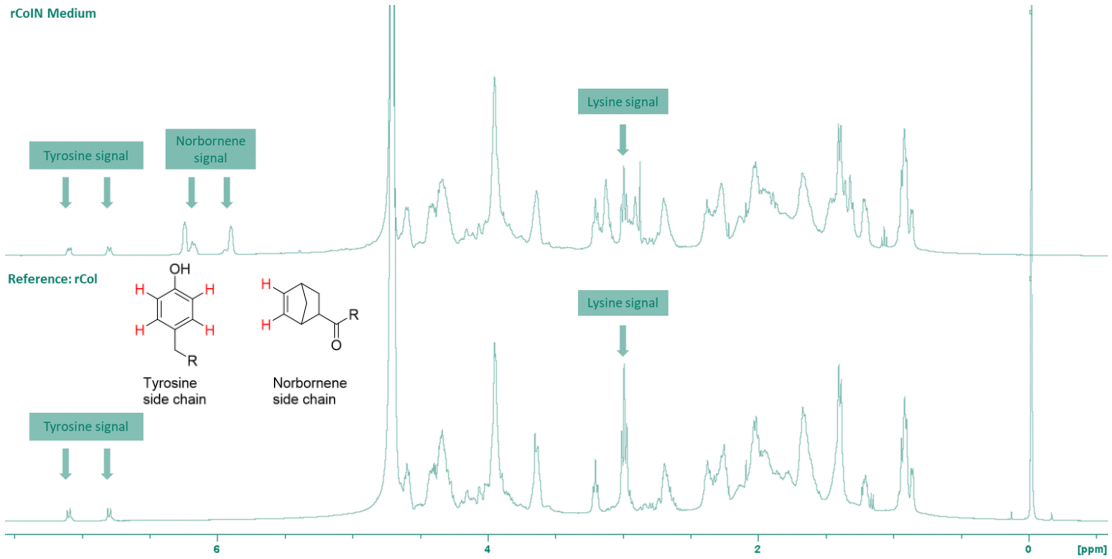

Figure 2-39: ^{1}H-NMR spectrum of rCol and rColN_medium. Relevant protons responsible for the measured signal were highlighted in red. The lysine signal is represented by the two protons at the epsilon carbon atom of the side chain.

2.3.2.1.3 TNBSA Assay implementation

Another way to determine the DoF was done with a colorimetric assay. Extracting from literature, the 2,4,6-Trinitrobenzene-1-sulfonic acid (TNBSA)-Assay was selected to detect primary amines which were not conjugated during the derivatization.[344] During the functionalization reaction, the number of primary amines was reduced which resulted in a reduced absorbance signal which meant a higher DoF. To establish the assay, pure rCol was used. As shown in Scheme 2-3, the signal can be detected at 420 nm and 335 nm. By measuring at 335 nm a higher signal intensity was measured (see Figure 2-40). Thus, 335 nm was chosen as detection wavelength. Also, both curves entered a plateau phase at rCol conc. >200 µg/ml. 200 µg/ml remained within the linear range and was chosen as sample concentration for further measurements due to the expected signal decrease during derivatization resulted from the lysine conjugation with norbornene units (see Figure 2-40).

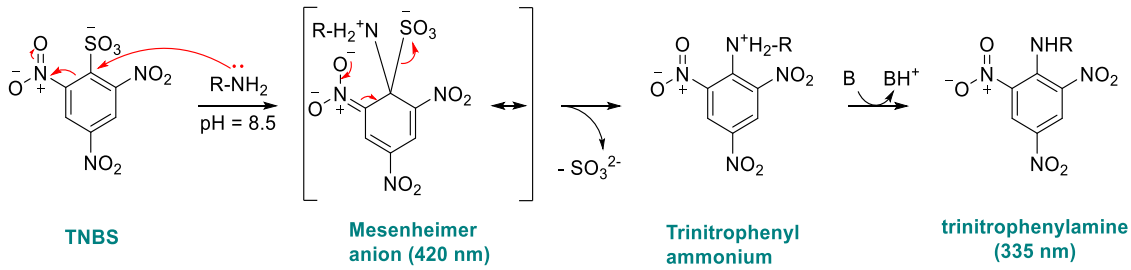

Scheme 2-3: TNBSA reaction mechanism for the synthesis of the trinitrophenylamine. TNBSA is deprotonated in basic buffer to form trinitrobenzene sulfonate followed by a nucleophilic attack of the primary amines yielding in substitution of the sulfate. The basic pH binds protons from the solution yielding in an orange-colored derivative. As a side reaction TNBSA can react with hydroxonium ions to picric acid. The reaction mechanism was extracted from Cayot *et. al.*[346]

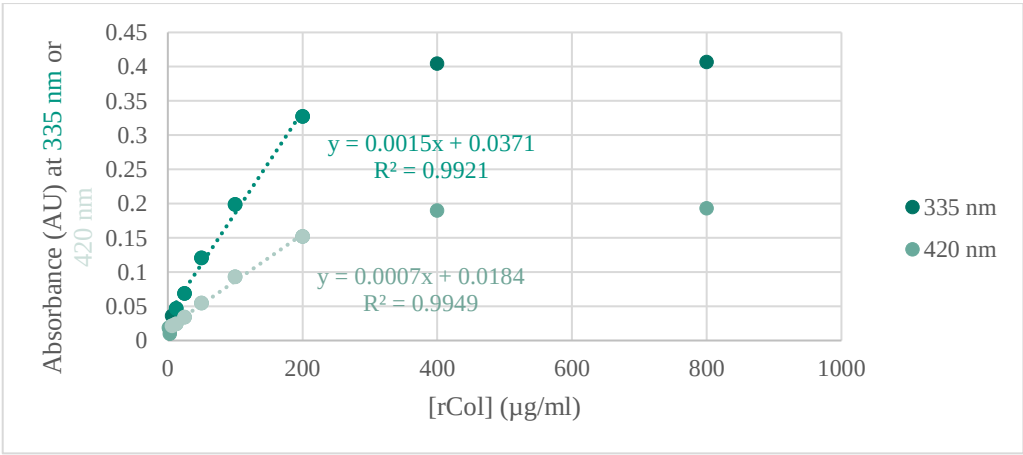

Figure 2-40: TNBSA Assay calibration curve with rCol detected at 420 nm (Mesenheimer complex) and 335 nm (Triphenylamine derivative). The assay was performed according to chapter 4.2.5.1.

2.3.2.1.4 rColN reaction optimization

For the one-pot reaction to modify rCol with norbornene units (see Scheme 2-2) the carbodiimide 1-Ethyl-3-(3-dimethylaminopropyl)carbodiimide (EDC) was used to activate norbornene acid for subsequent chemical coupling. The detailed reaction mechanism of EDC was described in chapter 1.3.3.2.2, Scheme 1-1. EDC is a commonly used chemical but it is highly reactive, hazardous (GHS06, GHS8, GHS09) and susceptible to hydrolysis. Due to the used one-pot reaction, some carboxylic acids may have been activated by EDC without *N*-Hydroxysuccinimide (NHS) substitution, which could reduce the biocompatibility of the products by secondary reactions with biological material or by later released EDU side products. To achieve a higher DoF, excess of EDC was required. Thus, longer purification times were expected. To avoid these issues, pre-activated, commercially available norbornene acid *N*-Hydroxysuccinimide ester (NCA-NHS) was applied. Due to high conversion rates of NHS activated esters, the need for chemical excess was not expected. This resulted in fewer byproducts and shorter dialysis times due to the single non-hazardous byproduct NHS. Using identical molar ratios (MRs) compared to previously applied Norbornene acid (NCA) (one-pot PoC experiment) a comparable DoF (~ 50%) was synthesized. Therefore, NCA-NHS was used for all following rColN syntheses. The water solubility of NCA and NCA-NHS was poor. According to a publication using the anhydride pathway, acetone was used to pre-dissolve norbornene anhydride.[146] Prior to the reaction, the compatibility of the acetone volume ratio with rCol was tested. By applying the same volume ratio, no solvent-induced precipitation of rCol was observed and the volume ratio was rated as feasible for the reaction. NCA-NHS was added as acetone solution or directly as powder, which led to white precipitation in both cases. The optimal pH for NHS ester coupling has been published to be between 7.2 and 9.[329] Therefore, two buffer systems were tested (1×PBS pH 7.4 and 0.1 M HEPES buffer pH 8.0). Within the first hours, the pH dropped stronger with 1×PBS and the turbidity increased. The addition of (1 M) NaOH cleared the solution again. White flocculation remained in both cases. Turbidity was not observed with HEPES buffer, and no manual pH adjustment was needed. It was assumed, that 0.1 M HEPES buffer had a better buffer capacity than 1×PBS to avoid a pH drop. Within the reaction time of 24 h, flocculation vanished in all formulations and a clear solution formed (see Figure 2-41). It was assumed that NCA-NHS precipitated in aqueous solution and that regaining transparency indicated reaction progress. Reaction product analysis using the TNBSA assay showed no benefit by adding acetone to the reaction mixture. The DoF was also higher with the HEPES buffer, and no subsequent pH adjustment was needed to maintain the pH. As a result, Nor-NHS was added directly, no acetone was used, and HEPES buffer pH 8 was used resulting in a controlled, organic solvent free reaction without the need pH adjustment.

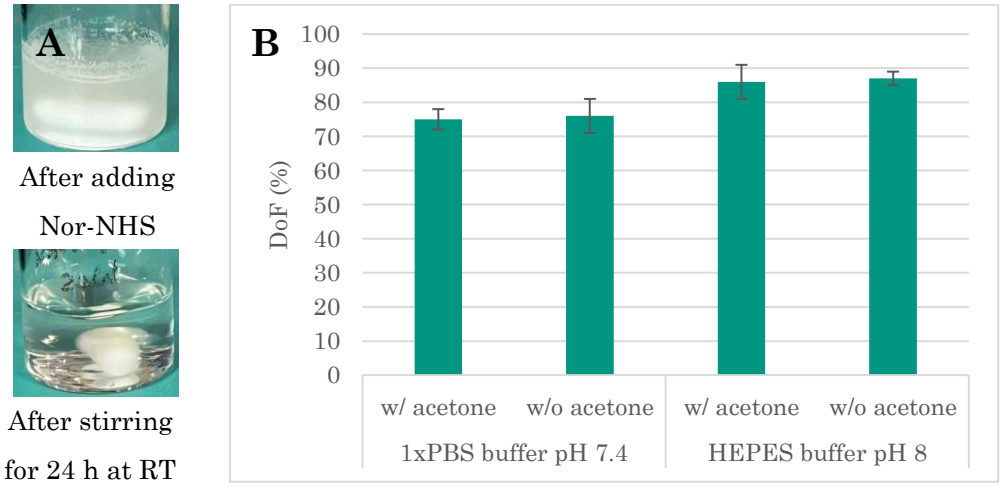

Figure 2-41: (A) Change in transparency with ongoing reaction process. **(B)** DoF analysis *via* TNBSA assay of different reaction products synthesized with (w/) or without (w/o) acetone using two different buffer systems (1x PBS pH 7.4 and 100 mM HEPES buffer pH 8.0) (N=3). All data was normally distributed.

During purification by dialysis against ddH_2O, a white precipitate formed within the dialysis tube. The amount of precipitate correlated with the targeted DoF (higher DoF → more precipitation) and increased with every water exchange. Freeze drying of the supernatant resulted in a poor mass yield. When the white solid was submerged in 0.1 M HEPES buffer pH 8.0, it dissolved completely. By modifying primary amines, the basic side chains (NH_2), the pI of the protein was assumed to change which potentially made it less to non-soluble in an acidic environment (less NH_2 groups, which could get protonated). To maintain a neutral to basic pH, dialysis against 1×PBS pH 7.4 was tested. For the last dialysis step, the 1×PBS buffer was exchanged by alkalified ddH_2O (pH of 7.5-8.5) to remove most buffer salts. By doing so, no precipitation was observed during the dialysis. To further lower the production costs, the 1×PBS was replaced completely by alkalized water.

2.3.2.1.5 rColN screening

rColN screening was executed with different MR of NCA-NHS to rCol. Based on the previous experiment where a MR of rCol:Norbornene acid of 1:0.5 led to a DoF of 48%, five different MRs (1:0.1 to 1:1) were tested with 200 mg starting material each to approach a DoF of 10-100%. The reaction products were dialyzed, freeze-dried and analyzed *via* ^{1}H-NMR and TNBSA assay. By comparing the data from both analytical methods, similar results were gained. The difference between both methods increased with increased DoF of the rColN from 5-13%. Resulting DoF were shown in Figure 2-42.

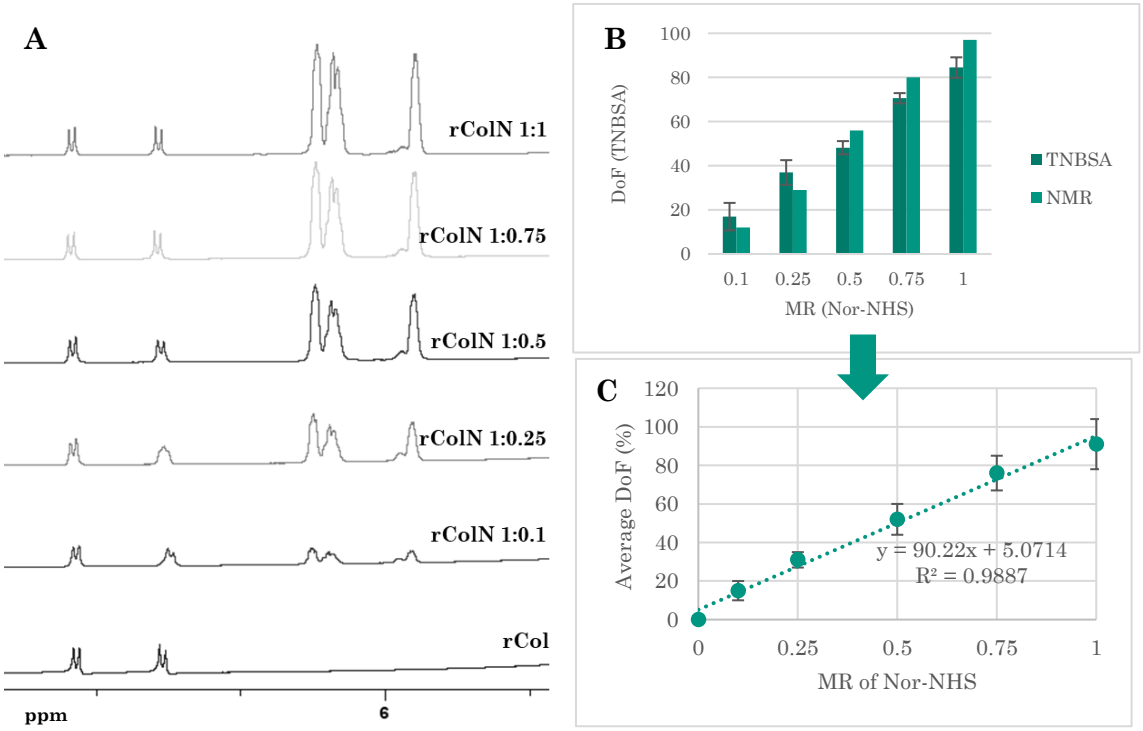

Figure 2-42: (A) ^{1}H-NMR spectra of differently modified rColN products comparing the crucial peaks for quantification **(B)** DoF determination by TNBSA-Assay (N = 3) and ^{1}H-NMR in correlation to the applied equivalents of Nor-NHS. **(C)** Correlation of average DoF (TNBSA-Assay and ^{1}H-NMR) and applied equivalents of Nor-NHS to rCol. All data was normally distributed.

Within the rCol development phase, also methacrylated rCol was synthesized, which resulted in very high DoF of >90% (data not shown here). By using methacrylic acid anhydride in excess, methacrylation of hydroxyl groups was proven by ^{1}H-NMR by the chemical shift of the aromatic protons of the tyrosine signal. To explore the observed effect for the norbornene functionalization, Nor-NHS was used in excess (two equivalents). ^{1}H-NMR showed a DoF of 98% (nearly complete turnover) and no tyrosine modifications. In summary, the DoF could be adjusted by the applied equivalents of Nor-NHS to rCol. A linear correlation between the applied molar ratio of Nor-NHS to rCol and the resulting DoF was identified. Quantification was successfully demonstrated by ^{1}H-NMR and colorimetric TNBSA-Assay. By comparing the measured DoF from the TNBSA assay and ^{1}H-NMR, led to signal variations between 4% -13% for all tested MRs which was rated as acceptable (see Figure 2-42; C).

2.3.2.1.6 Cytotoxicity Analysis

To analyze possible cytotoxic side effects of rColN, a cell viability study using the MTS-assay was performed (see Figure 2-43). The assay determined the metabolic activity of selected cells (here: HFF) during compound exposure. As reference, unmodified rCol was tested. The assay procedure was described in more detail in chapter 4.2.3.1.1. Sample concentrations between

0.1 and 20 mg/ml were tested showing cell viabilities between 83–110%. This surpassed the threshold of 70% (which was extracted from the ISO standard 10993-5). Resulting from the generated data, an LD_{50} of >20 mg/ml was determined for all tested samples. The materials were determined as non-cytotoxic under the test conditions.

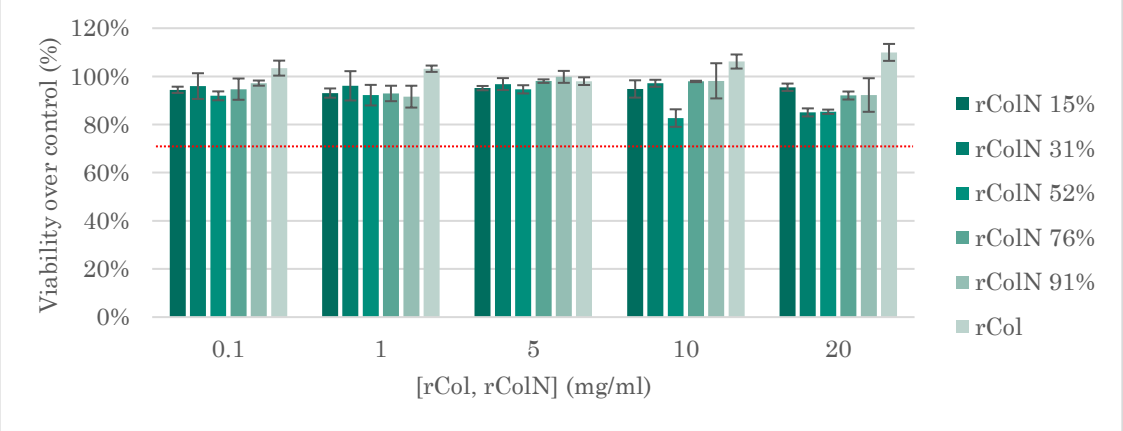

Figure 2-43: MTS cell viability assay based on the metabolic activity of HFF fibroblasts after exposure to rCol and rColN for 24 h under culture conditions. rCol was dissolved in cell culture medium prior to exposure (N = 3). All data was normally distributed. The threshold for viability of 70% given by ISO standard 10993-5 was indicated by a red dotted line.

To reduce the sample size for subsequent experiments, three different DoF were synthesized: Low (25% ± 12%), medium (50% ± 12%) and high (75% ± 12%). Only these three material variants were used in the following thesis. Materials with a lower DoF (extra low: <12%) and a higher DoF (extra high >88%) were not taken into consideration due to their poor or extreme gelation behaviors. While rColN_low required high concentrations for gelation (see chapter 2.3.3.2), the high functionalization of rCol (rColN_high) might have altered the helical structure strongly or cause extreme network densities during crosslinking. Larger amounts of all three derivatives were synthesized for all follow up experiments to calculate different DoFs resulting in the material characteristics in Table 2-5.

Table 2-5: rColN synthesis table showing the applied equivalents (eq.) of Nor-NHS, the applied mass of Nor-NHS per gram rCol, the analyzed DoF, the calculated molecular weight of the products (M_w) and the resulting yield.

Sample	Eq.	m (NCA-NHS)	M_w (g/mol)	DoF (NMR)	Molecular yield
rColN_low	1:0.2	45 mg	23,431	**21%**	99%
rColN_medium	1:0.5	116 mg	24,330	**53%**	79%
rColN_high	1:0.8	185 mg	25,005	**77%**	82%

2.3.2.1.7 Secondary structure

CD spectra can reveal the potential triple helical structure of collagens. To determine the DoF after synthesis, the three variants (low, medium and high) from Table 2-5 were compared to unmodified rCol (native and denatured). All curves showed the typical curve behavior for a triple helical structure (see Figure 2-44. Compared to rCol, the minimum at ~197 nm and the maximum at ~220 nm decreased for all rColN variants. For data extraction, the CD signal was normalized to a wavelength instead to a concentration. It is possible that chemical changes due to the introduced norbornene units alter the absorption properties of the molecule, resulting in slightly different normalized values. Nevertheless, the triple helical structure could be demonstrated and was comparable for all three derivatives.

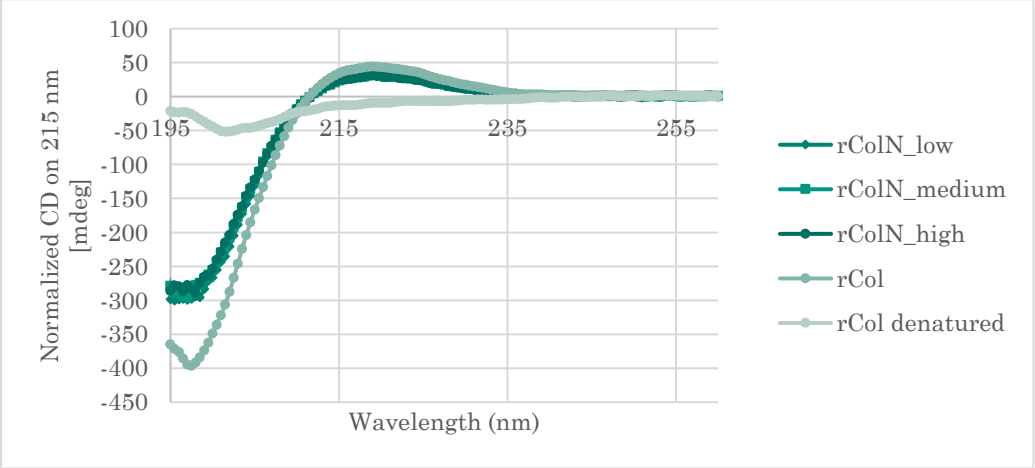

Figure 2-44: CD spectra of rCol and rColN. All data was normalized to UV absorption at 215 nm and smoothed using a second order polynomial equation with 5 neighboring points in size (5 nm). The smoothing was performed with GraphPad Prism 9.4.1. All samples were prepared with 0.1 g/kg 50 mM sodium phosphate buffer pH 7.2 and dissolved in a thermomixer for one hour at 20 °C before usage. The denatured rCol was incubated at 40 °C for 10 min prior to the measurement. The measurement itself was performed at 20 °C.

To determine the temperature stability of rColN, CD spectra were recorded at different temperatures. After a sigmoidal fit, the following T_m were calculated from the turning points of the sigmoidal fits: 33.1 °C (rCol); 33.0 °C (rColN_low); 31.9 °C (rColN_medium) and 30.9 °C (rColN_high). Gained data indicated a reduced thermal stability for norbornene modified rCol of up to 2.2 °C. For rColN handling a material incubation of max. 30 °C was recommended to maintain the triple helical structure.

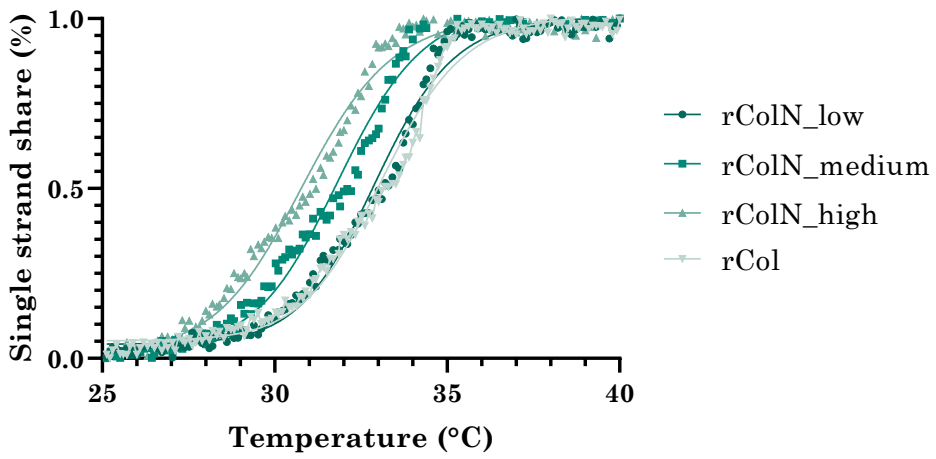

Figure 2-45: Melting temperature of rColN variants determined *via* CD spectra. 10 mg/ml rColN and rCol solutions in 50 mM sodium phosphate buffer pH 7.2 were prepared at 20 °C, diluted to 0.1 mg/ml and analyzed with a heating speed of 1 °C per 10 min from 25 – 40 °C. Applied procedures were described in chapter 4.2.5.6.

In Figure 2-4 (chapter 2.1.1.4) unmodified rCol showed refolding of the material over time measured by size exclusion chromatography (SEC). The same approach was followed to evaluate the refolding capacity of the rColN materials. Refolding of rColN_low and rColN_medium was observed (data not shown). For rColN_high, the applied SEC method needs to be optimized due to shift of retention time which made peak integration and peak resolution impossible. The experiment should be repeated with an optimized measurement method to validate and to determine potential backfolding for rColN_high. Refolding of denatured rColN was of importance to reuse denatured material by e.g. wrong storage conditions. Still, several repetitions need to be performed to the long-term stability of the protein in aqueous solution or powder form to get a better insight into the shelf life. Also, by preparing a stock solution and storage between 2 and 15 °C could always ensure the maximum degree of triple helical folding, which ensures identical material performance.

2.3.2.2 Thiolated recombinant collagen-like protein (rColS)

2.3.2.2.1 Introduction

Cysteine is rarely found in native collagen.[347] The applied rCol contains no cysteine. The introduction of thiols has several advantages like disulfide bond formation to strengthen the proteinogenic 3D structure and the chemical crosslinking *via* thiol-ene chemistry. The introduction of thiol groups can be achieved *via* genetic modifications or by post-translationally modifications. Here, the thiols were added post-translationally by chemical functionalizations. Several reagents can be used to modify primary amines. One of the most prominent reagent is 2-iminothiolane (2-IT or Traut's Reagent).[348] Also, sodium thioparaconate[349], γ-thiobutyrolactone[350], benzoyl homocysteine thiolactone[351] and *N*-acetyl homocysteine thiolactone (AcHCT)[352] can be used. According to a recent publication from Gockler *et al.* (thiolated gelatin), *N*-acetyl homocysteine thiolactone was selected due to its relative novelty and its price. All the listed structure were visualized in Figure 2-46.

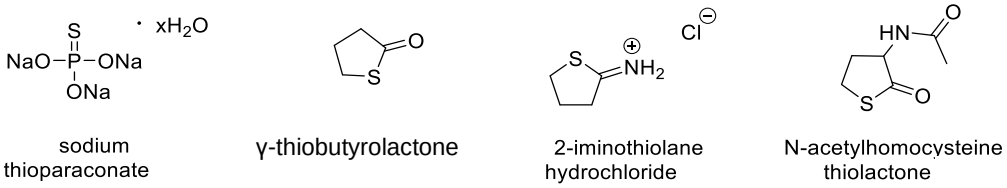

Figure 2-46: Overview of diverse thiolation reagents for proteins.

2.3.2.2.2 Ellman-Assay establishment

To quantify the DoFs of thiolated rCol, the calorimetric Ellman-Assay was established. The assay is based on the Ellman's reagent cleavage (5,5′-dithiobis-2-nitrobenzoic acid or DTNB) due to disulfide exchange with thiols in the sample. Formed 2-nitro-5-thiobenzoate (TNB^-) ionizes to TNB^{2-} dianion in water at neutral and alkaline pH which appears in a dark yellow color. The assay was ideal for rCol due to the lack of cysteines in the unmodified protein.

2.3.2.2.3 Proof of concept (PoC) synthesis

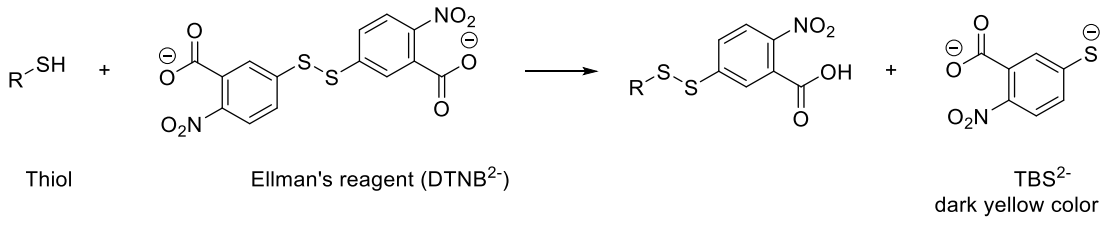

Scheme 2-4: Reaction scheme for the Ellman's assay.

rColS was synthesized comparable to GelS according to the protocol of Gockler *et al.* The reaction temperature was reduced (40 °C to 20 °C) and the starting material concentration

was increased to 40 mg/ml. A detailed reaction description was given in chapter 4.2.4.2. using the published ratios, 5 equivalents of *N*-acetyl homocysteine thiolactone (AcHCT) (5.03 mmol, 801.49 mg) were added to 1 g rCol (0.04 mmol, 1.01 mmol R-NH_2 moieties) in carbonate buffer under N_2 atmosphere. After synthesis (3 h at 20 °C) and purification, the material was analyzed *via* ^{1}H-NMR and Ellman's assay.

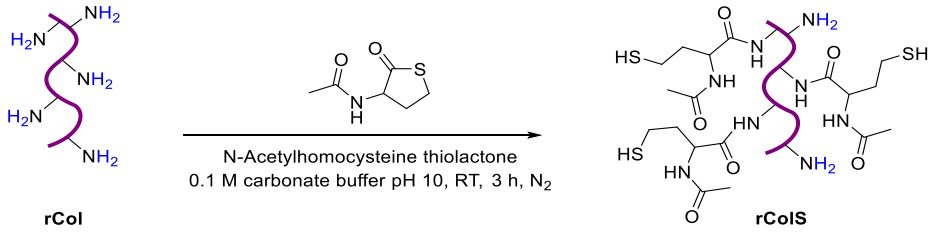

Scheme 2-5: Reaction scheme for the conjugation of *N*-Acetyl homocysteine thiolactone to rCol.

The DoF was determined *by* ^{1}H-NMR using formula 2-2. The two εCH$_2$ protons responsible for the lysine signal (δ = 2.96 to 3.03 ppm) were divided by the area of the four protons of the tyrosine signal (δ = 6.77 to 6.85 ppm and δ = 7.06 to 7.15 ppm), divided by the numbers of primary amines and multiplied with 100 to indicate the amount in percent. Subsequent subtraction from 100% resulted in the DoF. With an increase in DoF, the lysine signal diminished due to the conjugation with the thiolactone derivative. Another important peak appears at 2.015 ppm which corresponded to the introduced thiol moieties. Due to potential peak overlays in this area, the DoF calculations according to formula 2-2 proved as being sufficient.

$$\boldsymbol{DoF}\ (\%) = \mathbf{100} - \frac{\boldsymbol{A(lysine\ signal)/2}}{\boldsymbol{A\ (tyrosine\ signal)/4}} * \frac{\mathbf{1}}{\mathbf{23}} * \mathbf{100} \qquad \textbf{2-2}$$

Using an excess of 5 equivalents of AcHCT resulted in a DoF of 72% To achieve higher DoF longer reaction times could be tested with higher equivalents of AcHCT. Based on the generated data in chapter 2.3.2.1.6, a DoF of max. 75% was pursued. The same three functionalization variants were also pursued for rColS and required equivalents for the chemical modification were explored in the following screening.

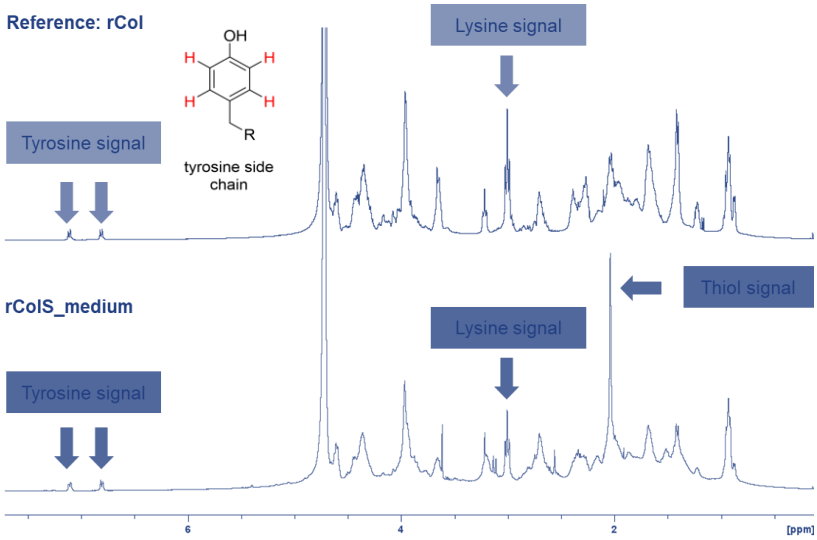

Figure 2-47: ^{1}H-NMR spectra of the first rColS batch made with 5 equivalents of *N*-acetyl homocysteine thiolactone. The protons responsible for the tyrosine signal and the lysine signal were highlighted in red. At δ = 2.015 ppm a third peak correlated with the introduced thiols.

2.3.2.2.4 rColS screening

Respectively 200 mg rCol was modified with five different molar ratios of AcHCT (1:0.25; 1:0.5; 1:1; 1:2; 1:5). Molar ratios were calculated by comparing the functional side chains in 1 mol rCol. Due to 23 reactive NH_2 groups, a molar ratio of 1 represented 1 mol functional side chains in 1/23 mol collagen molecules. The reaction was described in more detail in chapter 4.2.4.2. After product purification and freeze drying, the Ellman's assay was performed to quantify the DoF as well as ^{1}H-NMR spectra. By using more thiolactone (derivatization agent), an increased DoF was expected. To ensure signal quantification, the absorbance signal had to be in the linear range of the assay. To ensure this, different rColNS variants were screened in a concentration range from 1 to 10 mg/ml rColS (data not shown). The linear range was expected to differ for different DoF. Higher DoF were expected to have a lower linear concentration range compared to low functionalized rColS. For 1,2 and 5 mg/ml rColS a linear range was detected for all rColS variants (see Figure 2-48 (B). To receive a stronger signal intensity, 5 mg/ml sample concentration was chosen for subsequent quantification experiments. Reaction products of the screening were also analyzed by ^{1}H-NMR (see Figure 2-48 (A). A correlation of extracted DoFs *via* Ellman's assay and ^{1}H-NMR was compared in Figure 2-48 (C). A linear correlation was extracted. The formula of the resulting trendline could be used to calculate the DoF solely based on the Ellman's assay signal. The calculated DoFs were summarized in Figure 2-48 (E). By plotting the DoF against the applied equivalents of thiolactone (AcHCT), a logarithmic correlation was identified. By extrapolation, a DoF of 75% would theoretically require 5.8 equivalents of AcHCT and a DoF of 100% 20 equivalents of AcHCT. This finding correlated with Gockler *et al.* who used the same

chemistry with animal-derived gelatin.[344] Five (5) equivalents of thiolactone showed a similar DoF of 72% compared to the literature (73%)[175] and surpassed the DoF published for gelatin with 50%.[344]

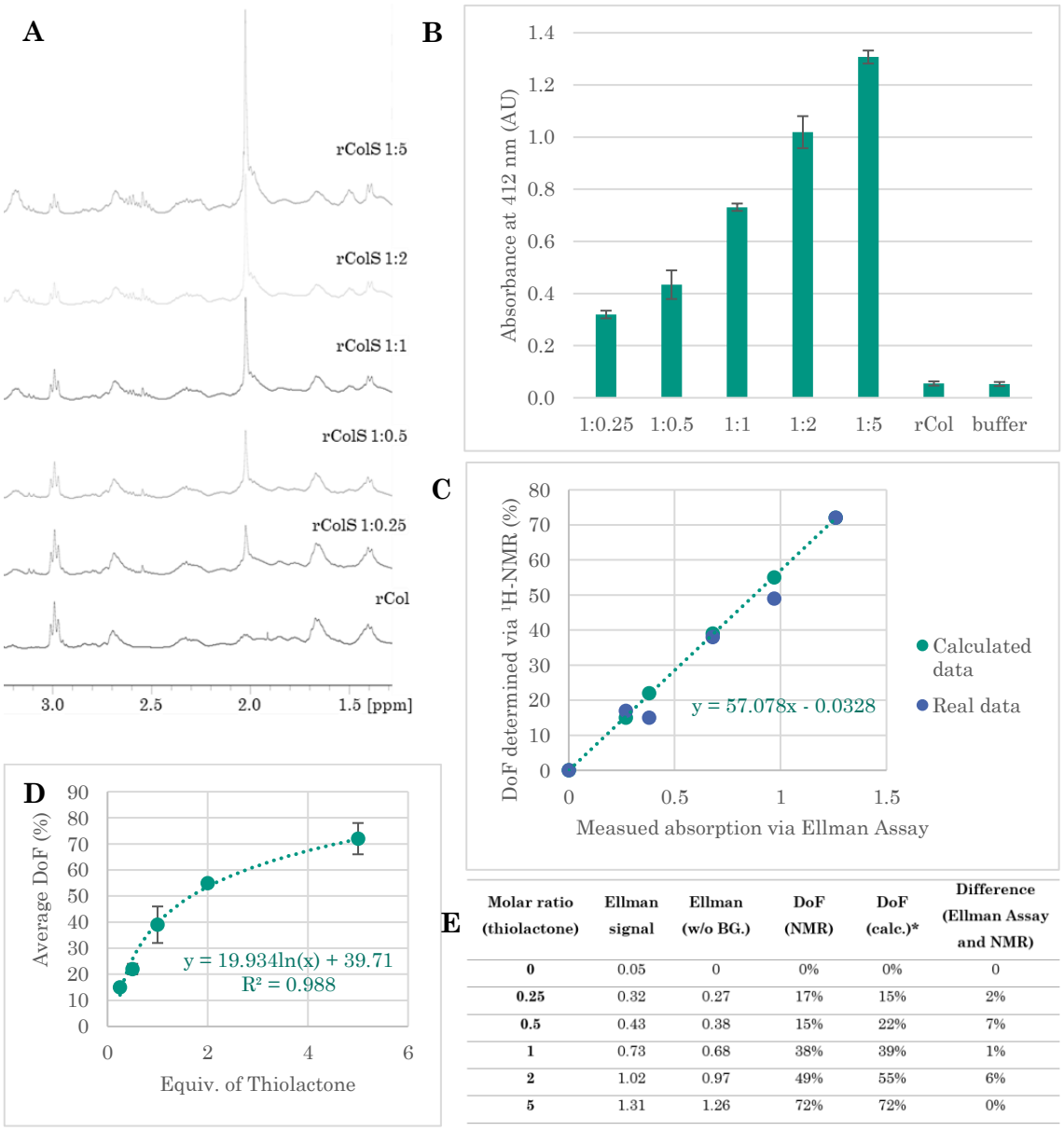

E

Molar ratio (thiolactone)	Ellman signal	Ellman (w/o BG.)	DoF (NMR)	DoF (calc.)*	Difference (Ellman Assay and NMR)
0	0.05	0	0%	0%	0
0.25	0.32	0.27	17%	15%	2%
0.5	0.43	0.38	15%	22%	7%
1	0.73	0.68	38%	39%	1%
2	1.02	0.97	49%	55%	6%
5	1.31	1.26	72%	72%	0%

Figure 2-48: (A) ¹H-NMR spectra of differently modified rColS products comparing the crucial peaks for quantification. **(B)** Ellman's assay signal comparison of rColS derivatives **(C)** DoF correlation based on ¹H-NMR data and Ellman's assay signal with a linear trendline. **(D)** Logarithmic correlation of DoF and applied equivalents of thiolactone. **(E)** Overview of applied MRs, resulting signals, recalculated DoFs and their difference in signal (N=3). All data was normally distributed.

2.3.2.2.5 Toxicological analysis

To analyze possible toxic side effects of the modified rColS material after purification, an MTS assay was performed with unmodified rCol as a reference (≤40 mg/ml collagen). The assay procedure was described in chapter 4.2.3.1.1. rColS showed an increased background signal, which correlated with the DoFs used and the rColS concentrations (data not shown). It was assumed that the introduced thiols interfered with the MTS reagent leading to an excess of formazan product. To obtain more reliable data, the color independent CellTiter-Glo® assay was performed with identical samples and controls. The experimental procedure was described in chapter 4.2.3.1.2. The background signal remained low for all samples tested. The excellent biocompatibility of unmodified rCol was already tested in previous experiments as shown in chapter 2.1.4, Figure 2-10 and in chapter 2.3.2.1.6, Figure 2-43. The experiment showed excellent viability of 86% - 109% which surpassed the ISO Norm 10993-5 threshold of 70%. Resulting from the generated data, an LD_{50} of >20 mg/ml was determined for all tested samples.

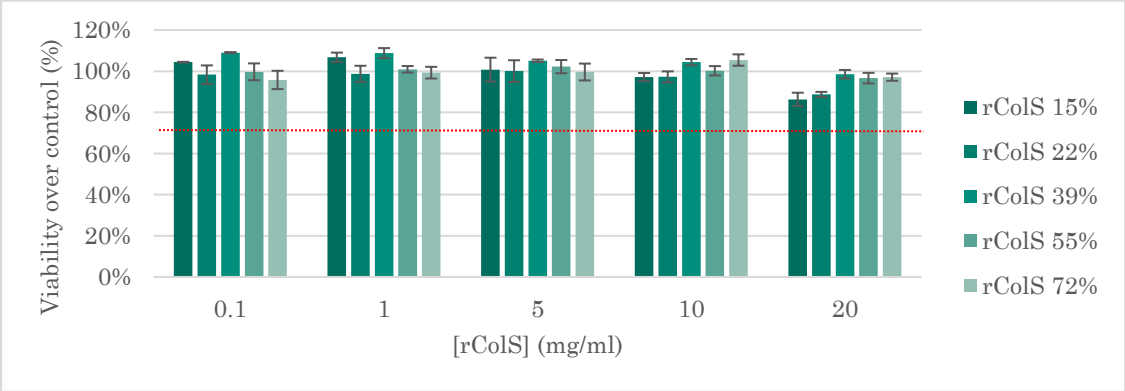

Figure 2-49: CellTiter-Glo® assay to determine the influence of different rColS samples on the metabolic activity of HFF fibroblasts after exposure for 24 h. rColS was dissolved in cell culture medium prior to exposure (N=3). All data was normally distributed. The threshold for viability of 70% given by ISO standard 10993-5 was indicated by a red dotted line.

2.3.2.2.6 DoF targeted synthesis

Based on the data generated, the reaction was repeated with the calculated equivalents of thiolactone for theoretically: 25% (0.5 equivalents), 50% (1.7 equivalents) and 75% thiolated collagen (5.8 equivalents). The DoF was quantified by Ellman's assay and ^{1}H-NMR resulting in the following products listed in Table 2-6. The resulting products showed excellent cell compatibility after purification (99-112% viability) and were considered as safe for subsequent experimental studies. All subsequent experiments were conducted with rColS_low (25% ±12%), _medium (50%±12%), or _high (75% ±12%). The numbers in brackets described the DoF range per product.

Table 2-6: rColS synthesis table showing the applied equivalents (Eq.) of thiolactone, the applied mass of thiolactone per gram of rCol, the analyzed DoF, the calculated molecular weight of the products (M_w) and the resulting yield.

Sample	Eq.	m (thio-lactone)	Mw (g/mol)	DoF (Ellman)	Molecular yield
rColS_low	1:0.5	77 mg	23,357	**14%**	99%
rColS_medium	1:1.7	268 mg	24,638	**49%**	97%
rColS_high	1:5.8	941 mg	25,224	**65%**	97%

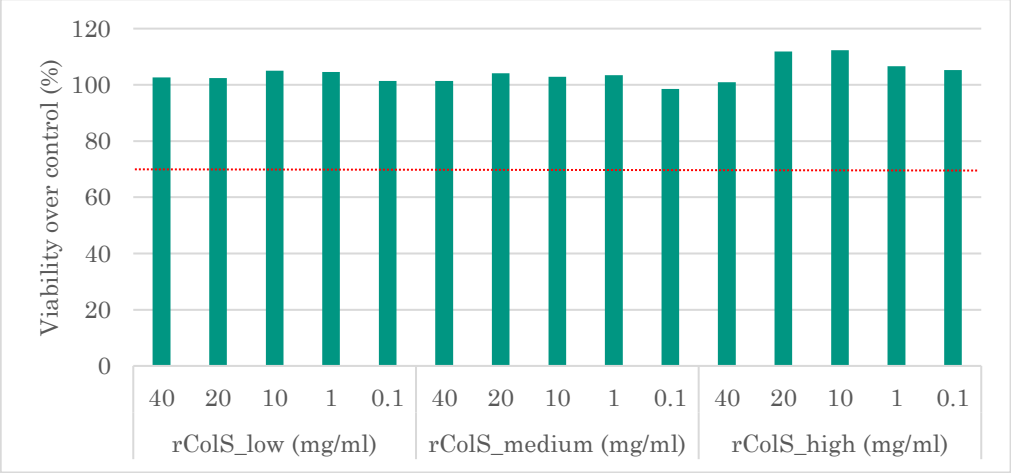

Figure 2-50: CellTiter-Glo® with different conc. of rColS_low, rColS_medium and rColS_high (N = 1). The threshold for viability of 70% given by ISO standard 10993-5 was indicated by a red dotted line.

As stated in chapter 2.1, collagen obtains a typical α-helical 3D structure. Due to this structure collagen obtains its unique properties, which differentiated it from its denatured random-coiled structure. Some of these properties like an increased material strength are listed in chapter 2.2.2. CD spectra were recorded to evaluate the rCol's secondary structure after thiolation (see Figure 2-51). Generated CD spectra showed a similar signal for the unmodified and folded rCol for all tested rColS variants. No denaturation was observed through the manufacturing process. Next, the melting temperature was determined by overlaying CD spectra. The following melting temperatures were extracted: 33.06 °C (rColS_low); 32.24 °C (rColS_medium) and 32.34 °C (rColS_high).

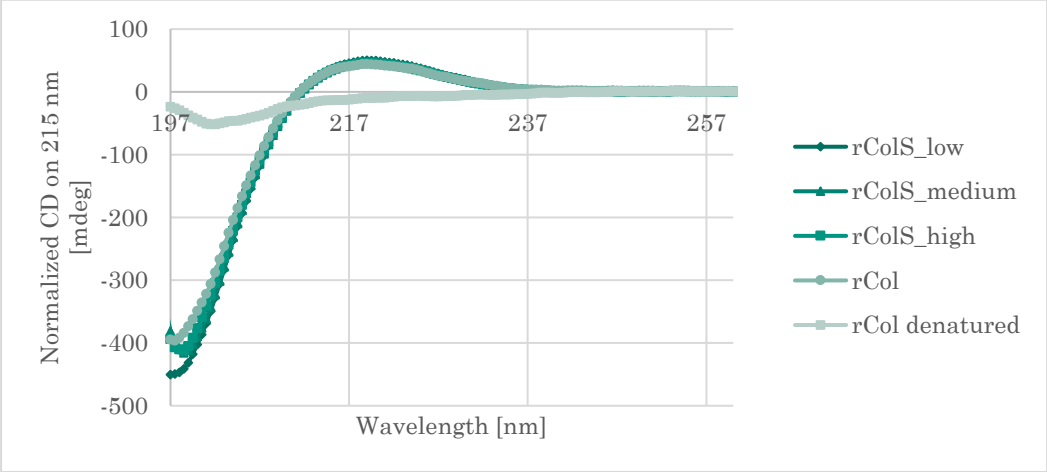

Figure 2-51: CD spectra of rCol and rColS. Measured data was normalized on material absorbance at 215 nm and smoothed using a second order polynomial equation with 5 neighboring points in size (5 nm). The smoothing was performed with GraphPad Prism 9.4.1. The denatured rCol was incubated at 40 °C for 10 min prior to the measurement. Detailed measurement descriptions were given in chapter 4.2.5.6.

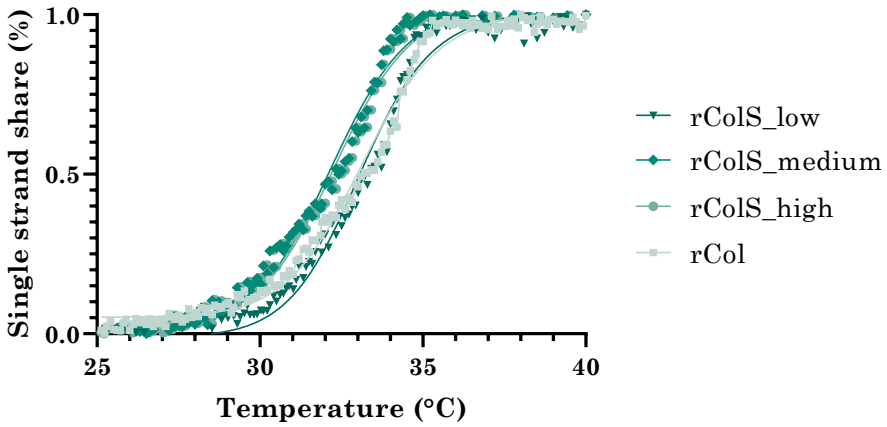

Figure 2-52: Melting curves of rColS_low, _medium and _high determined *via* CD melting curves. 10 mg/ml rColS and rCol solutions in 50 mM sodium phosphate buffer pH 7.2 were prepared at 20 °C, diluted to 0.1 mg/ml and analyzed with a heating speed of 1 °C per 10 min from 25 – 40 °C. Applied procedures were described in chapter 4.2.5.6. A sigmoidal curve fit was done with GraphPad Prism.

2.3.3 Hydrogel synthesis

2.3.3.1 Choice of Photoinitiator

One of the first and still commonly used water-soluble type I photoinitiators (PI) is Irgacure 2959. Disadvantages are limited molar absorptivity at 365 nm (ε ≈ 5 M−1 cm−1) and its low

water solubility of 5 g/l, which, however, is still acceptable for most applications. In comparison lithium phenyl(2,4,6-trimethylbenzoyl)phosphinate (LAP) showed a better water-solubility of 47 g/l. LAP also absorbs light at higher wavelengths of 365 nm (ε = 218 $M^{-1}cm^{-1}$).[153] For being less cytotoxic and allowing light absorbance at visible light, LAP became first choice in state-of-the-art water-soluble PIs for 3D biofabrication[353,354] To test for cytotoxicity before and after irradiation, Irgacure 2959 and LAP were compared with HFF cells.

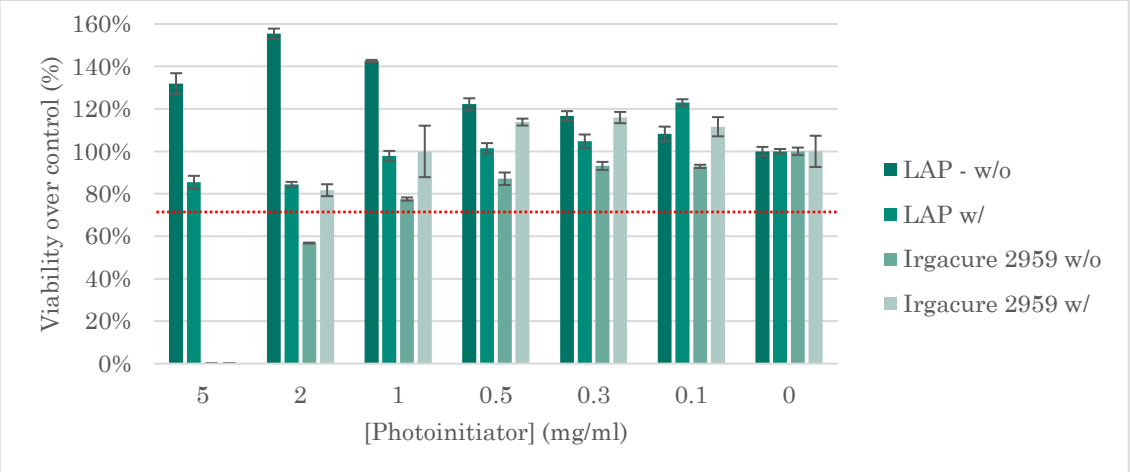

Figure 2-53: CellTiter-Glo® cytotoxicity assay of Irgacure 2959 and LAP solutions on HFF (P7) cells after 24 h exposure time with (w/) and without (w/o) prior irradiation (15 sec, Omnicure S2000, sample-light distance: 5 cm, intensity: 5.0 W/cm²). The PI was dissolved in medium. The background of the sample solution without cells was subtracted and the signal was normalized to the negative control (cells with culture medium). The relevant threshold for viability of 70% given by the ISO standard 10993-5 was visualized as dotted, red line at 70% (N=3). All data was normally distributed.

Resulting data from the cytotoxicity assay demonstrated differences between both photoinitiators. First, the non-irradiated samples were compared where no radical formation was expected. Between 0.1 and 1 mg/ml material, the cell viability remained above 70% (78-142%). Interestingly, non-irradiated LAP even had a positive effect on the measured signal especially between 1 and 5 mg/ml. The reason for showing such high viabilities above 100% remained unclear. By increasing the Irgacure 2959 concentration, already 2 mg/ml material resulted in cell viabilities below the threshold of 70% and a concentration of 5 mg/ml Irgacure 2959 was toxic for 100% of the tested cells. The irradiated samples demonstrated a reduced viability for LAP. Still, even with 5 mg/ml photoactivated material, the measured signal remained above the threshold. For Irgacure 2959, a slightly higher cell viability was measured with the irradiated samples. This was surprising because the radicals were expected to have a more severe influence on the cell viability. Based in the generated data, an LD_{50} value of >5 mg/ml was defined for LAP while Irgacure 2959 obtained a LD_{50} of 2-5 mg/ml. In

summary, LAP can be used in higher concentrations than Irgacure 2959. Even with 5 mg/ml activated LAP, the resulting cell viability remained above the threshold of 70%. Due to the good solubility and the sensitivity to blue light, further experiments were done with LAP.

2.3.3.2 First crosslinking trials

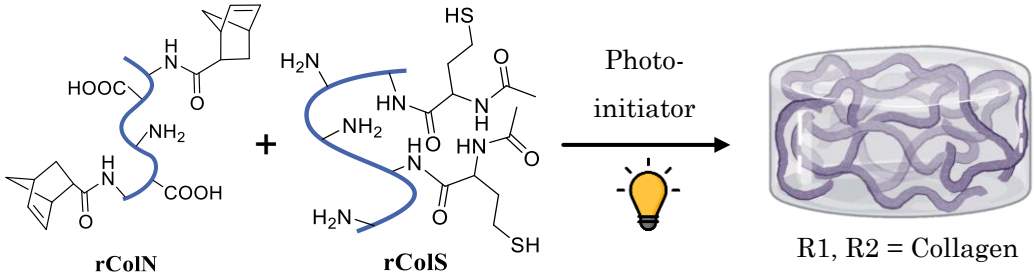

Scheme 2-6: Photopolymerization of rColN and rColS by adding a photoinitiator (here: LAP) and a light signal (here: blue light with the wavelength of 405 nm).

rColN and rColS were mixed in a 1:1 mass ratio (example: 20 mg/ml rColNS contains 10 mg/ml rColN and 10 mg/ml rColS) with similar or identical DoF. To better understand the rColNS concentration threshold for gelation, the following range was tested: DoF (8-81%) + rColNS concentrations (2.5-40 mg/ml). To reduce the number of experiments, the LAP concentration was set to 0.3 mg/ml in accordance with Gockler *et al.*[344] For photopolymerization, the Omnicure S2000 system was used. The Omnicure S2000 system can produced up to 16.5 W/cm² (see Figure 2-54). To compare the generated data, always the same light intensity was chosen. Here, a medium light intensity of 5.0 W/cm² was chosen for all following experiments. 100 µl sample volumes were prepared according to chapter 4.2.4.5 and 25 µl droplets were tested according to chapter 4.2.6.1 *via* droplet test.

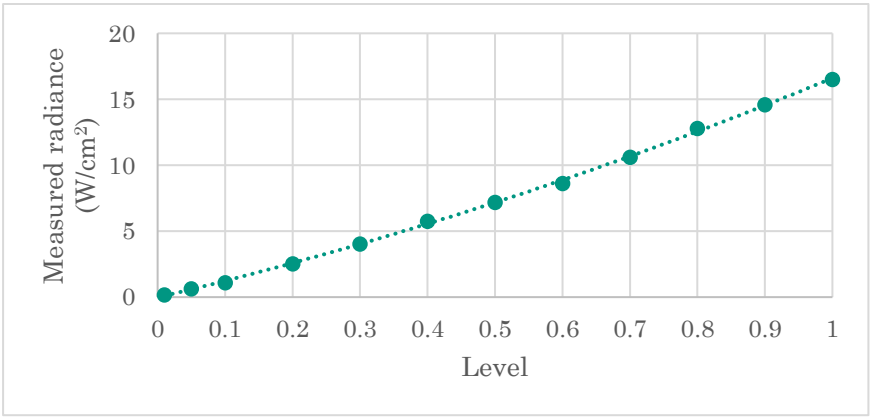

Figure 2-54: Correlation of measured radiance and adjustable level of the Omnicure S2000 lamp.

First, rColN was tested without rColS in a radical chain polymerization. Gained data showed a weak gelation performance with 0.3 mg/ml photoinitiator (see Table 2-7). No gelation was observed even with 40 mg/ml rColN_high (DoF of 80%). By applying longer irradiation times of up to 400% (15 → 60 seconds), tested formulations remained liquid. By increasing the LAP concentration ~ 3× (0.3 → 1 mg/ml) gelation was observed for some formulations starting from 10 mg/ml rColN_medium (DoF of 41-56%) (see Table 2-7). A correlation between collagen concentration and the applied DoF was observed with regards to successful gelation. Second, rColN was tested in combination with rColS in a step growth chain polymerization (SGP). The combination of rColNS and rColS showed improved gelation properties. Successful gelation was observed with only 2.5 mg/ml rColNS and 0.3 mg/ml LAP. In comparison to radical chain growth polymerization (RCP) with rColN_medium, a 4× reduction in required collagen while using 3× less photoinitiator for gelation was observed with rColNS. Furthermore, a correlation between collagen concentration and the applied DoF was observed. Increased DoF and rCol concentration improved gelation and *vice versa*. The data obtained confirmed the published results by Van Hoorick *et al.* that RCP required more photoinitiator and higher material concentrations for gelation.[126] In summary, the combination of rColN with a thiol significantly reduced the required material concentrations.

Table 2-7: Gelation experiments with rColN and LAP in 1×PBS. The total rCol was indicated in bold. (left) A LAP concentration of 0.3 mg/ml (left table) and 1 mg/ml (right table) was used for all formulations. All samples were irradiated with an Omnicure S2000 system with 5.0 W/cm² from a 5 cm distance between sample and optical fiber for up to one minute. Gelation was determined every 15 seconds of illumination. Successful (✓) and insufficient gelling (✗) was documented (with N = 2). Based on the defined DoF ranges the following DoF were assigned to rColN_very low (8% and 12%), rColN_low (29%), rColN_medium (41%, 48% and 56%) and rColN_high (80%).

0.3 mg/ml LAP							
[rColN]	**DoF (rColN) (%)**						
(mg/ml)	**8**	**12**	**29**	**41**	**48**	**56**	**80**
5	✗	✗	✗	✗	✗	✗	✗
10	✗	✗	✗	✗	✗	✗	✗
20	✗	✗	✗	✗	✗	✗	✗
40	✗	✗	✗	✗	✗	✗	✗

1 mg/ml LAP							
[rColN]	**DoF (rColN) (%)**						
(mg/ml)	**8**	**12**	**29**	**41**	**48**	**56**	**80**
5	✗	✗	✗	✗	✗	✗	✗
10	✗	✗	✗	✓	✓	✓	✗
20	✗	✗	✓	✓	✓	✓	✓
40	✓	✓	✓	✓	✓	✓	✓

Table 2-8: Gelation experiments with rColN, rColS and LAP in 1×PBS. The total rCol concentration is indicated in bold. rColN and rColS were applied in identical mass ratio (1:1) with a LAP concentration of 0.3 mg/ml. All samples were irradiated with an Omnicure S2000 system with 5.0 W/cm² from a 5 cm distance between sample and optical fiber for 15 seconds each. Successful (✓) and insufficient gelling (✗) was documented. All formulations were tested with N = 2.

Bioink Classification	DoF (rColN) (%)	DoF (rColS) (%)	Total rCol (mg/ml)				
			2.5	5	10	20	40
Extra low	**8**	**8**	✗	✗	✗	✗	✓
Extra low - low	**12**	**17**	✗	✗	✗	✓	✓
Low	**29**	**32**	✗	✓	✓	✓	✓
Medium	**41**	**45**	✓	✓	✓	✓	✓
Medium	**48**	**45**	✓	✓	✓	✓	✓
high	**80**	**81**	✓	✓	✓	✓	✓

2.3.3.3 Irradiation time

The minimal irradiation time for hydrogel formation is an important factor for 3D printing. Shorter irradiation times can speed up the printing process, which can save time and money. Furthermore, long lamp exposure and processing times bear the risk of hydrogel drying. To compare the gelation rate of radical chain polymerization with rColN to step-growth polymerization with rColNS, same concentrations of collagen (10-40 mg/ml) were applied along with three concentrations of LAP (0.3, 1, and 2 mg/ml). Gelation was detected with the droplet assay (see chapter 4.2.6.1; 25 µl droplets) and irradiation times of 1–60 seconds using the Omnicure S2000 instrument at 5.0 W/cm² and a sample to light source distance of 5 cm. After the indicated irradiation time, an attempt was made to move the droplet with a pipetting tip. When sufficiently solid, the droplet moved and was evaluated as gelated. Resulting data (Table 2-9) showed the expected discrepancy between radical chain polymerization with rColN to step-growth polymerization with rColNS. By using only rColN, only high concentrations of rColN and LAP led to stable hydrogels. This finding aligned with the trend observed in Table 2-7. Still some formulations were evaluated in Table 2-7 as hydrogel forming, which failed in the repetition (Table 2-9). It was assumed that the respective concentrations represented the border gelation concentration where gelation was difficult to determine. In general, a trend was observed that higher rColN and LAP concentrations led to hydrogel formation. By using rColN in combination with rColS, all tested formulations gelled within one second of irradiation. One exception was rColNS_low where irradiation times of up to 15 seconds were needed to induce gelation. Data demonstrated collagen and LAP correlations showing that less LAP and less collagen required longer irradiation times. In summary, gelation

was possible with all tested formulations of rColNS. Data validated the described superiority of step-growth polymerization. A DoF and collagen concentration dependent irradiation time was observed.

Table 2-9: Minimal gelation times of different collagen hydrogel formulations were noted in green with the applied irradiation time until gelation was observed as well as insufficient gelation (✗). All samples were irradiated with an Omnicure S2000 device with 5 cm between the optical fiber and a lamp power of 5 W/cm² for up to 60 seconds. Samples were evaluated after 1, 2, 3, 5, 10, 20, 30 and 60 seconds of irradiation. Samples were prepared on Tesafilm coated glass slide.

Formulation			LAP (mg/ml)				LAP (mg/ml)		
Total rCol	DoF		**0.3**	**1**	**2**		**0.3**	**1**	**2**
5 mg/ml	Low	rColN	✗	✗	✗	rColNS	**15**	**10**	**5**
10 mg/ml	Low	rColN	✗	✗	✗	rColNS	**5**	**2**	**1**
20 mg/ml	Low	rColN	✗	✗	✗	rColNS	**2**	**1**	**1**
40 mg/ml	Low	rColN	✗	✗	✗	rColNS	**1**	**1**	**1**
5 mg/ml	Medium	rColN	✗	✗	✗	rColNS	**2**	**1**	**1**
10 mg/ml	Medium	rColN	✗	✗	✗	rColNS	**1**	**1**	**1**
20 mg/ml	Medium	rColN	✗	✗	**15**	rColNS	**1**	**1**	**1**
40 mg/ml	Medium	rColN	✗	**1**	**1**	rColNS	**1**	**1**	**1**
5 mg/ml	High	rColN	✗	✗	✗	rColNS	**1**	**1**	**1**
10 mg/ml	High	rColN	✗	✗	✗	rColNS	**1**	**1**	**1**
20 mg/ml	High	rColN	✗	✗	✗	rColNS	**1**	**1**	**1**
40 mg/ml	High	rColN	✗	✗	**15**	rColNS	**1**	**1**	**1**

2.3.3.4 Reaction efficiency

Cell encapsulation requires an interconnected pore system for proliferation. The reaction efficiency was correlated with a more intertwined network which influences the pore size and pore distribution. To better understand the reaction efficiency of rColNS hydrogels, colorimetric studies were performed with the Ellman's assay (described in chapter 4.2.5.3) using ColNS_medium as PoC with different molar ratios of thiol:norbornene. To establish the assay for this purpose, hydrogels were prepared as described in chapter 4.2.4.5 in a 96-well plate with 5 mg/ml rColS_medium with different concentrations of rColN_medium and 0.3 mg/ml LAP with 100 µl total volume/well. After irradiation (Omnicure S2000, 320 – 500 nm, 15 sec., 5.0 W/cm²), samples were covered with 200 µl Ellman reagent of different concentrations (0.2%, 0.1% or 0.01% (w/v)) and stirred (orbital shaker; 200 rpm) for 2-6 h at RT. Absorbance was then recorded without discarding the supernatant. Similar results were measured for all

three regent concentrations. This finding indicated that all three concentrations were sufficient to modify all thiol side chains. Differences were measured in the incubation time until a stable signal was reached. The higher the Ellman reagent concentration the faster a stable signal was reached (data not shown). To reduce the reagent concentration while maintaining an adequate incubation time to reach a stable signal 0.1% (w/v) Ellman reagent was chosen and the experiment was repeated for validation and to determine the minimal required incubation time to reach a stable signal. By measuring every hour an incubation time of 2 h was sufficient to reach a stable value at RT (see Figure 2-55). Data obtained showed high efficiency of the rColN photopolymerization reaction. An equimolar ratio of norbornene to thiol led to less than 20% unreacted thiols while twice the excess of norbornene units led to ~100% turnover of the primary thiols present in rColS.

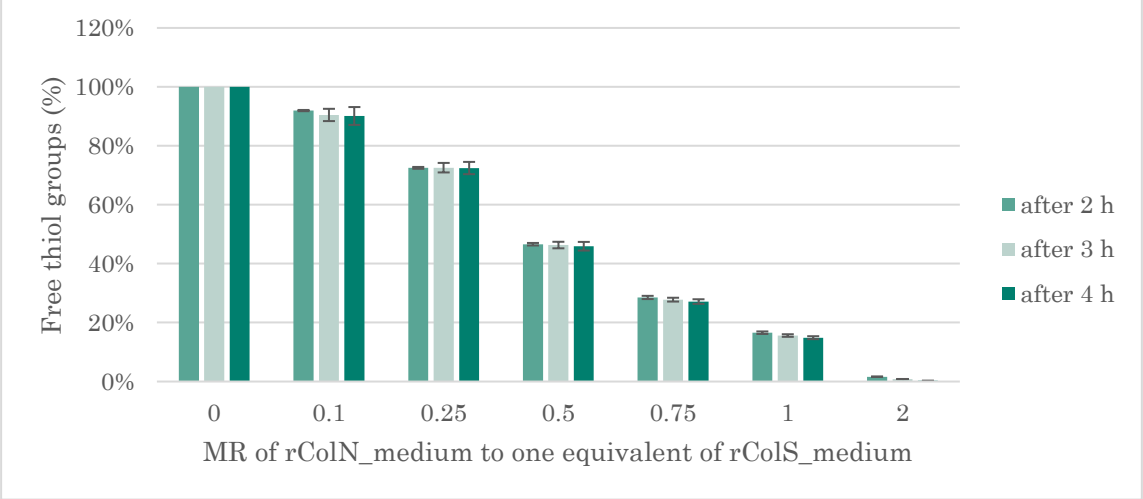

Figure 2-55: Assay establishment for reaction efficiency using the Ellman's assay. 0.1% (w/v) Ellman reagent was added to photopolymerization products of rColS_medium w/ or w/o rColN_medium. Ellman reagent in reaction buffer was used as blank. Sample groups were measured in triplicates. All data was normally distributed.

Within this thesis, rColN and rColS were not mixed with identical concentrations in (mol/l) but in 1:1 mass ratios (g/l). Thus, the experiment was repeated with defined mass concentrations (see Figure 2-56). Data showed the lowest free thiol content in rColNS_high and the highest free thiol content in rColS_low. rColNS_medium remained in the middle range. For rColNS_medium and rColNS_high no global trend was observed with respect to the applied concentrations. Considering also rColNS_low, the data showed a stronger difference by the applied type of rColNS (DoF) than by the applied concentration. The only exception remained the lowest tested rColNS_low concentration with a significantly higher signal compared to the other results. The average percentages of free thiols, excluding 5 mg/ml for rColNS_low,

were: rColNS_low = 9%; rColNS_medium = 6.6% and rColNS_high = 4.8%. The rather high signal of unreacted thiols for 5 mg/ml rColNS_low was assumed to result from the low density of reaction partners (steric availability) together with the low number of functional side chains per modified rCol molecule. Longer irradiation times could be tested for a possible increase of reacted side chains as well as alternating concentrations of LAP. Higher and lower concentrations of all three variants could also be tested to potentially identify additional concentration dependent trends. In conclusion and except for 5 mg/ml rColNS_low, a higher DoF resulted in more reacted side chains with shares of <10% of unreacted thiols.

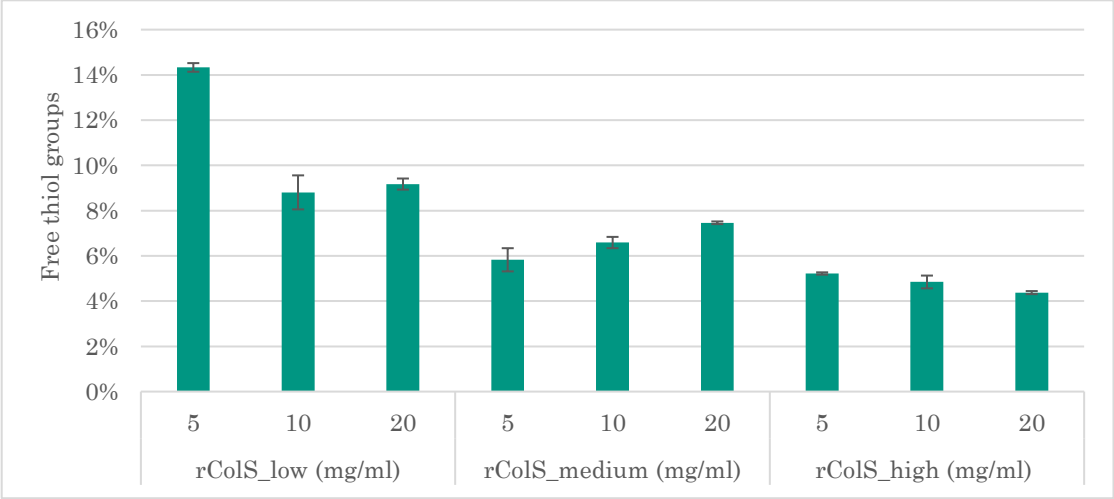

Figure 2-56: Ratio of free thiols after reaction of rColN and rColS with subsequent Ellman's assay quantification. 0.3 mg/ml LAP was used for the photopolymerization. The resulting signals were normalized on the applied final concentration of rColS_low, _medium or _high (N=3). Samples were diluted when needed to remain within the linear range of the unmodified rColS.

2.3.3.5 Self-gelation of rColS

2.3.3.5.1 Background

Disulfides are covalent bonds between thiols. The reaction occurs naturally between cysteine side chains, which essentially contribute to the secondary structure and tertiary of proteins. Disulfides are usually formed by the oxidation of sulfhydryl (-SH) groups.[355] Alternatively, disulfide bonds can form by thiol-disulfide exchange (see Ellman's assay; chapter 4.2.5.3). Collagen normally does not contain cysteine or if so only in small quantities.[356] By synthetically introducing thiols, disulfide bond formation could lead to hydrogel formation due to long time storage (cysteine can also be introduced genetically within the amino acid sequence). The self-gelation effect was observed, when rColS solution was stored between 4 °C - 25 °C for several days. To trigger disulfide bonds, several ways were described in literature like the

addition of an oxidation reagents like H_2O_2 or by the addition of several metals or enzymes which can catalyze the reaction.[357] The reaction is additionally triggered by pH.[358]

$$2\,R-SH \rightleftharpoons RS-SR+2H^{+}+2\,e^{-} \qquad \textbf{2-3}$$

$$RS-SR+R'SH \rightleftharpoons RS-SR'+RSH \qquad \textbf{2-4}$$

2.3.3.5.2 PoC and the influence of pH

As stated above, the pH plays an important role in disulfide bond formation. To test the influence of pH, rColS_low was dissolved with 100 mg/ml in three different buffer systems (1×PBS buffer, 0.1 M HEPES buffer pH 8.0 and carbonate buffer pH 10). Samples with pH 10 showed the fastest gelation, forming a gel even before complete dissolution which required the application of incubation at elevated temperatures to achieve a homogenous solution. After complete dissolution, all formulations were incubated at 2-8 °C. The solution dissolved at pH 10 let to the stiffest hydrogel formation with the fastest gelation kinetics. At pH 7.4 and pH 8.0 the hydrogel formed as well, but the gelation process took longer and the final hydrogel was softer. As a result, hydrogel formation was observed for all tested buffer systems when stored at 2-8 °C over different time periods. The higher the applied pH, the higher the resulting stiffness after identical time points. It was assumed that the basic pH accelerates the reaction to produce more crosslinks at the same time to form stiffer hydrogels.

2.3.3.5.3 The influence of temperature

Melting curves of rColS (Figure 2-52) demonstrated triple helical disintegration above ~30 °C. It was assumed that an elevated temperature (increase to 37 °C) might also change the rheological properties of rColS due to denaturation resulting in a liquid solution. To test this hypothesis and to reproduce the previous results, a freshly prepared 100 mg/ml rColS_low stock solution in carbonate buffer pH 10 was prepared overnight at RT followed by subsequent heating to 37 °C to allow full dissolution. The prepared solution was incubated over night at 2 to 8 °C which caused gelation. Subsequent incubation for 15 min at 37 °C dissolved the formulation again. The solution was stored for 14 h at 2 to 8 °C causing gelation again followed by incubation for only 1 min at 37 °C which was sufficient to dissolve the hydrogel again. Subsequent incubation at 2 to 8 °C for only 10 min caused gelation. This repetitive gelation and dissolution cycle was picturized in Figure 2-57. In summary, the self-gelation effect of rColS was reproducible and reversibility in repetitive warming and cooling cycles was proven.

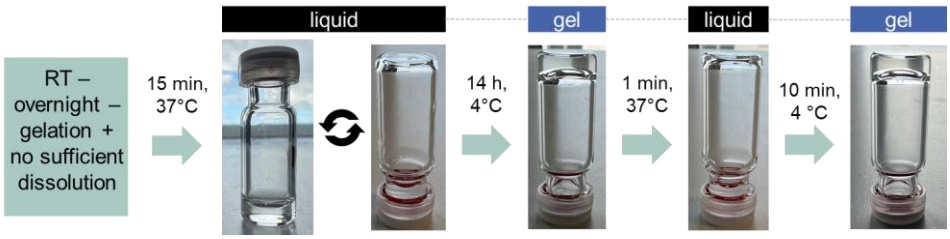

Figure 2-57: Gelation experiments with 100 mg/ml rColS_low in carbonate buffer pH 10 exposed to different temperatures for different time periods.

It was assumed that heat treatment disintegrated the triple helical structure and resulted single strands which didn't form a hydrogel anymore. This hypothesis aligns with the rColS melting temperatures extracted from Figure 2-52 (chapter 2.3.2.2.6) with T_m of 32-33 °C. By cooling down the formulation to ≤15 °C, the formulation gelated again. It was assumed that – based on the refolding experiments in Figure 2-60 (chapter 2.3.3.5.1) – temperatures below the melting temperature initiated refolding into the triple helical structure. To better understand the temperature dependent gelation and denaturation, the shear modulus of one selected formulation was recorded online with the ElastoSens™ Bio device (see chapter 4.2.6.3.2). To achieve a more intensive shear storage modulus (G') signal, rColS_medium was used (instead of rColS_low). By using identical repetitive heating and cooling cycles, the temperature dependent gelation was demonstrated. Briefly, the sample was initially heated to 40 °C followed by cooling to 5 °C. The sample was heated again with 1 °C/min until 40 °C was reached. Repetitive cycles of heating and cooling led to the data in Figure 2-58. Data demonstrated repetitive and reproducible increase and decrease in stiffness ranging from ~500 Pa until ~3500 Pa. To visualize the cyclic behavior, a sinus curve fit was applied. The longer the cooling phase lasted the higher the measured stiffness of the hydrogel (G'). A longer incubation time was associated with a higher share of refolding into the triple helix and thus an increased stiffness. To test this, the sample holder was incubated after the 3rd heating at 2 - 8 °C for 5 d which led to a further increase in a G' up to ~5000 Pa. By heating to 40 °C, comparable low G' values of ~500 Pa to preceding cycles were measured. The measured increased stiffness with longer cooling times was assumingly due to the ongoing refolding of the single strand into a triple helical structure. The disulfide formation has apparently not changed significantly during the measurements due to the similar stiffness after each heating cycle and the comparable melting temperature. In case of disulfide bond formation, a change in T_m was expected.

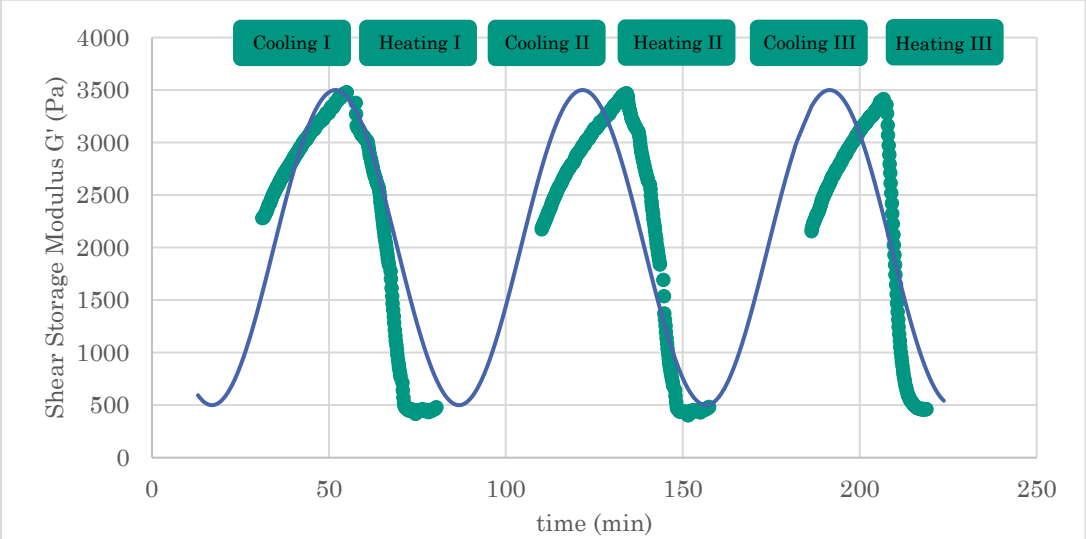

Figure 2-58: Increase and decrease of stiffness due to temperature changes of 2 ml of a 100 mg/ml rColS_medium solution in 1x PBS over time. Cooling meant a temperature change from 40 °C to 5 °C and heating *vice versa*. Anti-evaporation oil was used to avoid sample drying. The curve was fitted using Excel solver with a sinus fit (y=A*sin(wx)+B).

Generated data validated the temperature dependence and demonstrated a time-dependent gelation behavior as well. Based on these results, additional kinetic experiments were performed by a colleague (B. S. Thaqi; Evonik Operations GmbH) and displayed with her consent (see Figure 2-59). Samples were incubated at 2-8 °C and measured from time to time until a stable value was reached. Anti-evaporation oil was used to avoid sample drying. All tested samples showed a G' of 0.3 – 0.6 kPa after heating (40 °C) independently of the applied formulation (100 – 150 mg/ml rColS_low and rColS_medium). A rColS concentration dependent comparison of rColS_medium demonstrated a ~11× increase in G' (150 mg/ml vs. 100 mg/ml) during the 2nd cooling phase (18.4 vs. 1.7 kPa). For 150 mg/ml rColS_low a comparable G' to 150 mg/ml rColNS_medium of 18.5 kPa was measured. Differences appeared during the longer incubation phase at 2-8 °C. After 5 d at 2-8 °C G' values strongly increased to 4.8 kPa for 100 mg/ml rColS_medium (2.8× increase), 57 kPa for 150 mg/ml rColS_medium (3.1× increase) and 34 kPa for 150 mg/ml rColS_low (1.8× increase) were measured. Data showed an incubation time dependent increase in G' due to long time storage at 2-8 °C which revealed the effect of a lower or higher DoF on the hydrogel stiffness. In summary, the temperature, the rColS concentration and the DoF had a significant influence on the rheology of rColS solutions.

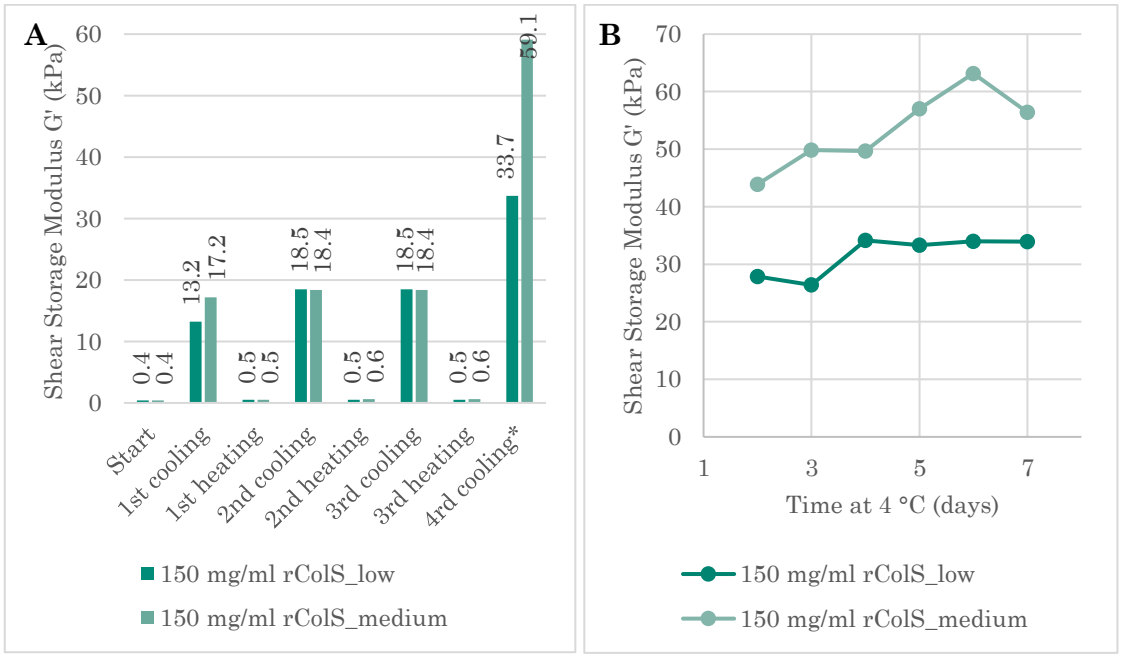

Figure 2-59: (A) Correlation of shear storage modulus of different rColS samples in 1×PBS when exposed to subsequent heating and cooling cycles (N=1). **(B)** Resulted shear storage modulus after temperature treatment in Figure A and subsequent storage at 4 °C for several days. Each sample was measured once per days at 4 °C machine temperature as a single measurement and was subsequently stored back art 4 °C. Anti evaporation oil was applied on the sample to avoid sample drying (N=1).

So far, all results demonstrated a reduction in G' when heated (40 °C) followed by hydrogel melting. This aligned with the identified melting curved for rColS (see chapter 2.3.2.2.6, Figure 2-52) of 32 – 33 °C. Additionally to the triple helical formation, disulfide bond formation was expected to contribute to the melting temperature. By increasing the pH from 7.4 (1×PBS) to 10 (carbonate buffer), gelation happened faster and a DoF and rColS concentration dependent increase in liquification temperature was observed (data not shown). By exploring this effect further and enabling the same effect in 1×PBS or 0.9% (w/w) NaCl the selected formulations could be relevant for injections. Ideally, the resulting temperature would be slightly higher than the human body temperature to ensure gelation after injection for e.g. cosmetic applications as dermal filler.

2.3.3.5.1 rColS refolding

In chapter 2.1.1.4, Figure 2-4 the temperature-dependent refolding of rCol was explored. In this chapter the experiment was repeated with rColS with another sample concentration (~25 mg/ml rColS each). The sample was denatured for 15 min at 40 °C and stored at 15 °C for up to 24 h. Samples before and after and after subsequent storage at 15 °C for 24 h were analyzed *via a* SEC chromatography with the method used in patent WO 2023/016892 A1.

The triple helix content was monitored at 1, 2, and 24 h as shown in Figure 2-60. Data were generated and provided by C. Banger, Evonik Operations GmbH and displayed with his consent**.** It showed a triple helical ratio of 83-91% before denaturation for all three samples. After denaturation (15 in at 4 °C) rColS_low remained the highest triple helical share of nearly 50% while rColS_medium showed 21% and rColS_high showed a triple helical ratio or amount of 13%. Within the next hours, the triple helical ratio increased for all samples leading to 90% refolding of rColS_low, 92% for rColS_medium and 84% for rColS_high after 24 °C incubation time at 15 °C in comparison to the triple helical share before denaturation. Triple helical unfolding was stronger with high DoF and refolding took longer to reach comparable shares of triple helical folding. In summary, this experiment demonstrated the capability of rColS to fold back in the triple helical state when stored at 15 °C over time. Longer refolding times (48 h or 72 °h) could increase triple helical share further. Based on this finding the hypothesis that changes in G' appeared from triple helical denaturation was strengthened. Also, the role of disulfide bond formation played an important role as shown in the long-term incubation at 4 °C (see Figure 2-59).

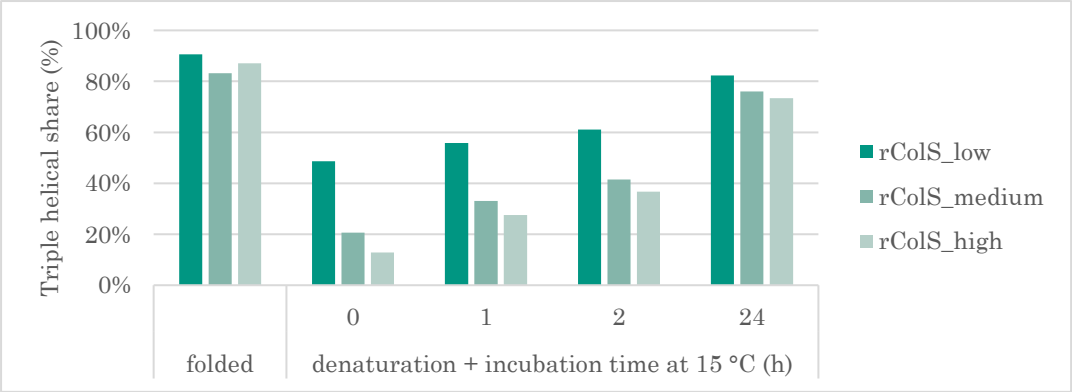

Figure 2-60: Temperature-dependent refolding of different rColS variants. ~25 mg/ml rColS solutions in 50 mM Na-Phosphate buffer pH 7.2 were measured, denatured and measured again *via* SEC-HPLC. The share in triple helical content was calculated based on the relevant peak integrals compared to the residual peak areas before and after denaturation. After denaturation, samples were incubated at 15 °C for 1-24 h prior to the analysis (N=1).

2.3.3.5.2 Application example

Due to the self gelation of rColS, injectables for e.g. dermal filler, cellular encapsulations or drug depots are highly appealing. To test the injectability of the formulation through a needle (G27), one formulation was chosen (100 mg/ml rColS_medium) in 1×PBS and in 0.9% NaCl solution. rColS was dissolved over night at RT forming a transparent solution which also gelated within this timeframe. The formulation was incubated at 37 °C followed by storage at 2-8 °C. After different minutes the formulation was ejected to visualize the increase in

viscosity (see Figure 2-61). After 8 min a visual increase in viscosity was observed which increased. After 15 min a strong but still ejectable hydrogel was formed (see Figure 2-61; B).

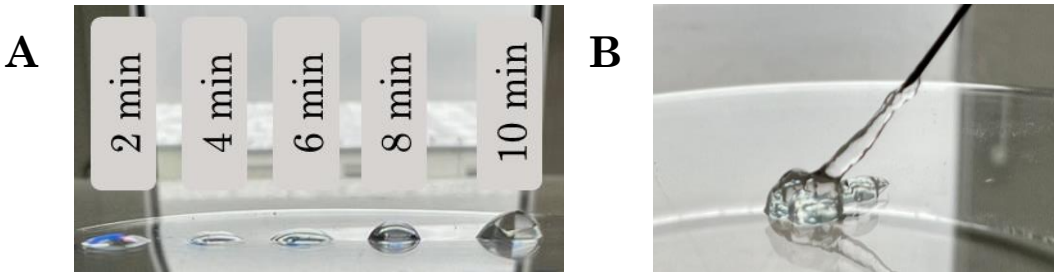

Figure 2-61: Ejected rColS hydrogel after different timepoints with 100 mg/ml rColS_medium. rColS_medium was dissolved in 0.9% NaCl. The formulation was heated to 37 °C for 5 min, filled in a 1 ml syringe with G27 needle attached and stored at 4 °C for up to 15 min. After different timepoint, the formulation was ejected. (B) after 15 min storage at 4 °C.

Based on literature, common injectable formulations for soft tissue fillers require stiffnesses from 7-600 Pa with viscosities (η) of 150-1630 Pas.[359] For a proper product development of an injectable hydrogels, several formulations might be screened including critical manufacturing steps like autoclaving of pre-filled syringes to ensure product sterility. Due to the medical focus of this thesis, this topic wasn't explored further. The self-gelation of rColS was demonstrated in different buffer systems and different rColS concentrations (100 – 150 mg/ml). A pH dependent effect in gelation was observed which was associated with pH triggered disulfide bond formation. Depending on the storage time at reduced temperatures (4-15 °C) strong differences in stiffness were recorded based on the applied rColS concentration and the applied DoF. The higher these parameters, the higher was the measured stiffness. Injectability was shown as a first PoC experiment and should also be explored further. Next steps could test the refolding effect after autoclaving of the rColS solution as well as testing 0.9% NaCl as alternative solvent. Also, the difference in melting temperature should be evaluated starting from a pre-gelated rColS formulation until full stiffness was reached. The increase in stiffness due to longtime storage was associated with disulfide bond formation. These links might have an increasing effect on the melting temperature. Based on the findings, rColS could be an interesting smart material for self-gelation.

2.3.4 Characterization of rColNS hydrogels

2.3.4.1 Porosity

The porosity was determined according to previous chapters (2.2.2.2.3 and 2.2.3.3.2) and correlated with the surface area of the material. The experimental procedure was described in chapter 4.2.6.4. A higher surface area was correlated with an increased water uptake (swelling). The more porous the surface, the better and faster was the expected swelling. Interconnected pores are also important for cell expansion within the matrix, and open porosity at the surface is necessary for cell infiltration.[360,361] In order to better understand the appearance of different formulations, rColNS hydrogel sponges were prepared according to chapters 4.2.4.5 and 4.2.4.8 with 5 mg/ml, 10 mg/ml and 20 mg/ml collagen resulting from 1:1 mixtures (w/w) of rColN and rColS in ddH_2O and three different DoF (low, medium and high). Cylindric hydrogels were prepared with 0.3 mg/ml LAP in self-made silicon molds (750 µl, 6.3 mm radius, 6 mm height). Hydrogel formulations were cured (Omnicure S2000; 5.04 W/cm²; 15 sec.) and lyophilized. The obtained hydrogel sponges were analyzed by SEM and the porosity and inner structure were analyzed (see Figure 2-62). The total porosity (detailed description in chapter 4.2.6.4) ranged from 83-96% for all tested formulations and increased slightly with amplified incubation time (83-94% after 1 h incubation, 88-96% after 24 h) (see Figure 2-62). Open porosity (detailed description in chapter 4.2.6.4) ranged from 12% to 35% and increased with amplified incubation time as well (12-29% after one hour, 24-35% after 24 . The lowest tested rColNS concentration (5 mg/ml rColNS) showed the highest open porosity and 20 mg/ml rColNS samples showed higher open porosity than 10 mg/ml rColNS samples. Cross section images validated this effect (see Figure 2-63). Additionally, the diameter of formed pore walls increased with the rColNS concentration for all DoF. An increase in pore diameters with 20 mg/ml rColNS samples was observed with an increased DoF. This effect was not observed with 10 mg/ml rColNS samples. An open porosity of max. 35% was not considered high compared to other crosslinking technologies using rCol which can reach open porosities of 50-80% (data not shown here). The same can be said for the total porosity, which can reach 95-99% with the DMTMM crosslinked reaction products (data not shown here).

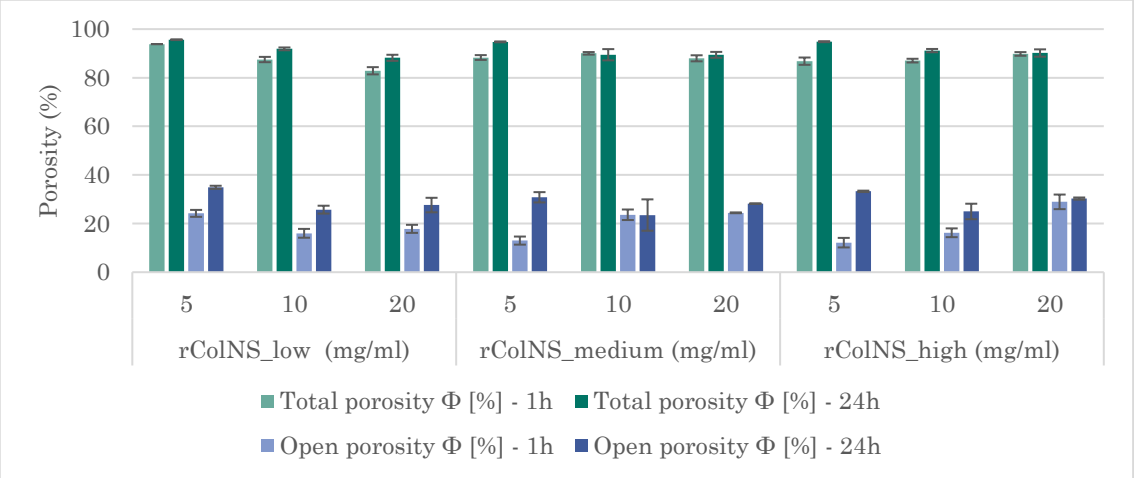

Figure 2-62: Porosity determination of 5-20 mg/ml total collagen made from rColNS (N=3). All data was normally distributed.

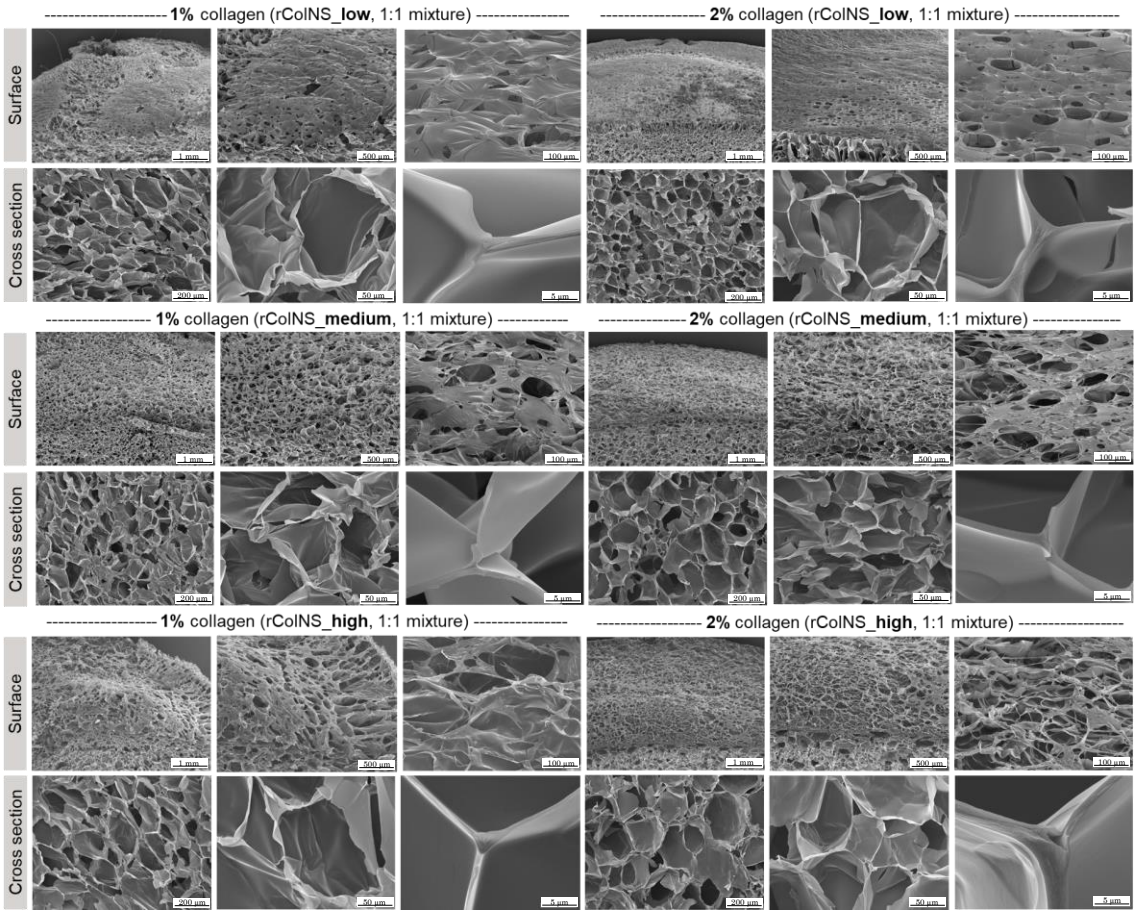

Figure 2-63: SEM imaging of rColN/S sponges. Sponges were prepared and analyzed according to chapter 4.2.4.8 and 4.2.6.2. Images were taken each from the surface of the sponge (1000 µm, 500 µm and 100 µm) and the cross chapter after freeze fracture (200 µm, 50 µm and 5 µm). 1% = 10 mg/ml; 2% = 20 mg/ml.

2.3.4.2 Swelling

The porosity was measured in analogy to chapter 2.2.2.2.3 and 2.2.3.3.2. Different formulations (5-20 mg/ml rColNS, all three DoF) were tested. Cylindrical samples were prepared according to chapter 4.2.4.8 (750 µl, 6.3 mm radius, 6 mm height) and incubated in 1× PBS at 37 °C for up to 72 h. The swelling ratio was calculated according to chapter 4.2.6.5. After 72 h swelling time, a swelling ratio between 8 - 14 was observed for all samples. The highest and fastest swelling was observed with the two highest rColNS concentrations with the two highest DoF (20 mg/ml rColNS_medium and 20 mg/ml rColNS_high). The increase in porosity and in pore size for the 20 mg/ml rColNS formulations from Figure 2-63 was aligned with an increased swelling (10.2 (low)→12.9 (medium)→14.1 (high). This effect was not reported for 5 and 10 mg/ml rColNS. One hypothesis was the more defined structure with higher rColNS concentrations.

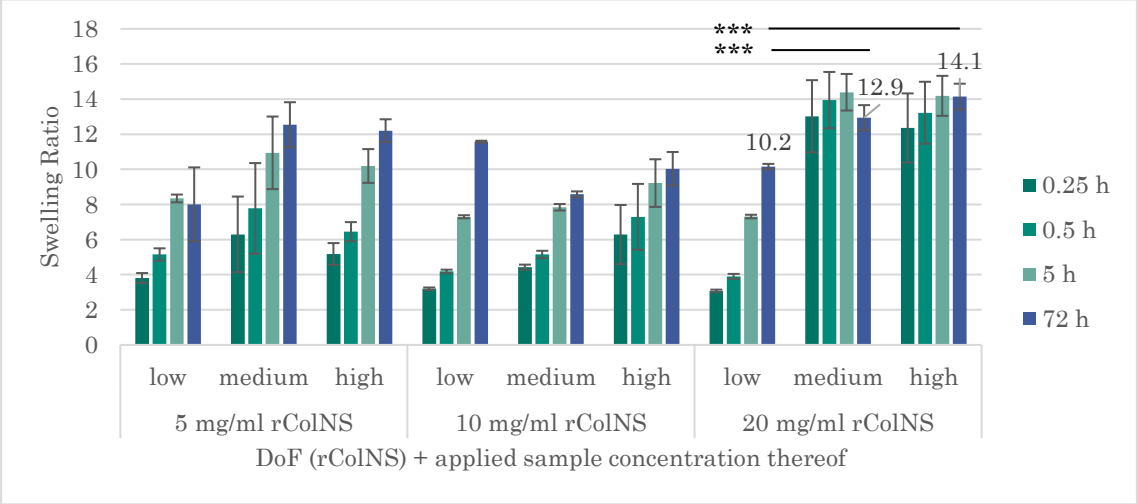

Figure 2-64: Swelling data of rColNS sponges in 1×PBS for 0.25-72 h at 37 °C (N=4). All data was normally distributed. A homoscedastic two-sided Student's t-test was performed with Excel *, **, *** represent $\alpha < 0.05$, 0.01, and 0.001, respectively.

2.3.4.3 Degradation

Biomaterials like collagens are naturally biodegradable and can be fully resorbed by mammalian organisms, which is favored especially for *in vivo* applications like sutures as they avoid later surgical removal. For different applications, different degradation times are desired. While some applications favor non to very slow degradation properties (like permanent implants, dermal filler) some applications benefit from a medium to fast degradation rate (long-term delivery scaffolds or resorbable tissue scaffolds). For bioinks, a medium degradation time is desired which ideally happens simultaneously tissue remodeling.

2.3.4.3.1 Hydrolysis

Hydrolysis was explored analog to chapter 2.2.2.2.4. Data showed an initial decrease in hydrogel mass within the first 24 h (see Figure 2-65). This effect increased with lower rColNS concentrations and lower DoF. The reason remained unclear but might be correlated with the significant higher numbers of unreacted side chains demonstrated in Figure 2-56 (chapter 2.3.3.4), which could leave collagen strands unreacted or cause insufficient structural integrity. Less structural integrity and a low number of intermolecular crosslinks could facility strand separation during denaturation (1×PBS solution; 37 °C). Additionally, non-crosslinked material could be flushed away or go into solution (depending on the fragment size). It was hypothesized that closer spherical distance (given by higher rColNS concentrations) and higher numbers of crosslinks (given by higher DoF) would reduce strand separation due to sterically hinderance and/or fragment entrapment. Extrapolated trendlines were calculated based on the remaining weight after 1 d of incubation (Figure 2-65; B), rColNS concentration of 30-40 mg/ml could lead to no material loss. After the initial decrease (after 1 d), no further decrease in weight was observed for any of the formulations tested over a monitoring time of 14 days. On the contrary, a slight increase in weight was measured for most of the formulations. The reason for this effect was not determined.

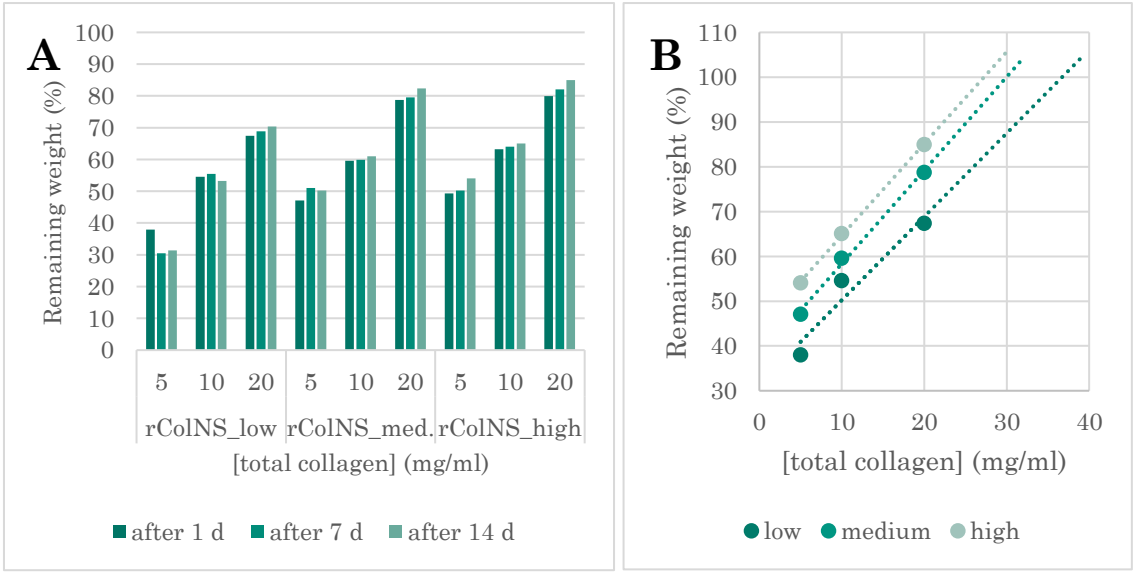

Figure 2-65: (A) Hydrolysis of rColNS hydrogel sponges over time under physiological conditions. **(B)** Blotting values from figure A with extrapolated linear trendlines.

2.3.4.3.2 Enzymatic degradation

Enzymatic degradation was performed in analogy to chapter 2.2.2.2.4 and 2.2.3.3.1 with a metalloproteinase mixture. The choice of enzymes was outlined in chapter 2.2.2.2.4. The decrease in wet weight was monitored after an initial swelling phase in reaction buffer for 24 h

according to chapter 4.2.6.6.2. A commercially available animal-derived bovine collagen reference (Lyostypt®, Braun) was used. The initial wet weight after soaking in enzyme buffer (24 h at 37 °C) was used as reference wet weight. After adding the enzyme solution, loss in wet weight was determined. All samples degraded completely within 24 hours. The DoF had a significant effect on the degradation rate, especially for rColNS_low (see Figure 2-66). A concentration-dependent degradation was observed. Samples made from higher rColNS concentrations had longer degradation times. After addition of the enzyme solution, all rColNS_low samples decreased in weight within 1 h, while surprisingly, all formulations with rColNS_medium or rColNS_high increased slightly in weight. One potential hypothesis could be that the enzymatic activity increased the pore size of rColNS_medium and high, which may have promoted swelling in the beginning of the experiment. It was assumed that this effect was not visible for rColNS_low due to the fast degradation. The bovine collagen reference was also hydrolyzed by the enzymatic activity but the degradation rate should not be directly compared due to the different sample surface areas. In summary, all formulations were degraded by the enzymatic activity. The degradation rate was highly dependent on the DoF during hydrogel synthesis. This knowledge could be used to find the optional rColNS composition for a specific application, followed by testing tissue specific metalloproteinases for side specific applications.

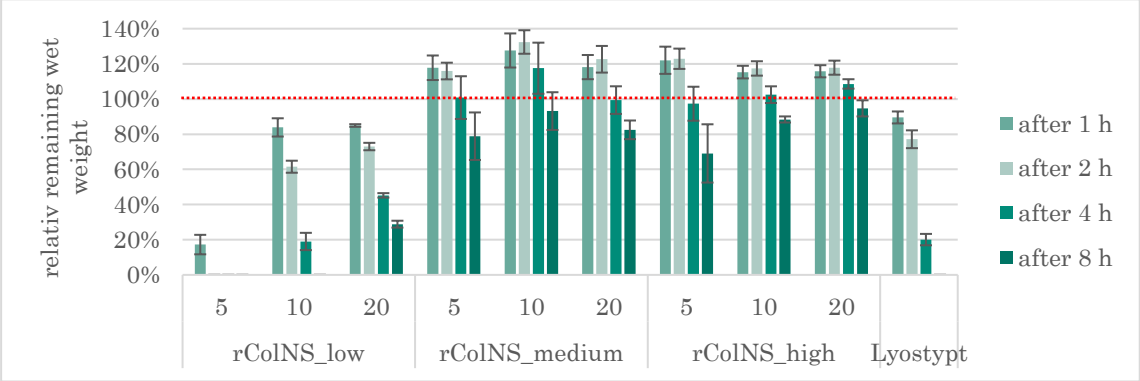

Figure 2-66: Enzymatic hydrolysis of different rColNS formulations with different DoF over a period of 8 d with Collagenase from *Clostridium histolyticum* in comparison to animal-derived Lyostypt®. All samples had a cylindrical shape with a diameter 6.3 mm and height 6 mm in dry state except for the animal-derived reference which was a flat sponge patch. The starting weight (100%) was depicted with a red dotted line (N=3). All data was normally distributed.

2.3.4.3.3 Rheology

As described in chapter 4.2.6.3 the gelation kinetics were recorded using the ElastoSens™ Bio device with the described method in chapter 4.2.6.3.2. To establish the device for photopolymerization, different formulations with polyethylene glycol diacrylate (PEG-DA,

benchmark material) were used. PEG-DA hydrogels showed a linear increase in shear storage modulus (G') until complete cure from 54 kPa with 20% (v/v) material in 1×PBS with 1 mg/ml LAP (see Figure 2-67).

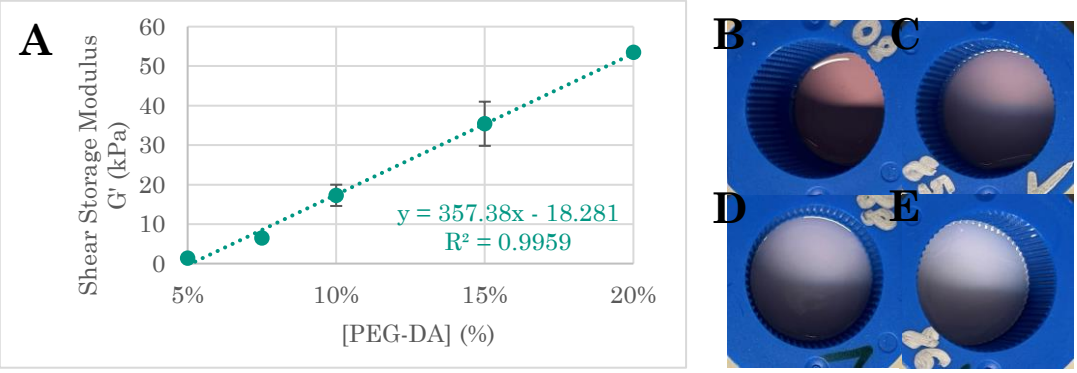

Figure 2-67: (A) Shear storage moduli (G') of different hydrogels made of different concentrations of PEG-DA (M_n = 575 g/mol) within the plateau phase of the gelation kinetic using the ElastoSens™ Bio **(B)** Different PEG-DA formulations after photopolymerization 2.5% (not solid); **(C)** 5% (solid); **(D)** 7.5% (solid) and **(E)** 10% (solid).

Next, rat tail collagen methacrylate (rtColMA) formulations were tested based on a 10 mg/ml stock solution in 20 mM acetic acid. The rtColMA stock solution was challenging to handle. The preparation of an 8 mg/ml rtColMA formulation caused issues like bubble formation, material loss and probably insufficient homogenization. Therefore, a maximum concentration of 6 mg/ml rtCol was evaluated. The stock solution was diluted to a final concentration of 2-6 mg/ml rtColMA in 1×PBS containing 1 mg/ml LAP. For the physical gelation, the sample was prepared on ice and transferred to the sample holder, followed by heating to 37 °C to reach a plateau phase to trigger physical gelation, followed by irradiation at 405 nm leading to a second plateau phase caused by chemical crosslinking (see Figure 2-68). Physical gelation showed a concentration dependent increase in G' with a low standard deviation from 0.8 kPa (2 mg/ml rtColMA) to 2.7 kPa (6 mg/ml rtColMA). Subsequent photopolymerization (see chapter 4.2.6.3.2) increased G' to 1.3 kPa (2 mg/ml rtColMA) and 6.8 kPa (6 mg/ml rtColMA). The standard deviation for chemical crosslinking was higher than physical crosslinking which could be conditioned by issues with photoinitiator homogenization within the formulation, as well as limited diffusion before photopolymerization and during physical gelation. In conclusion, the experimental data showed a rtColMA concentration-dependent increase in stiffness during physical gelation, which was further enhanced by chemical crosslinking. All formulations turned to cloudy white during the process, which is an obstacle for applications which require transparency for e.g. microscopic applications (see Figure 2-68; B). While the

resulting stiffness range is excellent for soft tissue applications (see Figure 1-7) the material might be too soft for stiffer tissues such as cartilage.

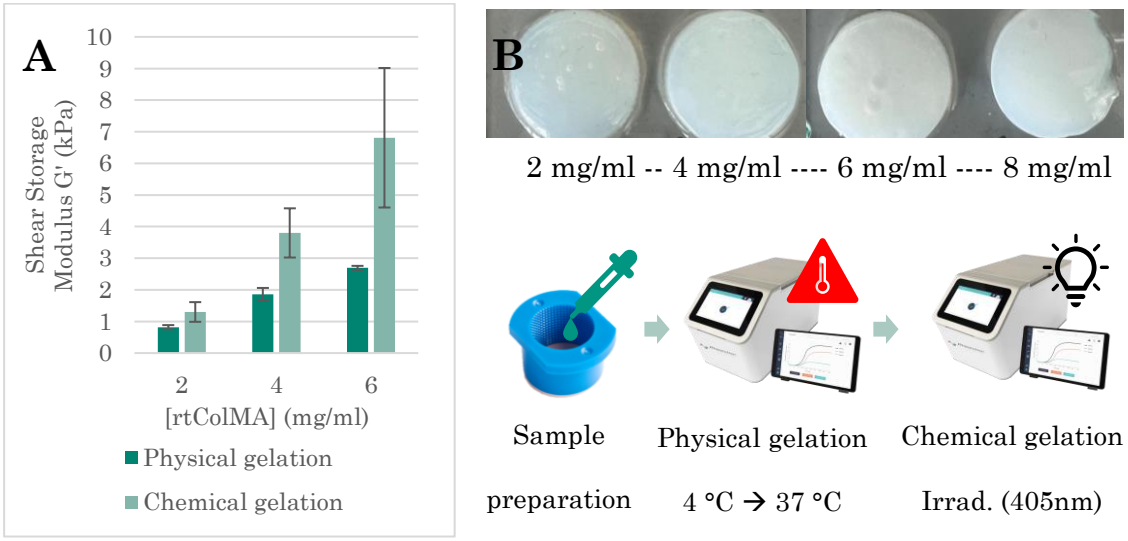

Figure 2-68: (A) Shear storage modulus (G') measurements of rtColMA samples in 1×PBS and 1 mg/ml LAP. Hydrogels made of different concentrations of rtColMA (Cellink) were analyzed with ElastoSens™ Bio (N=2). Sample groups were measured in duplicates. All data was normally distributed. **(B)** Visual hydrogel appearances after chemical crosslinking of 2-8 mg/ml rtColMA and subsequent experimental process steps of the measurement.

Next, different rColNS formulations were tested in a duplicate using photopolymerization, which showed a low standard deviation. Three example measurement with their standard deviation of duplicates were depicted in Figure 2-69 (A). The extracted and collected storage moduli were depicted in Figure 2-69 (B). Measurements with rColNS showed an adjustable G' based on the chosen rColNS concentration and the chosen DoF. The increase of both parameters increased the final stiffness (G'). As an example, 40 mg/ml rColNS_low resulted in 9.9 kPa, 40 mg/ml rColNS_medium in 19 kPa and 40 mg/ml rColNS_high in 26.2 kPa. To better understand the potential range of stiffness, a high concentration with the highest DoF was tested (100 mg/ml rColNS_high) resulting in a G' of 57 kPa.

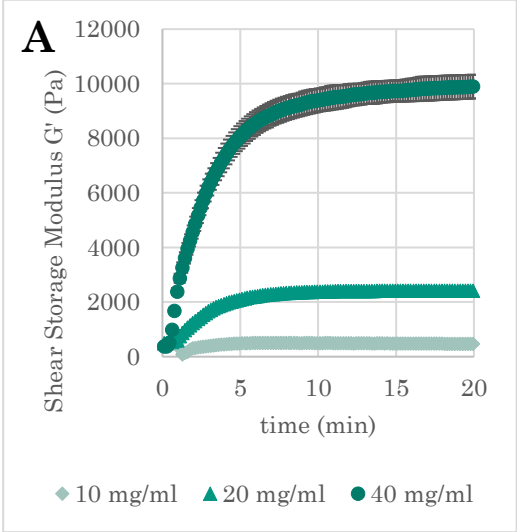

B

Total rColNS (1:1 mixture)	Final G' (kPa)		Average (G')
	Rep. I	Rep. II	
10 mg/ml low	0.5	0.5	0.5 ± 0.0
20 mg/ml low	2.4	2.4	2.4 ± 0.0
40 mg/ml low	10.2	9.6	9.9 ± 0.3
10 mg/ml medium	1.3	1.3	1.3 ± 0.0
20 mg/ml medium	5.7	5.6	5.7 ± 0.1
40 mg/ml medium	18.1	19.9	19 ± 0.9
10 mg/ml high	1.6	1.7	1.7 ± 0.1
20 mg/ml high	7.1	7.5	7.3 ± 0.2
40 mg/ml high	26.0	26.3	26 ± 0.2
100 mg/ml high	57	57	57

Figure 2-69: (A) Measured increase in shear storage modulus (G') of different rColNS hydrogel formulations induced by photopolymerization. Samples were tested in duplicates; the standard deviation was performed in Excel. **(B)** Rheological measurements of rColNS formulations (each 2 ml in 1×PBS, 0.3 mg/ml LAP) with the ElastoSens™ Bio device (N=2).

By correlating the measured stiffnesses, a polynomial fit was calculated with allows the stiffness prediction of intermediate formulations (see Figure 2-70).

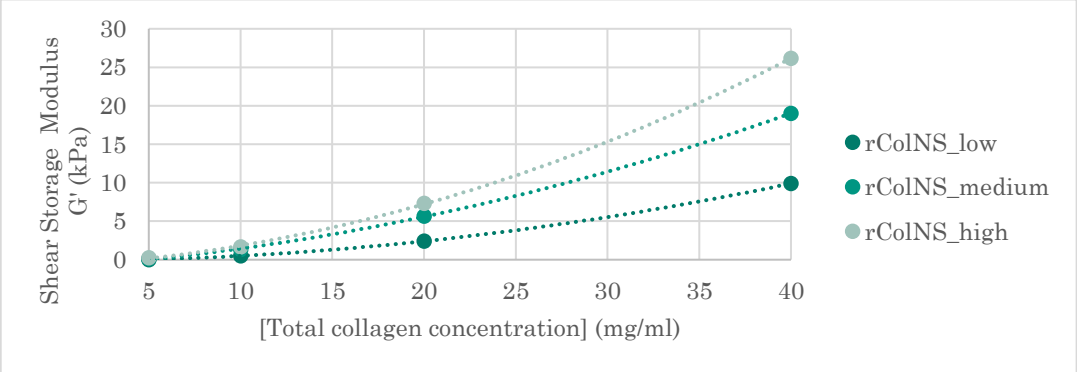

Figure 2-70: (A) Storage moduli of different rColNS formulations after complete gelation vs. applied rColNS mass concentration by 1:1 mixture of rColN and rColS with different DoF (low, medium and high).

In 2020, Tytgat *et al.* modified another recombinantly expressed collagen protein in a similar way. By using 100 mg/ml of the of norbornene-modified and thiolated collagen a G' of 16 kPa was genereated.[175] Compared to rColNS_high, the material from Tytgat *et al.* resulted in a 3.5× reduction of measured stiffness which highlighted to broad spectrum of rColNS in regards to the measured stiffness after crosslinking. Here, radical chain polymerization of rColN was used as reference to rColNS. Although it should be noted that norbornenes are

expected to be less reactive than terminal alkenes (including methacrylates), rColN was used as a first reference. Based on the generated data in chapter 2.3.3.2, Table 2-7, at least 1 mg/ml LAP was necessary to form a hydrogel with only rColN_high for 20 and 40 mg/ml material. Without rColS, rColN formed hydrogels with significantly lower G' even by increasing the LAP concentration (see Table 2-10). Increase in LAP concentration caused increase in G' for the radical chain polymerization with rColN. In chapter 2.3.3.4, Figure 2-56, only small shares of unreacted thiol side chains remained after crosslinking. Thus, only a small increase in G' was expected for rColNS by using a higher LAP concentration than 0.3 mg/ml. For 20 mg/ml rColNS_high only 4% unreacted thiols were determined. A similar share for 40 mg/ml rColNS_high was expected and no increase in G' was detected by increasing the photoinitiator concentration from 0.3 mg/ml to 2 mg/ml. This confirmed the high reaction efficiency known for thiol-ene chemistry. The low LAP concentration of 0.3 mg/ml LAP was used for follow up experiments to keep the PI concentration as low as possible to avoid potential PI induced cell damages from formed radicals. In summary, rColNS showed superior stiffness at identical concentrations and was evaluated as a superior technology compared to radical chain polymerization.

Table 2-10: Rheological measurements with rColN w/ and w/o rColS using the ElastoSens™ Bio. Constantly 1 mg/ml LAP was used with a sample volume of 2 ml. Depicted values were extracted from the plateau phase of the measured kinetics.

Sample	LAP (mg/ml)	Final G' (kPa)		Average (G')	Difference in stiffness (rColN vs. rColNS)
		Rep. I	Rep. II		
20 mg/ml rColNS_high	**0.3**	7.1	7.5	7.3 ± 0.2	**1.0×**
20 mg/ml rColN_high	**1**	0.58	0.54	0.56 ± 0.02	0.07×
20 mg/ml rColN_high	**2**	0.96	-	0.96	0.13×
40 mg/ml rColNS_high	**0.3**	28.50	-	28.50	**1.0×**
40 mg/ml rColNS_high	**1**	28.71	-	28.71	1.0×
40 mg/ml rColNS_high	**2**	27.82	-	27.82	1.0×
40 mg/ml rColN_high	**1**	1.27	1.04	1.16 ± 0.12	0.04×
40 mg/ml rColN_high	**2**	3.13	-	3.13	0.11×
40 mg/ml rColN_high	**5**	4.48	-	4.48	0.16×

2.3.4.3.1 Developing tissue specific scaffolds with elastic and shear modulus

Based on a recent market analysis, 3D tissue printing is currently being developed for cornea, vasculature, cartilage, bone, skin, cancer models, and adipose tissue.[247] Within this thesis, two relevant cell types were selected to estimate a potential use of the materials for skin and cartilage repair. Other applications, such as cancer models and vasculature were excluded due to high model complexity. Bone was also excluded due to the very high material stiffness

that is difficult to achieve with hydrogels. To test two different stiffnesses, skin (here fibroblast scaffold) and cartilage (chondrocyte scaffold) were selected. For the selected applications, elastic moduli (E) of ~3 kPa and ~14 ±1 kPa were reported for fibroblasts (skin) and for chondrocytes (cartilage), respectively.[362] As introduced in chapter 1.3.2, the stiffness of the hydrogel plays an important role on the cellular wellbeing and the integration into existing tissues. Although cells can sometimes remodel the scaffold and replace it by their own matrix which alternates the composite stiffness, matching the desired stiffness from the beginning might be beneficial for a great cellular well being. Based on equation 1-2 (chapter 1.3.2.3) (E' = 2.5G' to 3G'), the tensile strength can be recalculated into the shear storage modulus leading to a G' of ~1 kPa for skin tissue and a G' of ~4.7-5 kPa for cartilage. To find suitable formulations, the measured G' of rColNS formulations using the ElastoSens™ Bio can be used to find the optimal composition. Ideally, the measurement shall be repeated with cells incorporated into the formulations to depict the real matrix stiffness. Also, the cells should be incubated for 24 h before the measurement to reduce false negative results due to swelling or hydrolysis effects, which could occur within the first hours of incubation to get a more exact value. However, this is connected to different obstacles like the observed hydrogel shrinkage, which was reported in chapter 2.3.4.3.1 for lower concentrated formulations making ElastoSens measurements impossible. Direct molding into the sample holders would detach them during the cultivation which hinders a correct measurement. Also some cells like fibroblasts are known to develop strong contraction, which leads to a shrinkage of the scaffolds during cultivation.[363,364] In summary and to keep the experimental set up simple, measured values based on cell free scaffolds measured at 25 °C were considered as first orientation to predict an adequate material stiffness for different cell types and tissues. Based on these values formulations for fibroblasts and chondrocytes were tested in the biological chapter below.

2.3.4.4 Leachables

To evaluate the biocompatibility of the rColNS hydrogels, a leachable assay was applied as described in 4.2.3.2. To reduce toxic side effects from formed radicals during photoactivation, hydrogel extracts were prepared after crosslinking and a dose-depended toxicity assay was performed by exposing the extracts to pre-seeded HFF. After an incubation period of 24 h the cells viability was analyzed using the MTS assay (CellTiter 96® AQueous One Solution Cell Proliferation Assay, Promega).

Figure 2-71: Leachable assay of rColNS hydrogels tested on HFF. Exposure time was 24 h and detection happened with the CellTiter 96® Aqueous One Solution Cell Proliferation Assay (Promega) (N=3). All data was normally distributed.

2.3.4.5 Biomaterial sterility

The production of bioinks required sterile print components. Several methods have been reported in the literature to ensure sterility, including plasma sterilization, sterile filtration, gamma or UV light irradiation, and dry or wet heat sterilization. Due to the potential interference of UV light with the protein structure in terms of crosslinking effects such as tyrosine dimer formation in collagen[365] or protein degradation, as well as the heat sensitivity of rCol, some technologies were excluded. For animal-derived collagen (MW ~300 kDa) there were additional limitations. For example, sterile filtration of a rat tail collagen solution with a 0.2 µm pore size filter resulted in clogging. Due to the significantly lower molecular weight and viscosity of rCol, sterile filtration was tested for feasibility. Solution with 10 mg/ml rCol (unmodified and modified) were prepared in ddH_2O. 2 ml solutions with and without sterile filtration (0.2 µm filter) were transferred into 50 ml sterile Greiner tubes with filter caps ("non-sterile sample"). After subsequent lyophilization, dry weights were plotted (see Figure 2-72). No significant difference was observed between filtered and unfiltered samples and no trend was observed. Data indicated that there was no significant weight loss due to sterile filtration.

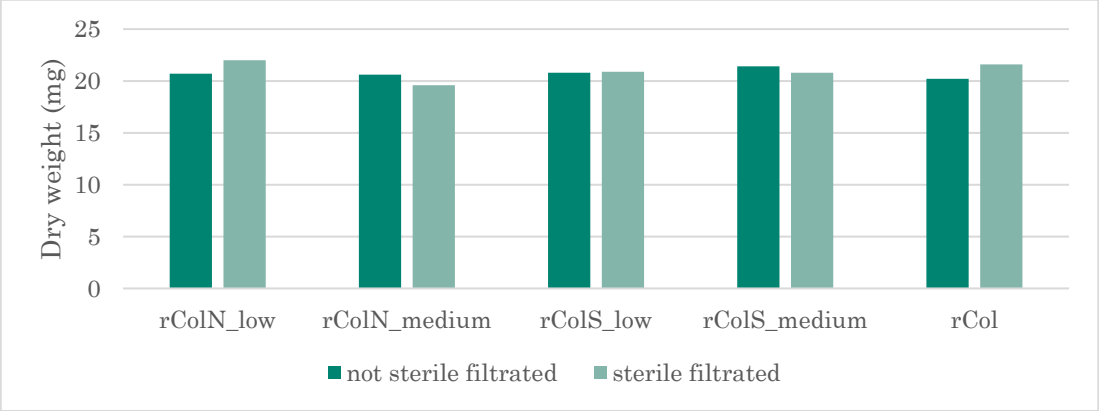

Figure 2-72: Dry weight comparison before and after sterile filtration of different samples. Animal-derived rat tail collagen (Sigma) was tested as well but sterile filtration (0.2 µm pore size) wasn't possible due to instant clogging (N=1).

Next, a sterility kit was used to determine biological contamination of unfiltered and filtered samples from Figure 2-72 by using ROTI®DipSlides (CASO/RBCenr, Carl Roth, 3934.1) according to the user manual (see chapter 4.2.3.6). Images were taken after 2 d and 5 d of culture (see Figure 2-73). After 5 d of culture (supplier's recommended incubation time), growth was seen on both sides of the control slide with 8 colony-forming units (CFU) for eukaryotes and 64 CFU for procaryotes. Partial bacterial growth without sterile filtration was observed for some samples (case 2) with 28 CFU and no growth was observed for all without sterile filtration (case 1). This indicated that some contamination occurred due to the non-sterile processing of the material which would be removed by sterile filtration. In summary, the data showed that sterile filtration does not result in drastic material loss for the tested formulations and no bacterial, fungal or yeast growth was observed with the ROTI®DipSlides used, demonstrating that sterile filtration is an excellent option for material sterilization or decontamination on a laboratory scale. The applicability for larger batch sizes has to be evaluated in the future.

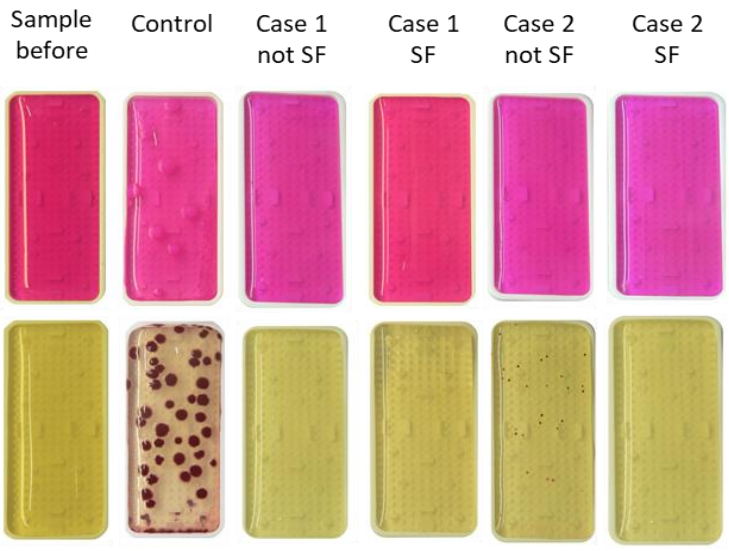

Figure 2-73: Sterility Assay after 5 d incubation time at 30 °C under humid conditions. "Sample before" shows an inoculated slide before the incubation time. The red agar fosters the growth of yeast and fungi, the yellow agar the growth of bacteria.

2.3.4.6 Cell Adhesion and cellular ingrowth

2.3.4.6.1 Initial screening

Unlike polysaccharide-based hydrogels, proteins contain recognition pattern for biological interactions like cell adhesion. Collagens derived from animals, for example, are known for their high abundance of cell binding sites such as the common integrin binding pattern RGD (Arg-Gly-Asp). rCol does not contain the RGD motif. In 1996, alternative integrin binding domains were published.[366,367] One example is the DGEA motif which occurs once per strand. To evaluate cell adhesion, human fibroblasts (HFF), human epithelial cells (HeLa) and murine fibroblasts (NIH3T3) were tested on different photopolymerized rColNS formulations according to chapter 4.2.3.3. Microscopic images were recorded within seven days followed by Hoechst 33342/Live/Dead staining (see Figure 2-74). Most cells were viable after seven days and a 2D cell layer had formed. In comparison the plasma-treated surface consistently showed better growth behavior compared to the hydrogel surfaces. Data also indicated cell type-specific cell adhesion. While fibroblasts showed strong cell adhesion on the rColNS formulations, HeLa cells did not adhere at all. Instead, they formed spheroids. Differences between HFF and NIH3T3 cells were observed already after one day of incubation. The NIH3T3 cells were proliferating faster. This could be due the immortalization of NIH3T3 cells compared to the primary HFF. Primary cells are known to grow slowly. Furthermore, a higher rColNS concentration showed more attached cells after seven days (10 mg/ml vs. 5 mg/ml)

and rColNS_medium showed better adhesion than the combination of rColN_medium and rColS_low. It was assumed that the stiffer rColNS_medium hydrogels accelerate cell adhesion. The exact reason for the difference in cell adhesion remained unclear. Cell adhesion was also cell type specific. While fibroblasts attached well, tested epithelial cells (HeLa) did not attach to the hydrogel surface. This effect needed to be validated by experimental replication and by testing more cell types, which was done in Figure 2-78. Selective cell adhesion could be exploited as feature for applications like selective cell isolation from e.g. a biopsy.

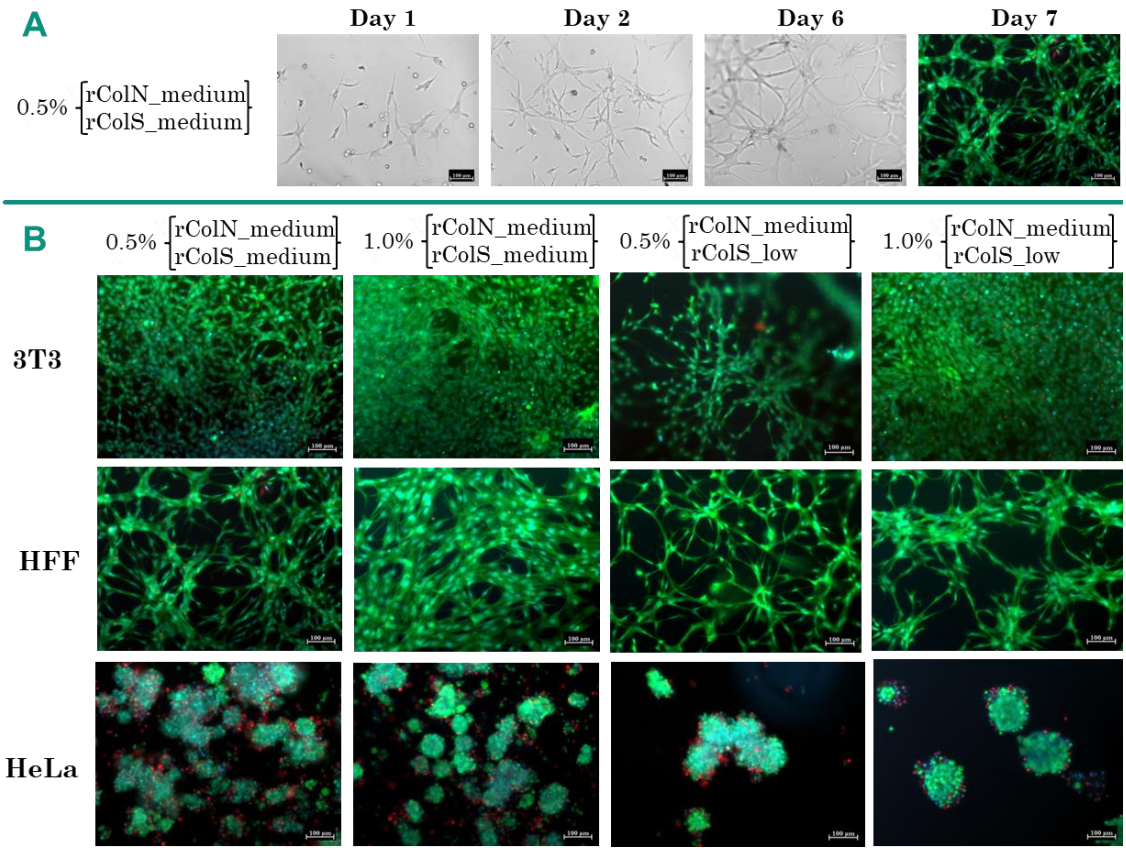

Figure 2-74: Cell adhesion experiment of different cell types (3T3, HFF and Hela) on different photopolymerized rColN/rColS hydrogel formulations. **(A)** Exemplary HFF behavior within the test period of seven days represented by brightfield imaging at day 1, 2 and 6 followed by LIVE/DEAD/Hoechst staining according to chapter 4.2.3.5.1 at day 7. **(B)** Different cell behavior after 7 days of culture and subsequent LIVE/DEAD/ Hoechst staining. Viable cells (green), dead cells (red) and cell nuclei (blue) were stained.

2.3.4.6.2 Confirmation study

To validate the obtained data, the experiment was repeated with additional formulations of rColNS (5 mg/ml and 10 mg/ml rColNS_low, rColNS_medium and rColNS_high) and additional cells (human chondrocytes (SW1353 cells). Cured hydrogels were topped by respective

culture medium (200 µl each) and incubated overnight at 4 °C to ensure no osmolar effects during the experiment. Within seven days, brightfield imaging was performed showing similar results as the previous experiment (see Figure 2-75). Plate controls again showed the best cell adhesion with confluence after 1-2 days. HeLa cells repeatedly failed to attach to the hydrogel surface. Formulations with 5 mg/ml rColNS_low dissolved within the first days of cultivation, and some formulations lost about half of their volume (10 mg/ml rColNS_low and 5 mg/ml rColNS_medium). Formulations with higher DoF or higher rCol concentration (10 mg/ml rColNS_medium, 5 mg/ml rColNS_high and 10 mg/ml rColNS_high) visually retained their volume and were depicted in Figure 2-75. For NIH3T3 cells, a higher rColNS concentration and DoF showed higher numbers of adhered cells. This effect was not observed for HFF and SW1353 cells. After 5 days of incubation cells showed between 60 and 100% confluency. The best results were achieved with NIH3T3 cells which showed a much higher cell adhesion with 10 mg/ml rColNS which arose the hypothesis, that the rColNS concentration is more crucial than the applied DoF. With HFF, the same trend was observed. For SW1353 cells no clear trend was observed and the best adhesion was reported on the stiffest hydrogel made from 10 mg/ml rColNS_high. In summary, cell adhesion was observed for 3T3, HFF and SW1353 cells as well as no cell adhesion for HeLa cells which aligned with the previous data. Also, stiffer or more concentrated rColNS formulations showed improved cell density after 5 d of incubation than softer hydrogel version.

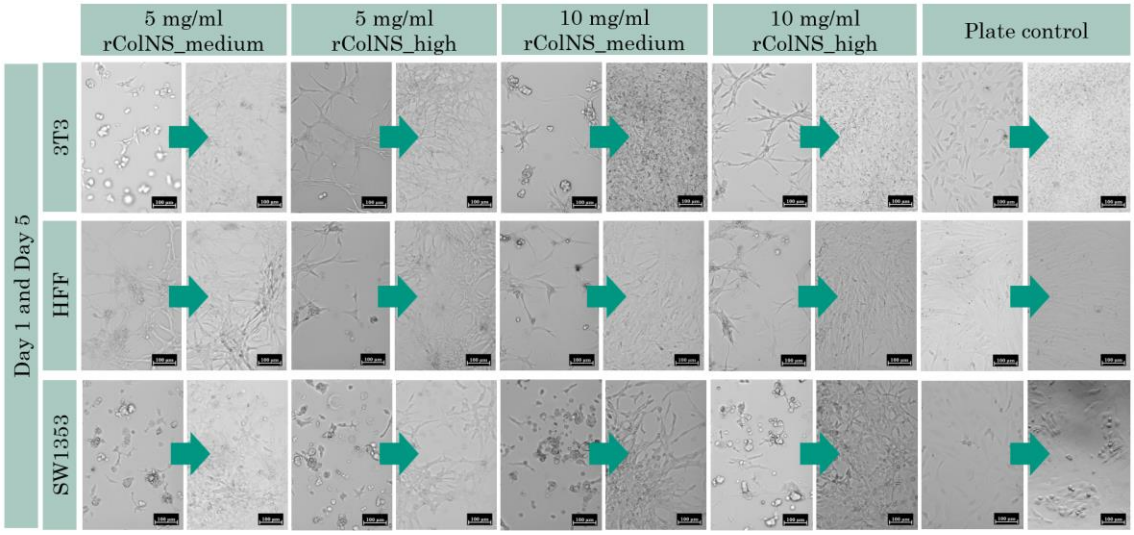

Figure 2-75: Cell adhesion of different cell types (NIH3T3, HFF and SW1353 cells) on different cured rColNS hydrogel formulations (0.3 mg/ml LAP; curing according to standard Omnicure S2000 settings) after one day and 5 days of incubation. Brightfield pictures of both timepoints were connected by an arrow. The experiment was conducted in a 48 well format as described in the method chapter 4.2.3.3.

2.3.4.6.1 Cellular ingrowth

In a third attempt, the cell adhesion experiment was repeated with only HFF cells for a prolonged incubation time (21 d) followed by Live/Dead staining to detect for long-term viability and cellular ingrowth. After 21 days, cells showed high viabilities with partially 100% confluency (plate control, 20 mg/ml rColNS_medium). After two weeks, cellular extensions were observed growing into the gel, as shown in see Figure 2-76. Cellular ingrowth started between day 7 and 14 with the lower concentrated formulations. The effect was stronger with a lower DoF (rColNS_low > rColNS_medium) (see Figure 2-77). On the other side, 2D cellular growth was more uniformly distributed on higher concentrated rColNS formulations which aligned with the previous results. The highest tested formulation with rColNS_low (20 g/ml total collagen) demonstrated the best cellular attachment, which was comparable to the plasma treated cell culture surface reference. However, the cellular attachment to the reference (plasma treated cell culture plate) was consistently superior to that of the tested hydrogels which also aligned with previous results. It was assumed that the high matrix stiffnesses and highly density of the collagen scaffold could lead to increased exposed number of binding sites to the surface, leading to a stronger cell adhesion. In summary, especially the lower concentrated formulations showed HFF ingrowth into the hydrogel matrix. The highest confluency was observed with the highest tested concentration of rColNS_medium (see Figure 2-77).

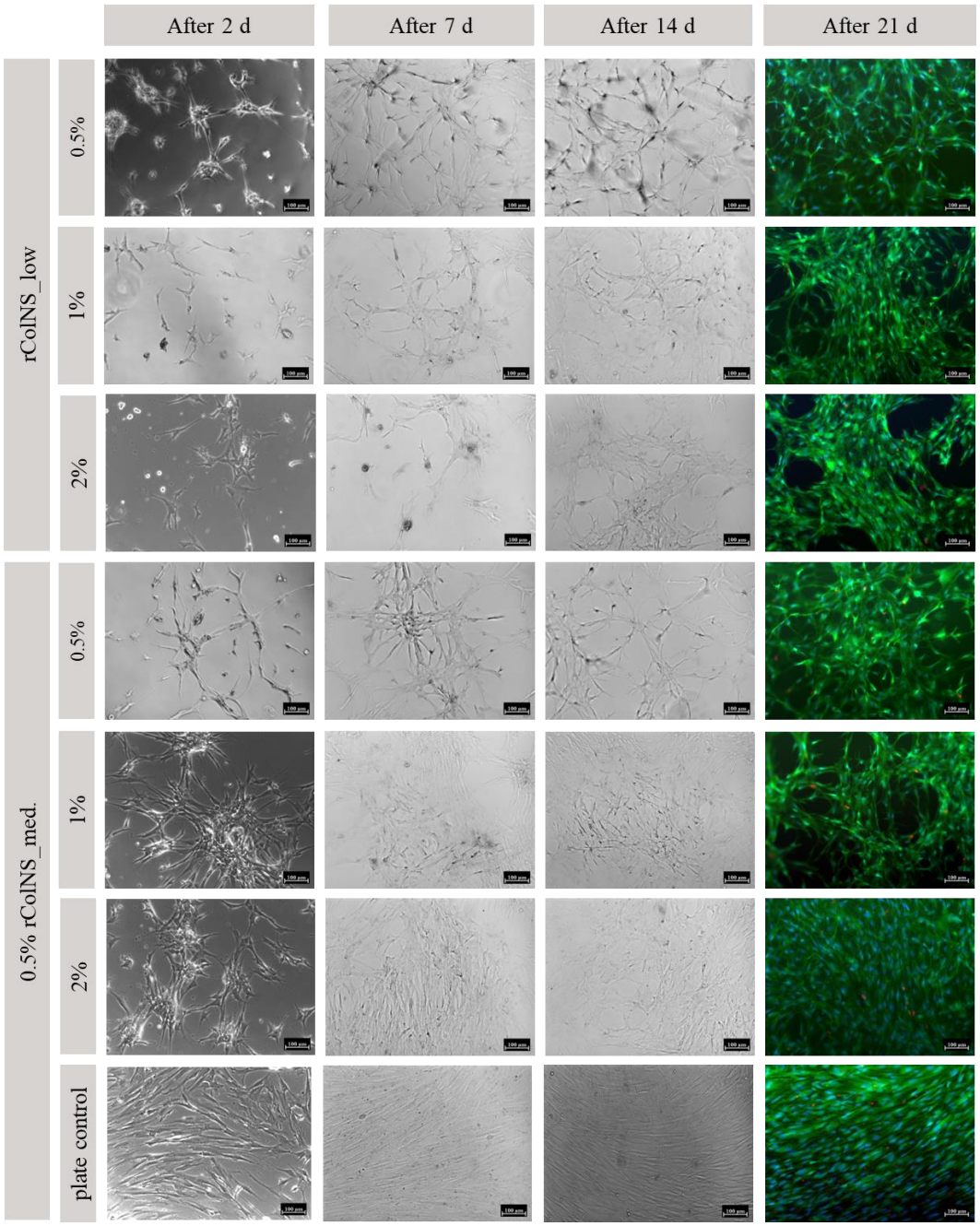

Figure 2-76: HFF growth on six different rColNS hydrogel formulations (200 µl formulation/well in 8 well chamber slide; 200 µl; $5x10^4$ cells/ml) over time under culture conditions. The cell morphology was evaluated after 2 d, 7 d and 14 d using brightfield imaging. After 21 d a LIVE/DEAD/Hoechst 33324 staining was performed. The scale bar equals 100 µm.

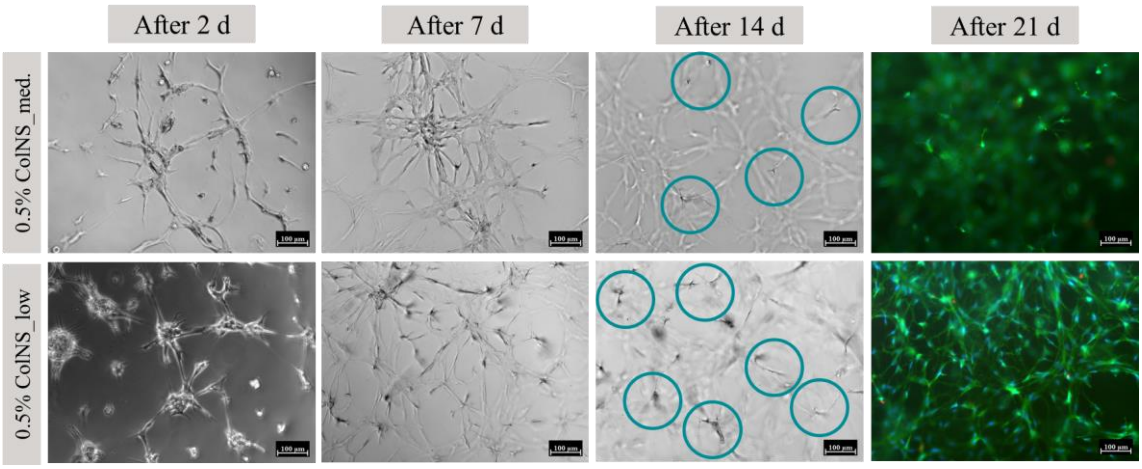

Figure 2-77: Formulations from Figure 2-76 which showed cellular ingrowth after different incubation times. Observed ingrowth was indicated with circles. The scale bar equals 100 µm.

2.3.4.6.2 Addition of RGD binding motif

The RGD peptide is the most known binding motif for cells. Thus, it was added to the liquid formulation before photopolymerization as peptide (Sigma, TrueGel3D RGD; TRUERGD-1EA) to determine potential change in cell adhesion. To achieve a strong effect, the peptide was used in excess (1:27). Based on the previous experiment the best formulation was tested (10 mg/ml rColNS_high) for this experiment. Already after one day, differences in cell adhesion were observed (see Figure 2-78). As mentioned above, cells seeded on plasma-treated culture flasks showed the best adhesion and the fastest proliferation but NIH3T3 cells showed nearly similar adhesion results in combination with the RGD peptide. While mouse fibroblasts (NIH3T3 cells) responded strongly to the presence or absence of the RGD peptide, human fibroblasts didn't show a significant difference in cell adhesion. The SW1353 cells on the other hand showed an improved cell adhesion in combination with the RGD peptide within the first days but the effect was not strong. HeLa cells repetitively didn't adhere even with the addition of the RGD peptide. In summary, cell adhesion was repeatedly supported for human and mouse fibroblasts without the addition of the RGD peptide as well as the tested human chondrocytes. By adding the RGD peptide strong differences were only observed with the NIH3T3 cells. Although the overall cell adhesion is not comparable to an optimized plasma-treated cell culture plate, the rColNS hydrogel represents an interesting, biocompatible and cell adhesive coating material which can be cured quickly on demand for e.g. implants or cell culture vessels.

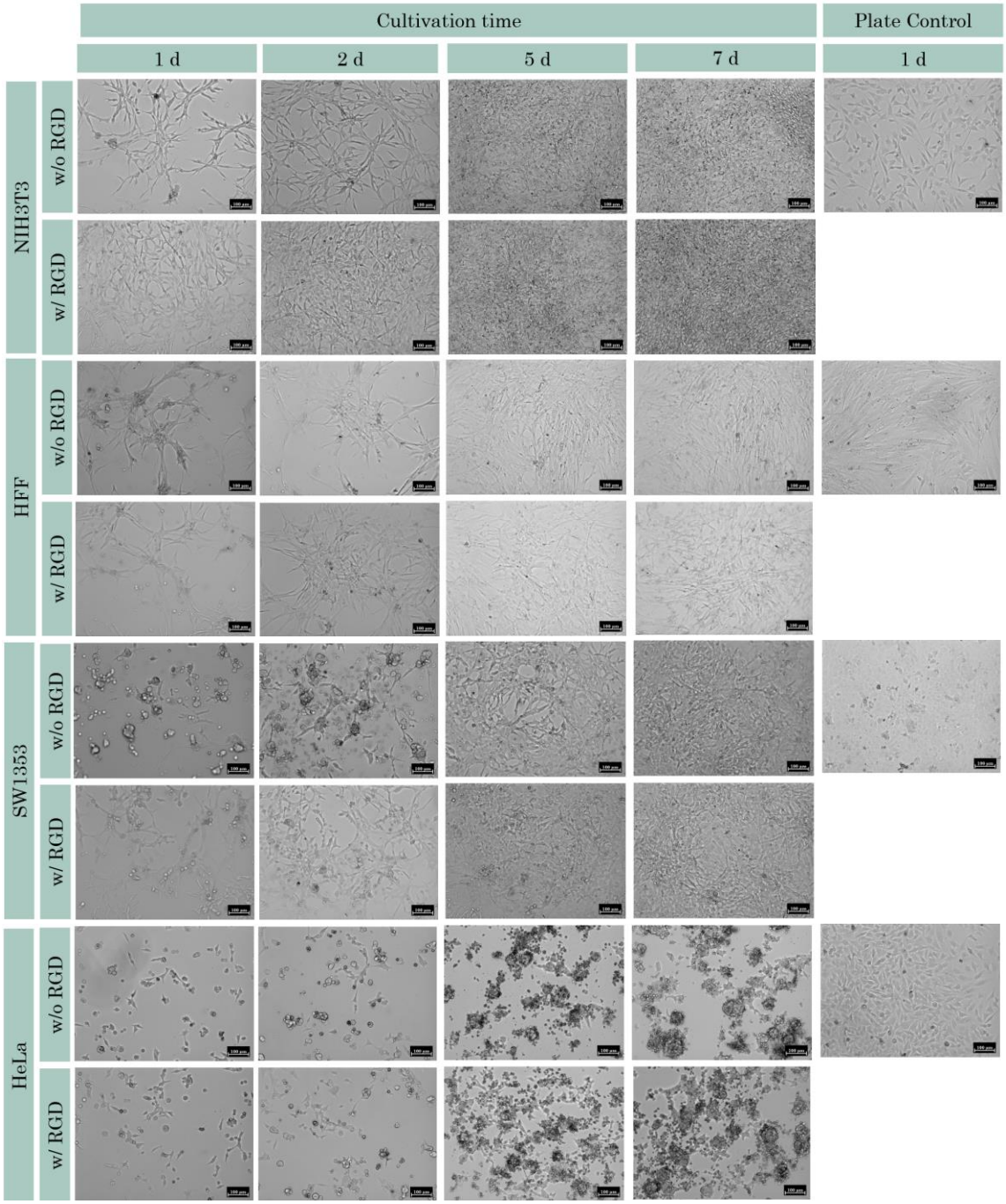

Figure 2-78: Brightfield imaging of cell adhesion experiment on 10 mg/ml rColNS_high formulations crosslinked with 0.3 mg/ml LAP as PoC with and without a RGD peptide. NIH3T3, HFF, HeLa and SW1353 cells were tested with the same starting number of cells/sample. The pictures show the cellular behavior on top of the hydrogels after 1. 2, 5 and 7 days of culture. The plate control represents a plasma treated cell culture plate surface (optimal culture conditions). The scale bar equals 100 µm.

2.3.4.6.3 Application: Cell adhesion for medical device coatings

Great cell adhesion was shown for rColNS hydrogels with different cell types. Finally, hydrogel adhesion to non-adherent surfaces were tested to improve the biocompatibility and integrity of medical devices for tissue implantations based on the results of the previous chapters. HFF cells were seeded on 6 well plates (w/ and w/o plasma treatment) with or without prior hydrogel coating. The coating was done according to chapter 4.2.3.3 by a thin hydrogel layer. Formulations were covered with full Dulbecco's Modified Eagle Medium (DMEM) and incubated for 72 h prior to usage at 37 °C. Medium was replaced by 2 ml fresh full DMEM medium containing HFF cells ($3x10^6$ cells/well). Brightfield pictures were recorded after 1 d, 2 d and 3 d. As expected, no cell adhesion was observed on the cell repellent plate surface and great cell adhesion on the plasma-treated surface already after 1 d (see Figure 2-79). The cell adhesion performance in the hydrogel coated wells was slightly weaker than on the positive control but remained similar in both plate systems showing great cell adhesion after 1 d as well. Proliferation was observed on the positive control as well as on the hydrogel coatings showing confluency on the positive control after 2 d and near confluency on the hydrogel coatings after 3 d.

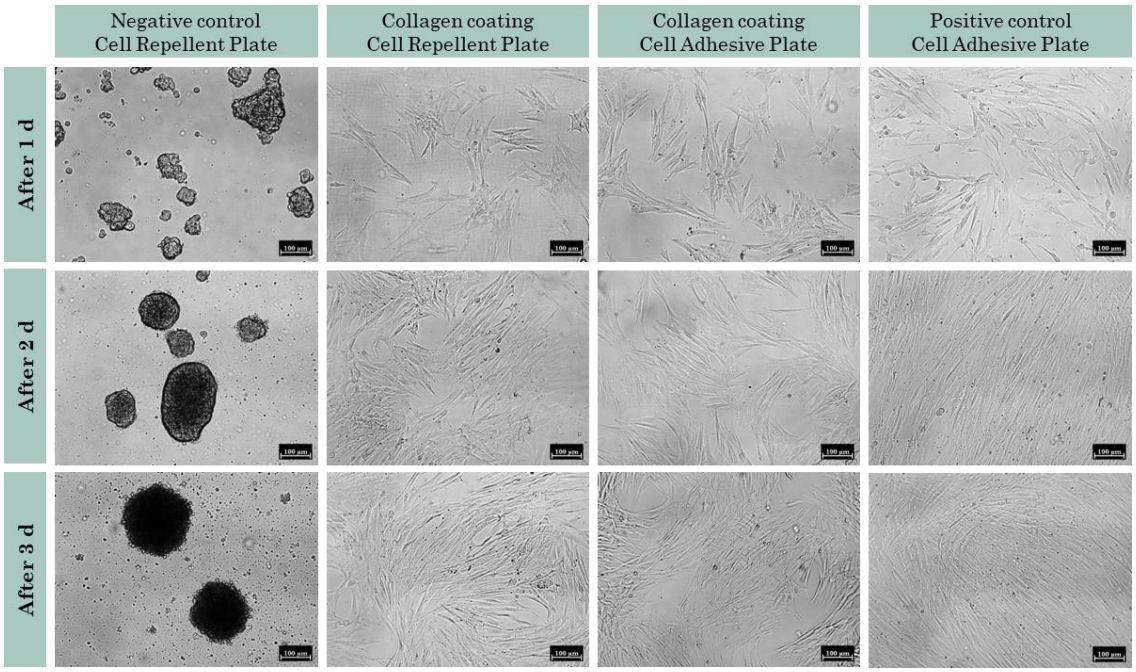

Figure 2-79: HFF cell adhesion on different surfaces using a 6-well plate with cell repellent surface and one with plasma-treated cell culture surface. A hydrogel coating (40 mg/ml rColNS_low in 1×PBS; 500 µl/well; 1 mg/ml LAP; Omnicure S2000 standard settings) was applied in both plate systems.

2.3.4.7 Cell encapsulation

Different parameters influence the viability of cells inside 3D scaffolds. These parameters have been classified into different hierarchies of difficulty. Basic parameters include a biocompatible material that has a low to non-inflammatory response and does not produce toxic byproducts during additive manufacturing. Furthermore, it should allow and promote cell proliferation. Hydrogels have been specifically studied here. Second, and more difficult to control, are the parameters that comprise the physical microstructure of the formed hydrogel scaffold. These include pore size, network density (influenced by material concentration and DoF), nutrient exchange, and matrix stiffness. Cells need sufficient space to migrate and proliferate. Especially for adherently growing cells, cell stretching will only occur if the cells have enough space. Third, and most difficult to control, is the cell-matrix interaction over time. This includes cell differentiation, cell viability and scaffold remodeling. All these parameters are only examples. A broader overview was given in Figure 2-80.

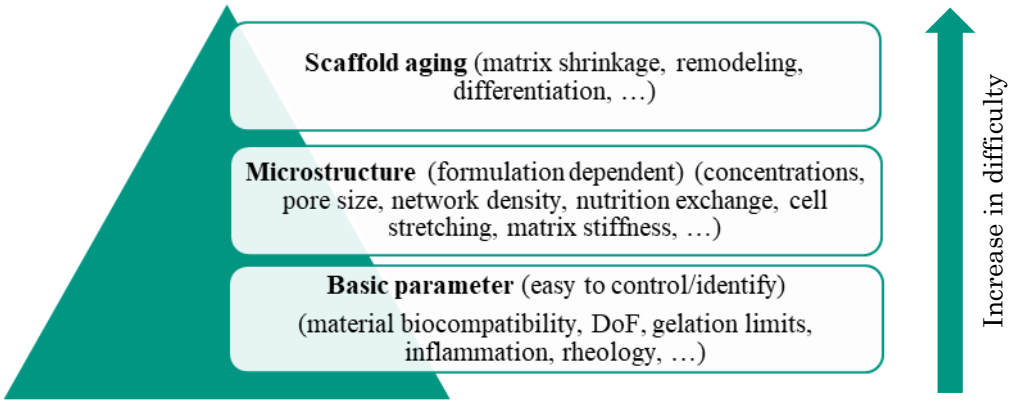

Figure 2-80: Overview of relevant parameters for the rCol bioink development based on rCol with identified and grouped challenges within the development phase.

2.3.4.7.1 Human fibroblasts

2.3.4.7.1.1 Initial screening

Broad formulations of rColN and rColS were tested (DoF range: very low (<12.5%) to medium (50±12.5%); rColNS concentration range: 2.5-40 mg/ml). Formulations with a very low DoF did not gel although higher rColNS concentrations were used like 20 mg/ml rColNS_low or the mixture of 20 mg/ml rColN_very low and 20 mg/ml rColS_low. Higher DoF allowed gelation with very low total collagen concentrations such as 2.5 mg/ml or 5 mg/ml rColNS_medium. During cultivation, very soft formulations disintegrated, stiffer formulations shrank in size and the stiffest formulations demonstrated a stable shape. These results align with the described initial mass loss in chapter 2.3.4.3.1. Although shrinkage is not desired, the

soft hydrogels showed the best cellular viability and stretching within the matrix, while stiffer formulations did not. Based on the accumulated results, a DoF and concentration dependent "cell stretching window" was identified (see Figure 2-81 (B)). If the DoF and the collagen concentration were too low no sufficient gelation occurred. If the DoF and the collagen concentration were too high, cells remained round shaped.

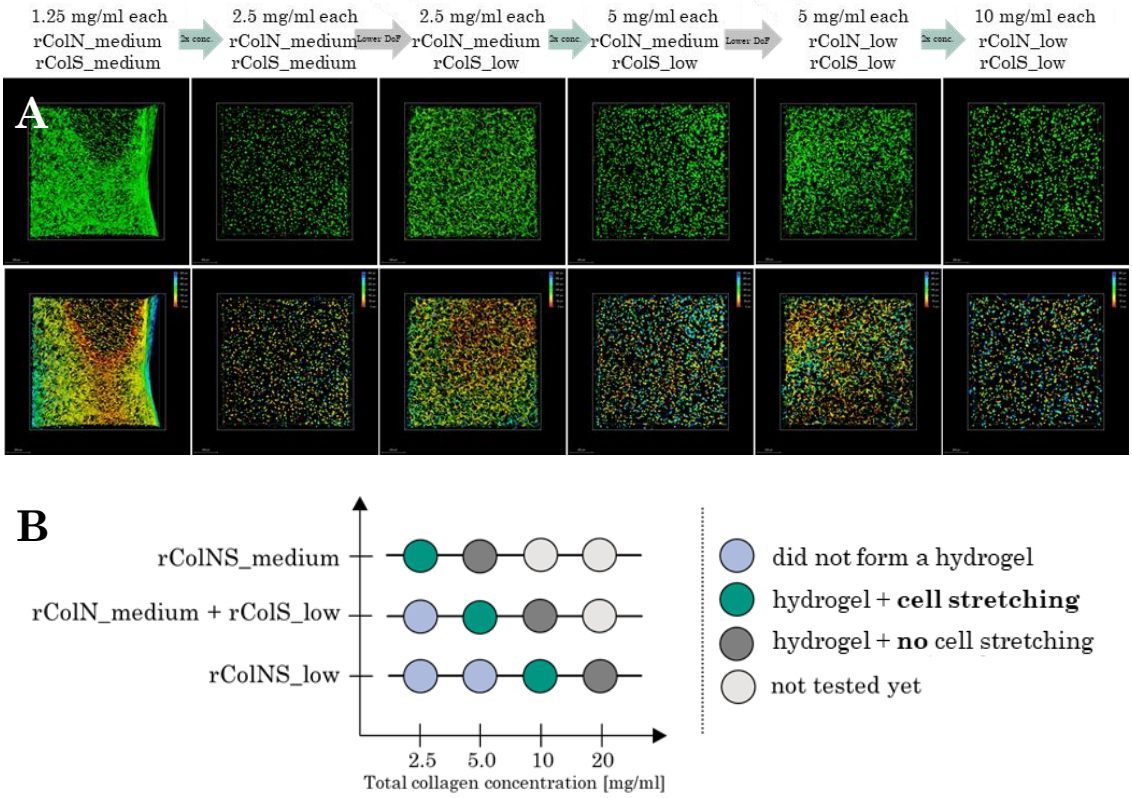

Figure 2-81: (A) HDF cell encapsulation in rColNS hydrogel scaffolds using 0.3 mg/ml LAP and the Omnicure S2000 standard curing settings. After incubation for 14 d under cell culture conditions, a LIVE/DEAD staining was performed, and pictures of the fluorescence imaging were depicted (upper row) as well as a depth coding thereof (lower row). Green arrows symbolized doubling of the rColN and rColS concentration. Grey arrows symbolized a reduction in DoF for one component. **(B)** Summarized comparison of tested formulations and the relevant concentration range where hydrogel formation and cellular stretching was observed.

2.3.4.7.1.2 Confirmation study

To show reproducibility, the experiment was repeated with the most successful formulations from Figure 2-81. Additionally, 3.5 mg/ml rColN_medium + 3.5 mg/ml rColS_low was tested based on the aligned data from Figure 2-81 (B). Each formulation was prepared with four replicates and respectively one per formulation was stained *via* LIVE/DEAD and Hoechst

staining after 1 d, 7 d, 14 d and 21 d of culture. The resulting fluorescence images after 21 d of culture as well as a depth coding thereof was depicted in Figure 2-82.

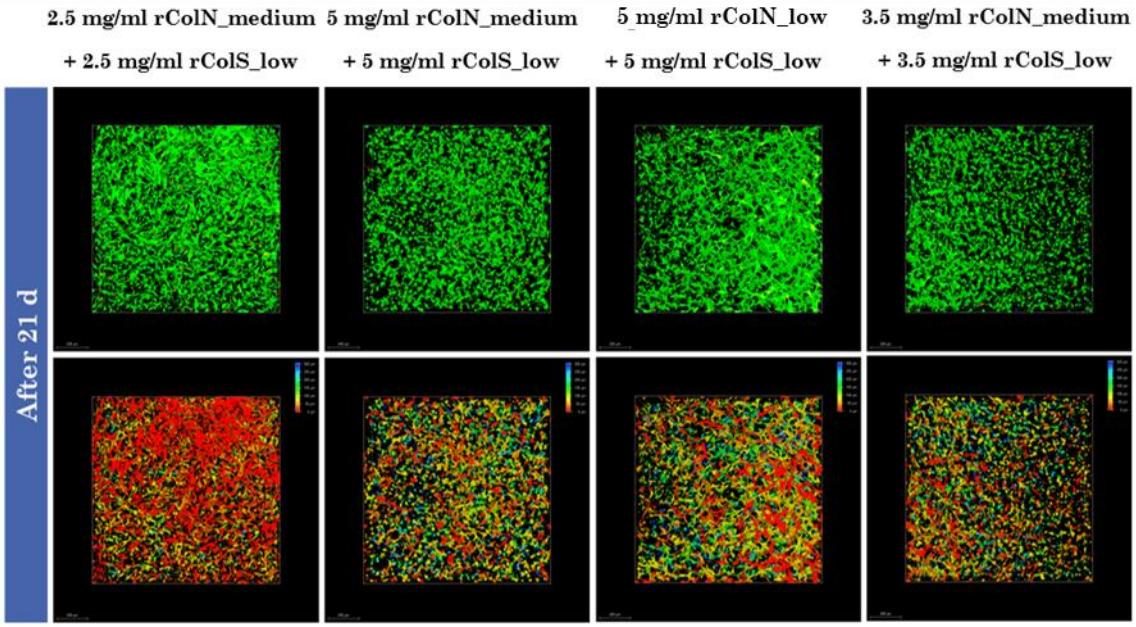

Figure 2-82: Reproduction of the cell encapsulation experiment from Figure 2-81 with additionally 3.5 mg/ml rColN_medium + 3.5 mg/ml rColS_low and 0.3 mg/ml LAP with encapsulated HFF cells. The upper row shows a LIVE/DEAD staining while the lower row shows a depth coding.

To better show the cellular stretching over time, one formulation (2.5 mg/ml rColNS_medium + 2.5 mg/ml rColS_low and 0.3 mg/ml LAP) was depicted at different time points in Figure 2-83. Data showed cellular stretching within one week together with cellular proliferation, which was observed by the increase in green dots (viable cells). Also, the relative ratio of dead cells (red) decreased slightly. After 14 d, the sample was damaged leading to a not-usable picture and after 21 d a great cellular stretching was observed in multiple layers as well as an additional increase in proliferation due to an increase in green dots. In summary, cellular stretching of HFF cells is possible within one week in selected rColNS hydrogels. An overview of functional formulations was visualized in Figure 2-81; B. Cellular stretching and proliferation were repetitively shown which increased over the weeks of the experiment as well as cellular wellbeing.

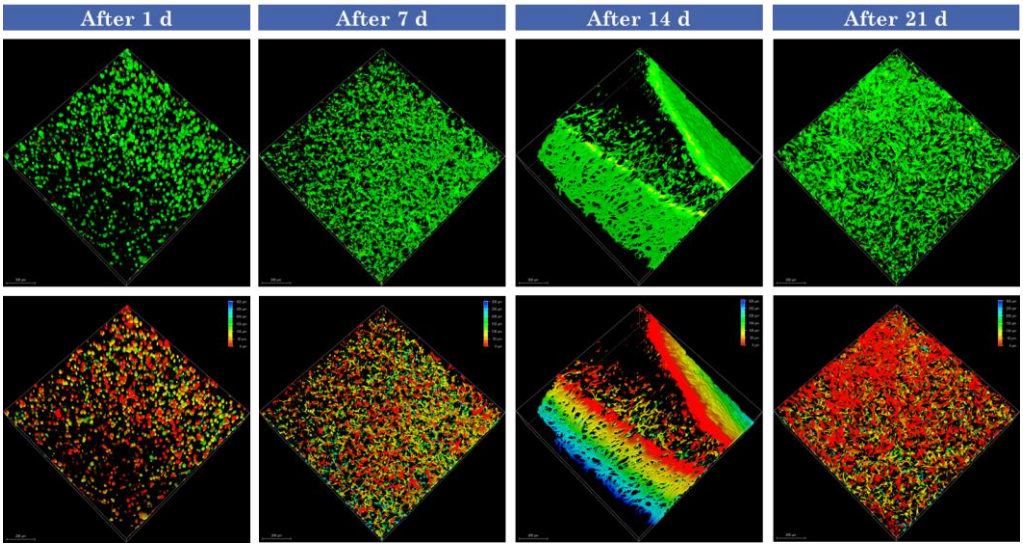

Figure 2-83: Selected formulation of Figure 2-82 (2.5 mg/ml rColN_medium + 2.5 mg/ml rColS_low) with more time steps. The upper row shows a LIVE/DEAD staining while the lower row shows a depth coding.

2.3.4.7.1.3 Final compositions

Based on the characterized formulations within the previous chapters, the experiment was repeated using 5 and 10 mg/ml rColNS_low, 2.5 and 5 mg/ml rColNS_medium. The goal of was a closer resolution of cellular behavior by daily observations. Already after one day, cell stretching was observed using 5 mg/ml rColNS_low and 2.5 mg/ml rColNS_medium (see Figure 2-84). The effect increased to day 2 up to day 7. Higher concentrated formulations (10 mg/ml rColNS_low and 5 mg/ml rColNS_medium) showed no cellular stretching after 1 - 2 days. Within the next days increased cellular stretching was observed up to day 7. The best cellular network formation was observed with the softest formulation (5 mg/ml rColNS_low) which was assumed to be relying on the relatively low number of crosslinks. Higher concentrated formulations showed also cellular stretching, but it took much longer to appear, and no sufficient networks were formed within 7 d incubation time. In summary, the two best formulations (5 mg/ml rColNS_low and 2.5 mg/ml rColNS_medium) showed great cellular stretching and network formation already after one day of incubation. These formulations could be tested in animal trials to show their performance for *in vivo* applications. Still an open issue remains the structural shrinkage of the material when incubated at 37 °C as reported in chapter 2.3.4.3.1. To circumvent this shrinkage, higher rColNS concentrations with very low modified rColN and rColS components could be evaluated as well as supporting structures like RESOMER® grids to keep the hydrogel material in place. Depending on the required softness, the soft hydrogel formulations could be also tested for injection purposes.

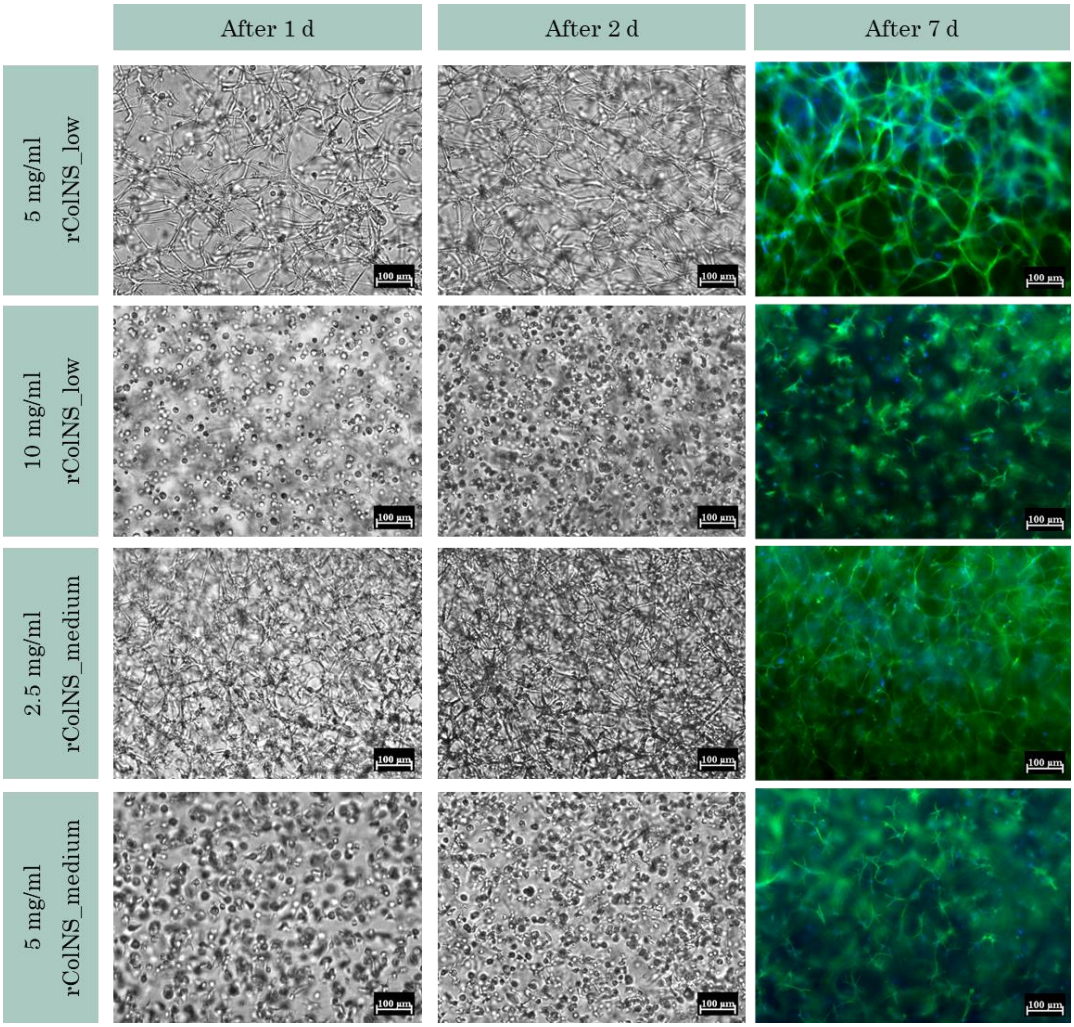

Figure 2-84: Brightfield imaging after 1 d and 2 d incubation time of encapsulated HFF cells (P8) in rColNS hydrogels followed by Phalloidin/Hoechst 33342 staining after 7 d. Cell loaded hydrogels were prepared in 8 well chamber slides with 200 µl formulation per well. 0.3 mg/ml LAP was applied and photopolymerization was done with the Omnicure S2000 standard curing settings. Green = actin filaments; Blue = cell nuclei.

2.3.4.7.1.4 rColS replacement

To show the versatility of the thiol-ene chemistry, rColS was replaced by another thiol. Here, a four times terminally modified polyethylene glycol was chosen (4-Arm-PEG-SH). This linker exists with different molecular weights. To reduce the sample number only the 10 kDa version was tested based on the previous experiments with 4-Arm-PEG-SG in chapter 2.2. Before applying the linker, its cytotoxicity on fibroblasts was evaluated according to chapter 4.2.3.1.2 (see Figure 2-85). No toxic side effects were detected. The observed, bell-shaped curve behavior remained unclear. Experimental repetition could reveal whether this effect is

reproducible. Due to the lack of any cytotoxic effect, the experiment was not repeated, and the linker was evaluated as save to use.

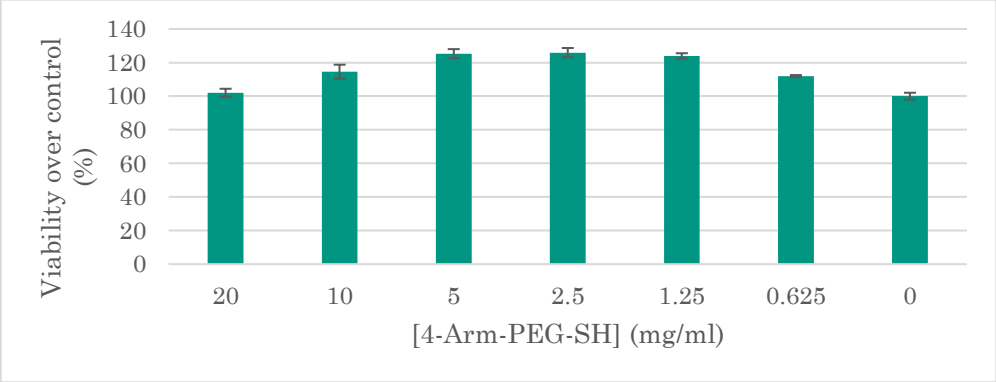

Figure 2-85: CellTiter-Glo® assay to test possible toxic effects of different 4-Arm-PEG-SH concentrations (molecular linker weight: 10 kDa) on mouse fibroblasts (3T3 cells; P11) after 24 h of exposure under culture conditions (N=3). All data was normally distributed.

To minimize the sample size, only rColN_medium was tested in combination with 4-Arm-PEG-SH with one molecular weight (10 kDa). Previous experiments showed that cell stretching of human fibroblasts was favored with lower rColNS concentrations and lower DoFs. Therefore, the linker was applied with low molar ratios (1:0.1; 1:0.2 and 1:0.3) in combination with three rColN_medium concentrations (5, 10 and 20 mg/ml). The sample preparation was described in chapter 4.2.4.6. All nine formulations gelated but some dissolved within 2 days under culture conditions (5 mg/ml rColN_medium with MR of 1:0.1 and 1:0.2; 10 mg/ml rColN_medium with MR of 1:0.1). All formulations which didn't dissolve shrank in their volume during cultivation. This finding correlates with the rColNS trials (see chapter 2.3.4.3.1, Figure 2-65). The G' of all gelated formulations was measured without cells leading to values between 0.5 and 1 kPa (data not shown here). Formulations with cellular stretching and high cell viabilities, were close to the gelation limit and thus very soft. In summary, the rColS replacement showed great cellular stretching and cellular wellbeing of encapsulated HFF cells within a certain" formulation window" (see Figure 2-86, B) as previously shown for rColNS formulations (see Figure 2-81; B). Depending on the application, a replacement of rColS could be interesting to craft copolymers with additionally properties. As an outlook for future research topics, thiolated bioactive molecules like the RGD peptide could be tested for covalent integration. This could lead to new formulations for drug delivery where the release is based on the degradation of the collagen matrix over time or to stimulate cells to interact with the matrix in a desired way. This could lead to now therapeutic approaches for hydrophilic APIs in case of a release matrix or as surface coating for e.g. a targeted cellular differentiation by covalently crosslinked growth factors or hormones in a flat cell culture plate

surface covering without the need to add special differentiation media. All these ideas could be relevant for future projects, but they were not pursued within this thesis.

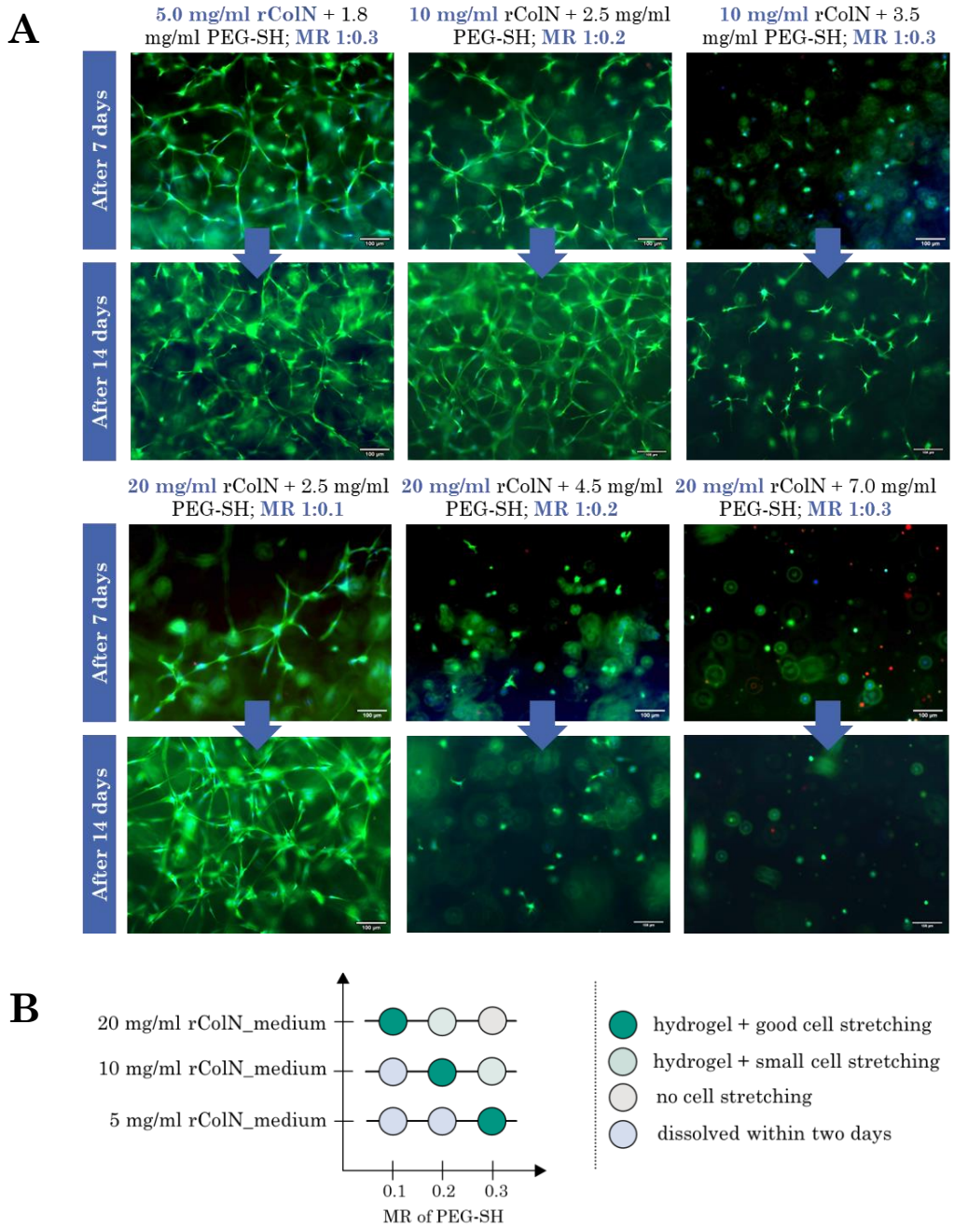

Figure 2-86: (A) HFF (P4) cell encapsulation trials in a matrix made from rColN_medium and 4-Arm-PEG-SH, 10 kDa. A final cell concentration of $5x10^5$ cells/ml was applied. Samples were prepared in 8 well chamber slides with 200 µl formulation per well. After 7 and 14 d under culture conditions for two weeks, a LIVE/DEAD/Hoechst 33342 staining was performed to visualize cell spreading and cellular wellbeing (viable cells = green; dead cells = read; blue dots = cell nuclei). **(B)** Overview of tested formulations.

2.3.4.7.1.5 Minimal medium

Fetal bovine serum (FBS) is an undesired medium component due to its animal-derived extraction from calves. Research is done to reduce or replace FBS for the development of minimal and defined media. Based on the previous encapsulation results, the experiment was prepared with two different media. These were full culture DMEM medium containing 15% FBS and CnT-Prime Fibroblast Proliferation Medium (CELLnTEC; CnT-PR-F; contains only 1% serum) with three different conc. (10 mg/ml, 20 mg/ml and 30 mg/ml rColN_medium) and different MR of 4-Arm-PEG-SH, 10 kDa. Based on the previous experiment, a MR of 1:0.2 showed the best results with 10 mg/ml rColN_medium (see Figure 2-87). Excellent cellular growth was determined with the minimal medium.

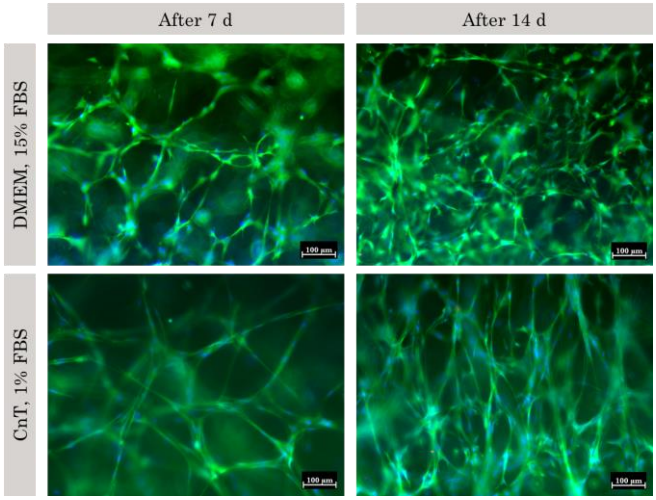

Figure 2-87: Encapsulated HFF cells (P4) in a rCol/PEG composite made from 10 mg/ml rColN_medium and 4-Arm-PEG-SH, 10 kDa with a MR of 1:0.2. A final cell concentration of $5x10^5$ cells/ml was applied. Formulations were cured with 200 µl each in an 8 well chamber slide format and incubated for up to 14 d followed by LIVE/DEAD/Hoechst 33342 staining (viable cells = green; dead cells = read; blue dots = cell nuclei).

2.3.4.7.2 Human chondrocytes

Besides fibroblasts for e.g. skin applications, cartilage cells were also interesting due to the predicted possible availability of 3D printed organs and tissues for humans from a recent market report study, which predicted a timeline of 2022-2025 for skin and 2021-2024 for cartilage.[247] To find a good scaffold for cartilage regeneration, the experiment from the previous chapter was repeated with adapted concentrations of rColNS to fit the shear storage modulus G' for the used chondrocytes (SW1353; ATCC). In chapter 2.3.4.3.1, the required shear storage modulus in cartilage tissue was calculated from the Young's modulus, resulting in a value of G' of ~ 4.7-5 kPa. In chapter 2.3.4.3.3, the shear stress moduli of different rColNS formulations were determined and set in correlation to the applied formulation. Although

these data were derived from cell-free scaffolds they were used as a rough guidance for potential rColNS formulations for chondrocytes. Based on these calculations, different formulations were calculated (see Table 2-11).

Table 2-11: Formulation calculations for rColNS hydrogels for cartilage applications. Formulations where cellular stretching was observed were highlighted in green.

DoF (Collagen)	[Total collagen] for G' = 4.7 kPa	[Total collagen] for G' = 5.0 kPa	[Total collagen]
rColNS_low	27.8 mg/ml	28.6 mg/ml	20, 25, 30, 35 mg/ml
rColNS_medium	18.2 mg/ml	18.8 mg/ml	10, 15, 20, 25 mg/ml
rColNS_high	16.0 mg/ml	16.5 mg/ml	10, 15, 20, 25 mg/ml

Each formulation was prepared in duplicate with 1×10^6 cells/ml, followed by 3D culture under standard conditions for three weeks. Most formulations showed initial shrinkage as reported earlier for other rColNS formulations when heated to 37 °C (see Figure 2-65, chapter 2.3.4.3.1) and the same effect was observed during HFF encapsulation experiments in chapter 2.3.4.7.1. rColNS_low and rColNS_medium performed best, while rColNS_high performed bad at all tested concentrations. This finding aligned with the rColNS performance for HFF encapsulation in the chapter 2.3.4.7.1. In cartilage, chondrocytes can appear with different morphologies. While juvenile chondrocytes are elliptic in shape, the shape can also take a round form.[368] In the present experiments, cellular stretching was observed for two formulations only (see Figure 2-88). Interestingly, both formulations (25 mg/ml rColNS_low and 20 mg/ml rColNS_medium) aligned with the calculated range from Table 2-11. In summary, the used human chondrocytes showed high viability after three weeks of culture in rColNS hydrogels. Depending on the formulation, some showed cellular stretching. For this work, the focus was on fibroblasts and this experiment served as a PoC that the rColNS material was also suitable for other cell types.

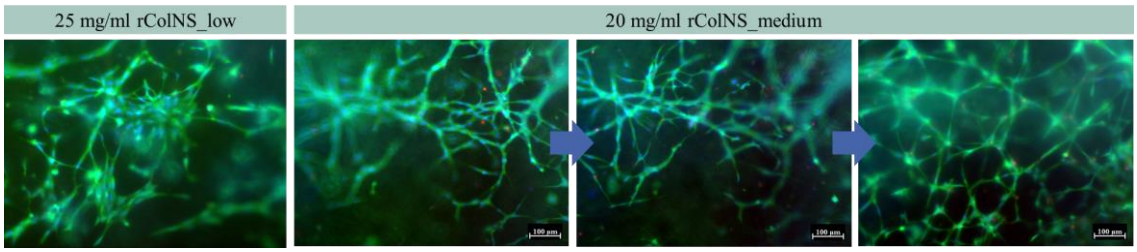

Figure 2-88: LIVE/DEAD/Hoechst 33342 staining of encapsulated SW1353 cell within rColNS formulations after 21 d incubation time. Both formulations were prepared with 0.3 mg/ml LAP. The formulation with 20 mg/ml rColNS_medium was depicted with three layers of a Z-stacking.

2.4 Crosslinker comparison

The application of all three tested crosslinking mechanism (DMTMM, rCol/PEG and rColNS) resulted in hydrogels synthesis. Identified differences and common properties were outlined in Table 2-12. The minimal required rCol concentration for hydrogel formation shifted per crosslinking procedure and was best with rColNS where only 1.25 mg/ml rColN and 1.25 mg/ml rColS was required. For the rCol/PEG composite, at least 5 mg/ml rCol and for the DMTMM crosslinker at least 10 mg/ml rCol were needed. The pH range for hydrogel synthesis showed a broad flexibility with rColNS and DMTMM, while the PEG linker required a neutral to basic pH. A big difference was observed in gelation speed, which was fastest with rColNS (seconds) followed by the rCol/PEG (seconds to minutes) and the DMTMM crosslinking reaction (minutes to hours). Hydrogel sponges made with DMTMM showed great swelling (720-2280%), followed by rColNS (800-1410%) and rCol/PEG (400-800%). Regarding porosity demonstrated rCol/PEG the highest density with less to no porosity. The porosity increased with the equilibrium swelling rates. The material integrity during lyophilization was best for DMTMM crosslinked rCol, followed by rColNS and rCol/PEG. In terms of enzymatic degradation, formulation-dependent degradation was observed for the PEG composite and rColNS hydrogels, while the DMTMM crosslinked hydrogels showed almost no degradation under the tested conditions. The measured stiffness of all three technologies with one concentration of rCol (20 mg/ml) had a wide range depending on the applied MR of the linker and the DoF (in case of rColNS). Therefore, it is difficult to include this parameter for the comparison. Nevertheless, a broad range of stiffnesses was identified for all technologies which could be adapted to the final application. For the biological evaluation, rColNS showed the best biocompatibility. The two other technologies allowed unspecific side reactions with surrounding cells or tissues during gelation which needs to be considered for the final application. The best cell adhesion was achieved with rColNS. Cells also adhered to DMTMM crosslinked rCol samples, but the results were difficult to reproduce. No cell adhesion was observed with rCol/PEG composites. For 3D cell encapsulation, only rColNS performed well. The other technologies are more suited for scaffolds which can be washed prior to cellular contact. The advantages of the DMTMM crosslinker were based on the high structural integrity and preservation after lyophilization, good porosity, high material swelling and good resistance to hydrolysis and enzymatic degradation. In addition, soft tissue patches prepared with this crosslinker showed excellent conditions for drug delivery. The developed rCol/PEG composite showed adjustable, formulation-dependent degradation together will cell repellent surface properties regardless of the tested cell type. This highly transparent hydrogel product didn't show hazardous properties in a first leachable experiment and is

therefore interesting for cell repellent surface coatings or implantable and biodegradable separation membranes to avoid cellular ingrowth. The fast gelation together with an adjustable degradation pattern could be explored further for immobilized API release due to matrix degradation by e.g. the use of microparticles. The developed thiol-ene chemistry has great gelation properties with minimal concentrations of rCol. The light-triggered, very fast gelation of rColNS formulations showed partial shrinkage when exposed to 37 °C with lower concentrations of rColNS which is reduced by higher rColNS concentrations. The product had average swelling properties and was susceptible to enzymatic degradation but so far it was stable against hydrolysis. The great biocompatibility, the good cell adhesion as well as the repetitively proven cellular wellbeing within the rColNS matrix made the established thiol-ene chemistry with rCol a great bioink material for tissue engineering and 3D cell culture. An overview comparing all technologies was given in Table 2-12.

Table 2-12: Comparison. The best crosslinking procedure per category was highlighted in **green**.

Characteristic	**Crosslinking procedure**		
	DMTMM	**rCol/PEG**	**rColNS**
Min. [rCol] for gelation (mg/ml)	10	5	**2.5**
pH range	**5-9**	7-9	**broad**
Gelation speed	slow	medium to fast	**very fast**
Storage modulus (hydrogel) (kPa) (20 mg/ml collagen)	1.5-11	3.6-14.1	2.4-7.3
Swelling	**+++**	+	++
Degradation - Hydrolysis	no	**yes**	no
Enzymatic degradation	no	**yes**	**yes**
Not cytotoxic / Leachables	-	+	**+++**
Usable for direct cell contact	--	+	**+++**
Transparency (sponges after swelling)	no	**yes**	no
Porosity	**++**	---	+
Sponge Form stability	**+++**	-	+
Price/ crosslinker (research prices) per Gramm	**++**	+	--
Cell encapsulation	---	--	**+++**
Cell Adhesion	+	---	**++**
Printability	--	--	**++**

2.5 Printability studies

Bioprinting can be done with many different technologies. Some prefer low viscosity, while others rely on highly viscous solutions. Due to the low viscosity of rColNS, technologies like stereolithography and drop-on demand were evaluated as methods of interest. The Regenate printer from Black Drop GmbH was used for the subsequent fabrication to apply jetting besides Fused filament Fabrication (FFF).

2.5.1 Drop on demand printing

2.5.1.1 Establishment of DoD printing

To establish the printing process, formulations without cells were evaluated with simple, physically gelling material (animal-derived gelatin and Blue Drop Agarose (Black Drop GmbH)). Both are liquid when heated and solid when cooled. Blue Drop was initially heated to 80 °C until liquification followed by a 1:1 dilution with 1xPBS and filled into a pre-heated printhead (32 °C). The used 10% (w/w) gelatin in ddH_2O was prepared by dissolving 10 g gelatin in 90 g ddH_2O at 60 °C. The prepared gelatin solution was stored at 4 °C and heated to 37 °C when needed until liquification occurred before transferring the solution into a pre-heated printhead (37 °C). After establishing material handling, cylindric structures were printed and compared (see Figure 2-89). The sliced file was provided by Black Drop GmbH and adapted on the respective material. For printing parameters, the recommended settings from Black Drop GmbH were used (see Table 2-13). Due to the better resolution and the much cheaper price, gelatin was chosen for further establishments.

Table 2-13: Recommendations Regenate printer settings provided by Black Drop for the processing of bioinks.

Parameter – Controller	Recommendations	Range
Temperature printing head (Jetting)	material dependent	4 °C – 42 °C
Temperature printing head (Printing bed)	material dependent	4 °C – 80 °C
Printing speed	300 - 1500	1 – 2000 mm/min
Lamp power	30%	0% - 100%
Distance lamp to printing surface	1 cm	1 - 1.5 cm
Pressured air	0.2 - 0.3 bar	0.2 – 1.5 bar
Opening time (Opening time (valve))	450 -800 µs	400 µs – 4500 µs
Droplet Distance (OC und IC)	0.75 - 1.5 (material dependent)	0.5 - 2

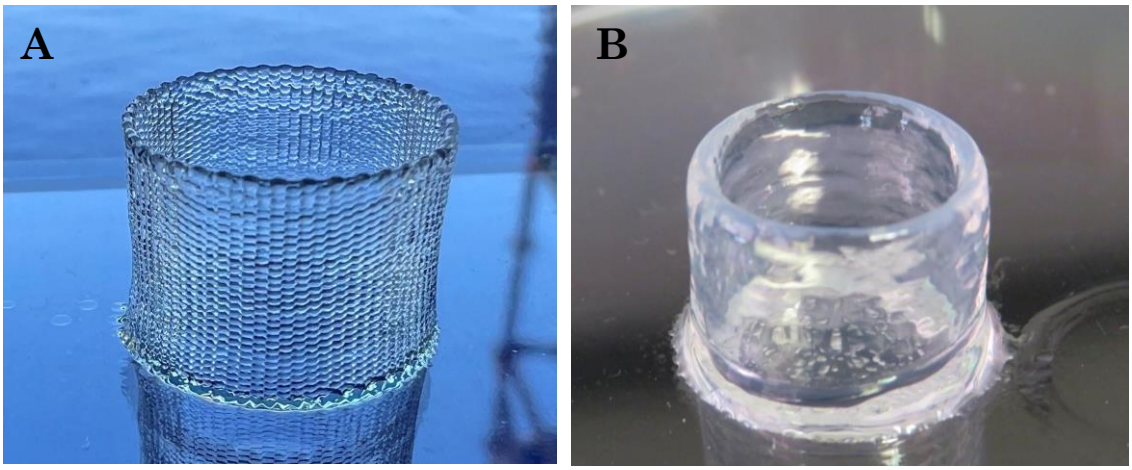

Figure 2-89: Cylindric prints (Ø14 mm; 10 mm height) made from **(A)** 10% (w/w) gelatin in ddH_2O and **(B)** Blue Drop agarose (Black Drop GmbH) in 1×PBS processed *via* Drop-on-Demand. For jetting a pressure of 0.2 bar was applied and droplets were printed on a cooled surface (4 °C).

2.5.1.2 Establishment of rColNS printing

2.5.1.2.1 Bioink viscosity

The high printing fidelity in Figure 2-89 was the result of an optimization experiment and printing effects are challenging to reproduce with another material like rColNS which obtains different material characteristics. The very low viscosity of the material, which is close to water, makes additive manufacturing even more challenging in terms of fidelity and droplet shape especially on hydrophilic surfaces like glass. Exploration of the contact angle of the bioink to the printing surface can reveal further insights to optimize the printing fidelity. To optimize the printing result, the formulation was adjusted in regards to the described optimal viscosity range in literature of 3.5-12 mPa*s.[254] To find the optimal concentration range for 3D printing with rColNS, the viscosities of different rColNS concentration was determined with rColNS_low. Starting from a 100 mg/ml rColNS (stock solution from a 1:1 mixture of rColN and rColS which was prepared fresh at RT), a dilution series was made in 1×PBS. An exponential correlation between concentration and viscosity was determined (see Figure 2-90). Interestingly, additional cooling over 40 h increased the viscosity of the solution further, which was demonstrated in chapter 2.3.3.5 for rColS. To adjust the formulation to the recommended viscosity a concentration range of 24.1 – 47.4 mg/ml was calculated. It is recommended to use the formulation directly after preparation and to consider the change of viscosity during longer storage times.

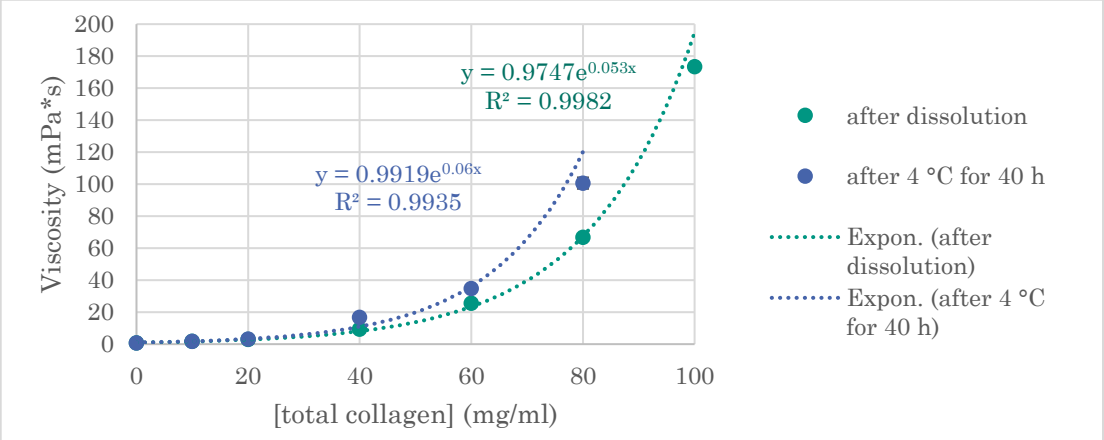

Figure 2-90: Correlation of viscosity and total collagen concentration of rColNS_low after dissolution. A 100 mg/ml stock solution was prepared by dissolving 50 mg rColN and 50 mg rColS in 1×PBS for 4 h at RT followed by viscosity determination according to chapter 4.2.6.3.1 (N = 3). The measurement temperature was 20 °C. Then, after an incubation of 40 h storage at 4 °C the measurement was repeated each with N = 3 followed by an exponential curve fit with Excel. All data was normally distributed.

2.5.1.2.2 Drop volume analysis

The printing resolution is depending on several factors. One of them is the droplet size which can go down to nl volumes. The smaller the droplets were, the higher the resulting resolution. To quantify the drop volume, a defined number of droplets was ejected and the resulting mass was compared. Different rColNS concentrations and different pneumatic pressure of the printing head were tested with the same gate opening time (450 µs). Produced data demonstrated a pressure dependent increase in droplet volume (see Figure 2-91). The higher the applied pressure, the more volume was ejected which led to bigger droplets. Also, the deviation in droplet mass was less dependent on the rColNS concentration with higher pressures. In summary, the pressure influenced the droplet size and lower pressures were recommended to ensure a max. resolution.

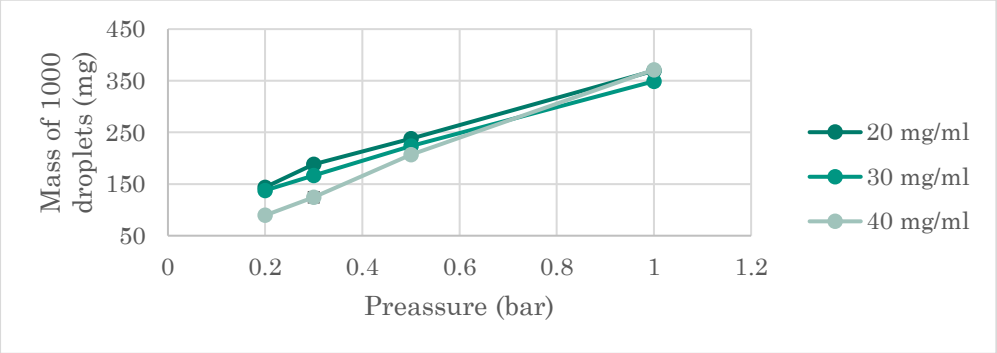

Figure 2-91: Droplet mass correlation with the applied pneumatic pressure. rColNS_medium was used. The measurement was performed at 22 °C (N=3). All data was normally distributed.

2.5.1.2.3 Printing rColNS

After identifying the optimal viscosity range to match the recommended range (25-50 mg/ml rColNS_low; see chapter 2.5.1.2.1), the material was processed to produce a column of droplets and a cylindrical structure of 8 mm in diameter (see Figure 2-92). The results showed the potential to print droplets on top of each other, but cylindrical printing caused inhomogeneous wall thickness (thick base and a thin top). Also, no distinct droplets were observed which was associated with an excess of droplets per layer and a nonsufficient gelation. Therefore, the number of drops per layer was reduced, which resulted in the same issue. Next, more LAP was tested (0.3 mg/ml →1 mg/ml) to allow faster curing leading to potentially stiffer structures. The results indicated the need for higher LAP concentrations. Alternatively, longer exposure times could be tested. Also, a brief experiment with rtCol was performed with even 2.5 mg/ml LAP and an increased irradiation time. The resulting cylinder showed no distinct droplet separation, and more LAP might be needed to improve the printing quality. In general, rtCol was evaluated as not being ideal for droplet printing due to the high viscosity and extrusion printing might be the better technology to process the material by also considering the higher toxicity of elevated LAP concentrations.

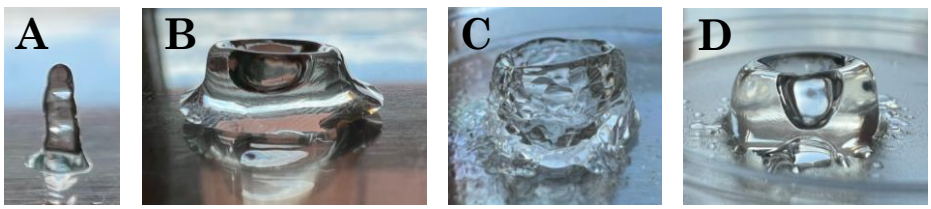

Figure 2-92: Printing trials of 50 mg/ml rColNS_low with **(A)** 0.3 mg/ml LAP in 1×PBS processed with 0.2 bar and a single droplet per layer and **(B)** 0.3 mg/ml LAP in a cylindric shape with Ø8 mm. **(C)** Same settings were applied with 1 mg/ml LAP in 1×PBS. **(D)** 4 mg/ml neutralized rtColMA (Cellink) solution with 2.5 mg/ml LAP with twice the irradiation time and post-curing for 30 seconds using the Omnicure S2000 with standard settings.

To confirm these findings, different formulations were tested with 1 mg/ml LAP, showing great resolution and efficacy in the indicated concentration range of 25-50 mg/ml rColNS_low, with great results using 40 mg/ml material, showing better resolution, more distinct droplets, and less droplet accumulation at the base of the print. Less splattering was also observed with 50 mg/ml. It was suggested that the higher concentrations resulted in stiffer hydrogels, which increased the bouncing effect of new droplets (Figure 2-93). Still, different additional concentrations should be tested to potentially find a better formulation.

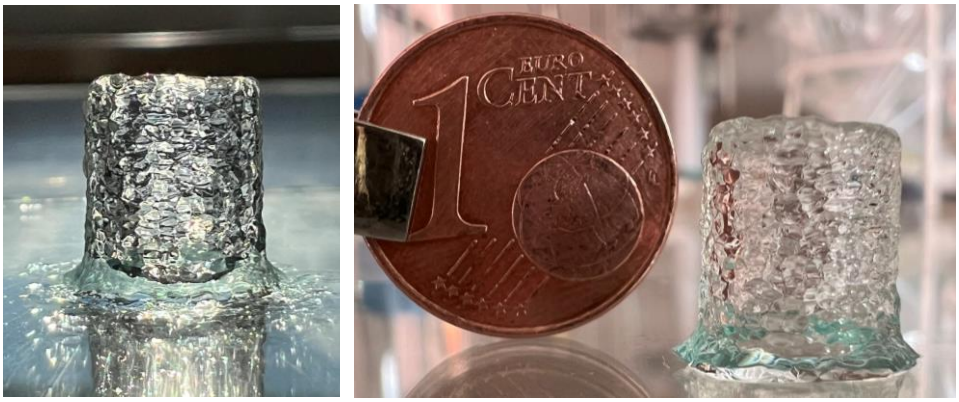

Figure 2-93: Printed cylinder made out of 40 mg/ml rColNS_low (1:1 mixture) with 1 mg/ml LAP in 1×PBS (100 layer; height of 9.3 mm; outer Ø8.5 mm; 0.09 mm layer height; 30 droplets per layer; AB droplet dispensing; curing after 15 and 30 droplets with 4x 1 sec curing time each; 40% lamp power). A pressure of 0.3 bar was used for jetting.

2.5.1.2.4 Bioink variations

Printing below 30 mg/ml rColNS_low remained challenging. A screening revealed that more LAP resulted in better printing results (data not shown here). Furthermore, higher DoF of rColNS (low → medium → high) correlated with less required rColNS concentrations for gelation and efficient printing in height (see Figure 2-94 (A) and (B)). This was expected in general due to the previously performed experiments in chapter 2.3.3.2 showing that hydrogel synthesis was possible with lower rColNS concentrations when higher DoF were applied. It was assumed that the low viscosity of rColNS (especially with low concentrations) complicated the droplet positioning without flowing them away prior to the viscosity increase by curing. By incorporating viscosity enhancers like a recombinant hyaluronic acid with high viscosity (see Figure 2-94 (C)), cylindrical structures were printed with only 10 mg/ml rColNS material. Although printing with less than 30 mg/ml is possible, the formed structures were easily destroyed under minimal stress. Therefore, printing with at least 30 mg/ml rColNS was recommended. Also, the surface properties of the material on which is printed on plays an important role within the printing process. Several materials were tested (glass and polystyrene in particular), which led to the assumption that plastic surfaces caused better

printing results while a glass surface led to stronger droplet splashing. Therefore, sole hydrogel prints with rColNS were done in 3.5 mm petri dishes made from polystyrene. It was assumed that the more hydrophobic surface led to better droplet formation of the hydrophilic formulation.

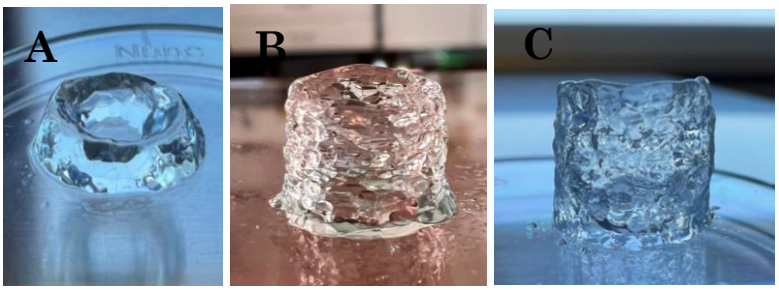

Figure 2-94: Cylindric prints (Ø8 mm) made from rColNS. **(A)** 20 mg/ml rColNS_low, 1 mg/ml LAP in 1×PBS. The print was halfway stopped. **(B)** 20 mg/ml rColNS_medium, 1 mg/ml LAP in 1×PBS. **(C)** 10 mg/ml rColNS_high, 1 mg/ml LAP with 0.25% (w/v) recombinant hyaluronic acid.

2.5.1.3 rColNS printing with cells

Cell growth within the rColNS matrix was demonstrated in chapter 2.3.4.7 with different cell types and the printability of the rColNS formulation was demonstrated in chapter 2.5.1.2.3. Finally, both was combined. One of the best formulations for cell stretching was 5 mg/ml rColNS_low with 0.3 mg/ml LAP (see chapter 2.3.4.7.1.3) but printability thereof failed. Higher concentrations of LAP and rColNS were needed to increase the viscosity and the printing fidelity. 40 mg/ml rColNS_low on the other side demonstrated good printability (see chapter 2.5.1.2.3, Figure 2-93). To explore the usability of 40 mg/ml rColNS_low for cell encapsulation, HFF cells were added to the liquid formulation and printed. Although the formulation gelated, cells remained round shaped and LIVE/DEAD staining revealed low cell viabilities (data not shown). To explore the influence of the printing technique on the cell viability, 5 mg/ml rColNS_low spiked with cells ($1x10^6$ HFF cells/ml) were processed by the printer head and ejected into an eight well chamber slide. The photopolymerized matrix was incubated for one week under culture conditions showing elongated and viable cells after one week *via* LIVE/DEAD staining (see Figure 2-95 (A)). To demonstrate cell stretching while maintaining a low rColNS_low concentration, viscosity modifiers like hyaluronic acid (e.g. HyaCare), dextran, PEG, polyvinyl alcohol (PVA), Xanthan Gum, Pectin, Carrageenan, Guar Gum, Cellulose and other materials could be accessed to stabilize the low viscous formulation.[369] Additionally, the implementation of another biopolymer could alternate the pore size of the formed hydrogel by acting as an placeholder which could induce cell stretching with higher rColNS concentrations. To reduce the rColNS_low concertation from 40 mg/ml to 30

or 20 mg/ml, recombinant hyaluronic acid was added to stabilize the print with HFF cells ($1x10^6$ cells/ml). While 20 mg/ml rColNS formulations showed weak resolution (distinct outer lining but repetitively caused an inner filling), 30 mg/ml rColNS allowed a cylindric print with good resolution (see Figure 2-95; B) but cells remained round shaped. The printing fidelity decreased with the increase in height. As an outlook, other material composition could be tested to further increase the printing fidelity and to allow cell stretching and cellular wellbeing within the formulation.

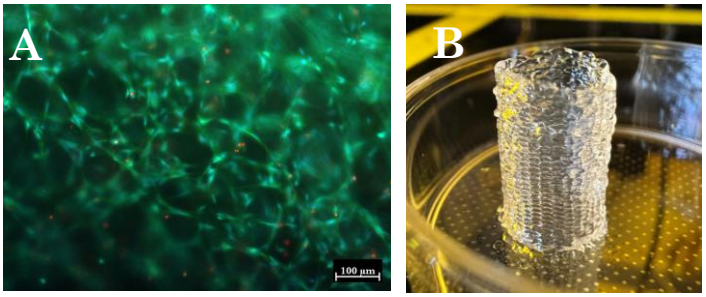

Figure 2-95: (A) LIVE/DEAD staining of encapsulated HFF cells (P3) in 5 mg/ml rColNS_low using 0.3 mg/ml LAP. The formulation was processed *via* DoD using the Black Drop Bioprinter with a pressure of 0.25 bar. The cured matrix (Omnicure S2000, 15 seconds, 5.04 W/cm²) was covered by cell culture medium and incubated for one week prior to staining. **(B)** Cellular print of HFF cells ($1x10^6$ cells/ml) using 30 mg/ml rColNS_low with 0.25% (w/v) recombinant hyaluronic acid and 1 mg/ml LAP. The cylinder has a diameter of 8 mm and consists of 72 layers.

2.5.1.4 RESOMER® – rCol hybrid print

Compared to hydrogels, RESOMER® polymers have a much higher stiffness. Combining both materials by using a core shell design can stabilize weak hydrogel structures and improve the biological response of RESOMER®. Therefore, PLA based RESOMER® was printed together with agarose hydrogel. Some impressions of an artificial heart valve (see Figure 2-96) and another structure with filled hydrogel cavities (Figure 2-97) were successfully tested. Also, porous or hollow structures could be interesting for subsequent hydrogel filling.

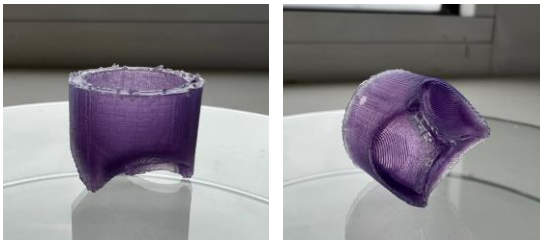

Figure 2-96: Hybrid print of a heart valve made from transparent PLA and agarose. The hydrogel fraction was stained using purple food dye. The printing file was provided by Blackdrop GmbH.

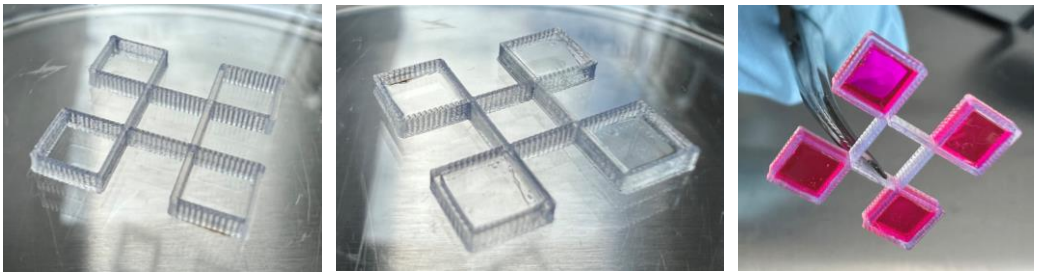

Figure 2-97: FFF print of transparent PLA filament to squares with a diameter of 5 mm. The squares were filled with 40 mg/ml rColNS_low (0.3 mg/ml LAP). After photopolymerization hydrogels were stained with 1 mg/ml rhodamine B in ddH_2O.

2.5.2 Stereolithographic printing

Besides DoD, stereolithography is another great printing technology for low viscous and photopolymerizable fluids. To explore feasibility for stereolithography of rColNS, a selected formulation was processed with the Bionova X from Cellink which demonstrated great potential for further trials. To increase the printing fidelity different parameters could be optimized. Examples are printing parameters like layer height, exposure time and curing intensity. Furthermore, the formulation could be optimized by testing a broader concentration range of rColNS, explore different viscosities, and have a deeper look into the surface tension. Interesting would also be the use of cell culture medium as solvent, the addition of rheology modifiers or post processing steps like additional curing or washing to achieve the desired material properties.

Figure 2-98: Stereolithographic print of 40 mg/ml rColNS_medium with 1 mg/ml LAP in 1×PBS using a Bionova X from Cellink as PoC experiment to craft a cuboid, a cubic and a pyramid-like structure.

3 Conclusion

3.1 The State of the Art – before the thesis

The 3D-bioprinting is a growing market with a reported CAGR forecast of 16.2% worldwide.[370] 3D-bioprinting inludes the development of 3D-cell culture systems and artificial tissues targeting new regenerative medicine therapies. Therefore, the need for efficient cell scaffolds is continuesly increasing. At the same time, we are living in a world with limited resources, where the idea of sustainability is more and more respected and followed. In order to combine the need for tissue matrices and sustainability while considering the advantages of proteinogenic biomaterials, Evonik Operations GmbH invested in a recombinant collagen (rCol) for which scaffold structures were explored within this thesis. Apart from synthetic polymers, which often show poor to non-biological interactions and partially no biodegradability, naturally derived biomaterials (polysaccharides, proteins, a.o.) have in general higher biodegradability, biocompatibility, non-toxicity and non-antigenicity. While most polysaccharides are plant-derived (alginate, agar, agarose, cellulose, ...), proteinogenic biomaterials are mostly animal-derived. Due to the mostly proteinogenic nature of tissues, proteinogenic bioinks may offer advantages over polysaccharide-based materials. Also their easy modification by genetic engineering and the natural interaction sites with cells and other components make proteins highly interesting. The aim of this work was to better understand rCol and to develop different hydrogels of it to develop different material applications while studying the characteristics and properties of the formed hydrogels. The rCol material was also compared to animal-derived collagen and the differences were determined. Various applications in the field of medical devices and bioprinting were explored by introducing three different crosslinking technologies for rCol based on a simple carbon acid activation reagent (DMTMM), a copolymer with PEG and finally a prior chemical functionalization to allow photopolymerization. The functionalization for photopolymerization was established for the first time for rCol based on thiol-ene chemistry (click chemistry). During the research and development phase, two application fields of interest were identified. First, a soft tissue patch for drug delivery and second a novel recombinant and photopolymerizable bioink made from rCol.

3.1.1 DMTMM and PEG linker

Numerous crosslinking methods have been reported to stabilize proteins. Some examples go back to 1983 where Weadock *et al.* used UV irradiation, dehydrothermal crosslinking (DHT),

carbodiimides, glutaraldehyde and combinations thereof to crosslinked bovine collagen films.[371] For DMTMM more recent literature was found. One of the earliest mentions of "collagen" and "DMTMM" on the patent database "Espacenet" was from 2009 where the authors synthesized an ultrafine fibrous membrane made from a biopolymer like collagen and DMTMM as crosslinker (2009; CN101703786A). More recent patents include a recombinant collagen-like protein expression and its subsequent crosslinking by DMTMM (2017; WO2018069873A1) or the DMTMM-guided crosslinking of collagen for cornea replacements (2023; CN115990969A) or for an ophthalmological device (2020; US2023035013A1). One patent application with similar protein sequence compared to rCol was filed. The rCol was crosslinked by carbon acid activation regents like EDC or DMTMM (2017; WO2019046943A1). By exceeding the research to market products and publications, no soft tissue patch application was found w/ or without the use for drug delivery made from a recombinant collagen-like protein. For 4-Arm-PEG-SG, the closest state-of art was identified by Lotz *et al.*[113], where chemical crosslinking of rat tail collagen with a PEG-SG linker was used to overcome the fibroblast-mediated contraction due to the poor stability of physically gelated collagen. The authors could show a reduction in contraction by using the linker. Still the material derived from animal-derived sources and does not fulfill the desire for sustainability. In summary, both technologies were chosen to evaluate hydrogel synthesis with rCol. Both linkers are state of the art for animal-derived collagens. Due to the unique properties of rCol, novel material properties of formed hydrogels were generated.

3.1.2 Photopolymerization

For rColN and rColS functionalization, the closest state of the art was published during the timeframe of this PhD thesis by others in 2021. A summary of these publications is listed in Table 3-1. Tytgat *et al.* reported the functionalization of a recombinant collagen like-protein using a comparable functionalization chemistry. Still novelties were introduced for the derivatization reaction due to the replacement of organic solvents and reduced reaction temperatures. Additionally, DoD as printing technology was not tested with rCol before using norbornene and thiol functionalizations. Also, the used collagen-like protein (Cellnest) has enough alterations within the primary sequence to be evaluated as different protein which was outlined in the following. First, Cellnest (RCPhC1) was assembled from four overlapping collagenous fragments of human type I collagen alpha 1 chain with a molecular weight of 571 amino acids.[372] rCol is of bacterial origin (based on the Scl2 protein), with half the size (240 amino acids) and labelled as type free. Second, the amino acid comparison was different. Similar shares for Gly, Leu, Cys, Hyl, Arg, His, Phe, Hyp were identified. RCPhC1 contains more Ala (2.5x), Val (2x), Ile, Met (4x) and Pr (1.3x) while rCol contains more Ser, Thr, Asp

(1.4x), Glu (1.6x), Gln (3.6x), Lys (1.6x) and Tyr. Ser, Thr and Tyr are only present in rCol; Ile only in RCPhC1. Third, rCol contains more lysine side chains which are relevant for the derivatization and the chemical crosslinking with the two described reagents (DTMMMM and 4PEG-SG) and the chemical derivatization for rColN and rColS. Fourth, both proteins lack cysteines side chains. Fifth, the share of hydrophobic side chains is higher in the RCPhC1 sequence which could negatively affect the solubility in water depending on the 3D folding of the protein and the exposure thereof to the aqueous surrounding. In another publication, Guo *et al.* used only ColN which was derived from an animal-derived collagen, and the authors used norbornene acid anhydride which introduced additional carbon acids with each conjugation position resulting in a different product. Gockler *et al.* used a comparable chemistry with elevated temperatures due to the use of animal-derived gelatin. Therefore, the reaction products are also not comparable to rColN and rColS. This leaves rColN and rColS to totally new material whose synthesis were never done before. The same accounted for the resulting hydrogel products which updated the state of the art with all the subsequent discoveries with the synthesized hydrogel made from rColNS.

Table 3-1: Summary of relevant literature for the state-of-the-art evaluation for rColN and rColS.

Author	Description	Differences to publication	Source
Tytgat *et al.*	Functionalization of a recombinant collagen (RCPhC1) with norbornene and thiol units by a similar chemistry for high resolution 2PP printing and the encapsulation of adipose tissue–derived stem cells (ASCs). This publication has the closest state of the art in regard to the overall procedure and the application idea.	Another collagen was used; no organic solvents were used for the synthesis; lower temperatures were applied during the reaction; DoD printing was used instead of 2PP.	[175]
Guo *et al.*	Norbornene functionalization of rtCol I with norbornene anhydride and subsequent photopolymerization with HS-PEG-SH (1000 Da) for the successful encapsulation of human dermal fibroblasts (HDFBs) allowing cellular spreading.	Another collagen was used; norbornene functionalization was done with norbornene acid instead of the anhydride; no 3D printing technique was used.	[146]
Gockler *et al.*	Functionalization of animal-derived gelatin with norbornene acid and thiolation with *N*-acetyl-homocysteine thiolactone. The used chemistry represented the closest state of the Art for the new rCol material and was further optimized.	A short collagen-like protein was used instead of gelatin; lower temperatures were used for the reactions; better reaction control using a preactivated norbornene acid	[344]

3.2 Identified novelties

The goal of this thesis was to evaluate the novel rCol material and to explore hydrogel synthesis technologies and to develop biomedical applications. Based on exclusive properties of

rCol, resulting hydrogels demonstrated exceptional material properties and fitting applications which were outlined in the following.

3.2.1 Material related

First, crosslinking rCol with DMTMM or the PEG-based linker was not obvious due to the different molecular weight of rCol in comparison to mammalian collagens. To synthesize hydrogels with rCol, the importance of the collagenous triple helix during gelation was explored. In Figure 2-3 (chapter 2.1.1.3), a T_m of 33 °C was identified for rCol. Exposure to different temperatures prior to crosslinking and during crosslinking significantly influenced the gelation and the final stiffness (see chapters 2.2.2.2.1 and 2.2.3.3.1, Figure 2-14 and Figure 2-23). These findings indicated the importance of the triple helical conformation required for hydrogel formation with low molecular weight collagens. Second, an elevated stiffness of rCol hydrogels was identified compared to mammalian collagens. All technologies reported in this thesis relied on lysine side chains for crosslinking. Due to the high ratio thereof (10%) in the rCol primary sequence, a variety of crosslinks could be established. As comparison, mammalian collagens contain ~3.7-3.9% lysines based on the following sequences from the database Uniprot: P02452, P02464 and P08123. Especially for the α1 chain, the number of lysine side chains is preserved in several mammalians (human, mouse, rat and bovine) based on the Uniprot sequences: P02452, P11087, P02454 and P02453.[373] The resulting hydrogels exceeded the known stiffnesses of mammalian collagens based on the generated data in Figure 2-68 and Figure 2-69 (chapter 2.3.4.3.3) roughly 21x compared to physically crosslinked rtColMA (57 kPa vs. 6.8 kPa) and ~8x compared to chemically crosslinked rtColMA (57 kPa vs. 6.8 kPa). These values are just for a rough estimation. Higher concentrations of both materials (rtColMA and rColNS) might alter the relative share. Furthermore, the high solubility (up to 200 mg/ml) allows high final concentrations with a broad range of material properties including a broad rheology range (tested from ~ 0.5 kPa to ~60 kPa). Third, rCol solution obtained remarkably low viscosities compared to mammalian collagens. Collagens are known to be quite viscous which restricts their usage for bioprinting. Only technologies which require a high viscosity are therefore suitable (like extrusion). The low viscosity of rColNS before crosslinking is ideal for Jetting and SLA. Fourth, rCol hydrogels revealed adjustable cell interaction properties regarding cell adhesion. Based on the applied crosslinking procedure and the formulation, none to great cell adhesion was observed. The best cell adhesion was observed with rColNS (except for HeLa cells), followed by DMTMM crosslinked rCol hydrogels (difficulties in reproduction) and the complete loss of cell adhesion with rCol/PEG composites. This cell-repellent effect was not observed by mixing the PEG linker with rat tail collagen. Concluding, the surface properties were adjustable depending in the final

application. The lack of cellular attachment with the PEG composite could be useful for cell-cell interaction studies for cell type specific adhesion, cell spheroid or organoid production and the use as biosensors with anti-fouling characteristics. Decreased biological recognition can also make the composite appealing for drug delivery or for biodegradable anti-fouling coatings. Especially in combination with blood, collagen is known to induce blood clotting. Thus, it can be risky for nanogel or microgel applications when thinking about injections. A blood clotting effect of the formulation needs to be tested in advance before investing in that direction. Due to the hydrophilicity of the hydrogel matrix, especially hydrophilic bioactive materials are interesting including antibodies, growth factors, antibiotics or vitamins while maintaining biodegradable properties. Cell repellent matrix properties can be also beneficial for cell encapsulation trials as published for chondrocytes for the formation of neocartilage.[374] Fifth, rCol solutions as well as resulting hydrogels have an unseen transparency unusual for mammalian collagen-based hydrogels. Most hydrogels are turbid or colored (like alginate, agarose or cellulose)[375] which makes them difficult for microscopic applications and they can decompose into acidic monomers (alginate) which might cause a regional pH drop when implanted or cause inflammation (chitosan). Here rCol based hydrogels offer a great advantage for applications where transparency is a must have. Sixth, the biodegradability was adjustable. Based on the formulation, different hydrolytic effects were observed with or without the presence of relevant enzymes. Due to the high accessible concentration range of rCol, the degradation time can be adjusted based on the application while no toxic side products form during rCol degradation due to the proteinogenic origin. Furthermore, rCol can be easily genetically modified to introduce several recognition patterns for e.g. enzymatic cleavage.

3.2.2 Applications

One application of rCol hydrogels is the usage as drug delivery matrix. Trials with DMTMM crosslinked rCol demonstrated a fast release of added APIs in the hydrogel solutions (tested with caffeine) as well as when using a nano emulsion (data not shown here). For the latter, microparticles were added prior to crosslinking and immobilized within the hydrogel. The release kinetic of the encapsulated model drug (meloxicam) was like loaded microparticles without being immobilized in the hydrogel, showing a sustained release profile as expected for the used polymer (PLGA). On the side, the direct API immobilized without microparticle showed an immediate release profile. These findings showed a great potential of the microparticle loaded DMTMM crosslinked rCol as well as the PEG composite for a sustained *in situ* API release for therapeutic applications. Especially the fast-gelling PEG composite with adjustable degradation patterns and a demonstrated injectability prior to crosslinking bear a huge potential for an injectable drug depot while showing no adverse effects of the released

NHS as shown by a leachable experiment. During this thesis, several application fields were evaluated and tested. An overview of tested applications was given in Figure 3-1. Due to the novelty of the material itself, most applications were evaluated as new state of the art. Based on the raw material, hydrogels were synthesized and used for the generation of microgels with microfluidics, as coatings for cell culture plates, films, freeze-dried hydrogels for collagen sponges and ultimately soft tissue patches. By the help of chemical derivatizations, also bioprinting was possible. A special case is electrospinning which was successfully tested and explored by another PhD student (C. Krauss, Evonik Operations GmbH).

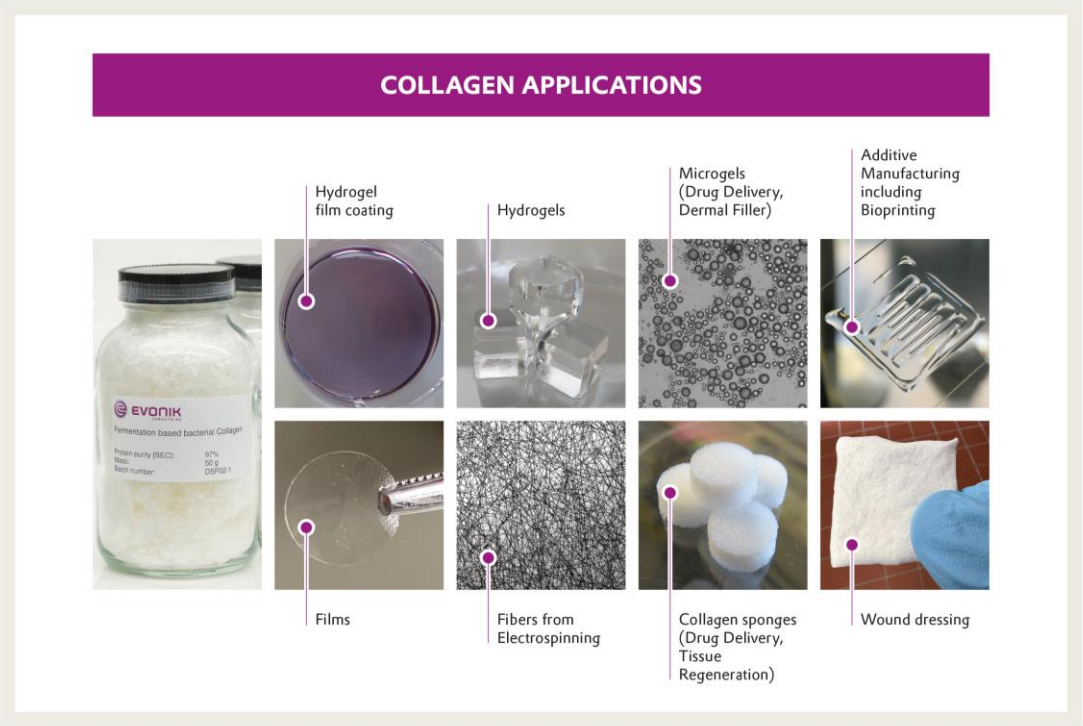

Figure 3-1: Overview of rCol-based medical, drug delivery and tissue engineering applications.

Regarding rColNS, a highly efficient bioink for bioprinting was developed which was never done with this material before and opened to range of printing technologies which rely on low viscous polymer solutions like DoD or vat-based methods. The fast and efficient crosslinking mechanism with minimal concentrations of photoinitiator, the large formulation spectrum and the great transparency were additional benefits. Microscopic imaging was ideal with rColNS hydrogels and allowed the long-term observation of encapsulation cells in multiple layers. This could be highly relevant for tissue development. The low concentrations of required material could be also interesting for e.g. subcutaneous injections. The performed DLP printing with this material composition could be interesting to printing high resolution structures for medical purposes.

3.3 The future of 3D bioprinting

3.3.1 Currents trends

3D bioprinting gained increasing awareness within the latest years mainly due to its ability to overcome some challenges in tissue engineering like spatial control of cell and biomaterial placement and to counteract the decrease in organ donors vs. the increasing demand for it.[376,377] Given a rapidly aging world population it is highly likely that market for bioprinted organs will steadily growth within the first half of the 21th century. In a recent paper[378], 3327 publications related to 3D bioprinting were analyzed by bibliometric analysis (2007-2022) demonstrating an increasing number of published articles over time and an expected growing trend with USA (n = 1,069) and China (n = 733) in the lead with top-ranked institutions like the Harvard Medical School and Tsinghua University. The top ten listed journals with most publications were identified with an impact factor (2021) of >4 which might be seen as indicator for the scientific relevance. The rapid increase in publications is partially owned due to the increase in printer commercialization and in bioink distribution.[378] By comparing the research from the past eight years to the last four years several changes were observed. 3D bioprinting became more prominent in tissue engineering. Also, the term "bioink" became an important keyword within the last 4 years and was described as highly relevant for the future research as well as the term "biomaterial" wherefore the authors expect significant developments within the next years. Also, the attention to hydrogels has significantly increased as well as its wide recognition as bioprinting material. Some early discovered materials like gelatin and alginate decreased in attention due to other, more promising materials and a decrease for these materials was forecast. Applications in the regenerative medicine field are expected to be highly focused on in the future as well. Based on a recent report from 2023, the main applications for bioprinting were described as cell culture and regenerative medicine applications comprising 3D cell systems, organ-on-a-chip designs, skin substitutes and organ printing (*in situ* printing).[370] According to another publication,[378] only a few bioinks were described before 2015. Between 2015 and 2018 a large number of new biomaterials emerged including alginate[379], hyaluronic acid[380], collagen[381], fibroin[382] and agarose[383]. Ding *et al.* also points out the often-used biomaterial combination with gelatin to maintain the shape during printing before crosslinking. Besides the increased attention to decellularized extracellular matrices, increasing numbers of studies combine two to three materials to receive additional benefits which was also considered as a hot research direction.[378] After 2018 more materials were evaluated as being suitable for 3D bioprinting including chitosan[384], gellan gum[385], cellulose[386] and others. All this ongoing research with different materials makes the bioink and hydrogel topic the most studied topic in 3D bioprinting.[378] Here, also

the combination of low viscous materials for polymerization with high viscous filler materials is interesting to increase the viscosity to allow a stable printing result. For photopolymerization applications also the choice of PI is a relevant topic. Ongoing research in this field within the last years allowed e.g. volumetric printing by Xolography using a dual color technique where a special PI is activated in the orthogonal intersection of light of two different wavelengths.[286] Another approach its the design of biocompatible PIs which react to light with a longer wavelength. In 2020, Urciuolo *et al.* used two photon cycloaddition of PEG molecules which were modified with 7-carboxymethoxy-4-methylcoumarin which reacts to light with wavelengths >850 nm. This technology allowed in depth curing under the skin due to the high penetration depths of infra-red light. The technology was successfully tested on mice and published in nature.[387] Applying this byproduct-free technology to other molecules including rCol could open the scope for specific form printing *in situ*. Still, ongoing challenges limit the current usage of bioprinting to simulate an environment which is as close as possible to native tissue. Examples are the ideal choice of biomaterial, the optimal manufacturing process and one of the biggest challenges, the formation of vascular networks and the scale up to craft complex 3D-architectures required for organ printing. Also, cellular *in vivo* and *in vitro* interactions with the respective biomaterials need to be understood better while maintaining the structural integrity of the printed structures over time. Also, the lack of specific ECM proteins in most bioinks, the potential of scaffold remodeling and adjusted matrix degradation remains challenging as well as the optimal final stiffness of the crafted composite to withstand external stress after implantation and to ensure excellent blending in the surrounding tissue. Despite all these challenges, bioprinting is expected to be a key player in personalized regenerative medicine in the future.[377,378,388,389]

3.3.2 Benefits of the recombinant collagen ink rColNS

As described in the previous chapter, bioinks represent a major part of bioprinting. Animal-derived GelMA describes one of the most promising materials due to its physical gelation by temperature changes, which allows deposition with high accuracy followed by photopolymerization to crosslink the printed object. Its proteinogenic nature allows cellular interactions, which is highly desirable for tissue applications. As described in the introduction, GelMA has several disadvantages as well as animal-derived collagens mainly due to the animal origin (see chapter 1.2.5). An alternative are recombinant materials like recombinant gelatin or collagen. Due to the advantages of collagen compared to gelatin including a better resemblance to tissue conditions, a better preservation of recognition sites and a stronger material stiffness recombinant, collagen represent the better option. Still, animal-derived collagens are hard to handle due to an acidic stock solution, high viscosities, inhomogeneity, the need

to neutralize the solution for cell contact, issue of bubble entry, the requirement to cool the collagen solution to avoid premature gelation during preparations and a limited concentration range. Gelation trials with rtColMA (photopolymerizable collagen version) demonstrated whitish and non-transparent hydrogel products which could make microscopic imaging impossible. The developed rColNS bioink resolved many of the issues. The material shows superior properties such as high solubility resulting in a material preparation in isotonic 1×PBS solution with very high concentrations of >150 mg/ml, which formed after a few hours at RT; low viscosity enabling a good homogenization behaviors and easy bubble removal prior to curing. The processing of the rCol solution at any temperature <30 °C is a huge benefit. Microscopic images of encapsulated cells were easy due to the high transparency, even with higher concentrations of rColNS. Besides cells, drugs were also attractive candidates for encapsulation. The triple helical structure, which contributes to stability, was also retained. Compared to commercially available rtColMA, rColNS could be synthesized with several DoFs, that can be adjusted based on the application. The biological performance was also different. While rtColMA can show problems with cellular well-being after encapsulation, rColNS showed reproducible well-being for encapsulated fibroblasts. It was assumed that rColNS formed a more homogeneous network compared to rtColMA. This was also supported by previous publications with GelMA.[126] Due to the flexible thiol-ene chemistry platform, rColN and rColS offers a chemistry that can be mixed with other norbornene-modified or thiolated polymers to synthesize copolymers with additional benefits and potentially unique material properties, which aligned with the described trend for copolymers. In addition to the tested 4-arm PEG-SH, other polymers such as DTT or peptide with terminal thiols could be used, as well as cysteine-containing or modified proteins for covalent attachment to form hydrogels with additional properties. Therefore, rColNS is an excellent bioink choice whose components preserve the triple helical structure while ensuring quality and performance with consistent results. In summary, the developed rColNS bioink has a great potential for bioprinting and represents a very promising candidate for commercialization to contribute internationally to the emerging field of tissue engineering.

4 Materials and Methods

4.1. Material

4.1.1 Used Cell lines and Primary Cells

Table 4-1: Overview of applied cells. Cells labelled with "*" are cell lines.

Abbr.	Cell Type / morphology / Origin	Supplier
Cal72*	Cell line / fibroblastic / human osteosarcoma	DSMZ - ACC 439
HeLa*	cell line / epithelial-like / human cervix carcinoma	DMSZ - ACC57
HFF-1	Primary fibroblast / fibroblast-like / human skin	ATCC - SCRC-1041™
NIH3T3*	Fibroblasts / fibroblast-like / Swiss albino mouse	DMSZ - ACC173
SW1353*	Chondrocytes / fibroblast-like / human chondrosarcoma	DMSZ – HTB-94™

4.1.2 Prepared Solutions

Table 4-2: Table of prepared solutions for the experimental part.

Fin. conc.	Sample description	V or m	components
66 µM (400x)	Phalloidin stock solution	150 µl	anhydrous DMSO
		+	vial content (ThermoFisher)
0.165 µM (1x)	Phalloidin staining solution	2.5 µl	Phalloidin stock solution
		+ 1 ml	1% (w/v) BSA in 1×PBS
100 mg/ml	rCol stock solution	100 mg	rCol
		+ 1 ml	ddH_2O
0.1%(w/w)	Cell permeabilization buffer	10 µl	Triton X-100
		+ 10 ml	1×PBS
20% (v/v)	Triton X100	20 ml	Triton X-100
		+ 80 ml	ddH_2O
0.1 M (w/v)	Na_2HPO_4	14.20 g	Na_2HPO_4
		+ 1 L	ddH_2O
0.1 M (w/v)	NaH_2PO_4	12.00 g	NaH_2PO_4
		+ 1 L	ddH_2O
0.1 M (pH 8.0)	Ellman reaction buffer	93.2 ml	0.1 M Na_2HPO_4
		+ 6.6 ml	0.1 M NaH_2PO_4
		+0.2 ml	0.5 M EDTA pH 8.0
0.01% (w/v)	Ellman staining solution	1 mg	5,5′-dithio-bis-(2-nitrobenzoic acid)
		+ 10 ml	Ellman reaction buffer
0.4% (w/v)	Ellman staining solution	4 mg	5,5′-dithio-bis-(2-nitrobenzoic acid)
		+ 1 ml	0.1 M Ellman reaction buffer pH 8.0

1.5 mM	Cysteine stock solution	18.17 mg + 100 ml	L-Cysteine Ellman reaction buffer
0.1 M (pH 8.5)	TNBSA reaction buffer	5 ml + 95 ml	Na_2CO_3 (0.1 M) $NaHCO_3$ (0.1 M)
0.01% (v/v)	TNBSA stock solution	20 µl + 9980 µl	5% (w/v) TNBSA TNBSA reaction buffer pH 8.5
50 mM (pH 7.2) (w/v)	CD measurement buffer	8.93 g + 2.31 g + 1 L	$Na_2HPO_4 \cdot 7{\times}H_2O$ $NaH_2PO_4 \cdot 1{\times}H_2O$ ddH_2O
0.5 M	$CaCl_2$ stock solution	7.35 g + 100 ml	$CaCl_2 \cdot 1{\times}H_2O$ ddH_2O
0.1 M Tris, 50 mM $CaCl_2$	Enzymatic degradation buffer	10 ml + 10 ml + 80 ml	50 mM $CaCl_2$ 1 M TRIS-HCl pH 7.4 ddH_2O
0.1 M	$NaHCO_3$ solution	8.40 g + 1 L	$NaHCO_3$ ddH_2O
0.1 M	Na_2CO_3 solution	10.60 g + 1 L	Na_2CO_3 ddH_2O
0.1 M (pH 10)	rColS reaction buffer	40 ml + 60 ml	$NaHCO_3$ (0.1 M) Na_2CO_3 (0.1 M)
201.37 mg/ml	PEG-SG stock solution	201.37 mg + 1 ml	4-Arm-PEG-SG, 10 kDa in ddH_2O
196.25 mg/ml	DMTMM stock solution	196.25 mg + 1 ml	DMTMM in ddH_2O
30 mg/ml	LAP stock solution	30 mg + 1 ml	LAP ddH_2O
1% (w/v)	Ninhydrin solution	100 mg 10 ml	Ninhydrin DMSO

4.1.3 Chemicals

Table 4-3: Overview of used chemicals.

Denotation	Provider	Cat. number
0.4% trypan blue staining solution	Invitrogen™	T10282
5,5′-dithiobis-(2-nitrobenzoic acid (DTNB)	Sigma	D8130-5G
5-Norbornene-2-NHS Ester (26% exo; 73% endo)	BroadPharm®	BP-24407
Alexa Fluor™ 488 phalloidin	Invitrogen™	A12379
BlueDrop Agarose	Black Drop GmbH	D8130-1G
Caffeine	Merck Millipore	1025841000
Calcium chloride ($CaCl_2$)	Sigma // Merck	C5670-100G
CellTiter 96® Aqueous Non-Radioactive Cell Prolif. Assay	Promega GmbH	G5421
CellTiter-Glo® Luminescent Cell Viability Assay	Promega GmbH	G7571
CnT minimal medium	CELLnTEC	CnT-PR-F

Coll 1 Lyophilizate	Cellink	VL5000000010
Collagen from rat tail (rtCol)	Sigma	C7661
Collagenase from *Clostridium histolyticum*	Sigma-Aldrich // Merck	C0130-100MG
Dimethyl sulfoxide (DMSO)	Merck	1.02952.1000
DL-Homocysteine thiolactone hydrochloride	Sigma-Aldrich // Merck	53530-25G-F
DMEM, high glucose, pyruvate, no glutamine	Gibco® life technologies	21969035
DPBS (1x), w/o calcium, w/o magnesium	Gibco® life technologies	14190-144
Ethylenediaminetetraacetic acid (EDTA)	Sigma-Aldrich	E9884-100G
Gelatine (extra pure, gold, 180 Bloom)	Roth	4274.3
Gentamycin solution (50 mg/ml)	Gibco® life technologies	11520506
Gibco™ Fetal Bovine Serum	Gibco® life technologies	16000044
GlutaMAX™-I (100x)	Gibco® life technologies	35050-061
HEPES Buffer pH 8.0 (1M) sterile	Apollo Scientific	BIA6906
Hoechst 33342, 10 mg/ml aqueous solution	Invitrogen™	H3570
HyaCare	Evonik Operations GmbH	
L-Cysteine	Merck	168149-2.5G
Lithium phenyl-2,4,6-trimethylbenzoylphosphinate	Sigma Aldrich	900889-1G
LIVE/DEAD™ Viability/Cytotoxicity Kit	Invitrogen™	L3224
Meloxicam	Fisher Scientific	AAJ6063506
$Na_2HPO_4 \cdot 7{\times}H_2O$	Sigma	S9390-1KG
$NaH_2PO_4 \cdot 1{\times}H_2O$	Sigma	567549-1KG
Ninhydrin	Sigma-Aldrich // Merck	151173-10G
PhotoCol® Methacrylated Type I Collagen	Cellink	#5198-100MG
Picrylsulfonic acid solution (5% (w/v) in ddH_2O)	Sigma-Aldrich	P2297-10ML
Pierce™ BCA Protein Assay Kits	Thermo Scientific™	23225
Poly (ethylene glycol) diacrylate (PEG-DA), M_n 575	Sigma // Merck	437441-100ML
Sodium bicarbonate ($NaHCO_3$)	Merck	1063290500
Sodium Carbonate (Na_2CO_3)	Merck	1063921000
Sodium Dodecyl Sulfate (SDS), Lauryl	Thermo Scientific™	28365
Sodium hydroxide pellets (NaOH)	Spectrum Chemical	SO170-500GM
TRIS, 1.0 M solution pH 7.4	ThermoFisher	J60202.K2
Triton™ X-100	Sigma	1086031000
TrypLE™ Express w/o phenol red	Gibco® life technologies	12604-021
UltraPureTM Distilled water DNAse & RNAse free	Invitrogen	10977-035
UltraPure™ 0.5 M EDTA, pH 8.0	Invitrogen™	15575020
VECOLLAN® (rCol)	Evonik Operations GmbH	
α-Hydroxy-4-(2-hydroxyethoxy)-α-methylpropiophenon	Sigma-Aldrich	410896-10G

4.1.4 Consumables

Table 4-4: Table of used consumables.

Material	Manufacturer	Article number
µ-slide 8 well high ibiTreat	Ibidi GmbH	80806
1.5 ml reaction tubes, transparent	Eppendorf	30120086
15 ml CELLSTAR®, blue screw cap	Greiner Bio-One	188271
2.0 ml reaction tubes, black	Eppendorf	30120248
2.0 ml reaction tubes, transparent	Eppendorf	30120094
50 ml CELLSTAR®, blue filter screw cap	Greiner Bio-One	227245
50 ml CELLSTAR®, blue screw cap	Greiner Bio-One	227261
Cell culture flask, 250 ml, 75 cm²	Greiner Bio-One	658175
Cell culture flask, 550 ml, 175 cm²	Greiner Bio-One	660175
Combitips® advanced, 1 ml, yellow	Eppendorf	30089642
Combitips® advanced, 2.5 ml, green	Eppendorf	30089650
Combitips® advanced, 5 ml, blue	Eppendorf	30089669
ep Dualfilter T.I.P.S.® blue tip, 50-1000 µl	Eppendorf	30078578
ep Dualfilter T.I.P.S.® grey tip, 0.1-10 µl	Eppendorf	30078810
ep Dualfilter T.I.P.S.® orange tip, 20-300 µl	Eppendorf	30078560
ep Dualfilter T.I.P.S.® yellow tip, 2-200 µl	Eppendorf	30078551
Injekt®-F syringe, 1 ml	B. Braun	9166017V
Injekt™ syringe, 10 ml	B. Braun	9205766
Mr. Frosty™	Thermo Scientific™	5100-0001
MTP, 48 well, sterile, w/ lid, transparent	Greiner Bio-One	677180
MTP, 6 well, sterile w/ lid, transparent	Greiner Bio-One	657160
MTP, 6 well, sterile, w/ lid, transparent, cell repellent	Greiner Bio-One	657970
MTP, 96 well, sterile, w/ lid, black	Greiner Bio One	655086
MTP, 96 well, sterile, w/ lid, transparent	Greiner Bio-One	655180
MTP, 96 well, sterile, w/ lid, white	Greiner Bio One	655083
MTP, 96 well, transparent, UV-Star	Greiner Bio One	655801
Omnifix® syringe, 30 ml	B. Braun	4617320N
Omnifix® syringe, 50 ml	B. Braun	8508577FN
Petri dish (Ø3.5 mm)	Greiner Bio-One	627161
Petri dishes (Ø9.4 mm)	Greiner Bio-One	632181
Polyester mesh, 200 µm pore size	NeoLabs®	2-4063
ROTI® DipSlides	Carl Roth	3934.1
Serological pipette (CELLSTAR®, 10 ml)	Greiner Bio One	607180
Serological pipette (CELLSTAR®, 25 ml)	Greiner Bio One	760180
Serological pipette (CELLSTAR®, 5 ml)	Greiner Bio One	606180
Spectra/Por 7 Dialysis Tubing 3.5kD 45mm 16ft	Repligen	132111
Sterican Disposable Needle, 21G x 4 3/4" - 120mm	B. Braun	4665643
Sterican Disposable Needle, 27G x ¾"	B. Braun	16010256E
Sterile filters (Filtropur S 0.2)	Sarstedt AG &Co. KG	83.1826.001

4.1.5 Devices

Table 4-5: Table of used devices.

Device	Provider	Model
3D bioprinter	Black Drop GmbH	Regenate
3D printer	Anycubic	Mega S
Analytical balance	Sartorius AG	Cubis MCE225S-2S00-I
Autoclave	Systec GmbH	DB-23
Automated Cell Counter	Invitrogen AG	Countess™ 3
Centrifuge I	Eppendorf	5425 R
Centrifuge II	Eppendorf	5910i
Fluorescence microscope 1	Carl Zeiss AG	Axio Observer Z1
Fluorescence microscope 2	Leica	Stellaris 5
Freeze dryer	Martin Christ Gefriertrocknungsanlagen GmbH	EPSILON
Heat cabinet	Memmert GmbH & Co. KG	UNB 200
Magnetic stirrer	IKA-Werke GmbH & Co. KG	C-MAG HS 7 control
Mechanical Pipette	Eppendorf	Research® plus
Multi-Dispenser Pipette	Eppendorf	Repeater® M4
NanoDrop	Thermo Fisher Scientific	One
NMR device	Bruker	Avance III HD 400 MHz
Platform shaker	Heidolph Instruments GmbH & Co. KG	Vibramax 100
Rheometer	AntonPaar	MCR 502 WESP
Rheometer (online)	Rheolutions GmbH	ElastoSens™ Bio
Routine microscope	Carl Zeiss AG	Primo Vert
Safety workbench	Thermo Electron LED GmbH	2030i 1.2
SEM	JEOL Ltd.	JSM-IT300 InTouchScope™
Spot UV Curing System	Excelitas Technologies® Corp.	Omnicure S2000
Tecan Multiplate Reader	Tecan Group AG	Infinite M200 Pro
Vibratory shaker	Scientific Industries, Inc.	Genie 2
Water bath	Julabo GmbH	PURA 14
Device	Provider	Model

4.1.6 Software

Table 4-6: Used software for this thesis.

Name	Softwareprovider	Version
ChemDraw Professional®	PerkinElmer Informatics, Inc.	21.0.0.28
Endnote™20	Clarivate™	20.5
Fiji ImageJ	National Institute of Mental Health, Bethesda, Maryland, USA.	1.53q
Fusion 360	Autodesk, Inc.	2
LasX	Leica Microsystems	03.05.2007
Microsoft Office 365	Microsoft Corporation	2302
Prism 9.4.1	GraphPad	09.04.2001
RheoCompass	Anton Paar GmbH	1.31.70
Tinkercad	Autodesk, Inc.	/
TopSpin	Bruker Corporation	04.01.2001
Zen (blue edition)	Carl Zeiss Microscopy GmbH	3.3.89.0006
Minitab	Minitab, LLC.	21.4.1 (64-bit)

4.2 Methods

Unless otherwise stated, "cell culture conditions" meant humid atmosphere at 37 °C and 5% CO_2. “Complete culture medium” represented the used cell-dependent culture medium with all required supplements, FBS, and antibiotics used to culture the respective cells, whereas “culture medium” represented the unsupplemented high-glucose DMEM medium with pyruvate and without glutamine. Also, room temperature is abbreviated with RT and comprises 21 °C -25 °C.

4.2.1 Data extraction and Statistics

Generated data were processed with Microsoft Excel and processed into figures. In case of duplicates or more replicates, the standard deviation was calculated with the formula STABW.N. The test for normal distribution was performed with Minitab with the help of a probability blot. Significance calculations were performed with Minitab as well using a one-way ANOVA or a 2-Sample t Test.

4.2.2 Cell Culture

The work with cell cultures was done under sterile conditions in a Herasafe™ safety cabinet, and all vessels or bottles were disinfected before placement (Bacillol® AF or 70-80% (v/v) isopropanol in ddH_2O). Only sterilized consumables were used in contact with cells and UV

irradiation was used for sterilization at the end of a workday. Disposable nitrile gloves were worn during work, and all cell cultures and supernatants were inactivated before disposal by autoclavation. Regular tests for mycoplasma were performed as well.

4.2.2.1 Cell Thawing

Vials of frozen cells (1 ml volume, typically 1×10^6 cells) were removed from liquid nitrogen storage and gently agitated in a 37 °C water bath. Once 50% of the cell suspension was thawed (approx. 30-90 sec.), the vial was removed and decontaminated by immersion or spraying with 70%-80% isopropanol. From here, proper aseptic techniques were applied using a laminar flow hood. The contents of the vial were diluted in 8 ml of prewarmed (37 °C) culture medium and rinsed once with 1 ml of fresh prewarmed culture medium. The cell suspension (10 ml) was gently homogenized and centrifuged (500 rcf, 5 min, 4 °C). After discarding the supernatant, the cells were resuspended in fresh pre-warmed (37 °C) medium and transferred to a new sterile T75 flask. The flask was incubated under culture conditions until cell passaging was required.

4.2.2.2 Cryopreservation

Table 4-7: Cryopreservation media. ** high glucose, w/o L-glutamine, w/ sodium pyruvate. All formulations contain 0.3 ml of a 50 mg/ml gentamycin stock solution (final concentration: 30 µg/ml).

Cells	Cryo medium	Culture medium
HFF	• 70% (v/v) DMEM** • 20% (v/v) FBS • 10% (v/v) DMSO	• 500 ml DMEM, high glucose** • 75 ml FBS (final concentration 15%) • 5 ml GlutaMAX™ (final conc. 1x)
NIH3T3	• 70% (v/v) DMEM** • 20% (v/v) FBS • 10% (v/v) DMSO	• 500 ml DMEM** • 50 ml FBS (final concentration: 10%) • 5 ml GlutaMAX™ (final conc. 1x)
HeLa	• 70% (v/v) DMEM** • 20% (v/v) FBS • 10% (v/v) DMSO	• 500 ml DMEM, high glucose** • 50 ml FBS (final concentration: 10%) • 5 ml GlutaMAX™ (final conc. 1x)
SW1353	• 60% (v/v) DMEM** • 30% (v/v) FBS • 10% (v/v) DMSO	• 500 ml DMEM, high glucose** • 50 ml FBS (final concentration: 10%) • 5 ml GlutaMAX™ (final conc. 1x)
Cal72	• 70% (v/v) DMEM** • 20% (v/v) FBS • 10% (v/v) DMSO	• 500 ml DMEM, high glucose** • 50 ml FBS (final concentration: 10%) • 5 ml GlutaMAX™ (final conc. 1x)

Cell-type dependent cryopreservation media were prepared in accordance with Table 4-7. Cells were detached as described in chapter 0, counted, precipitated by centrifugation (500 rcf, 5 min., 4 °C) and resuspended in cryopreservation medium with 1×10^6 cells/ml. Respectively 1 ml cell suspension was transferred into a cryo vial followed by linear cooling to - 80 °C with 1 °C/min using a Mr. Frosty™ cryo device (ThermoScientific™; order number: 5100-0001).

4.2.2.3 Passaging and standard culture

Adherent cells were split before they reached confluency (100% coverage of the culture surface). Cells were split when they reached ~80% confluency with the indicated seeding density in Table 4-8. Used culture medium for standard cultivation are listed in Table 4-7.

Table 4-8: Used seeding densities and subcultivation ratios for applied cells.

Cell Type	Seeding density (cells/cm²)	Inoculation cell density (total cell number/flask)			Detachment solution	Subcultivation ratio
		T175	T75	T25		
NIH3T3	0.5×10^4	0.9×10^6	4×10^5	1×10^5	TrypLE	1:10
HFF	$\geq0.8\times10^4$	1.4×10^6	6×10^5	2×10^5	TrypLE	1:5 to 1:7
SW1353	1×10^4	1.75×10^6	7.5×10^5	2.5×10^5	TrypLE	1:2 to 1:5
Cal72	1.25×10^4	2.2×10^6	9.4×10^5	3.1×10^5	TrypLE	1:3 to 1:10
HeLa	2×10^4	3.5×10^6	15×10^5	5×10^5	TrypLE	1:10 to 1:15

Prior to detachment, the culture medium was removed, and the cells were rinsed once or twice with 1×PBS (RT) to remove traces of serum (containing trypsin inhibitors), detached cells and cell debris. Cells were incubated with detachment solution at 37 °C under culture conditions (inside an incubator) until ~ 90-100% of the cells detached. Frequently the cell vessel was removed from the incubator and the cell morphology was observed with a light microscope. Gentle tapping of the flask may help to dislodge cells. The indicated volume of culture medium (pre-heated; 37 °C) was added to quench enzymatic activities and the cells were transferred to a sterile Falcon tube. Repeated pipetting (up and down) was used to break up remaining cell aggregates while bubble formation during pipetting was prevented as much as possible. Enzymatic incubation was kept short to avoid irreversible cell damage (especially with trypsin).[390] Then the same was precipitated by centrifugation (500 rcf, 5 min, 4 °C). After removing the supernatant, cells were resuspended in 1 ml culture medium which was preheated to 37 °C. The cell concentration was determined by the Countess™ 3 Automated Cell Counter (Invitrogen™; catalog number: AMQAX2000) according to the user's manual (1:1 mixture of cell suspension and 0.4% trypan blue staining solution (Invitrogen™; catalog

number: T10282). After the measurement, the following formula was used to adjust the desired cell concentration (equation 4-1):

$$V_1 = \frac{c_2 * V_2}{c_1}\,;\; V_{Medium\ to\ add} = V_2 - V_1 \qquad \textbf{4-1}$$

- C_1 = detected cell concentration of the homogenized stock suspension.
- C_2 = desired cell concentration.
- V_1 = volume of stock suspension (needed to be calculated)
- V_2 is the desired final volume of the desired concentration.

Pre-heated (37 °C) $V_{Medium\ to\ add}$ was first added to the desired culture vessel followed by V_1. The vessel was gently moved several times in the shape of an infinity symbol (∞) before placing it into the incubator. Every 2-5 days, the cells are washed with 1×PBS (RT) and the medium was replenished, or cells were detached again for sub cultivation reasons.

Table 4-9: Used volumes for cell passaging regarding cell washing with 1x PBS, cell detachment and subsequent quenching of the enzymatic reaction and the total volume for cell cultivation.

Flask/dish	Growth Area (cm^2)	1×PBS (ml)	Detachment solution (ml)	Quenching volume (ml)	Growth Medium (ml)
T175	175	15	7	7	30
T75	75	5	3	7	12
T25	25	3	1	3	4

4.2.3 Biological Assays

4.2.3.1 Cytotoxicity Assays

4.2.3.1.1 MTS Assay

The CellTiter 96® AQueous Non-Radioactive Cell Proliferation Assay (Promega; catalog number: G5430) detected the number of viable cells after exposure to a test solution by quantifying the concentration of reduction equivalents (NADH & NADPH) produced by viable cells during glycolysis. By reducing the MTS reagent to a measurable purple formazan product, the metabolic activity of exposed cells was measured as an indirect indicator of cell viability. The assay was designed based on the manufacturer's protocol and ISO standard 10993-5. Briefly, cells were seeded at 1×10^4 cells/well (1×10^5 cells/ml, 0.1 ml) into a transparent 96-well plate. 20 mg/ml sample stock solutions in complete culture medium were diluted with complete culture medium to the final test concentrations. After 14-24 h of incubation under culture conditions, the cell medium was replaced with 100 µL of test solution. Each

formulation was tested in triplicate. For background control, the formulation was tested without cells. Complete culture medium was used as a negative control. Cells were exposed to the test formulations for 24 h under cell culture conditions. The test solution was then replaced with 100 µl of fresh complete culture medium and 20 µl of premixed MTS reagent solution per well (prepared according to the user's manual). For the positive control, 5 µl of 20% (v/v) Triton X-100 was added 10 min before the addition of the MTS solution. The test plate was incubated for 4 h (37 °C, 5% CO_2). The absorbance was read at 490 nm (multiplate reader, Tecan Pro200). The background signal was subtracted from each test sample, followed by signal normalization to the negative control. The sample mean and standard deviation were calculated.

4.2.3.1.2 CellTiter-Glo® Assay

The CellTiter-Glo® Luminescent Cell Viability Assay was performed to evaluate potential cytotoxic effects of solubilized materials according to the manufacturer's protocol. Cells of interest were pre-seeded at 1×10^4 cells/well (1×10^5 cells/ml, 0.1 ml) in a white 96-well plate. As an adhesion control, 3 wells of a transparent 96-well plate were filled with the same number of cells. After 14-24 h of incubation (37 °C, 5% CO_2), the complete culture medium was replaced by 100 µl of test solution. A 20 mg/ml stock solution in complete culture medium was prepared for each formulation, followed by a dilution series with complete culture medium. Each formulation was tested in triplicate. The formulation without cells was analyzed as a reference. 150 µg/ml digitonin in complete culture medium (positive control) and complete culture medium (negative control) were used as controls. Cells were exposed to the test formulations for 24 h under cell culture conditions. The CellTiter-Glo® reagent was then prepared (1:1 mixture of CellTiter-Glo® Substrate and CellTiter-Glo® Buffer) and equilibrated to RT together with the cell containing MTP for 30 min. Reagent was added at 100 µl/well. The plate was vortexed for 2 min (multiplate reader, Tecan Pro200) followed by an incubation period of 10 min. Luminescence was then measured with an integration time of 0.1 sec. per well. The average signal of the positive control was subtracted from each test sample and the sample signals were normalized to the negative control. The average of the sample values and the standard deviation were calculated.

4.2.3.2 Leachables

2 mm thick hydrogels were prepared in a sterile 48-well plate (220 µl of liquid hydrogel formulation) and incubated for 16-24 h at RT. Separately, adherent growing cells were seeded into a white 96-well plate for luminescence measurements at 1×10^4 cells/well (100 µl of a homogenized cell stock solution containing 1×10^5 cells/ml). The next day, each well was

washed in the 48 well plate with twice the hydrogel volume (440 µl) of complete culture medium at RT with orbital shaking (300 rpm) for 1 h each. Wash solutions were collected with a total of three wash cycles. The medium in the culture plates with adherent cells from the previous day was replaced by 100 µl of washing solution. Each wash solution was tested in triplicate. Cells exposed to culture medium were used as a negative control. Exposed cells were incubated under culture conditions for 24 h. The next day, the MTS assay was performed.

4.2.3.3 Cell Adhesion

All steps for hydrogel preparation were performed under proper aseptic technique in a laminar flow hood and were performed either in 48 well MTPs, 6 well MTPs or 8 well chamber slides. The preparation of hydrogel formulations is described in chapter 4.2.4. In case of photopolymerization, samples were cured and used right away. Wells filled with non-photopolymerizable formulations were cured overnight at RT by plate sealed to prevent drying. If not stated otherwise, they were washed twice with twice the hydrogel volume for 1 h each to remove potentially toxic components and to generate isotonic conditions within the hydrogel. For rColNS samples, this step wasn't mandatory because rColN and rColS proved to be non-toxic and LAP was used in a non-toxic concentration as well. After washing detached cells were added (according to Table 4-10). The culture plate was incubated under culture conditions for up to 7 d. Brightfield imaging was performed within this time period. Optionally, a cell staining can be applied to determine the cell viability or to label cell structures like actin-filaments. As reference, chemically and physically gelated rtCol was used and prepared according to chapter 4.2.4.7. The required concentration of PEG linker was calculated based on the number of lysine side chains in rat tail collagen and based on the molecular weight of the PEG linker to yield in identical MRs to the rCol sample.

Table 4-10: Applied cells and volumes for cell adhesion experiments regarding the applied vessel.

Format	Hydrogel volume/well	V (cell suspension)	Applied cell suspension	Final culture volume
8 well ibidi slide	200 µl	200 µl	$5x10^4$ cells/ml	200 µl
48 well MTP	220 µl	300 µl	$1×10^5$ cells/ml	300 µl
6 well MTP	500 µl	100 µl	$3×10^6$ cells/ml	2000 µl

4.2.3.4 Cell injections + Staining

To determine cellular metabolic activity within hydrogel sponges crosslinked by DMTMM, they were prepared according to chapter 4.2.4.3 and 4.2.4.8. For the subsequent injections, HFF and SW1353 cells were used. Hydrogel sponges were prepared according to chapter (750 µl, 6.3 mm radius, 6 mm height) prepared from 750 µl hydrogel volume were soaked in EtOH for 20 min followed by overnight incubation in 25 ml sterile 1×PBS containing 30 µg/ml gentamicin each. The next day, the sponges were transferred to a 12-well plate, followed by 500 µl of complete culture medium injections to remove residual EtOH and to equilibrate the interior with medium. Then, cells were injected (500 µl, $2x10^6$ cells/ml each for HFF cells and 500 µl, $3x10^6$ cells/ml for SW1353 cells) using a 27G×3/4 needle, followed by immersion in cell culture medium for 7 d. Then, cells were stained by replacing the cell culture medium with 3 ml of 1 mg/ml MTT reagent in 1×PBS for 4 h incubation time. Then, the macroscopic images of the surface and interface were taken by cutting the sponge in half. The sponges were then squeezed to remove excess liquid and incubated with 80% (v/v) isopropanol for 1 h in a sealed reaction tube. Additional squeezing ensured a homogeneous solution. The absorbance of 250 µl extraction solution was measured at 570 nm.

4.2.3.5 Cell staining

4.2.3.5.1 LIVE/DEAD + Hoechst 33342

LIVE/DEAD staining was performed using the LIVE/DEAD™ Viability/Cytotoxicity Kit for Mammalian Cells according to the user's manual (Invitrogen™; catalog number: L3224). The kit is based on calcein-AM and ethidium homodimer-1 (EthD-1). The aqueous working solution was freshly prepared before each staining experiment due to the susceptibility of calcein-AM to hydrolysis by adding 2.5 µl 4 mM calcein AM and 10 µl 2 mM EthD-1 to 5 ml sterile 1×PBS. Additionally, 2 µl of 10 mg/ml Hoechst 33342 solution (Invitrogen™; catalog number: H3570) was added. The resulting working solution was added directly to the cells (200 µl / well / 8 well slide; 220 µl / well / 48 well plate. Cells were incubated for 20-40 min at 37 °C in the dark. Then, dye emissions were detected using a fluorescence microscope with the following wavelength settings:

- **Calcein**: Excitation / Emission: 494 nm / 517 nm
- **EthD-1:** Excitation / Emission: 528 nm / 617 nm
- **Hoechst 33342**: Excitation / Emission: 352 nm / 454 nm

4.2.3.5.2 Phalloidin/Hoechst 33342

Phalloidin staining is based on Alexa Fluor 488® Phalloidin Reagent (Invitrogen™; catalog number: A12379). The water-soluble, small-molecule bicyclic peptide conjugate binds to F-actin with nanomolar affinity. The staining procedure is based on four sequential steps: Fixation, Permeabilization, Blocking/Staining and Readout. This protocol describes the staining procedure for adherent cells in a 48-well plate format. The volumes required can be adapted to other vessel sizes by multiplying each volume by the volume change factor.

Cell fixation: Remove supernatant; wash cells twice with pre-warmed 1×PBS (500 µl each). Discard washing solution and add 300 µl 4% methanol-free paraformaldehyde solution. Incubate the mixture for 15 min at RT.

Cell Permeabilization: Remove fixation solution; wash twice with 500 µl 1×PBS each. Replace washing solution by 300 µl "Permeabilization buffer". Incubate 15 min at RT.

Blocking and staining: Discard "Permeabilization solution". Wash twice with 500 µl 1×PBS each. Add 200 µl "Phalloidin staining solution"/well. Incubate 30-60 min at RT in the dark. Remove staining solution. Wash twice with 1×PBS (500 µl each). Remove the washing solution and add 200 µl/well of a Hoechst staining solution. 10 mg/ml Hoechst stock solution is diluted 1:5000 to a work concentration of 2 µg/ml.

Readout: Fluorescence microscope imaging with λ_{ex} 499 nm / λ_{em} 520 nm (Phalloidin) and λ_{ex} 352 nm / λ_{em} 454 nm (Hoechst 33342). Record pictures and prepare image overlays using the software ImageJ.

4.2.3.6 Sterility test

To allow sterile production of collagen derivatives, sterile filtration (0.2 µm pore size) was used after dialysis. Each 2 ml of reaction product (w/ and w/o sterile filtration, 1% (w/v) each) was lyophilized in a 50 ml sterile Greiner tube with filter inlet in the cap (0.2 µm). The weight of the lyophilizate obtained was compared with the tare weight to determine any weight loss due to sterile filtration. 20 mg of each lyophilizate was dissolved in 40 ml of sterile 0.9% NaCl solution and assayed using ROTI® DipSlides (CASO/RBCenr, Carl Roth, 3934.1) according to the manufacturer's instructions (0.5 mg/ml). Briefly, the DipSlides were immersed in the 40 ml test samples for 10 seconds each. *E. coli* (bacterium) and *P. pastoris* (yeast) strains were used as positive controls. The slides were incubated at 30 °C for 120 h. Photographs were taken after 48 and 120 hours.

4.2.3.7 3D cell encapsulation

This method described the cell encapsulation in rCol hydrogels followed by longtime cultivation. All steps were done under proper aseptic techniques within a laminar flow hood with sterile materials only. If not stated otherwise, rColN and rColS were used in identical concentrations with 0.3 mg/ml Lithium phenyl(2,4,6-trimethylbenzoyl)phosphinate (LAP). All components were dissolved in 1×PBS. Cells of interest were detached and adjusted to a concentration of 1×10^7 cells/ml in full culture medium. Cells were used with final concentrations of 1×10^6 cells/ml. 1×PBS, $rColN_{(aq)}$, $rColS_{(aq)}$, cells and $LAP_{(aq)}$ were mixed in a suitable vessel based on Table 4-11, molded and exposed to light. If not stated otherwise either 8-well ibidi slides with 200 µl/mold or 48-well plates with 220 µl/mold were applied and the Omnicure S2000 system was used for irradiation with 5.04 W/cm² for 15 seconds and a lamp-sample distance of 5 cm. After irradiation, hydrogels were covered by the identical volume of pre-heated full cell culture medium followed by incubation under culture conditions. The medium was exchanged after 1 h, 24 h and then every second day.

Table 4-11: Example formulations for rColNS with cells for 1000 µl each. 50 mg/ml rColN and 50 mg/ml rColS stock solution in 1×PBS was used as well as 30 mg/ml LAP. Cells were prepared with $1x10^7$ cells/ml and homogenized before adding to achieve a final cell concentration of $1x10^6$ cells/ml.

Final concentrations				Needed volumes per component				
rColN	**rColS**	**LAP**	**Cells**	**rColN**	**rColS**	**LAP**	**Cells**	**1×PBS**
mg/ml			**nb/ml**	**µl**				
2.5	2.5	0.3	1.0×10^6	50	50	10	100	790
5.0	5.0	0.3	1.0×10^6	100	100	10	100	690
7.5	5.0	0.3	1.0×10^6	150	150	10	100	590
10	10	0.3	1.0×10^6	200	200	10	100	490
12.5	12.5	0.3	1.0×10^6	250	250	10	100	350
15	15	0.3	1.0×10^6	300	300	10	100	250
17.5	17.5	0.3	1.0×10^6	350	350	10	100	150
20	20	0.3	1.0×10^6	400	400	10	100	50

4.2.4 Chemical Synthesis

4.2.4.1 Synthesis of recombinant norbornene-modified collagen (rColN)

4.2.4.1.1 rColN – preliminary synthesis

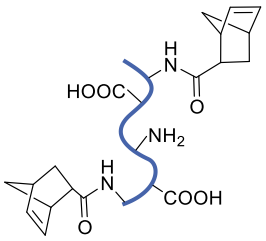

rColN

The protocol of Gockler *et al.* was adapted.[344] Briefly, 1.5 g rCol was dissolved overnight at RT in 37 ml 0.5 M MES buffer pH 6.0. Subsequently, 110.3 mg NBCA, 305.96 mg EDC*HCl, and 91.84 mg NHS were dissolved in 1 ml each of 0.5 M MES buffer, mixed, and heated to 50 °C for 15 min. The solution was cooled to RT and rCol solution was then added dropwise, followed by pH adjustment to 7.56 with 10 M NaOH. The reaction was stirred overnight (14-16 h) at RT. After seven days of dialysis against ddH_2O (cellulose tube; cut-off: 3.5 kDa), the product was lyophilized, resulting in a white, spongy material.

Table 4-12: Used quantities for the synthesis of GelN and rColN using an adapted procedure of Gockler *et al.*[344] Used molar masses are highlighted in green.

Compounds	**Approach 1: Gelatin**	**Approach 2: rCol**
Gelatine: m (g) / $n_{(molecule)}$ (mmol) / n_{NH2} (mmol)	1 / - / **0.27**	-
rCol: m (g) / $n_{(molecules)}$ (mmol) / n_{NH2} (mmol)	-	1 / 0.044 / **1.007**
NCA: m (mg) / $n_{(molecules)}$ (mmol)	73.5 / 0.53	73.5 / 0.53
EDC*HCl: m (mg) / $n_{(molecules)}$ (mmol)	204.0 / 1.06	204.0 / 1.06
NHS: m (mg) / $n_{(molecules)}$ (mmol)	61.3 / 0.53	61.3 / 0.53
Molar ratio of NH_2: NCA : EDC*HCl : NHS	**1:2:4:2**	**1:0.5:1.1:0.5**

4.2.4.1.2 rColN synthesis

All subsequent steps were performed as sterile as possible. A clear solution of 40 mg/ml rCol (Evonik Operations GmbH) in 0.1 M HEPES buffer pH 8.0 was prepared overnight at RT on an orbital shaker (450 rpm). Different amounts of 5-norbornene-2-NHS ester (NCA-NHS; BroadPharm; BP-24407) were added to clean and sealable glass vials, followed by rCol solution. The covered reaction was stirred for up to 48 h at RT. Initial flocculation disappeared within the reaction time and visualized the progress of the reaction. The solution was diluted 1:2 with reaction buffer followed by dialysis (cellulose tubing; cut-off: 3.5 kDa) for 1 d against alkaline ddH_2O (pH ~ 8.0). Water was changed regularly (every 1-2 h; at least 3× per day). The purified product was lyophilized to produce a white sponge-like material, which was

stored at 4 °C for further use. Optionally, the product can be sterile filtered (0.2 µm pore size) prior to lyophilization to ensure material sterility.

^{1}H-NMR (400 MHz, D_2O, 315 K): *δ*/ppm = 7.13-6.75 (*4H*$_{aromat}$, Collagen (*Tyr*)), 6.44-6.11 (2H, Norbornene (sp^2-C-*H*)), 2.99 (t, 2H, ε-CH_2 (Lys)).

Table 4-13: Calculation table for the synthesis of rColN.

material	equiv.	m (mg)	M (g/mol)	n (mmol)	n (reac. side chains, mmol)
rCol	1	1000	22844	0.044	1.007
NCA-NHS	0.1	23.68	235.24	0.101	0.101
	0.25	59.21	235.24	0.252	0.252
	0.5	118.42	235.24	0.503	0.503
	0.75	177.63	235.24	0.755	0.755
	1	236.85	235.24	1.007	1.007
	1.5	355.28	235.24	1.511	1.511
	2	473.70	235.24	2.014	2.014

4.2.4.2 Synthesis of recombinant thiol-modified collagen (rColS)

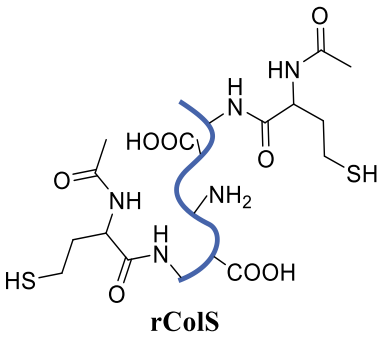

rColS

A 40 mg/ml rCol solution in 0.1 M carbonate buffer (pH 10) was mixed with 1 mM EDTA (to avoid thiol oxidation by metal ions[391]) and transferred into a 2-neck flask. The solution was degassed and flushed with N_2 (3x each; 1-3 min/step). 1.0 M (160.3 mg/ml) DL-*N*-acetyl homocysteine thiolactone (short: AcHCT; Sigma & Aldrich; Cat. No.: A16602-25G) was dissolved in degassed 0.1 M carbonate buffer (pH 10) and added *via* syringe and septum at the indicated volumes in Table 4-14. After stirring for 3 h at RT, the reaction mixture was dialyzed for 24 h at RT against degassed ddH_2O (cut-off: 3.5 kDa). The water was replaced four times with new degassed water. 1 mM EDTA was added to the first two washings. The purified product was lyophilized to produce a white sponge-like material, which was stored under N_2 at -80 °C for further use.

^{1}H-NMR (400 MHz, D_2O, 315 K): *δ*/ppm = 7.13-6.75 (*4H*$_{aromat}$, Collagen (*Tyr*)), 2.99 (t, 2H, ε-CH_2 (Lys)), 2.02 (s, 3H, CO-CH_3).

Table 4-14: rColS synthesis calculation table. A 160.3 mg/ml AcHCT stock solution in carbonate buffer was used.

material	equiv.	m (mg)	M (g/mol)	n (mmol)	n (reac. side chains, mmol)	V (AcHCT stock, µl)
rCol	1	1000	22844	0.04	1.01	-
AcHCT	0.25	40.07	159.21	0.25	-	250
	0.5	80.15	159.21	0.50	-	500
	1	160.30	159.21	1.01	-	1000
	2	320.59	159.21	2.01	-	2000
	5	801.49	159.21	5.03	-	5000

4.2.4.3 Synthesis of rCol hydrogels with DMTMM

A 100 mg/ml rCol stock solution was pre-dissolved in ddH_2O overnight at RT on an orbital shaker. 196.25 mg/ml crosslinker (0.71 M; TCI Chemicals) was freshly prepared in ddH_2O (this takes up to 5 min, RT). The molecular ratio of collagen to crosslinker was based on the reactive side chains in both components. The recombinant collagen contains 36 acidic side chains (19 Asp and 16°Glu + 1 terminal carboxyl group), while the DMTMM activation reagent contains one functional group per molecule.

Table 4-15: Pipetting scheme for rCol and DMTMM (1500 µl volume each).

Final concentrations (mg/ml)			Stock concentrations (mg/ml)		Volumes of stock solutions (µl)		
MR	**rCol**	**DMTMM**	**rCol**	**DMTMM**	**rCol**	**DMTMM**	**ddH_2O**
0.1	**10**	0.436	100	196.25	150	3.3	1347
0.5	**10**	2.18	100	196.25	150	16.7	1333
1	**10**	4.36	100	196.25	150	33.3	1317
3	**10**	13.08	100	196.25	150	100	1250
0.1	**20**	0.872	100	196.25	300	6.7	1193
0.5	**20**	4.36	100	196.25	300	33.3	1167
1	**20**	8.72	100	196.25	300	66.6	1133
3	**20**	26.17	100	196.25	300	200	1000
0.1	**30**	1.308	100	196.25	450	10.0	1040
0.5	**30**	6.54	100	196.25	450	50.0	1000
1	**30**	13.08	100	196.25	450	100	950
3	**30**	39.25	100	196.25	450	300	750
0.1	**40**	1.744	100	196.25	600	13.3	887
0.5	**40**	8.72	100	196.25	600	66.6	833
1	**40**	17.44	100	196.25	600	133	767
3	**40**	39.25	100	196.25	600	300	600

0.1	**50**	2.18	100	196.25	750	16.7	733
0.5	**50**	10.9	100	196.25	750	83.3	667
1	**50**	21.8	100	196.25	750	167	583
3	**50**	65.41	100	196.25	750	500	250

4.2.4.4 Synthesis of collagen-PEG composites

100 mg/ml rCol was pre-dissolved in ddH_2O overnight at RT on an orbital shaker. 201.37 mg/ml crosslinker (0.02 M; 4-arm PEG-SG 10 kDa, Jenkem Technology) was freshly prepared in ddH_2O (this takes up to 5 min, RT). The molecular ratio of collagen to crosslinker was based on the reactive side chains in both components. The recombinant collagen contains 23 primary amines (22 lysine + 1 terminal NH_2), while the 4-arm PEG-SG linker contains four functional groups per molecule. This results in a molar ratio of 23:4. The components were added in the following order: ddH_2O, 0.1 M HEPES buffer pH 8.0 (1:10 dilution from 1 M stock solution), rCol stock solution and the crosslinker stock solution. The mixture was homogenized and transferred into the appropriate mold. Gelation takes place within seconds to hours (depending on the formulation). To avoid dehydration, gelation was performed in a humid atmosphere. In some cases, 4-arm PEG-SG linkers with an aberrated molecular weight were used (2 kDa, 20 kDa, 40 kDa).

Table 4-16: Pipetting scheme for rCol and 4-Arm-PEG-SG, **10 kDa** linker from Jenkem Technologies. (1000 µl Formulation volume each).

Final concentrations (mg/ml)			**Stock concentrations (mg/ml)**		**Volumes of stock solutions (µl)**			
MR	**rCol**	**PEG-SG**	**rCol**	**PEG-SG**	**rCol**	**PEG-SG**	**Buffer**	**ddH_2O**
0.2	5	2.517	100	201.37	50	12.5	100	838
0.4	5	5.034	100	201.37	50	25	100	825
0.8	5	10.07	100	201.37	50	50	100	800
1.6	5	20.14	100	201.37	50	100	100	750
0.2	10	5.034	100	201.37	100	25	100	775
0.4	10	10.07	100	201.37	100	50	100	750
0.8	10	20.14	100	201.37	100	100	100	700
1.6	10	40.27	100	201.37	100	200	100	600
0.2	20	10.07	100	201.37	200	50	100	650
0.4	20	20.14	100	201.37	200	100	100	600
0.8	20	40.27	100	201.37	200	200	100	500
1.6	20	80.55	100	201.37	200	400	100	300
0.2	40	20.14	100	201.37	400	100	100	400
0.4	40	40.27	100	201.37	400	200	100	300
0.8	40	80.55	100	201.37	400	400	100	100

Table 4-17: Pipetting scheme for rCol and 4-Arm-PEG-SG, 5 ka, **20 kDa and 40 kDa** linker from Jenkem Technologies (1000 µl Formulation volume each).

Final concentrations (mg/ml)						Volumes of stock solutions (µl)						
MR	rCol	PEG-SG				rCol	PEG-SG				1 M buffer	ddH₂O
		5	10	20	40		5	10	20	40		
0.2	5	1.26	2.52	5.04	10.1	50	6.25	12.5	25	50	100	Rest
0.4	5	2.52	5.03	10.1	20.1	50	12.5	25	50	100	100	Rest
0.8	5	5.05	10.1	20.2	40.4	50	25	50	100	200	100	Rest
0.2	10	2.52	5.03	10.1	20.1	100	12.5	25	50	100	100	Rest
0.4	10	5.05	10.1	20.2	40.4	100	25	50	100	200	100	Rest
0.8	10	10.1	20.1	40.2	80.4	100	50	100	200	400	100	Rest
0.2	20	5.05	10.1	20.2	40.4	200	25	50	100	200	100	Rest
0.4	20	10.1	20.1	40.2	80.4	200	50	100	200	400	100	Rest
0.8	20	20.1	40.3	80.6	161	200	100	200	400	-	100	Rest
0.2	40	10.1	20.1	40.2	80.4	400	50	100	200	400	100	Rest
0.4	40	20.2	40.3	80.6	161	400	100	200	-	-	300	Rest

4.2.4.5 Synthesis of rColN/rColS Hydrogels

Hydrogels made of rColN and rColS will be referred to as rColNS hydrogels. If not stated otherwise in the respective chapters, the hydrogels were synthesized the following:

4.2.4.5.1 The applied light source

Depending on the final DoF and the concentrations of rColN, rColS and LAP used, different irradiation times were also required. The minimum irradiation for optical gelation was given in chapter 2.3.3.3. Depending on different applications, different lamps had to be used:

- The Omnicure S2000 unit was used for most of the experiments (broadband lamp from 365 nm – 500 nm; 5.04 W/cm²; lamp-sample distance of 5 cm). Unless otherwise noted, this lamp was used with a 15 s exposure time.
- For rheological kinetics described in chapter 2.3.4.3.3 (ElastoSens™ Bio), a built-in lamp with a specific wavelength of 405 nm and an irradiance of 11.6 mW/cm² had to be used.
- For 3D printing, a high-power UV LED spot P lamp (Opsytec Dr. Gröbel GmbH) with a maximum wavelength of 405 nm and a bandwidth of ~ 40 nm was used. The "standard" lamp emitted different irradiance intensities [W/cm²] depending on the sample distance and the distance from the lamp center. An excerpt from the data sheet is shown below. Due to the different print structures, the lamp distance and the lamp power were adjusted individually for each print.

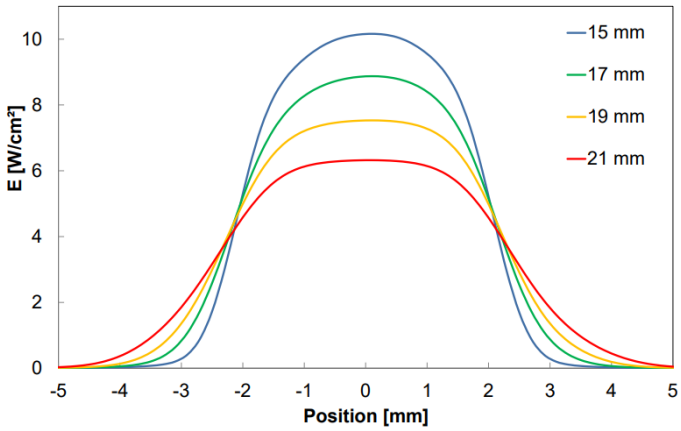

Figure 4-1: Correlation of measured E [W/cm²] and the lamp position of the standard lamp version with 100% lamp power. The figure was taken from the technical data sheet.

4.2.4.5.2 Hydrogels without cells

Stock solutions of 50 mg/ml rColN, 50 mg/ml rColS and 30 mg/ml LAP (use brown or black light protected vessel) were prepared in 1×PBS until a clear solution was obtained. 1×PBS, $rColN_{(aq)}$, $rColS_{(aq)}$ and $LAP_{(aq)}$ were mixed in a suitable vessel and exposed to light with the Omnicure S2000 standard settings if not stated otherwise. The preparation of hydrogels with cells was described in chapter 4.2.3.7.

Table 4-18: Example formulations for rColNS without cells for 1000 µl each with 0.3 mg/ml LAP as final concentration diluted from a 30 mg/ml stock solution. rColN and rColS were applied as a 50 mg/ml stock solution in 1×PBS.

Fin. rCol concentration (mg/ml)	Fin. concentrations (mg/ml)			Volumes of stock solutions (µl)				
	rColN	rColS	LAP	rColN	rColS	LAP	1×PBS	Sum
5	2.5	2.5	0.3	50	50	10	890	1000
10	5.0	5.0	0.3	100	100	10	790	1000
20	10	10	0.3	200	200	10	590	1000
30	15	15	0.3	300	300	10	390	1000
40	20	20	0.3	400	400	10	190	1000
5	2.5	2.5	1.0	50	50	33	867	1000
10	5.0	5.0	1.0	100	100	33	767	1000
20	10	10	1.0	200	200	33	567	1000
30	15	15	1.0	300	300	33	367	1000
40	20	20	1.0	400	400	33	167	1000

4.2.4.6 Synthesis of rColN/4-Arm-PEG-SH composites

rColN and 4-Arm-PEG-SH (10 kDa) were dissolved with 50 mg/ml in 1×PBS until a clear solution formed. 30 mg/ml LAP was dissolved in 1×PBS for at least 2 h prior to the experiment. 1×PBS, $rColN_{(aq)}$, $4\text{-Arm-PEG-SH}_{(aq)}$, $LAP_{(aq)}$ (and cells) were mixed in a suitable vessel and exposed to light of a wavelength of 365-405 nm using the Omnicure S2000 system with standard settings. If not stated otherwise 200 µl sample was used per well in an eight well chamber slide (ibidi). Cells were resuspended in full culture medium and used with $5x10^5$ cells/ml as final concentration. After curing the sample was topped by 200 µl full culture medium and subsequent cultivation under culture conditions. The medium was exchanged every 2-3 days. For curing, the Omnicure S2000 system was used. If not stated otherwise, the standard settings were applied as described in chapter 4.2.4.5.1. An example pipetting scheme was given in Table 4-19.

Table 4-19: Example formulations for rColN and 4-Arm-PEG-SH (abbreviated with PEG-SH) without cells for 2200 µl each. 50 mg/ml rColN and 50 mg/ml PEG-SH stock solutions in 1×PBS were applied. The PI (LAP) was used with a stock concentration of 30 mg/ml in 1×PBS. Cells were prepared with $1x10^7$ cells/ml and homogenized before adding.

Final conc.				Volumes to add					
rColN	**PEG-SH**	**LAP**	**HFF**	**rColN**	**PEG-SH**	**LAP**	**1×PBS**	**Cells**	**Sum**
	mg/ml		**cells/ml**			**µl**			
5	1.8	0.3	$5x10^5$	220	79	22	1769	110	2200
10	2.5	0.3	$5x10^5$	440	110	22	1518	110	2200
10	3.5	0.3	$5x10^5$	440	154	22	1474	110	2200
20	2.5	0.3	$5x10^5$	880	110	22	1078	110	2200
20	4.5	0.3	$5x10^5$	880	198	22	990	110	2200
20	7.0	0.3	$5x10^5$	880	308	22	880	110	2200

4.2.4.7 Gelation of rat tail collagen

Lyophilized rat tail collagen (Sigma, C7661) was reconstituted in 0.1% CH_3COOH to a stock solution of 6 mg/ml. During dissolution, the solution was kept at 4 °C. For the hydrogel formation, all stock solutions were preincubated on ice for at least 15 min. Physically crosslinked rtCol was prepared by combining the following ingredients on ice: 10×PBS, rtCol stock solution, ddH_2O and 1 M NaOH. The final formulation contained 1×PBS and a pH of 7.2-7.4. The mixture was homogenized thoroughly by pipetting followed by brief centrifugation to remove bubbles. Reverse pipetting was used with special pipetting tips into the final vessel and the sample was incubated at 37 °C under humid conditions for 1 h to allow physical gelation. For chemical crosslinking, the sample preparation was identically to the physical

gelation but after temperature incubation, a crosslinker solution was added on top with identical volume to the underlaying hydrogel with 2x the final crosslinker concentration in 0.1 M HEPES buffer pH 8.0. The crosslinking solution remained 2 h on top at RT under humid conditions. Then, the residual supernatant was discarded, and the hydrogel was washed 3x with 1×PBS buffer. The chemical crosslinker wasn't directly added to the solution due to the rapid gelation speed which increased the already high viscosity too fast, to deposit the material.

4.2.4.8 Sponge preparation by freeze drying

Hydrogel based sponges can be made from hydrogels *via* freeze drying. Prepared hydrogels were processed with a freeze dryer (Epsilon, Martin Christ Gefriertrocknungsanlagen GmbH) according to the depicted procedure in Figure 4-2.

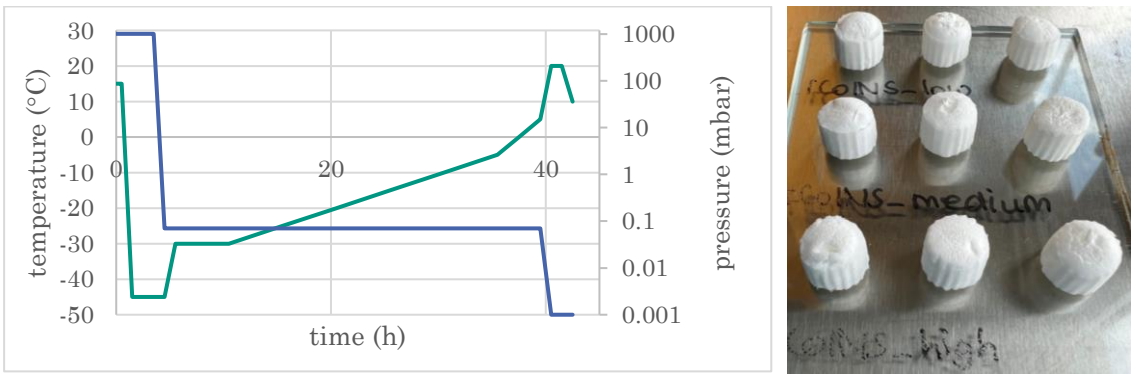

Figure 4-2: (left) rCol freeze drying protocol regarding pressure and temperature over time containing a loading phase (0 h – 0.5 h), a freezing phase (0.5 h – 4.5 h), a main drying phase (4.5 h – 40.5 h) and a final drying phase (40.5 h – 42.5 h). (right) Example rColNS sponges after freeze drying using rColNS_low; _medium and _high. In each row, final collagen concentrations of 5, 10 and 20 mg/ml were used from left to right.

4.2.4.9 Patch preparation

DMTMM crosslinked hydrogel sponge patches were prepared as described in the following with or without the addition of APIs with and without the prior encapsulation in microparticles. If not stated otherwise, 2 mm thick hydrogel layers were prepared with a standard formulation of 10 mg/ml rCol and a MR of DMTMM of 1:1. Flat silicon molds with rim were filled with a freshly prepared hydrogel solution according to chapter 4.2.4.3. Enough volume was used to achieve a layer thickness of 2 mm. Prior to adding the solution to the mold, APIs were spiked as solution into the water fraction of the formulation or alternatively a

microparticle suspension. Furthermore, when microparticles were applied, the formed suspension was incubated until first viscosity increases were visually observed prior to molding. Alternatively, fully closed molds containing the suspension were constantly rotated until gelation occurred to ensure a homogenous particle distribution. After gelation under humid conditions, formed hydrogels were freeze-dried according to chapter 4.2.4.7.

4.2.4.10 3D (bio)printing

If not stated otherwise, the following settings were applied with the Regenate printer from Black Drop GmbH. The biopolymer solution was filled into one of the printer heads. During printing, the printing platform was cooled 4-15 °C for hydrogel printing and kept at RT for hybrid extrusion printing with filament. For each biopolymer solution, the printer head was heated or cooled accordingly (rColNS 4 °C-RT). For droplet generation a chamber pressure of 0.2-0.3 bar was used on the printer heads with a valve opening time of 450 µs. The droplet to surface distance was kept around 1 cm. Printing files were either provided by Blackdrop or self-made using an Autodesk 3D crafting software. The file was sliced accordingly to the printer company's instructions with the companies owned slicer software.

4.2.5 Analytics

4.2.5.1 TNBSA-Assay

2,4,6-Trinitrobenzene Sulfonic Acid (TNBSA) can be used to quantify primary amines by the formation of a chromogenic derivative with an absorption maximum at 335 nm. Primary amines are present in lysine side chains as well as in the *N*-terminus of the used rCol. During the synthesis of rColN and rColS, lysine side chains are modified. By comparing the primary amines of modified and unmodified rCol, the degree of functionalization (DoF) can be quantified.

4.2.5.1.1 Liquid rCol and its derivatives

The TNBSA assay was performed according to the manufacturer's protocol from Promega. Briefly, 500 µl of sample (200 µg/ml) was dissolved in reaction buffer (0.1 M sodium bicarbonate (Na_2CO_3/$NaHCO_3$) pH 8.5) and mixed with 250 µl of freshly diluted TNBSA solution (0.01% (v/v)). The TNBSA working solution was prepared from an aqueous 5% TNBSA stock solution diluted with reaction buffer. The reaction mixture was incubated at 37 °C for 2 h in the dark. The reaction was then quenched with 125 µl of 1 M HCl followed by 250 µl of sodium dodecyl sulfate solution (SDS, 10% w/v). Unmodified rCol was used as a reference. For each sample, a blank was prepared by directly quenching 500 µl sample with 125 µl 1 M HCl

followed by 250 µl TNBSA solution (0.01% (v/v)) and then incubating at 37 °C for 2 h in the dark. Then 250 µl SDS solution (10% (w/v)) was added to all samples and the absorbance was measured in transparent UV/VIS 96-well plates with 250 µl sample volume per well followed by absorbance detection at 335 nm using a TecanReader Pro200. A glycine dilution series (2-12 µg/ml) was recorded for evaluation. For the unmodified proteins, a sample concentration of 20-200 µg/ml is recommended. If needed, the sample was diluted for a signal intensity between 0.1 and 1.0.

Table 4-20: Pipetting scheme for TNBSA Assay.

Sample	Blank
500 µl sample dissolved in buffer **250 µl** TNBSA solution (0.01% (v/v))	**500 µl** sample dissolved in buffer **125 µl** 1 M HCl **250 µl** TNBSA solution (0.01% (v/v))
---------- Incubation at 37 °C for 2 h in the dark ----------	
125 µl 1 M HCl **250 µl** SDS solution (10% (w/v))	**250 µl** SDS solution (10% (w/v))
---------- 250 µl / well in 96 well plate and absorption scan at 335 nm ----------	

4.2.5.2 Ninhydrin-Assay

To determine the degree of crosslinking within DMTMM and PEG-SG induced hydrogels, a ninhydrin staining of the final hydrogels can be performed. 100 µl fully gelated hydrogel sample within a 2 ml reaction tube was covered by 170 µl DMSO and 30 µl 1% (w/v) Ninhydrin in DMSO. The mixture was incubated within a water bath for 2 h at 80 °C. Then 100 µl was removed and analyzed within a 96 well plate by using an Absorption wavelength of 590 nm. If needed, the sample was diluted for a signal intensity between 0.1 and 1.0. The wavelength was chosen due to an absorption scan with one sample. 100 µl DMSO was used as blank.

4.2.5.3 Ellman's Assay

4.2.5.3.1 Liquid collagen

The Ellman's assay was used to determine the conjugated free thiol moieties in thiolated collagen (rColS). The assay was performed according to a literature protocol (Thermo Fisher Scientific Inc.). A stock solution of 0.5% (w/v) lyophilized rColS or rCol in reaction buffer (0.1 M sodium phosphate, pH 8.0, containing 1 mM EDTA) was prepared. 125 µl collagen stock solution was mixed with 1250 µl reaction buffer and 25 µl freshly prepared 0.4% (w/v) Ellman reagent solution and incubated for 15 min at RT. Buffer was used as blank. After

incubation, 200 µl was transferred into a 96-well plate and the absorbance was measured at 412 nm. For data extraction, the average blank was subtracted from all data and the resulting values were plotted. For calibration purposes, a cysteine calibration curve was recorded according to the manufacturer protocol showing a linear curve behavior between 0-1.5 mM L-Cysteine. If needed, the sample was diluted for a signal intensity between 0.1 and 1.0.

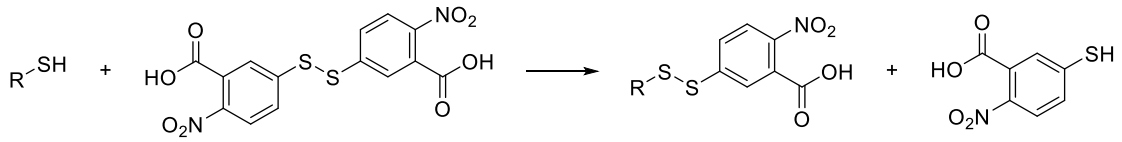

Scheme 4-1: Reaction scheme for the Ellman's assay. A thiol containing test substance (X) reacts with 5,5′-Disulfanediylbis (2-nitrobenzoic acid) (X) by cleaving the reagents thiol group and forming 2-nitro-5-thiobenzoate (TNB−). The basic reaction buffer reduces TNB− to TNB^{2-} which has a yellow color.

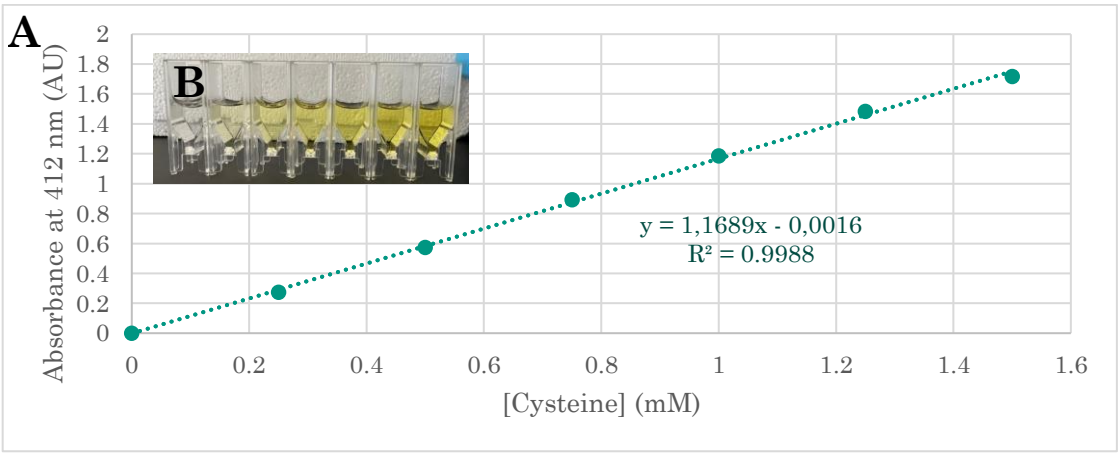

Figure 4-3: (A) Ellman's assay calibration curve with L-Cysteine. **(B)** Color change of the different tested samples (f.l.t.r) reaction buffer, 0.25 mM, 0.5 mM, 0.75 mM, 1 mM, 1.25 mM and 1.5 mM.

4.2.5.3.2 Determination of free thiols after photopolymerization

Ellman's assay was also used to quantify the amount of free thiol groups in photopolymerized rColNS hydrogels by keeping the same concentration of rColS and changing the concentration of rColN. Hydrogels were prepared in 1×PBS with 100 µl sample volume/well in a 96-well plate with N = 3. Outer wells were filled with 200 µl of 1× PBS to ensure a moist environment. After irradiation (Omnicure S2000, 15 sec. 5.04 W/cm², 320-500 nm, 5 cm sample/lamp distance), samples were covered with 200 µl of 0.01% Ellman reagent (0.1 M sodium phosphate, pH 8.0, containing 1 mM EDTA). Hydrogels were incubated for 2-4 h at RT in the dark and optical absorbance was measured at 412 nm. rColS in 1×PBS was used as a positive

control identical to the rColS concentration in the hydrogel formulation (1/2 of the total collagen concentration). To keep within the linear range of the assay the applied rColS concentration was reduced. For a concentration range of 2.5 – 10 mg/ml, applied rColS concentrations were 0.625-2.5 mg/ml. Results were multiplied with the dilution factor. 100 µl 1×PBS was used as a background control. The average background signal was subtracted from all signals followed by signal normalization to the positive control to calculate free thiol groups in %.

Table 4-21: Calculation table for MR calculations of rColN_medium (Mw = 24330 g/mol; 53% DoF) and rColS_medium (Mw = 24,638 g/mol; 49% DoF). 5 mg rColS_medium contains 0.2 mmol rColS and 2.3 mmol thiol groups. rColN_medium contains 12.2 norbornene moieties per molecule.

Sample	m (rColS)	n (thiol)	n (Nor)	n (rColN)	m (rColN)	Signal
1:0	5.00 mg	2.29 mmol	0.00 mmol	0.000 mmol	0 mg	100%
1:0.1	5.00 mg	2.29 mmol	0.23 mmol	0.019 mmol	0.46 mg	90%
1:0.25	5.00 mg	2.29 mmol	0.58 mmol	0.047 mmol	1.15 mg	72%
1:0.5	5.00 mg	2.29 mmol	1.15 mmol	0.094 mmol	2.29 mg	46%
1:0.75	5.00 mg	2.29 mmol	1.72 mmol	0.141 mmol	3.44 mg	27%
1:1	5.00 mg	2.29 mmol	2.29 mmol	0.188 mmol	4.58 mg	15%
1:2	5.00 mg	2.29 mmol	4.58 mmol	0.376 mmol	9.15 mg	0%

4.2.5.4 Protein quantification assay

4.2.5.4.1 Bradford Protein Assay

Marion Bradford's 1976 paper on the Bradford protein assay, which is a very common and widely-used laboratory method for quantifying proteins in solutions, is one of the most cited papers in history and was used for this method description.[392] The Bradford protein assay is based on the absorbance shift of Coomassie Brilliant Blue G-250 (465 nm to 595 nm) when binding to protein occurs. This is due to hydrophobic and ionic interactions that stabilize the anionic form of the dye, causing a visible color change. Variability of the response of the assay to different proteins due to the dye's specificity is the main disadvantage, so it is recommended to use a protein standard that is likely to give absorbance values close to those of the protein samples of interest. The assay is more accurate for neutral proteins and can be affected by high concentrations of detergents. For this thesis, a ready-to-use Coomassie Brilliant Blue G-250 working solution from AppliChem GmbH (article number: A6932,0500) was applied. The assay was performed in a 96 well MTP plate format using transparent plates. Every sample was prepared in triplicate. A 2 mg/ml protein stock solution was prepared in ddH_2O and diluted to 100 µg/ml using ddH_2O. 0, 2, 4, 6, 10, 15 and 20 µl protein stock solution

was added per well and filled up to 20 µl total volume with ddH_2O. 200 µl Bradford reagent was added on top per well. After incubation for 30 min at RT the absorbance was measured at 595 nm and received data were blotted against the applied protein concentration. The standard deviation was depictured as well as a linear curve fit to identify the linear range of the test substance. If needed, the sample was diluted further in ddH_2O for a signal intensity between 0.1 and 1.0.

4.2.5.4.2 BCA Protein Assay

The assay protocol was taken from the Pierce™ BCA Protein Assay Kit (Thermo Scientific™; catalog number: 23227). The bicinchoninic acid assay (BCA assay) has a resolution of (20–2000 µg/ml and is similar to the Lowry protein assay, the Bradford assay and the biuret reaction. It is based on an alkaline solution containing BCA, Na_2CO_3, $NaHCO_3$, $Na_2C_4H_4O_6$ (sodium tartrate) and $CuSO_4 \times 5\ H_2O$ (copper (II) sulfate pentahydrate). Peptide bonds within the protein reduce Cu^{2+} to Cu^{+} (temperature dependent, endotherm). Then, two molecules of bicinchoninic acid chelate with Cu^{+} ion each by forming a purple-colored complex whose absorbance can be measured at 562 nm. An advantage of the assay is the high tolerance towards additional compounds within the reaction mixture like urea and guanidinium chloride.[393] The assay was performed in the 96 well MTP format. 20 mg/ml rCol stock solution was prepared in ddH_2O and diluted with ddH_2O to the following concentrations: 1500, 1000, 750, 500, 250, 125 and 25 µg/ml. ddH_2O was used as reference. Next the working reagent (WR) was prepared (50:1; Regent A:B). After mixing, a cloudiness may be observed which quickly disappears due to homogenization during mixing. A color change to a clear green solution is observed. The solution can be stored at RT in the dark for several days. Each sample was tested in triplicate. 25 µl (diluted) sample was added per well (96-well plate) followed by 200 µl working solution. The plate was vortexed on an orbital shaker at 300 rpm at RT for 30 seconds. The plate was covered and incubated at 37 °C for 30 minutes in the dark. The plate was cooled to RT for 5 minutes and the absorbance was then measured at 562 nm using a Tecan Pro200 plate reader. The average background signal (blank: ddH_2O + WR) was subtracted from all test samples. The sample average was plotted with standard deviation against the applied sample concentration.

4.2.5.5 ^{1}H Nuclear Magnetic Resonance (NMR)

The degree of functionalization was quantified using ^{1}H-NMR spectra from a 400 MHz spectrometer (Bruker Avance III HD 400 MHz NMR Spectrometer). Before the measurement, 50 mg of the sample was dissolved in 1 ml deuterium oxide at 30 °C.

4.2.5.6 Circular dichroism + CD melting curves

Collagenous samples were dissolved in 50 mM sodium phosphate buffer pH 7.2 to a concentration of 10 g/kg and dissolved in a thermomixer for one hour at 20 °C. Samples were diluted by a factor of 100 to a final concentration of 0.1 g/kg in the same buffer. CD measurements were performed on a Jasco J-810 CD Spectropolarimeter using a 2 mm quartz cuvette and a volume of 400 µl at 20 °C if not indicated else. All CD spectra were baseline corrected against the same buffer. Spectra were taken from 260 to 190 nm using a bandwidth of 1 nm and scanning speed of 50 nm/min with 5 accumulations each. CD spectra were smoothed using a Savitski-Golay filter with a window of 5 points (5nm) and normalized to UV absorption signal at 215 nm. Melting curves were recorded from 25 °C to 40 °C at 200 nm with a heating speed of 1 °C per 10 min. and a bandwidth of 1 nm.

4.2.5.7 API release from rCol patches

Release experiments were performed either with the API added to the liquid formulation (as with caffeine) or after the API was encapsulated in PLGA microparticles and added to the still-liquid formulation. In the case of lyophilization, the resulting patches are no longer transparent, making it difficult to observe the particles within the patch. Therefore, the hydrogels were semi-dried in a heat cabinet at 40 °C for 20 hours. After drying, the patches were immersed in 1× PBS and incubated in a 37 °C warm water bath on an orbital shaker (85 rpm) in 50 ml Greiner tubes. The volume of the extraction medium was chosen in accordance with the solubility limit of the encapsulated drug in 1×PBS and the loading density of the patch/particles to ensure complete theoretical solubility and to avoid any drawback effects due to solubility limitations. After various time points, 1 ml samples were taken from the supernatant. The reduced volume was replaced with 1 ml fresh 1×PBS and the sample was analyzed using a Tecan multiplate reader with an absorbance wavelength of 365 nm for meloxicam and 275 nm for caffeine. Quantification was performed using calibration curves in 1×PBS and the initial caffeine applied was normalized to the recalculated measured signal. In the case of PLGA particles, when no further signal increase was reported, the 1×PBS buffer was completely removed and replaced with 5 ml DMSO to dissolve the remaining particles as well as the remaining meloxicam from the patch. After 3 and 24 hours of incubation at RT, absorbance was measured at 365 nm to ensure complete release after 3 h. The sum of released Meloxicam was normalized to 100%.

4.2.6 Mechanical characterizations

4.2.6.1 Gelation limitation & gelation time

The minimal conc. for gelation was determined *via* two different methods based on the applied crosslinker. For photopolymerizations, the droplet test was performed and for all other formulations the upside-down vial assay. Gained data provided the min. conditions for optical gelation. Although the hydrogel appeared solid, post-gelation procedures by additional curing increase the stiffness significantly within time. Therefore, it must not be mistaken with the maximum final stiffness whose determination was described in chapter 4.2.6.3.

Droplet test: 25 µl formulation droplets were dispensed onto a tesafilm® coated glass slide followed by irradiation for a varying amount of time (Omnicure S2000; broad spectrum lamp; 365 nm – 500 nm; 5.04 mW/cm²; lamp-sample distance of 5 cm; 1-60 seconds). Hydrogel formation was proven by droplet movement with a pipetting tip after irradiation. Solid hydrogels can be moved as one piece while liquid formulations could not.

Vial upside-down assay: 300 µl hydrogel formulation was filled into a 2 ml HPLC vial. The vial was sealed and turned upside down within different time points. Formed hydrogels immobilized the formulation and the needed time was documented.

4.2.6.2 SEM imaging

Collagen sponges were frozen in liquid nitrogen and cut with a blade to create a cross-section surface. Chapters were fixed with a sticky pad on a SEM sample stub. The sample surface was sputtered with gold-palladium, thereby increasing electrical conductivity. Secondary electron pictures were captured in various magnifications with a JEOL JSM-IT300 Scanning Electron Microscope (SEM, high vacuum, 10kV, SE-mode). The device uses a Tungsten cathode with a theoretical magnification range of 10× to 300,000×. A secondary electron detector (SED) was used for the measurement. Applying an image analysis software, the pore size of several cells was measured (n ≥8).

4.2.6.3 Rheology

4.2.6.3.1 Viscosity measurement

The Anton-Paar MCR 502 WESP system equipped with a plate-cone extension was used to determine the viscosity. The lower plate was flat (stainless steel, Ø 50 mm, CP50) while the cupper cone had a 1° angle (stainless steel, Ø 50 mm, CP50-1) with a truncation of 99 µm.

The stock solution was made one day in advance and left for complete dissolution on an orbital shaker at RT overnight. A sample load of 750 µl was applied. Excess sample was removed with a tissue after reaching the measurement position (0.099 mm measurement gap). The shear rate was measured at constant 20 °C with 21 data points between 0.01 and 10^4 1/s as logarithmic ramp. The shear rate for different solutions was adapted depending on the viscosity. For highly viscous solutions, a lower shear rate was needed than for low viscous solutions. Each sample was measured in triplicate and the average within the linear range of three measurements was calculated as well as the standard deviation.

4.2.6.3.2 Online shear modulus measurement

After optical gelation, further stiffening occurs within the hydrogel due to ongoing crosslinking. Using an endpoint measurement, the required time for complete gelation is time consuming to determine. Here the Anton-Paar MCR 502 WESP system equipped with a plate-plate extension could have been applied. Instead, the ElastoSens™ Bio device from Rheolution Live Sciences was used. The non-destructive non-contact measurement relies on induced vibration of the sample holder silicon bottom whose amplitude is recoded by a laser. The stiffer the formulation, the lesser the response in amplitude. For photopolymerization, hydrogel formulation with 2.2 ml were prepared. 2 ml was transferred into the calibrated sample holder using reverse pipetting. The sample was irradiated with 405 nm (50% lamp power; equals a light power of 11.6 mW/cm² according to the providers light power chart) until a stable Shear Storage Modulus (G'). The stiffness was measured every 10 seconds. The hydrogel height was recorded by the device ensuring no significant decrease. If not stated otherwise, the reaction temperature was kept constant at 25 °C. If the recorded Shear Storage modulus (G') was below 500 Pa using the standard stiff mode, the measurement was repeated with 7 ml of the same formulation according to the user manual in soft mode. For crosslinker induced gelation, a hydrogel volume of 5.5 ml was prepared, and 2-5 ml was transferred into the calibrated sample holder using reverse pipetting. Data was recorded until a stable Shear Storage Modulus (G') was measured. Due to longer gelation times, compared with photopolymerization, the liquid formulation was covered with a special occlusive oil shipped with the machine to avoid water evaporation. The hydrogel height was recorded by the device ensuring the oil's function. If not stated otherwise, the reaction temperature was kept constant at 25 °C. If the recorded Shear Storage modulus (G') was below 500 Pa using the standard stiff mode, the measurement was repeated with 7 ml of the same formulation according to the user manual in soft mode. For rtColMA 2 ml samples were applied and exposed to an increasing temperature ramp from 20 to 37 °C with 1 °C/min, followed by incubation at 37 °C for 5 min. Photopolymerization followed as described above with 405 nm (50% lamp power; equals a light power of 11.6 mW/cm² according to the providers light power chart) until a

stable Shear Storage Modulus (G'). For the disulfide bond formation of rColS, solutions of 50, 100 or 150 mg/ml rColS with different DoF were dissolved in 1x PBS or carbonate buffer pH 10 and dissolved completely. For some formulations additional heat treatment was required to achieve a clear and transparent solution. 2 ml solution was filled into a sample holder which was topped with anti-evaporation oil from the supplier. The sample was cooled to 10 °C and measured over time. The increase in storage modulus was recorded until a stable plateau phase was reached. Then, the temperature was slowly increased in 10 min steps with an increment of 5 °C each until 40 °C was reached. Once the storage modulus didn't decrease further, the sample was incubated at 4 °C once more until no increase in stiffness was measured. The process of heating and cooling was repeated several times. Data extraction was done by documenting the storage modulus (G') and the time once the plateau phase was reached. Both values originate from the same data point.

4.2.6.4 Porosity (ϕ)

For this thesis, two different kinds of porosity were determined: open porosity and total porosity. To determine both methods, the ethanol replacement method was used. First, the volume of the test specimen (collagen sponge) was determined. Here cylindric samples were used and the volume was determined by formula 4-2.

$$\boldsymbol{V\ (cylinder) = \pi * r^2 * h} \qquad \textbf{4-2}$$

Next, the dry weight of the samples was measured and submerged in sufficient volume of pure ethanol to cover the sample specimen completely. Here 5 ml EtOH were used. Samples were incubated in sealed tubes to avoid solvent evaporation and all weighing steps were proceed as fast as possible out of the same reason.

The following formula were applied:

$$\boldsymbol{total\ porosity\ \phi}\ [\%] = \frac{\boldsymbol{EtOH_{added} - EtOH_{remaining}}}{\boldsymbol{Sponge_{dry} + EtOH_{added} - EtOH_{remaining}}} * \mathbf{100} \qquad \textbf{4-3}$$

$$\boldsymbol{open\ porosity\ \phi}\ [\%] = \frac{\boldsymbol{Sponge_{wet} - Sponge_{dry}}}{\boldsymbol{V_{Sponge} * \rho_{EtOH}}} = \frac{\boldsymbol{Sponge_{wet} - Sponge_{dry} * \rho_{sponge}}}{\boldsymbol{m_{Sponge} * 0.789\ g/cm^3}} \qquad \textbf{4-4}$$

4.2.6.5 Hydrogel swelling

Hydrogels are mainly made of water. Complete drying results in sponge-like structures that can increase their weight multifold by swelling in an aqueous environment. This property can be useful for drug loading or other biologically active compounds. Various methods for hydrogel swelling are described in the literature. Here, a method according to Alonso et. al. was applied. Fully gelated hydrogels were freeze-dried, and their initial dry weight (w_{dry} (t=0)) was measured using an analytical balance with high sensitivity (at least 10−3 – 10−4 g) followed by submerging in 37 °C warm 1×PBS at for up to 72 h. At various time intervals, the swollen hydrogels were removed from the soaking solution, excess surface water was removed with a filter paper and the wet weight (w_{wet} (t = x)) at different time points was determined. The swelling ratio was calculated using equation 4-5 and plotted against the time. A curve area with no incline represents the respective equilibrium state. Sample triplicates were used.[394]

$$\textbf{\textit{Swelling ratio}}\ (\%) = \frac{\boldsymbol{W_{wet\ (t=x)} - W_{dry\ (t\,=\,0)}}}{\boldsymbol{W_{dry\ (t\,=\,0)}}} * \mathbf{100} \qquad \textbf{4-5}$$

4.2.6.6 Degradation

4.2.6.6.1 Hydrolysis

In alignment with ASTM International (F1635 − 16), the degradation via hydrolysis under physiological conditions was determined by weight loss. After preparing cylindric hydrogel sponges according to previously described methods (750 µl, 6.3 mm radius, 6 mm height), their initial dry weight (w_{dry} (t = 0)) was determined by using a high precision balance (precision of 0.1% of the total sample mass). Samples were fully immersed in 1×PBS (pH of 7.4 ± 0.2) containing 30 µg/ml gentamycin with a solution-to-sample mass ratio of >30:1. The samples were incubated at 37 °C ± 1 °C. The degradation solution was refreshed every 2-3 d. After 1, 7, 14 and 21 days, the hydrogel samples were gently rinsed in ddH_2O to remove superficial phosphate salts followed by freeze drying. Subsequently, the remaining dry weight (w_{dry} (t = x)) was measured and correlated with the respective w_0 by using equation 4-6. Each sample represented an endpoint measurement.

$$\textbf{\textit{Remaining mass}}\ (\%) = \mathbf{100} - \left(\frac{\boldsymbol{W_{dry\ (t\,=\,0)} - W_{dry\ (t\,=\,x)}}}{\boldsymbol{W_{dry\ (t\,=\,0)}}} * \mathbf{100}\right) \qquad \textbf{4-6}$$

4.2.6.6.2 Enzymatic hydrolysis

Enzymatic degradation was determined by wet weight determination according to Li_2016 with minor modifications.[395] Instead of hydrogels, swollen hydrogel sponges were used (cylindric; 750 µl, 6.3 mm radius, 6 mm height) whose dry weight was measured followed by swelling in digestion buffer (50 mM $CaCl_2$ in 0.1 M TRIS-HCl pH 7.4) until max. hydration was reached. Max. hydration was ensured by constant weight measurements or by a previous swelling experiment. If not stated otherwise, 24 h at 37 °C were used. The wet weight (w_{wet}; t=0) was measured by removing the sample from the buffer, removing surficial excess water with a tissue prior to weighing. Then the buffer was exchanged by 2 ml fresh, pre-heated (37 °C) warm digestion buffer containing collagenase (10 U/ml Collagenase IV from *Clostridium histolyticum*). Buffer without enzyme was used as negative control. All samples were incubated at 37 °C. After different time points (0.5, 1, 2, 4, 8, 24 and 48 h) the wet weight (w_{wet}; t=x) was determined after removing excess surface water carefully with a tissue. A decrease in wet weight was plotted against the time. The degree of degradation was determined by normalizing the residual hydrogel wet weight to the initial wet weight according to the following formula. Three samples were used at every time point for the measurement to calculate means and standard deviations.

$$\boldsymbol{Remaining\ weight}\ (\%) = \frac{\boldsymbol{W_{wet\ (t=0)} - W_{wet\ (t=x)}}}{\boldsymbol{W_{wet\ (t=0)}}} * \mathbf{100} \qquad \textbf{4-7}$$

5 References

1 Kumar Gupta, G., De, S., Franco, A., Balu, A. M. & Luque, R. Sustainable Biomaterials: Current Trends, Challenges and Applications. *Molecules* **21**, E48, doi:https://doi.org/10.3390/molecules21010048 (2015).

2 Montero, F. E., Rezende, R. A., da Silva, J. V. L. & Sabino, M. A. Development of a Smart Bioink for Bioprinting Applications. *Frontiers in Mechanical Engineering* **5**, doi:https://doi.org/10.3389/fmech.2019.00056 (2019).

3 Chen, Z., Fan, D. & Shang, L. Exploring the potential of the recombinant human collagens for biomedical and clinical applications: a short review. *Biomed Mater* **16**, 012001, doi:https://doi.org/10.1088/1748-605X/aba6fa (2020).

4 Vert, M. *et al.* Terminology for biorelated polymers and applications (IUPAC Recommendations 2012). *Pure and Applied Chemistry* **84**, 377-410, doi:https://doi.org/10.1351/PAC-REC-10-12-04 (2012).

5 Choi, S. M., Chaudhry, P., Zo, S. M. & Han, S. S. in *Cutting-Edge Enabling Technologies for Regenerative Medicine* 161-210 (Springer, 2018).

6 Zimmermann, L. M. & Veith, I. *Great Ideas in the History of Surgery*. 1st edition edn, (Norman Publishers, 1993).

7 Avila Rodriguez, M. I., Rodriguez Barroso, L. G. & Sanchez, M. L. Collagen: A review on its sources and potential cosmetic applications. *J Cosmet Dermatol* **17**, 20-26, doi:https://doi.org/10.1111/jocd.12450 (2018).

8 Barnes, M. J., Knight, C. G. & Farndale, R. W. The collagen-platelet interaction. *Curr Opin Hematol* **5**, 314-320, doi:https://doi.org/10.1097/00062752-199809000-00002 (1998).

9 Wintermantel, E. & Ha, S.-W. *Medizintechnik: Life Science Engineering*. 5th edn, (2009).

10 Sood, A., Gupta, A. & Agrawal, G. Recent advances in polysaccharides based biomaterials for drug delivery and tissue engineering applications. *Carbohydrate Polymer Technologies and Applications* **2**, doi:https://doi.org/10.1016/j.carpta.2021.100067 (2021).

11 Dong, C. & Lv, Y. Application of Collagen Scaffold in Tissue Engineering: Recent Advances and New Perspectives. *Polymers (Basel)* **8**, doi:https://doi.org/10.3390/polym8020042 (2016).

12 Liu, X. *et al.* Novel Collagen Surgical Patches for Local Delivery of Multiple Drugs. *Molecular Pharmaceutics* **20**, 3403-3411, doi:https://doi.org/10.1021/acs.molpharmaceut.3c00048 (2023).

13 Terzopoulou, Z., Michopoulou, A., Palamidi, A., Koliakou, E. & Bikiaris, D. Preparation and Evaluation of Collagen-Based Patches as Curcumin Carriers. *Polymers* **12**, 2393, doi:https://doi.org/10.3390/polym12102393 (2020).

14 Tummalapalli, M., Singh, S., Sanwaria, S. & Gurave, P. M. Design and development of advanced glucose biosensors via tuned interactions between marine polysaccharides and diagnostic elements – A survey. *Sensors International* **3**, 100170, doi:https://doi.org/10.1016/j.sintl.2022.100170 (2022).

15 Lovegrove, A. *et al.* Role of polysaccharides in food, digestion, and health. *Crit Rev Food Sci Nutr* **57**, 237-253, doi:https://doi.org/10.1080/10408398.2014.939263 (2017).

16 Kular, J. K., Basu, S. & Sharma, R. I. The extracellular matrix: Structure, composition, age-related differences, tools for analysis and applications for tissue engineering. *J Tissue Eng* **5**, 2041731414557112, doi:https://doi.org/10.1177/2041731414557112 (2014).

17 Werkmeister, J. A. & Ramshaw, J. A. Recombinant protein scaffolds for tissue engineering. *Biomed Mater* **7**, 012002, doi:https://doi.org/10.1088/1748-6041/7/1/012002 (2012).

18 Kim, E. *et al.* Microbially Synthesized Repeats of Mussel Foot Protein Display Enhanced Underwater Adhesion. *ACS Applied Materials & Interfaces* **10**, 43003-43012, doi:https://doi.org/10.1021/acsami.8b14890 (2018).
19 Tomblyn, S. *et al.* Keratin hydrogel carrier system for simultaneous delivery of exogenous growth factors and muscle progenitor cells. *Journal of Biomedical Materials Research Part B: Applied Biomaterials* **104**, 864-879, doi:https://doi.org/10.1002/jbm.b.33438 (2016).
20 Gough, C. R., Rivera-Galletti, A., Cowan, D. A., Salas-de la Cruz, D. & Hu, X. Protein and Polysaccharide-Based Fiber Materials Generated from Ionic Liquids: A Review. *Molecules* **25**, doi:https://doi.org/10.3390/molecules25153362 (2020).
21 Navarro, S., Stegner, D., Nieswandt, B., Heemskerk, J. W. M. & Kuijpers, M. J. E. Temporal Roles of Platelet and Coagulation Pathways in Collagen- and Tissue Factor-Induced Thrombus Formation. *Int J Mol Sci* **23**, doi:https://doi.org/10.3390/ijms23010358 (2021).
22 Varanko, A., Saha, S. & Chilkoti, A. Recent trends in protein and peptide-based biomaterials for advanced drug delivery. *Adv Drug Deliv Rev* **156**, 133-187, doi:https://doi.org/10.1016/j.addr.2020.08.008 (2020).
23 Chu, S., Wang, A. L., Bhattacharya, A. & Montclare, J. K. Protein Based Biomaterials for Therapeutic and Diagnostic Applications. *Prog Biomed Eng (Bristol)* **4**, doi:https://doi.org/10.1088/2516-1091/ac2841 (2022).
24 Abascal, N. C. & Regan, L. The past, present and future of protein-based materials. *Open Biol* **8**, doi:https://doi.org/10.1098/rsob.180113 (2018).
25 Nie, L., Hou, R. & Shavandi, A. Editorial: Advances in protein-based biomaterials for tissue engineering. *Front Bioeng Biotechnol* **10**, 1022733, doi:https://doi.org/10.3389/fbioe.2022.1022733 (2022).
26 Fang, H. & Chen, Q. Applications and challenges of biomaterial mediated mRNA delivery. *Explor Target Antitumor Ther* **3**, 428-444, doi:https://doi.org/10.37349/etat.2022.00093 (2022).
27 Kozielski, K. L. *et al.* Cancer-selective nanoparticles for combinatorial siRNA delivery to primary human GBM in vitro and in vivo. *Biomaterials* **209**, 79-87, doi:https://doi.org/10.1016/j.biomaterials.2019.04.020 (2019).
28 Hua, Y., Ma, J., Li, D. & Wang, R. DNA-Based Biosensors for the Biochemical Analysis: A Review. *Biosensors (Basel)* **12**, doi:https://doi.org/10.3390/bios12030183 (2022).
29 Wang, F., Li, P., Chu, H. C. & Lo, P. K. Nucleic Acids and Their Analogues for Biomedical Applications. *Biosensors (Basel)* **12**, doi:https://doi.org/10.3390/bios12020093 (2022).
30 Damiati, L. A. & El-Messeiry, S. An Overview of RNA-Based Scaffolds for Osteogenesis. *Frontiers in Molecular Biosciences* **8**, doi:https://doi.org/10.3389/fmolb.2021.682581 (2021).
31 Dey, S. *et al.* DNA origami. *Nature Reviews Methods Primers* **1**, 13, doi:https://doi.org/10.1038/s43586-020-00009-8 (2021).
32 Jo, J. I., Gao, J. Q. & Tabata, Y. Biomaterial-based delivery systems of nucleic acid for regenerative research and regenerative therapy. *Regen Ther* **11**, 123-130, doi:https://doi.org/10.1016/j.reth.2019.06.007 (2019).
33 D'souza, Z. *et al.* Collagen – structure, function and distribution in orodental tissues. *Journal of Global Oral Health* **2**, 134-139, doi:https://doi.org/10.25259/jgoh_4_2020 (2020).
34 Deshmukh, S. N., Dive, A. M., Moharil, R. & Munde, P. Enigmatic insight into collagen. *J Oral Maxillofac Pathol* **20**, 276-283, doi:https://doi.org/10.4103/0973-029x.185932 (2016).
35 Schweitzer, M. H. *et al.* Analyses of Soft Tissue from Tyrannosaurus rex Suggest the Presence of Protein. *Science (New York, N.Y.)* **316**, 277-280, doi:https://doi.org/doi:10.1126/science.1138709 (2007).

36 Rinnerthaler, M., Bischof, J., Streubel, M. K., Trost, A. & Richter, K. Oxidative Stress in Aging Human Skin. *Biomolecules* **5**, 545-589, doi:https://doi.org/doi:10.3390/biom5020545 (2015).

37 *Nutrition Source - Collagen*, https://www.hsph.harvard.edu/nutritionsource/collagen/

38 Kahan, V., Andersen, M. L., Tomimori, J. & Tufik, S. Can poor sleep affect skin integrity? *Medical Hypotheses* **75**, 535-537, doi:https://doi.org/10.1016/j.mehy.2010.07.018 (2010).

39 Ricard-Blum, S. The collagen family. *Cold Spring Harb Perspect Biol* **3**, a004978, doi:https://doi.org/10.1101/cshperspect.a004978 (2011).

40 George, J., Jegan, S. R. & Mahija, S. P. Collagen and its therapeutical applications in regenerative medicine. *International Journal for Scientific Research and Development* **6**, 1-10, doi:https://doi.org/10.3390/jfb14070363 (2018).

41 Hay, E. D. in *Cell Biology of Extracellular Matrix* (ed Elizabeth D. Hay) 379-409 (Springer US, 1981).

42 Gelse, K., Poschl, E. & Aigner, T. Collagens-structure, function, and biosynthesis. *Adv Drug Deliv Rev* **55**, 1531-1546, doi:https://doi.org/10.1016/j.addr.2003.08.002 (2003).

43 Wang, H. A Review of the Effects of Collagen Treatment in Clinical Studies. *Polymers (Basel)* **13**, doi:https://doi.org/10.3390/polym13223868 (2021).

44 Cheah, K. S. E. Collagen genes and inherited connective tissue disease. *The Biochemical journal* **229 2**, 287-303, doi:https://doi.org/10.1042/bj2290287 (1985).

45 Eyre, D. Articular cartilage and changes in Arthritis: Collagen of articular cartilage. *Arthritis Research & Therapy* **4**, 30, doi:https://doi.org/10.1186/ar380 (2001).

46 Wang, C. *et al.* Type III collagen is a key regulator of the collagen fibrillar structure and biomechanics of articular cartilage and meniscus. *Matrix biology : journal of the International Society for Matrix Biology* **85-86**, 47-67, doi:https://doi.org/10.1016/j.matbio.2019.10.001 (2020).

47 Holmes, D., Lu, Y., Starborg, T. & Kadler, K. Current Topics in Developmental Biology. (2018).

48 Naomi, R., Ridzuan, P. M. & Bahari, H. Current Insights into Collagen Type I. *Polymers (Basel)* **13**, doi:https://doi.org/10.3390/polym13162642 (2021).

49 Sorushanova, A. *et al.* The Collagen Suprafamily: From Biosynthesis to Advanced Biomaterial Development. *Advanced Materials* **31**, 1801651, doi:https://doi.org/10.1002/adma.201801651 (2019).

50 Krane, S. M. The importance of proline residues in the structure, stability and susceptibility to proteolytic degradation of collagens. *Amino Acids* **35**, 703-710, doi:https://doi.org/10.1007/s00726-008-0073-2 (2008).

51 Phang, J. M. The regulatory mechanisms of proline and hydroxyproline metabolism: Recent advances in perspective. *Front Oncol* **12**, 1118675, doi:https://doi.org/10.3389/fonc.2022.1118675 (2022).

52 Brodsky, B. & Ramshaw, J. A. The collagen triple-helix structure. *Matrix biology : journal of the International Society for Matrix Biology* **15**, 545-554, doi:https://doi.org/10.1016/s0945-053x(97)90030-5 (1997).

53 Gelse, K., Pöschl, E. & Aigner, T. Collagens—structure, function, and biosynthesis. *Advanced Drug Delivery Reviews* **55**, 1531-1546, doi:https://doi.org/10.1016/j.addr.2003.08.002 (2003).

54 Shoulders, M. D. & Raines, R. T. Collagen structure and stability. *Annu Rev Biochem* **78**, 929-958, doi:https://doi.org/10.1146/annurev.biochem.77.032207.120833 (2009).

55 Arseni, L., Lombardi, A. & Orioli, D. From Structure to Phenotype: Impact of Collagen Alterations on Human Health. *Int J Mol Sci* **19**, doi:https://doi.org/10.3390/ijms19051407 (2018).

56 Rezvani Ghomi, E., Nourbakhsh, N., Akbari Kenari, M., Zare, M. & Ramakrishna, S. Collagen-based biomaterials for biomedical applications. *Journal of Biomedical Materials Research Part B: Applied Biomaterials* **109**, 1986-1999, doi:https://doi.org/10.1002/jbm.b.34881 (2021).

57 Li, J. & Kirsner, R. S. in *Surgery of the Skin* (eds June K. Robinson *et al.*) 97-115 (Mosby, 2005).
58 Wu, M., Cronin, K. & Crane, J. S. in *StatPearls* (StatPearls Publishing Copyright © 2023, StatPearls Publishing LLC., 2023).
59 Abdemami, B., Shokrgozar, M. A., Shahreza, H. K. & Ghavami, M. Design and construction of two yeast shuttle vectors containing human procollagen genes expression cassette for expression in yeast. *Avicenna J Med Biotechnol* **3**, 11-18 (2011).
60 insights), P. P. M. Collagen Market is estimated to be US$ 23.1 billion by 2030 with a CAGR of 10.8% during the forecast period-BY PMI. (2023).
61 ltd, S. I. p. Medical Collagen Market Size, Share & Segment by Source (Porcine, Bovine, Others), By Product (Hydrolysed Collagen, Gelatine, Native Collagen, Others), By Application (Wound Care, Cartilage Repair, Bone Grafts, Tissue Scaffolds, Diagnostics, Vascular Grafts, Haemostats, Other), and by Regions | Global Market Forecast 2023-2030. Report No. SNS/HC/1777, 125 (2023).
62 Liu, W. *et al.* A regulatory perspective on recombinant collagen-based medical devices. *Bioact Mater* **12**, 198-202, doi:https://doi.org/10.1016/j.bioactmat.2021.10.031 (2022).
63 Farajollahi, M. M., Hamzehlou, S., Mehdipour, A. & Samadikuchaksaraei, A. Recombinant proteins: hopes for tissue engineering. *Bioimpacts* **2**, 123-125, doi:https://doi.org/10.5681/bi.2012.010 (2012).
64 Eriksson, A., Burcharth, J. & Rosenberg, J. Animal derived products may conflict with religious patients' beliefs. *BMC Med Ethics* **14**, 48, doi:https://doi.org/10.1186/1472-6939-14-48 (2013).
65 Olsen, D. *et al.* Recombinant collagen and gelatin for drug delivery. *Adv Drug Deliv Rev* **55**, 1547-1567, doi:https://doi.org/10.1016/j.addr.2003.08.008 (2003).
66 Wilesmith, J. W., Ryan, J. B. & Atkinson, M. J. Bovine spongiform encephalopathy: epidemiological studies on the origin. *Vet Rec* **128**, 199-203, doi:https://doi.org/10.1136/vr.128.9.199 (1991).
67 Fertala, A., Shah, D. M., Hoffman, A. R. & Arnold, V. W. Designing Recombinant Collagens for Biomedical Applications. *Current Tissue Engineering (Discontinued)* **5**, 73-84, doi:http://dx.doi.org/10.2174/2211542005666160616124053 (2016).
68 Woodley, D. T. *et al.* Intravenously Injected Recombinant Human Type VII Collagen Homes to Skin Wounds and Restores Skin Integrity of Dystrophic Epidermolysis Bullosa. *Journal of Investigative Dermatology* **133**, 1910-1913, doi:https://doi.org/10.1038/jid.2013.10 (2013).
69 Podrebarac, J. *Development of Recombinant Human Collagen Type I and Type III Injectable Hydrogels for Cardiac Therapy*, University of Ottawa, (2017).
70 Sionkowska, A., Skrzyński, S., Śmiechowski, K. & Kołodziejczak, A. The review of versatile application of collagen. *Polymers for Advanced Technologies* **28**, 4-9, doi:https://doi.org/10.1002/pat.3842 (2017).
71 Naomi, R., Bahari, H., Ridzuan, P. M. & Othman, F. Natural-Based Biomaterial for Skin Wound Healing (Gelatin vs. Collagen): Expert Review. *Polymers (Basel)* **13**, doi:https://doi.org/10.3390/polym13142319 (2021).
72 Shen, J., Zhang, W., Gao, P., Xu, Y. & Xia, W. The role of endogenous serine proteinase on disintegration of collagen fibers from grass carp (Ctenopharyngodon idellus). *LWT* **156**, 113003, doi:https://doi.org/10.1016/j.lwt.2021.113003 (2022).
73 Fonkwe, L. G., Narsimhan, G. & Cha, A. S. Characterization of gelation time and texture of gelatin and gelatin–polysaccharide mixed gels. *Food Hydrocolloids* **17**, 871-883, doi:https://doi.org/10.1016/S0268-005X(03)00108-5 (2003).
74 Holder, A. J. *et al.* Control of collagen gel mechanical properties through manipulation of gelation conditions near the sol–gel transition. *Soft Matter* **14**, 574-580, doi:https://doi.org/10.1039/C7SM01933E (2018).

75 Aswathy, S. H., Narendrakumar, U. & Manjubala, I. Commercial hydrogels for biomedical applications. *Heliyon* **6**, e03719, doi:https://doi.org/10.1016/j.heliyon.2020.e03719 (2020).

76 Ahmed, E. M. Hydrogel: Preparation, characterization, and applications: A review. *J Adv Res* **6**, 105-121, doi:https://doi.org/10.1016/j.jare.2013.07.006 (2015).

77 Hu, W., Wang, Z., Xiao, Y., Zhang, S. & Wang, J. Advances in crosslinking strategies of biomedical hydrogels. *Biomater Sci* **7**, 843-855, doi:https://doi.org/10.1039/c8bm01246f (2019).

78 Melchels, F. P. W. *et al.* Additive manufacturing of tissues and organs. *Progress in Polymer Science* **37**, 1079-1104, doi:https://doi.org/10.1016/j.progpolymsci.2011.11.007 (2012).

79 Cha, G. D. *et al.* Multifunctional Injectable Hydrogel for In Vivo Diagnostic and Therapeutic Applications. *ACS Nano* **16**, 554-567, doi:https://doi.org/10.1021/acsnano.1c07649 (2022).

80 Davari, N. *et al.* Protein-Based Hydrogels: Promising Materials for Tissue Engineering. *Polymers (Basel)* **14**, doi:https://doi.org/10.3390/polym14050986 (2022).

81 Oyen, M. L. Mechanical characterisation of hydrogel materials. *International Materials Reviews* **59**, 44-59, doi:https://doi.org/10.1179/1743280413Y.0000000022 (2014).

82 Li, J. & Mooney, D. J. Designing hydrogels for controlled drug delivery. *Nat Rev Mater* **1**, doi:https://doi.org/10.1038/natrevmats.2016.71 (2016).

83 Onaciu, A., Munteanu, R. A., Moldovan, A. I., Moldovan, C. S. & Berindan-Neagoe, I. Hydrogels Based Drug Delivery Synthesis, Characterization and Administration. *Pharmaceutics* **11**, doi:https://doi.org/10.3390/pharmaceutics11090432 (2019).

84 Butcher, D. T., Alliston, T. & Weaver, V. M. A tense situation: forcing tumour progression. *Nat Rev Cancer* **9**, 108-122, doi:https://doi.org/10.1038/nrc2544 (2009).

85 Cao, H., Duan, L., Zhang, Y., Cao, J. & Zhang, K. Current hydrogel advances in physicochemical and biological response-driven biomedical application diversity. *Signal Transduct Target Ther* **6**, 426, doi:https://doi.org/10.1038/s41392-021-00830-x (2021).

86 Madhu. *What is the Difference Between Elastic Modulus and Young's Modulus*, <https://www.differencebetween.com/what-is-the-difference-between-elastic-modulus-and-youngs-modulus/#:~:text=Among%20them%2C%20Young's%20modulus%20tends,acting%20upon%20by%20opposing%20forces.> (2022).

87 Guimarães, C. F., Gasperini, L., Marques, A. P. & Reis, R. L. The stiffness of living tissues and its implications for tissue engineering. *Nature Reviews Materials* **5**, 351-370, doi:https://doi.org/10.1038/s41578-019-0169-1 (2020).

88 Pereira, R. F. & Bártolo, P. J. 3D Photo-Fabrication for Tissue Engineering and Drug Delivery. *Engineering* **1**, 090-112, doi:https://doi.org/10.15302/j-eng-2015015 (2015).

89 Amaral, C. N. R., Oliveira, P. F., Pedroni, L. G. & Mansur, C. R. E. Viscoelastic behavior of hydrogel-based xanthan gum/aluminum lactate with potential applicability for conformance control. *Journal of Applied Polymer Science* **138**, doi:https://doi.org/10.1002/app.50640 (2021).

90 Javanmardi, Y., Colin-York, H., Szita, N., Fritzsche, M. & Moeendarbary, E. Quantifying cell-generated forces: Poisson's ratio matters. *Communications Physics* **4**, 237, doi:https://doi.org/10.1038/s42005-021-00740-y (2021).

91 Karoyo, A. H. & Wilson, L. D. A Review on the Design and Hydration Properties of Natural Polymer-Based Hydrogels. *Materials (Basel)* **14**, doi:https://doi.org/10.3390/ma14051095 (2021).

92 Mantha, S. *et al.* Smart Hydrogels in Tissue Engineering and Regenerative Medicine. *Materials (Basel)* **12**, doi:https://doi.org/10.3390/ma12203323 (2019).

93 Abasalizadeh, F. *et al.* Alginate-based hydrogels as drug delivery vehicles in cancer treatment and their applications in wound dressing and 3D bioprinting. *Journal of Biological Engineering* **14**, 8, doi:https://doi.org/10.1186/s13036-020-0227-7 (2020).
94 Lukin, I. *et al.* Progress in Gelatin as Biomaterial for Tissue Engineering. *Pharmaceutics* **14**, doi:https://doi.org/10.3390/pharmaceutics14061177 (2022).
95 Jiang, F. *et al.* Extraction, Modification and Biomedical Application of Agarose Hydrogels: A Review. *Marine Drugs* **21**, 299 (2023).
96 Wang, G., Wang, X. & Huang, L. Feasibility of chitosan-alginate (Chi-Alg) hydrogel used as scaffold for neural tissue engineering: a pilot study in vitro. *Biotechnology & Biotechnological Equipment* **31**, 766-773, doi:https://doi.org/10.1080/13102818.2017.1332493 (2017).
97 Sarrigiannidis, S. O. *et al.* A tough act to follow: collagen hydrogel modifications to improve mechanical and growth factor loading capabilities. *Materials Today Bio* **10**, 100098, doi:https://doi.org/10.1016/j.mtbio.2021.100098 (2021).
98 Friess, W. Collagen--biomaterial for drug delivery. *European journal of pharmaceutics and biopharmaceutics : official journal of Arbeitsgemeinschaft fur Pharmazeutische Verfahrenstechnik e.V* **45**, 113-136, doi:https://doi.org/10.1016/s0939-6411(98)00017-4 (1998).
99 van Luyn, M. J. *et al.* Secondary cytotoxicity of cross-linked dermal sheep collagens during repeated exposure to human fibroblasts. *Biomaterials* **13**, 1017-1024, doi:https://doi.org/10.1016/0142-9612(92)90153-f (1992).
100 Charulatha, V. & Rajaram, A. Dimethyl 3,3′-dithiobispropionimidate: A novel crosslinking reagent for collagen. *Journal of Biomedical Materials Research* **54**, 122-128, doi:https://doi.org/10.1002/1097-4636(200101)54:1<122::AID-JBM15>3.0.CO;2-N (2001).
101 Nishi, C., Nakajima, N. & Ikada, Y. In vitro evaluation of cytotoxicity of diepoxy compounds used for biomaterial modification. *J Biomed Mater Res* **29**, 829-834, doi:https://doi.org/10.1002/jbm.820290707 (1995).
102 van Wachem, P. B. *et al.* In vivo degradation of processed dermal sheep collagen evaluated with transmission electron microscopy. *Biomaterials* **12**, 215-223, doi:https://doi.org/10.1016/0142-9612(91)90203-m (1991).
103 Haque, M., Forte, N. & Baker, J. R. Site-selective lysine conjugation methods and applications towards antibody–drug conjugates. *Chemical Communications* **57**, 10689-10702, doi:https://doi.org/10.1039/D1CC03976H (2021).
104 Nakajima, N. & Ikada, Y. Mechanism of Amide Formation by Carbodiimide for Bioconjugation in Aqueous Media. *Bioconjugate Chemistry* **6**, 123-130, doi:https://doi.org/10.1021/bc00031a015 (1995).
105 Gatto, V., Conca, S., Bardella, N. & Beghetto, V. Efficient Triazine Derivatives for Collagenous Materials Stabilization. *Materials (Basel)* **14**, doi:https://doi.org/10.3390/ma14113069 (2021).
106 D'Este, M., Eglin, D. & Alini, M. A systematic analysis of DMTMM vs EDC/NHS for ligation of amines to hyaluronan in water. *Carbohydr Polym* **108**, 239-246, doi:https://doi.org/10.1016/j.carbpol.2014.02.070 (2014).
107 Valeur, E. & Bradley, M. Amide bond formation: beyond the myth of coupling reagents. *Chemical Society Reviews* **38**, 606-631, doi:https://doi.org/10.1039/B701677H (2009).
108 Risse, F., Gedig, E. T. & Gutmann, J. S. Carbodiimide-mediated immobilization of acidic biomolecules on reversed-charge zwitterionic sensor chip surfaces. *Analytical and Bioanalytical Chemistry* **410**, 4109-4122, doi:https://doi.org/10.1007/s00216-018-1048-0 (2018).
109 Sheehan, J., Cruickshank, P. & Boshart, G. Notes- A Convenient Synthesis of Water-Soluble Carbodiimides. *The Journal of Organic Chemistry* **26**, 2525-2528, doi:https://doi.org/10.1021/jo01351a600 (1961).
110 Kunishima, M. *et al.* 4-(4,6-dimethoxy-1,3,5-triazin-2-yl)-4-methyl-morpholinium chloride: an efficient condensing agent leading to the formation of amides and esters.

Tetrahedron **55**, 13159-13170, doi:https://doi.org/10.1016/S0040-4020(99)00809-1 (1999).

111 Asawa, R. R. *et al.* Transient cellular adhesion on poly(ethylene-glycol)-dimethacrylate hydrogels facilitates a novel stem cell bandage approach. *PLoS One* **13**, e0202825, doi:https://doi.org/10.1371/journal.pone.0202825 (2018).

112 Veronese, F. M. & Pasut, G. PEGylation, successful approach to drug delivery. *Drug Discovery Today* **10**, 1451-1458, doi:https://doi.org/10.1016/S1359-6446(05)03575-0 (2005).

113 Lotz, C. *et al.* Cross-linked Collagen Hydrogel Matrix Resisting Contraction To Facilitate Full-Thickness Skin Equivalents. *ACS Appl Mater Interfaces* **9**, 20417-20425, doi:https://doi.org/10.1021/acsami.7b04017 (2017).

114 Tian, H. *et al.* Fabrication, properties and applications of soy-protein-based materials: A review. *Int J Biol Macromol* **120**, 475-490, doi:https://doi.org/10.1016/j.ijbiomac.2018.08.110 (2018).

115 Espino, M., Fernández, M. d. l. Á., Gomez, F. J. V., Boiteux, J. & Silva, M. F. Green analytical chemistry metrics: Towards a sustainable phenolics extraction from medicinal plants. *Microchemical Journal* **141**, 438-443, doi:https://doi.org/10.1016/j.microc.2018.06.007 (2018).

116 Fujimoto, N., Kohta, R., Kitamura, S. & Honda, H. Estrogenic activity of an antioxidant, nordihydroguaiaretic acid (NDGA). *Life Sciences* **74**, 1417-1425, doi:https://doi.org/10.1016/j.lfs.2003.08.012 (2004).

117 Jayachandran, B., Parvin, T. N., Alam, M. M., Chanda, K. & Mm, B. Insights on Chemical Crosslinking Strategies for Proteins. *Molecules* **27**, doi:https://doi.org/10.3390/molecules27238124 (2022).

118 *K. Barry Sharpless – Facts – 2022*, <https://www.nobelprize.org/prizes/chemistry/2022/sharpless/facts/> (

119 Bednarek, C., Schepers, U., Thomas, F. & Bräse, S. Bioconjugation in Materials Science. *Advanced functional materials* **n/a**, 2303613, doi:https://doi.org/10.1002/adfm.202303613.

120 Wang, W. *et al.* In situ activation of therapeutics through bioorthogonal catalysis. *Adv Drug Deliv Rev* **176**, 113893, doi:10.1016/j.addr.2021.113893 (2021).

121 Azagarsamy, M. A. & Anseth, K. S. Bioorthogonal Click Chemistry: An Indispensable Tool to Create Multifaceted Cell Culture Scaffolds. *ACS Macro Lett* **2**, 5-9, doi:https://doi.org/10.1021/mz300585q (2013).

122 Sletten, E. M. & Bertozzi, C. R. From Mechanism to Mouse: A Tale of Two Bioorthogonal Reactions. *Accounts of Chemical Research* **44**, 666-676, doi:https://doi.org/10.1021/ar200148z (2011).

123 Hang, H. C., Yu, C., Kato, D. L. & Bertozzi, C. R. A metabolic labeling approach toward proteomic analysis of mucin-type O-linked glycosylation. *Proceedings of the National Academy of Sciences* **100**, 14846-14851, doi:https://doi.org/10.1073/pnas.2335201100 (2003).

124 *Carolyn Bertozzi – Facts – 2022*, <https://www.nobelprize.org/prizes/chemistry/2022/bertozzi/facts/> (2023).

125 Scinto, S. L. *et al.* Bioorthogonal chemistry. *Nature Reviews Methods Primers* **1**, 30, doi:https://doi.org/10.1038/s43586-021-00028-z (2021).

126 Van Hoorick, J. *et al.* (Photo-)crosslinkable Gelatin Derivatives for Biofabrication Applications. *Acta biomaterialia* **97**, doi:https://doi.org/10.1016/j.actbio.2019.07.035 (2019).

127 Makris, E. A., Responte, D. J., Paschos, N. K., Hu, J. C. & Athanasiou, K. A. Developing functional musculoskeletal tissues through hypoxia and lysyl oxidase-induced collagen cross-linking. *Proc Natl Acad Sci U S A* **111**, E4832-4841, doi:https://doi.org/10.1073/pnas.1414271111 (2014).

128 Nair, D. P. *et al.* The Thiol-Michael Addition Click Reaction: A Powerful and Widely Used Tool in Materials Chemistry. *Chemistry of Materials* **26**, 724-744, doi:https://doi.org/10.1021/cm402180t (2014).
129 Guvendiren, M. *3D Bioprinting in Medicine: Technologies, Bioinks, and Applications*. (Springer International Publishing, 2019).
130 Lee, M., Rizzo, R., Surman, F. & Zenobi-Wong, M. Guiding Lights: Tissue Bioprinting Using Photoactivated Materials. *Chem Rev* **120**, 10950-11027, doi:https://doi.org/10.1021/acs.chemrev.0c00077 (2020).
131 Nguyen, K. T. & West, J. L. Photopolymerizable hydrogels for tissue engineering applications. *Biomaterials* **23**, 4307-4314, doi:https://doi.org/10.1016/s0142-9612(02)00175-8 (2002).
132 Shirai, M. in *Encyclopedia of Polymeric Nanomaterials* (eds Shiro Kobayashi & Klaus Müllen) 1579-1585 (Springer Berlin Heidelberg, 2015).
133 Graeme Moad, D. H. S. *The Chemistry of Radical Polymerization*. 600 (Elsevier Science Ltd., 2019).
134 O'Brien, A. K. & Bowman, C. N. Modeling the Effect of Oxygen on Photopolymerization Kinetics. *Macromolecular Theory and Simulations* **15**, 176-182, doi:https://doi.org/10.1002/mats.200500056 (2006).
135 O'Brien, A., Cramer, N. & Bowman, C. Oxygen inhibition in thiol–acrylate photopolymerizations. *Journal of Polymer Science Part A: Polymer Chemistry* **44**, 2007-2014, doi:https://doi.org/10.1002/pola.21304 (2006).
136 Fouassier, J. P. & Rabek, J. F. *Radiation Curing in Polymer Science and Technology-Volume II: Photoinitiating Systems*. 718 (Springer Netherlands, 1993).
137 Kannurpatti, A. R., Anseth, J. W. & Bowman, C. N. A study of the evolution of mechanical properties and structural heterogeneity of polymer networks formed by photopolymerizations of multifunctional (meth)acrylates. *Polymer* **39**, 2507-2513, doi:https://doi.org/10.1016/S0032-3861(97)00585-5 (1998).
138 Bowman, C. N. & Peppas, N. A. Coupling of kinetics and volume relaxation during polymerizations of multiacrylates and multimethacrylates. *Macromolecules* **24**, 1914-1920, doi:https://doi.org/10.1021/ma00008a032 (1991).
139 Lee, T. Y., Roper, T. M., Jönsson, E. S., Guymon, C. A. & Hoyle, C. E. Influence of Hydrogen Bonding on Photopolymerization Rate of Hydroxyalkyl Acrylates. *Macromolecules* **37**, 3659-3665, doi:https://doi.org/10.1021/ma0305277 (2004).
140 Lu, H., Stansbury, J. W. & Bowman, C. N. Towards the elucidation of shrinkage stress development and relaxation in dental composites. *Dental Materials* **20**, 979-986, doi:https://doi.org/10.1016/j.dental.2004.05.002 (2004).
141 Wiley, K. L., Ovadia, E. M., Calo, C. J., Huber, R. E. & Kloxin, A. M. Rate-based approach for controlling the mechanical properties of 'thiol–ene' hydrogels formed with visible light. *Polymer Chemistry* **10**, 4428-4440, doi:https://doi.org/10.1039/C9PY00447E (2019).
142 Reddy, S. K., Okay, O. & Bowman, C. N. Network Development in Mixed Step-Chain Growth Thiol−Vinyl Photopolymerizations. *Macromolecules* **39**, 8832-8843, doi:https://doi.org/10.1021/ma060249m (2006).
143 Zhao, C. *et al.* Thiol-Rich Multifunctional Macromolecular Crosslinker for Gelatin-Norbornene-Based Bioprinting. *Biomacromolecules* **22**, 2729-2739, doi:https://doi.org/10.1021/acs.biomac.1c00421 (2021).
144 Deng, J.-R. *et al.* Chemoselective and photocleavable cysteine modification of peptides and proteins using isoxazoliniums. *Communications Chemistry* **2**, 93, doi:https://doi.org/10.1038/s42004-019-0193-5 (2019).
145 Rydholm, A. E., Reddy, S. K., Anseth, K. S. & Bowman, C. N. Controlling Network Structure in Degradable Thiol−Acrylate Biomaterials to Tune Mass Loss Behavior. *Biomacromolecules* **7**, 2827-2836, doi:https://doi.org/10.1021/bm0603793 (2006).

146 Guo, K. *et al.* Collagen-Based Thiol-Norbornene Photoclick Bio-Ink with Excellent Bioactivity and Printability. *ACS Appl Mater Interfaces* **13**, 7037-7050, doi:https://doi.org/10.1021/acsami.0c16714 (2021).
147 Ooi, H. W. *et al.* Thiol–Ene Alginate Hydrogels as Versatile Bioinks for Bioprinting. *Biomacromolecules* **19**, 3390-3400, doi:https://doi.org/10.1021/acs.biomac.8b00696 (2018).
148 Anderson, S. B., Lin, C.-C., Kuntzler, D. V. & Anseth, K. S. The performance of human mesenchymal stem cells encapsulated in cell-degradable polymer-peptide hydrogels. *Biomaterials* **32**, 3564-3574, doi:https://doi.org/10.1016/j.biomaterials.2011.01.064 (2011).
149 Lin, C.-C., Raza, A. & Shih, H. PEG hydrogels formed by thiol-ene photo-click chemistry and their effect on the formation and recovery of insulin-secreting cell spheroids. *Biomaterials* **32**, 9685-9695, doi:https://doi.org/10.1016/j.biomaterials.2011.08.083 (2011).
150 Van Hoorick, J. *et al.* Thiol-Norbornene gelatin hydrogels: influence of thiolated crosslinker on network properties and high definition 3D printing. *Biofabrication*, doi:https://doi.org/10.1088/1758-5090/abc95f (2020).
151 Choi, J. R., Yong, K. W., Choi, J. Y. & Cowie, A. C. Recent advances in photo-crosslinkable hydrogels for biomedical applications. *BioTechniques* **66**, 40-53, doi:https://doi.org/10.2144/btn-2018-0083 (2019).
152 Methods for Photocrosslinking Alginate Hydrogel Scaffolds with High Cell Viability. *Tissue Engineering Part C: Methods* **17**, 173-179, doi:10.1089/ten.tec.2009.0582 (2011).
153 Benedikt, S. *et al.* Highly efficient water-soluble visible light photoinitiators. *Journal of Polymer Science Part A: Polymer Chemistry* **54**, 473-479, doi:https://doi.org/10.1002/pola.27903 (2016).
154 Elkhoury, K., Zuazola, J. & Vijayavenkataraman, S. Bioprinting the future using light: A review on photocrosslinking reactions, photoreactive groups, and photoinitiators. *SLAS Technology* **28**, 142-151, doi:https://doi.org/10.1016/j.slast.2023.02.003 (2023).
155 Bryant, S. J., Nuttelman, C. R. & Anseth, K. S. Cytocompatibility of UV and visible light photoinitiating systems on cultured NIH/3T3 fibroblasts in vitro. *Journal of Biomaterials Science, Polymer Edition* **11**, 439-457, doi:https://doi.org/10.1163/156856200743805 (2000).
156 Gou, M. *et al.* Bio-inspired detoxification using 3D-printed hydrogel nanocomposites. *Nature Communications* **5**, 3774, doi:https://doi.org/10.1038/ncomms4774 (2014).
157 Lim, K. S. *et al.* Visible Light Cross-Linking of Gelatin Hydrogels Offers an Enhanced Cell Microenvironment with Improved Light Penetration Depth. *Macromolecular Bioscience* **19**, 1900098, doi:https://doi.org/10.1002/mabi.201900098 (2019).
158 Balzani, V. *et al.* Fluorescent guests hosted in fluorescent dendrimers. *Tetrahedron* **58**, 629-637, doi:https://doi.org/10.1016/S0040-4020(01)01094-8 (2002).
159 Chen, Y., Shen, Z., Pastor-Pérez, L., Frey, H. & Stiriba, S.-E. Role of Topology and Amphiphilicity for Guest Encapsulation in Functionalized Hyperbranched Poly(ethylenimine)s. *Macromolecules* **38**, 227-229, doi:https://doi.org/10.1021/ma047837p (2005).
160 Krowczynski, L. [Technological methods for improving the solubility and increasing the dissolution rate of slightly soluble drugs (author's transl)]. *Pharmazie* **37**, 79-83 (1982).
161 Koziol, J. Studies on Flavins in organic solvents. Spectral characteristics of riboflavin tetrabutyrate and lumichrome. *Photochemistry and Photobiology* **5**, 41-54, doi:https://doi.org/10.1111/j.1751-1097.1966.tb05759.x (1966).
162 Shih, H. & Lin, C.-C. Visible-Light-Mediated Thiol-Ene Hydrogelation Using Eosin-Y as the Only Photoinitiator. *Macromolecular Rapid Communications* **34**, 269-273, doi:https://doi.org/10.1002/marc.201200605 (2013).

163 Ash, C., Dubec, M., Donne, K. & Bashford, T. Effect of wavelength and beam width on penetration in light-tissue interaction using computational methods. *Lasers Med Sci* **32**, 1909-1918, doi:https://doi.org/10.1007/s10103-017-2317-4 (2017).
164 Fancy, D. A. *et al.* Scope, limitations and mechanistic aspects of the photo-induced cross-linking of proteins by water-soluble metal complexes. *Chemistry & Biology* **7**, 697-708, doi:https://doi.org/10.1016/S1074-5521(00)00020-X (2000).
165 Chuang, C. H., Lin, R. Z., Melero-Martin, J. M. & Chen, Y. C. Comparison of covalently and physically cross-linked collagen hydrogels on mediating vascular network formation for engineering adipose tissue. *Artif Cells Nanomed Biotechnol* **46**, S434-s447, doi:https://doi.org/10.1080/21691401.2018.1499660 (2018).
166 Jiang, Y. H. *et al.* Cross-linking methods of type I collagen-based scaffolds for cartilage tissue engineering. *Am J Transl Res* **14**, 1146-1159 (2022).
167 Gaudet, I. D. & Shreiber, D. I. Characterization of methacrylated type-I collagen as a dynamic, photoactive hydrogel. *Biointerphases* **7**, 25, doi:10.1007/s13758-012-0025-y (2012).
168 Lin, K. *et al.* Advanced Collagen-Based Biomaterials for Regenerative Biomedicine. *Advanced functional materials* **29**, doi:https://doi.org/10.1002/adfm.201804943 (2019).
169 Sagi, I. & Afratis, N. *Collagen Methods and Protocols: Methods and Protocols*. (2019).
170 Senadheera, T. R. L., Dave, D. & Shahidi, F. Sea Cucumber Derived Type I Collagen: A Comprehensive Review. *Mar Drugs* **18**, doi:https://doi.org/10.3390/md18090471 (2020).
171 Tytgat, L. *et al.* Photo-crosslinkable recombinant collagen mimics for tissue engineering applications. *J Mater Chem B* **7**, 3100-3108, doi:https://doi.org/10.1039/c8tb03308k (2019).
172 Ben, C. *et al.* A recombinant human collagen hydrogel for the treatment of partial-thickness burns: A prospective, self-controlled clinical study. *Burns* **47**, 634-642, doi:https://doi.org/10.1016/j.burns.2020.01.006 (2021).
173 Au - Suarez Muñoz, M., Au - Confalonieri, D., Au - Walles, H., Au - van Dongen, E. M. W. M. & Au - Dandekar, G. Recombinant Collagen I Peptide Microcarriers for Cell Expansion and Their Potential Use As Cell Delivery System in a Bioreactor Model. *JoVE*, e57363, doi:https://doi.org/10.3791/57363 (2018).
174 Furihata, T. *et al.* Bone forming ability of recombinant human collagen peptide granules applied with ß-tricalcium phosphate fine particles. *Journal of Biomedical Materials Research Part B: Applied Biomaterials* **108**, 3033-3044, doi:https://doi.org/10.1002/jbm.b.34632 (2020).
175 Tytgat, L. *et al.* High-Resolution 3D Bioprinting of Photo-Cross-linkable Recombinant Collagen to Serve Tissue Engineering Applications. *Biomacromolecules* **21**, 3997-4007, doi:https://doi.org/10.1021/acs.biomac.0c00386 (2020).
176 McLaughlin, S. *et al.* Injectable human recombinant collagen matrices limit adverse remodeling and improve cardiac function after myocardial infarction. *Nature Communications* **10**, 4866, doi:https://doi.org/10.1038/s41467-019-12748-8 (2019).
177 Amit Kumar, V. in *Collagen Biomaterials* (eds Mazumder Nirmal & Chakrabarty Sanjiban) Ch. 5 (IntechOpen, 2022).
178 Adepu, S. & Ramakrishna, S. Controlled Drug Delivery Systems: Current Status and Future Directions. *Molecules* **26**, doi:https://doi.org/10.3390/molecules26195905 (2021).
179 Liu, D., Yang, F., Xiong, F. & Gu, N. The Smart Drug Delivery System and Its Clinical Potential. *Theranostics* **6**, 1306-1323, doi:https://doi.org/10.7150/thno.14858 (2016).
180 Sahiner, M., Alpaslan, D. & Bitlisli, B. O. Collagen-based hydrogel films as drug-delivery devices with antimicrobial properties. *Polymer Bulletin* **71**, 3017-3033, doi:https://doi.org/10.1007/s00289-014-1235-x (2014).

181 Xeroudaki, M. *et al.* A porous collagen-based hydrogel and implantation method for corneal stromal regeneration and sustained local drug delivery. *Sci Rep* **10**, 16936, doi:https://doi.org/10.1038/s41598-020-73730-9 (2020).
182 Davidson, B. S. *et al.* Collagen matrix cisplatin prevents local tumor growth after margin-positive resection. *J Surg Res* **58**, 618-624, doi:https://doi.org/10.1006/jsre.1995.1097 (1995).
183 Slavin, J., Nash, J. R. & Kingsnorth, A. N. Effect of transforming growth factor beta and basic fibroblast growth factor on steroid-impaired healing intestinal wounds. *Br J Surg* **79**, 69-72, doi:https://doi.org/10.1002/bjs.1800790124 (1992).
184 Chak*, V., Kumar, D. & Visht, S. A Review on Collagen Based Drug Delivery Systems. *International Journal of Pharmacy Teaching & Practices* **4**, 811-820 (2013).
185 Minabe, M., Takeuchi, K., Tamura, T., Hori, T. & Umemoto, T. Subgingival administration of tetracycline on a collagen film. *J Periodontol* **60**, 552-556, doi:https://doi.org/10.1902/jop.1989.60.10.552 (1989).
186 Cascone, M. G., Sim, B. & Sandra, D. Blends of synthetic and natural polymers as drug delivery systems for growth hormone. *Biomaterials* **16**, 569-574, doi:https://doi.org/10.1016/0142-9612(95)91131-H (1995).
187 Chen, M. M. *et al.* Collagen/chitosan film containing biotinylated glycol chitosan nanoparticles for localized drug delivery. *Colloids Surf B Biointerfaces* **128**, 339-346, doi:https://doi.org/10.1016/j.colsurfb.2015.02.024 (2015).
188 Berthold, A., Cremer, K. & Kreuter, J. Collagen microparticles: carriers for glucocorticosteroids. *European journal of pharmaceutics and biopharmaceutics : official journal of Arbeitsgemeinschaft fur Pharmazeutische Verfahrenstechnik e.V* **45**, 23-29, doi:https://doi.org/10.1016/S0939-6411(97)00119-7 (1998).
189 Zhong, R. *et al.* Hydrogels for RNA delivery. *Nature Materials*, doi:https://doi.org/10.1038/s41563-023-01472-w (2023).
190 Lefebvre, F., Pilet, P., Bonzon, N., Daculsi, G. & Rabaud, M. New preparation and microstructure of the EndoPatch elastin-collagen containing glycosaminoglycans. *Biomaterials* **17**, 1813-1818, doi:https://doi.org/10.1016/0142-9612(95)00346-0 (1996).
191 Buitrago, J. O. *et al.* Silk fibroin/collagen protein hybrid cell-encapsulating hydrogels with tunable gelation and improved physical and biological properties. *Acta biomaterialia* **69**, 218-233, doi:https://doi.org/10.1016/j.actbio.2017.12.026 (2018).
192 Chaudhary, S. & Chakraborty, E. Hydrogel based tissue engineering and its future applications in personalized disease modeling and regenerative therapy. *Beni-Suef University Journal of Basic and Applied Sciences* **11**, 3, doi:https://doi.org/10.1186/s43088-021-00172-1 (2022).
193 Ersanli, C., Tzora, A., Skoufos, I., Voidarou, C. C. & Zeugolis, D. I. Recent Advances in Collagen Antimicrobial Biomaterials for Tissue Engineering Applications: A Review. *Int J Mol Sci* **24**, doi:https://doi.org/10.3390/ijms24097808 (2023).
194 Mallick, M., Are, R. P. & Babu, A. R. An overview of collagen/bioceramic and synthetic collagen for bone tissue engineering. *Materialia* **22**, 101391, doi:https://doi.org/10.1016/j.mtla.2022.101391 (2022).
195 Liu, Y., Shah, K. M. & Luo, J. Strategies for Articular Cartilage Repair and Regeneration. *Front Bioeng Biotechnol* **9**, 770655, doi:https://doi.org/10.3389/fbioe.2021.770655 (2021).
196 Tang, Y., Wang, Z., Xiang, L., Zhao, Z. & Cui, W. Functional biomaterials for tendon/ligament repair and regeneration. *Regen Biomater* **9**, rbac062, doi:10.1093/rb/rbac062 (2022).
197 Amirrah, I. N. *et al.* A Comprehensive Review on Collagen Type I Development of Biomaterials for Tissue Engineering: From Biosynthesis to Bioscaffold. *Biomedicines* **10**, doi:https://doi.org/10.3390/biomedicines10092307 (2022).
198 Dinescu, S. *et al.* in *Cellulose-Based Superabsorbent Hydrogels* (ed Md Ibrahim H. Mondal) 1-21 (Springer International Publishing, 2018).

199 Sheokand, B. *et al.* Natural polymers used in the dressing materials for wound healing: Past, present and future. *Journal of Polymer Science* **61**, 1389-1414, doi:https://doi.org/10.1002/pol.20220734 (2023).
200 Liu, J., Qu, S., Suo, Z. & Yang, W. Functional hydrogel coatings. *National Science Review* **8**, doi:https://doi.org/10.1093/nsr/nwaa254 (2020).
201 Naahidi, S. *et al.* Biocompatibility of hydrogel-based scaffolds for tissue engineering applications. *Biotechnology Advances* **35**, 530-544, doi:https://doi.org/10.1016/j.biotechadv.2017.05.006 (2017).
202 Mitura, S., Sionkowska, A. & Jaiswal, A. Biopolymers for hydrogels in cosmetics: review. *Journal of materials science. Materials in medicine* **31**, 50, doi:https://doi.org/10.1007/s10856-020-06390-w (2020).
203 Sato, K. The presence of food-derived collagen peptides in human body-structure and biological activity. *Food Funct* **8**, 4325-4330, doi:https://doi.org/10.1039/c7fo01275f (2017).
204 Zague, V. *et al.* Collagen hydrolysate intake increases skin collagen expression and suppresses matrix metalloproteinase 2 activity. *J Med Food* **14**, 618-624, doi:https://doi.org/10.1089/jmf.2010.0085 (2011).
205 Sionkowska, A., Adamiak, K., Musial, K. & Gadomska, M. Collagen Based Materials in Cosmetic Applications: A Review. *Materials (Basel)* **13**, doi:https://doi.org/10.3390/ma13194217 (2020).
206 Atieh, M. A., Alsabeeha, N., Tawse-Smith, A. & Payne, A. G. T. Xenogeneic collagen matrix for periodontal plastic surgery procedures: a systematic review and meta-analysis. *Journal of Periodontal Research* **51**, 438-452, doi:https://doi.org/10.1111/jre.12333 (2016).
207 Binlateh, T., Thammanichanon, P., Rittipakorn, P., Thinsathid, N. & Jitprasertwong, P. Collagen-Based Biomaterials in Periodontal Regeneration: Current Applications and Future Perspectives of Plant-Based Collagen. *Biomimetics (Basel)* **7**, doi:https://doi.org/10.3390/biomimetics7020034 (2022).
208 Kato, A. *et al.* Combination of Root Surface Modification with BMP-2 and Collagen Hydrogel Scaffold Implantation for Periodontal Healing in Beagle Dogs. *Open Dent J* **9**, 52-59, doi:https://doi.org/10.2174/1874210601509010052 (2015).
209 d'Aquino, R. *et al.* Human mandible bone defect repair by the grafting of dental pulp stem/progenitor cells and collagen sponge biocomplexes. *European cells & materials* **18**, 75-83, doi:https://doi.org/10.22203/ecm.v018a07 (2009).
210 Brent Allan, R. R., Euphemie Landao-Bassonga, Nicholas Gillman, Tao Wang, Junjie Gao, Yonghua Ruan, Yuan Xu, Clair Lee, Mithran Goonewardene, and Minghao Zheng. Collagen Membrane for Guided Bone Regeneration in Dental and Orthopedic Applications. *Tissue Engineering Part A* **27**, 372-381, doi:https://doi.org/10.1089/ten.tea.2020.0140 (2021).
211 Wang, E., Han, J., Zhang, X., Wu, Y. & Deng, X.-L. Efficacy of a mineralized collagen bone-grafting material for peri-implant bone defect reconstruction in mini pigs. *Regenerative Biomaterials* **6**, 107-111, doi:https://doi.org/10.1093/rb/rby029 (2019).
212 Abdelaziz, M., Shaaban, R., Abdelhalim, S. & Sadaka, M. Effect of CollaPlug® on the healing of extraction sockets in patients under oral anticoagulant therapy (clinical study). *Alexandria Dental Journal* **40**, 166-172, doi:https://doi.org/10.21608/adjalexu.2015.59145 (2015).
213 N. Poornima Sowjanya, N. R., N.V.V. Satya Bhushan, Gokkula Krishnan. Versitality of the Use of Collagen Membrane in Oral Cavity. *Journal of Clinical and Diagnostic Research* **10**, ZC30-ZC33, doi:https://doi.org/10.7860/jcdr/2016/.7205 (2016).
214 Haleem, A., Javaid, M., Singh, R. P., Suman, R. & Rab, S. Biosensors applications in medical field: A brief review. *Sensors International* **2**, 100100, doi:https://doi.org/10.1016/j.sintl.2021.100100 (2021).

215 Naresh, V. & Lee, N. A Review on Biosensors and Recent Development of Nanostructured Materials-Enabled Biosensors. *Sensors (Basel)* **21**, doi:https://doi.org/10.3390/s21041109 (2021).
216 Nguyen, H. H., Lee, S. H., Lee, U. J., Fermin, C. D. & Kim, M. Immobilized Enzymes in Biosensor Applications. *Materials (Basel)* **12**, doi:https://doi.org/10.3390/ma12010121 (2019).
217 Xu, M., Obodo, D. & Yadavalli, V. K. The design, fabrication, and applications of flexible biosensing devices. *Biosens Bioelectron* **124-125**, 96-114, doi:https://doi.org/10.1016/j.bios.2018.10.019 (2019).
218 Song, Z. *et al.* Flexible and Wearable Biosensors for Monitoring Health Conditions. *Biosensors* **13**, 630, doi:https://doi.org/10.3390/bios13060630 (2023).
219 Guo, J. *et al.* Soft and plasmonic hydrogel optical probe for glucose monitoring. *Nanophotonics* **10**, 3549-3558, doi:https://doi.org/10.1515/nanoph-2021-0360 (2021).
220 Fedi, A., Vitale, C., Giannoni, P., Caluori, G. & Marrella, A. Biosensors to Monitor Cell Activity in 3D Hydrogel-Based Tissue Models. *Sensors (Basel)* **22**, doi:https://doi.org/10.3390/s22041517 (2022).
221 Ravichandran, R., Martinez, J. G., Jager, E. W. H., Phopase, J. & Turner, A. P. F. Type I Collagen-Derived Injectable Conductive Hydrogel Scaffolds as Glucose Sensors. *ACS Applied Materials & Interfaces* **10**, 16244-16249, doi:https://doi.org/10.1021/acsami.8b04091 (2018).
222 Shuichi, S., Fujio, T., Ikuo, S. & Nobuyuki, S. Ethanol and Lactic Acid Sensors Using Electrodes Coated with Dehydrogenase—Collagen Membranes. *Bulletin of the Chemical Society of Japan* **48**, 3246-3249, doi:https://doi.org/10.1246/bcsj.48.3246 (1975).
223 Fenghong, C. *et al.* Cholesterol biosensing based on hydrogel optical fiber immobilization with cholesterol oxidase. *Optik* **286**, 170995, doi:https://doi.org/10.1016/j.ijleo.2023.170995 (2023).
224 Völlmecke, K. *et al.* Hydrogel-Based Biosensors. *Gels* **8**, doi:https://doi.org/10.3390/gels8120768 (2022).
225 Shen, P. *et al.* Aptamer-functionalized smart photonic hydrogels: application for the detection of thrombin in human serum. *NPG Asia Materials* **14**, 94, doi:https://doi.org/10.1038/s41427-022-00443-y (2022).
226 Zhang, Z. *et al.* Antifouling and sensitive biosensor based on multifunctional peptide and urease@ZIFs for metal matrix protease-7. *Sensors and Actuators B: Chemical* **364**, 131844, doi:https://doi.org/10.1016/j.snb.2022.131844 (2022).
227 Ren, H. *et al.* Self-assembled peptides-modified flexible field-effect transistors for tyrosinase detection. *iScience* **25**, 103673, doi:https://doi.org/10.1016/j.isci.2021.103673 (2022).
228 Wang, W., Han, R., Chen, M. & Luo, X. Antifouling Peptide Hydrogel Based Electrochemical Biosensors for Highly Sensitive Detection of Cancer Biomarker HER2 in Human Serum. *Analytical Chemistry* **93**, 7355-7361, doi:https://doi.org/10.1021/acs.analchem.1c01350 (2021).
229 D'Amico, E. *et al.* Hemostatic Collagen Sponge with High Porosity Promotes the Proliferation and Adhesion of Fibroblasts and Osteoblasts. *Int J Mol Sci* **24**, doi:10.3390/ijms24097749 (2023).
230 Glowacki, J. & Mizuno, S. Collagen scaffolds for tissue engineering. *Biopolymers* **89**, 338-344, doi:10.1002/bip.20871 (2008).
231 Dimatteo, R., Darling, N. J. & Segura, T. In situ forming injectable hydrogels for drug delivery and wound repair. *Adv Drug Deliv Rev* **127**, 167-184, doi:10.1016/j.addr.2018.03.007 (2018).
232 Ho, T.-C. *et al.* Hydrogels: Properties and Applications in Biomedicine. *Molecules* **27**, 2902 (2022).
233 ASTM. (ASTM International, West Conshohocken, PA, 2012).

234 Mhetre, G. N., Jadhav, V. S., Deshmukh, S. P. & Thakar, C. M. A Review on Additive Manufacturing Technology. *ECS Transactions* **107**, 15355, doi:https://doi.org/10.1149/10701.15355ecst (2022).
235 Gebler, M., Schoot Uiterkamp, A. J. M. & Visser, C. A global sustainability perspective on 3D printing technologies. *Energy Policy* **74**, 158-167, doi:https://doi.org/10.1016/j.enpol.2014.08.033 (2014).
236 Mehrpouya, M. *et al.* The Potential of Additive Manufacturing in the Smart Factory Industrial 4.0: A Review. *Applied Sciences* **9**, 3865 (2019).
237 Sutherland, W. J. *et al.* A horizon scan of global conservation issues for 2014. *Trends in Ecology & Evolution* **29**, 15-22, doi:https://doi.org/10.1016/j.tree.2013.11.004 (2014).
238 Petrovic, V. *et al.* Additive layered manufacturing: sectors of industrial application shown through case studies. *International Journal of Production Research* **49**, 1061-1079, doi:10.1080/00207540903479786 (2011).
239 Bobbio, L. D. *et al.* Additive manufacturing of a functionally graded material from Ti-6Al-4V to Invar: Experimental characterization and thermodynamic calculations. *Acta Materialia* **127**, 133-142, doi:https://doi.org/10.1016/j.actamat.2016.12.070 (2017).
240 Carroll, B. E., Palmer, T. A. & Beese, A. M. Anisotropic tensile behavior of Ti–6Al–4V components fabricated with directed energy deposition additive manufacturing. *Acta Materialia* **87**, 309-320, doi:https://doi.org/10.1016/j.actamat.2014.12.054 (2015).
241 Baumers, M., Dickens, P., Tuck, C. & Hague, R. The cost of additive manufacturing: machine productivity, economies of scale and technology-push. *Technological Forecasting and Social Change* **102**, 193-201, doi:https://doi.org/10.1016/j.techfore.2015.02.015 (2016).
242 Attaran, M. The rise of 3-D printing: The advantages of additive manufacturing over traditional manufacturing. *Business horizons* **60**, 677-688 (2017).
243 Frazier, W. E. Metal additive manufacturing: a review. *Journal of Materials Engineering and performance* **23**, 1917-1928 (2014).
244 Research, G. V. *Additive Manufacturing Market Size, Share & Trends Analysis Report By Component, By Printer Type, By Technology, By Software, By Application, By Vertical, By Material, By Region, And Segment Forecasts, 2022 - 2030*, <https://www.grandviewresearch.com/industry-analysis/additive-manufacturing-market> (2022).
245 Research, G. V. *3D Printing Market Size, Share & Trends Analysis Report By Component (Hardware, Software, Services), By Printer Type, By Technology, By Software, By Application, By Vertical, By Region, And Segment Forecasts, 2022 - 2030*, <https://www.grandviewresearch.com/industry-analysis/3d-printing-industry-analysis> (2022).
246 Research, G. V. *3D Bioprinting Market Size, Share & Trends Analysis Report By Technology (Magnetic Levitation, Inkjet-based), By Application (Medical, Dental, Biosensors, Bioinks), By Region, And Segment Forecasts, 2023 - 2030*, <https://www.grandviewresearch.com/industry-analysis/3d-bioprinting-market> (2022).
247 LLC, B. R. Laboratory Animal Models, 3D Cultures and Organoids: Global Markets. 213 (2022).
248 Groll, J. *et al.* A definition of bioinks and their distinction from biomaterial inks. *Biofabrication* **11**, 013001, doi:https://doi.org/10.1088/1758-5090/aaec52 (2019).
249 Heid, S. & Boccaccini, A. R. Advancing bioinks for 3D bioprinting using reactive fillers: A review. *Acta biomaterialia* **113**, 1-22, doi:https://doi.org/10.1016/j.actbio.2020.06.040 (2020).
250 Ji, S. & Guvendiren, M. Complex 3D bioprinting methods. *APL Bioengineering* **5**, doi:https://doi.org/10.1063/5.0034901 (2021).

251 Wang, Z. *et al.* A simple and high-resolution stereolithography-based 3D bioprinting system using visible light crosslinkable bioinks. *Biofabrication* **7**, 045009, doi:https://doi.org/10.1088/1758-5090/7/4/045009 (2015).

252 Murphy, S. V. & Atala, A. 3D bioprinting of tissues and organs. *Nat Biotechnol* **32**, 773-785, doi:https://doi.org/10.1038/nbt.2958 (2014).

253 Sundaramurthi, D., Rauf, S. & Hauser, C. 3D bioprinting technology for regenerative medicine applications. *International Journal of Bioprinting* **2**, doi:https://doi.org/10.18063/ijb.2016.02.010 (2016).

254 Madou, M. J. *Fundamentals of microfabrication: the science of miniaturization*. (CRC press, 2002).

255 Jones, N. Science in three dimensions: the print revolution. *Nature* **487**, 22-23, doi:https://doi.org/10.1038/487022a (2012).

256 Guillotin, B. *et al.* Laser assisted bioprinting of engineered tissue with high cell density and microscale organization. *Biomaterials* **31**, 7250-7256, doi:https://doi.org/10.1016/j.biomaterials.2010.05.055 (2010).

257 Saunders, R. E. & Derby, B. Inkjet printing biomaterials for tissue engineering: bioprinting. *International Materials Reviews* **59**, 430-448, doi:https://doi.org/10.1179/1743280414Y.0000000040 (2014).

258 Smith, C. M. *et al.* Three-dimensional bioassembly tool for generating viable tissue-engineered constructs. *Tissue Eng* **10**, 1566-1576, doi:https://doi.org/10.1089/ten.2004.10.1566 (2004).

259 Dai, X. *et al.* Coaxial 3D bioprinting of self-assembled multicellular heterogeneous tumor fibers. *Scientific Reports* **7**, doi:https://doi.org/10.1038/s41598-017-01581-y (2017).

260 Sinha, R. P. & Häder, D. P. UV-induced DNA damage and repair: A review. *Photochemical and Photobiological Sciences* **1**, 225-236, doi:https://doi.org/10.1039/b201230h (2002).

261 Ozbolat, I. T. & Yu, Y. Bioprinting toward organ fabrication: Challenges and future trends. *IEEE Transactions on Biomedical Engineering* **60**, 691-699, doi:https://doi.org/10.1109/TBME.2013.2243912 (2013).

262 Xu, T., Baicu, C., Aho, M., Zile, M. & Boland, T. Fabrication and characterization of bio-engineered cardiac pseudo tissues. *Biofabrication* **1**, 035001, doi:https://doi.org/10.1088/1758-5082/1/3/035001 (2009).

263 Sekitani, T., Noguchi, Y., Zschieschang, U., Klauk, H. & Someya, T. Organic transistors manufactured using inkjet technology with subfemtoliter accuracy. *Proceedings of the National Academy of Sciences* **105**, 4976-4980, doi:https://doi.org/10.1073/pnas.0708340105 (2008).

264 Derakhshanfar, S. *et al.* 3D bioprinting for biomedical devices and tissue engineering: A review of recent trends and advances. *Bioact Mater* **3**, 144-156, doi:https://doi.org/10.1016/j.bioactmat.2017.11.008 (2018).

265 Udofia, E. & Zhou, W. *Microextrusion Based 3D Printing -A Review*. (2019).

266 Compaan, A. M., Song, K. & Huang, Y. Gellan Fluid Gel as a Versatile Support Bath Material for Fluid Extrusion Bioprinting. *ACS Appl Mater Interfaces* **11**, 5714-5726, doi:https://doi.org/10.1021/acsami.8b13792 (2019).

267 Zhao, S. *et al.* Additive manufacturing of silica aerogels. *Nature* **584**, 387-392, doi:https://doi.org/10.1038/s41586-020-2594-0 (2020).

268 Ouyang, L. *et al.* Expanding and optimizing 3D bioprinting capabilities using complementary network bioinks. *Sci Adv* **6**, doi:https://doi.org/10.1126/sciadv.abc5529 (2020).

269 Duarte Campos, D. F. *et al.* Three-dimensional printing of stem cell-laden hydrogels submerged in a hydrophobic high-density fluid. *Biofabrication* **5**, 015003, doi:https://doi.org/10.1088/1758-5082/5/1/015003 (2013).

270 Hua, W. *et al.* Fluid Bath-Assisted 3D Printing for Biomedical Applications: From Pre- to Postprinting Stages. *ACS Biomaterials Science & Engineering* **7**, 4736-4756, doi:10.1021/acsbiomaterials.1c00910 (2021).
271 Lei, I. M. *et al.* Soft Hydrogel Shapeability via Supportive Bath Matching in Embedded 3D Printing. *Advanced Materials Technologies* **n/a**, 2300001, doi:https://doi.org/10.1002/admt.202300001 (2023).
272 Gudapati, H., Dey, M. & Ozbolat, I. A comprehensive review on droplet-based bioprinting: Past, present and future. *Biomaterials* **102**, 20-42, doi:https://doi.org/10.1016/j.biomaterials.2016.06.012 (2016).
273 Wijshoff, H. The dynamics of the piezo inkjet printhead operation. *Physics Reports* **491**, 77-177, doi:https://doi.org/10.1016/j.physrep.2010.03.003 (2010).
274 Cui, X. & Boland, T. Human microvasculature fabrication using thermal inkjet printing technology. *Biomaterials* **30**, 6221-6227, doi:https://doi.org/10.1016/j.biomaterials.2009.07.056 (2009).
275 Singh, M., Haverinen, H. M., Dhagat, P. & Jabbour, G. E. Inkjet Printing—Process and Its Applications. *Advanced Materials* **22**, 673-685, doi:https://doi.org/10.1002/adma.200901141 (2010).
276 Nishiyama, Y. *et al.* Development of a Three-Dimensional Bioprinter: Construction of Cell Supporting Structures Using Hydrogel and State-Of-The-Art Inkjet Technology. *Journal of Biomechanical Engineering* **131**, doi:https://doi.org/10.1115/1.3002759 (2008).
277 Demirci, U. & Montesano, G. Single cell epitaxy by acoustic picolitre droplets. *Lab on a Chip* **7**, 1139-1145, doi:https://doi.org/10.1039/B704965J (2007).
278 Chen, K. *et al.* The acoustic droplet printing of functional tumor microenvironments. *Lab Chip* **21**, 1604-1612, doi:https://doi.org/10.1039/d1lc00003a (2021).
279 Wohlers, T. G., T. History of additive manufacturing. 1-34 (Wohlers Associates, Inc., 2014).
280 Huang, J., Qin, Q. & Wang, J. A Review of Stereolithography: Processes and Systems. *Processes* **8**, 1138, doi:https://doi.org/10.3390/pr8091138 (2020).
281 Chaudhary, R. *et al.* Additive manufacturing by digital light processing: a review. *Progress in Additive Manufacturing* **8**, 331-351, doi:https://doi.org/10.1007/s40964-022-00336-0 (2023).
282 Tumbleston, J. R. *et al.* Continuous liquid interface production of 3D objects. *Science (New York, N.Y.)* **347**, 1349-1352, doi:https://doi.org/10.1126/science.aaa2397 (2015).
283 Bachmann, J. *et al.* Cavity vat photopolymerisation for additive manufacturing of polymer-composite 3D objects. *Communications Materials* **2**, 107, doi:10.1038/s43246-021-00211-5 (2021).
284 O'Halloran, S., Pandit, A., Heise, A. & Kellett, A. Two-Photon Polymerization: Fundamentals, Materials, and Chemical Modification Strategies. *Advanced Science* **10**, 2204072, doi:https://doi.org/10.1002/advs.202204072 (2023).
285 I., I. *Startup3D: xolo und der volumetrische 3D-Druck*, <https://www.3dnatives.com/de/xolo-volumetrischer-3d-druck-160320211/#!> (2021).
286 Regehly, M. *et al.* Xolography for linear volumetric 3D printing. *Nature* **588**, 620-624, doi:https://doi.org/10.1038/s41586-020-3029-7 (2020).
287 Marques, I. A. *et al.* Magnetic-Based Human Tissue 3D Cell Culture: A Systematic Review. *International Journal of Molecular Sciences* **23**, 12681, doi:https://doi.org/10.3390/ijms232012681 (2022).
288 De Moor, L. *et al.* Hybrid Bioprinting of Chondrogenically Induced Human Mesenchymal Stem Cell Spheroids. *Front Bioeng Biotechnol* **8**, 484, doi:https://doi.org/10.3389/fbioe.2020.00484 (2020).
289 Momeni, F., M.Mehdi Hassani.N, S., Liu, X. & Ni, J. A review of 4D printing. *Materials & Design* **122**, 42-79, doi:https://doi.org/10.1016/j.matdes.2017.02.068 (2017).
290 Caswell, C. C. *et al.* Identification of the First Prokaryotic Collagen Sequence Motif That Mediates Binding to Human Collagen Receptors, Integrins α2β1 and α11β1*.

Journal of Biological Chemistry **283**, 36168-36175, doi:https://doi.org/10.1074/jbc.M806865200 (2008).

291 Yu, Z., An, B., Ramshaw, J. A. & Brodsky, B. Bacterial collagen-like proteins that form triple-helical structures. *J Struct Biol* **186**, 451-461, doi:https://doi.org/10.1016/j.jsb.2014.01.003 (2014).

292 Munoz-Pinto, D. J. *et al.* Collagen-mimetic hydrogels promote human endothelial cell adhesion, migration and phenotypic maturation. *J Mater Chem B* **3**, 7912-7919, doi:https://doi.org/10.1039/C5TB00990A (2015).

293 Parmar, P. A. *et al.* Temporally degradable collagen-mimetic hydrogels tuned to chondrogenesis of human mesenchymal stem cells. *Biomaterials* **99**, 56-71, doi:https://doi.org/10.1016/j.biomaterials.2016.05.011 (2016).

294 Wang, X., Bank, R. A., TeKoppele, J. M. & Mauli Agrawal, C. The role of collagen in determining bone mechanical properties. *Journal of Orthopaedic Research* **19**, 1021-1026, doi:https://doi.org/10.1016/S0736-0266(01)00047-X (2001).

295 Todoh, M., Tadano, S. & Imari, Y. in *13th International Conference on Biomedical Engineering.* (eds Chwee Teck Lim & James C. H. Goh) 2034-2037 (Springer Berlin Heidelberg).

296 Zhang, Y. Z., Ran, L. Y., Li, C. Y. & Chen, X. L. Diversity, Structures, and Collagen-Degrading Mechanisms of Bacterial Collagenolytic Proteases. *Appl Environ Microbiol* **81**, 6098-6107, doi:https://doi.org/10.1128/aem.00883-15 (2015).

297 Greenfield, N. J. Using circular dichroism collected as a function of temperature to determine the thermodynamics of protein unfolding and binding interactions. *Nature Protocols* **1**, 2527-2535, doi:https://doi.org/10.1038/nprot.2006.204 (2006).

298 Bentz, H., Bachinger, H. P., Glanville, R. & Kuhn, K. Physical evidence for the assembly of A and B chains of human placental collagen in a single triple helix. *Eur J Biochem* **92**, 563-567, doi:https://doi.org/10.1111/j.1432-1033.1978.tb12778.x (1978).

299 Drzewiecki, K. E., Grisham, D. R., Parmar, A. S., Nanda, V. & Shreiber, D. I. Circular Dichroism Spectroscopy of Collagen Fibrillogenesis: A New Use for an Old Technique. *Biophys J* **111**, 2377-2386, doi:https://doi.org/10.1016/j.bpj.2016.10.023 (2016).

300 Jafari, H. *et al.* Fish Collagen: Extraction, Characterization, and Applications for Biomaterials Engineering. *Polymers (Basel)* **12**, doi:10.3390/polym12102230 (2020).

301 Krishna, A., V.T, A., D, G., Joji, J. & John, N. in *Advances in Bionanocomposites* (eds Bhasha Sharma *et al.*) 211-224 (Elsevier, 2024).

302 Wright, N. T. & Humphrey, J. D. Denaturation of collagen via heating: an irreversible rate process. *Annu Rev Biomed Eng* **4**, 109-128, doi:https://doi.org/10.1146/annurev.bioeng.4.101001.131546 (2002).

303 Hoermann, H. & Schlebusch, H. Reversible and irreversible denaturation of collagen fibers. *Biochemistry* **10**, 932-937, doi:https://doi.org/10.1021/bi00782a003 (1971).

304 Antoine, E. E., Vlachos, P. P. & Rylander, M. N. Review of collagen I hydrogels for bioengineered tissue microenvironments: characterization of mechanics, structure, and transport. *Tissue Eng Part B Rev* **20**, 683-696, doi:https://doi.org/10.1089/ten.TEB.2014.0086 (2014).

305 Morris, N. P., Watt, S. L., Davis, J. M. & Bächinger, H. P. Unfolding intermediates in the triple helix to coil transition of bovine type XI collagen and human type V collagens alpha 1(2) alpha 2 and alpha 1 alpha 2 alpha 3. *Journal of Biological Chemistry* **265**, 10081-10087, doi:https://doi.org/10.1016/S0021-9258(19)38782-4 (1990).

306 Leikina, E., Mertts, M. V., Kuznetsova, N. & Leikin, S. Type I collagen is thermally unstable at body temperature. *Proceedings of the National Academy of Sciences* **99**, 1314-1318, doi:https://doi.org/10.1073/pnas.032307099 (2002).

307 Persikov, A. V. & Brodsky, B. Unstable molecules form stable tissues. *Proceedings of the National Academy of Sciences* **99**, 1101-1103, doi:https://doi.org/10.1073/pnas.042707899 (2002).

308 Fujii, K. K. *et al.* The Thermal Stability of the Collagen Triple Helix Is Tuned According to the Environmental Temperature. *International Journal of Molecular Sciences* **23**, 2040 (2022).
309 Chen, G., Kawazoe, N. & Tateishi, T. in *Natural-Based Polymers for Biomedical Applications* (eds Rui L. Reis *et al.*) 396-415 (Woodhead Publishing, 2008).
310 Kramer, R. M., Shende, V. R., Motl, N., Pace, C. N. & Scholtz, J. M. Toward a molecular understanding of protein solubility: increased negative surface charge correlates with increased solubility. *Biophys J* **102**, 1907-1915, doi:https://doi.org/10.1016/j.bpj.2012.01.060 (2012).
311 Ahn, H.-C., Juranić, N., Macura, S. & Markley, J. L. Three-Dimensional Structure of the Water-Insoluble Protein Crambin in Dodecylphosphocholine Micelles and Its Minimal Solvent-Exposed Surface. *Journal of the American Chemical Society* **128**, 4398-4404, doi:https://doi.org/10.1021/ja057773d (2006).
312 Wu, W. U., Hettiarachchy, N. S. & Qi, M. Hydrophobicity, solubility, and emulsifying properties of soy protein peptides prepared by papain modification and ultrafiltration. *Journal of the American Oil Chemists' Society* **75**, 845-850, doi:https://doi.org/10.1007/s11746-998-0235-0 (1998).
313 Hanaë A. Henke, A. R. *Application note No. 376: ViscoTip®: Optimized Performance for Highly Viscous Liquids*, <https://www.eppendorf.com/product-media/doc/en/340779/Liquid-Handling_Application-Note_376_ViscoTip_ViscoTip-Optimized-Performance-Highly-Viscous-Liquids.pdf> (
314 Sionkowska, A., Lewandowska, K. & Adamiak, K. The Influence of UV Light on Rheological Properties of Collagen Extracted from Silver Carp Skin. *Materials (Basel)* **13**, doi:https://doi.org/10.3390/ma13194453 (2020).
315 Aitken, A. & Learmonth, M. in *The Protein Protocols Handbook* (ed John M. Walker) 3-6 (Humana Press, 1996).
316 Mahalingam, V., Hazra, C. & Samanta, T. A Resonance Energy Transfer Approach for the Selective Detection of Aromatic Amino Acids. *J. Mater. Chem. C* **2**, doi:10.1039/C4TC01954G (2014).
317 Leikina, E., Mertts, M. V., Kuznetsova, N. & Leikin, S. Type I collagen is thermally unstable at body temperature. *Proc Natl Acad Sci U S A* **99**, 1314-1318, doi:10.1073/pnas.032307099 (2002).
318 Gutierrez, C. B. *et al.* Developing an Acidic Residue Reactive and Sulfoxide-Containing MS-Cleavable Homobifunctional Cross-Linker for Probing Protein-Protein Interactions. *Anal Chem* **88**, 8315-8322, doi:https://doi.org/10.1021/acs.analchem.6b02240 (2016).
319 Sigma&Aldrich. *SAFETY DATA SHEET: 4-(4,6-Dimethoxy-1,3,5-triazin-2-yl)-4-methylmorpholinium chloride*, <https://www.sigmaaldrich.com/DE/en/sds/ALDRICH/74104?userType=undefined> (2024).
320 Takallu, S., Mirzaei, E., Azadi, A., Karimizade, A. & Tavakol, S. Plate-shape carbonated hydroxyapatite/collagen nanocomposite hydrogel via in situ mineralization of hydroxyapatite concurrent with gelation of collagen at pH = 7.4 and 37 degrees C. *J Biomed Mater Res B Appl Biomater* **107**, 1920-1929, doi:https://doi.org/10.1002/jbm.b.34284 (2019).
321 Kaviani, A., Zebarjad, S., Javadpour, S., Ayatollahi, M. & Bazargan-Lari, R. Fabrication and characterization of low-cost freeze-gelated chitosan/collagen/hydroxyapatite hydrogel nanocomposite scaffold. *International Journal of Polymer Analysis and Characterization* **24**, 1-13, doi:https://doi.org/10.1080/1023666X.2018.1562477 (2019).
322 Patel, J. M., Jackson, R. C., Schneider, G. L., Ghodbane, S. A. & Dunn, M. G. Carbodiimide cross-linking counteracts the detrimental effects of gamma irradiation on the physical properties of collagen-hyaluronan sponges. *Journal of Materials*

Science: Materials in Medicine **29**, 75, doi:https://doi.org/10.1007/s10856-018-6056-2 (2018).

323 Song, X. *et al.* A Novel Human-Like Collagen Hydrogel Scaffold with Porous Structure and Sponge-Like Properties. *Polymers (Basel)* **9**, doi:https://doi.org/10.3390/polym9120638 (2017).

324 Stark, M. & Kühn, K. The properties of molecular fragments obtained on treating calfskin collagen with collagenase from Clostridium histolyticum. *Eur J Biochem* **6**, 534-541, doi:https://doi.org/10.1111/j.1432-1033.1968.tb00477.x (1968).

325 Suh, H. & Park, J.-C. Evaluation of calcification in porcine valves treated by ultraviolet ray and glutaraldehyde. *Materials Science and Engineering: C* **13**, 65-73, doi:https://doi.org/10.1016/S0928-4931(00)00178-8 (2000).

326 Wassenaar, J. W., Braden, R. L., Osborn, K. G. & Christman, K. L. Modulating In Vivo Degradation Rate of Injectable Extracellular Matrix Hydrogels. *J Mater Chem B* **4**, 2794-2802, doi:10.1039/c5tb02564h (2016).

327 Mallya, S. K., Mookhtiar, K. A. & Van Wart, H. E. Kinetics of hydrolysis of type I, II, and III collagens by the class I and IIClostridium histolyticum collagenases. *Journal of Protein Chemistry* **11**, 99-107, doi:10.1007/BF01025096 (1992).

328 Hanoune, J., Stengel, D., Lacombe, M. L., Feldmann, G. & Coudrier, E. Proteolytic activation of rat liver adenylate cyclase by a contaminant of crude collagenase from Clostridium histolyticum. *J Biol Chem* **252**, 2039-2045, doi:https://doi.org/10.1016/S0021-9258(18)71861-9 (1977).

329 Scientific, T. *Amine-Reactive Crosslinker Chemistry*, <https://www.thermofisher.com/de/de/home/life-science/protein-biology/protein-biology-learning-center/protein-biology-resource-library/pierce-protein-methods/amine-reactive-crosslinker-chemistry.html#:~:text=NHS%2Dester%20crosslinking%20reactions%20are,temperature%20or%204%C2%B0C> (

330 Scientific, T. *Supplemente für Zellkulturmedien*, <https://www.thermofisher.com/de/de/home/life-science/cell-culture/mammalian-cell-culture/media-supplements.html#:~:text=The%20level%20of%20HEPES%20in,used%20concentration%20is%2025%20mM> (

331 Kim, D.-N., Park, J. & Koh, W.-G. Control of cell adhesion on poly(ethylene glycol) hydrogel surfaces using photochemical modification and micropatterning techniques. *Journal of Industrial and Engineering Chemistry* **15**, 124-128, doi:https://doi.org/10.1016/j.jiec.2008.08.001 (2009).

332 Tee, H. T., Zipp, R., Koynov, K., Tremel, W. & Wurm, F. R. Poly(methyl ethylene phosphate) hydrogels: Degradable and cell-repellent alternatives to PEG-hydrogels. *European Polymer Journal* **141**, doi:https://doi.org/10.1016/j.eurpolymj.2020.110075 (2020).

333 Cosgriff-Hernandez, E. *et al.* Bioactive hydrogels based on Designer Collagens. *Acta biomaterialia* **6**, 3969-3977, doi:10.1016/j.actbio.2010.05.002 (2010).

334 Jee, H. J., Lee, S. G., Bormate, K. J. & Jung, Y. S. Effect of Caffeine Consumption on the Risk for Neurological and Psychiatric Disorders: Sex Differences in Human. *Nutrients* **12**, doi:10.3390/nu12103080 (2020).

335 Tinjacá, D. A., Martínez, F., Almanza, O. A., Jouyban, A. & Acree, W. E. Solubility, Dissolution Thermodynamics and Preferential Solvation of Meloxicam in (Methanol + Water) Mixtures. *Journal of Solution Chemistry* **50**, 667-689, doi:https://doi.org/10.1007/s10953-021-01084-5 (2021).

336 Mohiuddin, K. & Swanson, S. J. Maximizing the benefit of minimally invasive surgery. *J Surg Oncol* **108**, 315-319, doi:https://doi.org/10.1002/jso.23398 (2013).

337 Ghobrial, S., Ott, J. & Parry, J. P. An Overview of Postoperative Intraabdominal Adhesions and Their Role on Female Infertility: A Narrative Review. *J Clin Med* **12**, doi:10.3390/jcm12062263 (2023).

338 Vrijland, W. W., Jeekel, J., van Geldorp, H. J., Swank, D. J. & Bonjer, H. J. Abdominal adhesions: intestinal obstruction, pain, and infertility. *Surg Endosc* **17**, 1017-1022, doi:10.1007/s00464-002-9208-9 (2003).
339 Frank, K. *et al.* Influence of Rheological Properties and Needle Size on Extrusion Forces of Hyaluronic Acid Based Soft Tissue Fillers. *J Drugs Dermatol* **20**, 498-502, doi:10.36849/jdd.5237 (2021).
340 Wang See, C., Kim, T. & Zhu, D. Hernia Mesh and Hernia Repair: A Review. *Engineered Regeneration* **1**, 19-33, doi:https://doi.org/10.1016/j.engreg.2020.05.002 (2020).
341 Faulk, D. M. *et al.* ECM hydrogel coating mitigates the chronic inflammatory response to polypropylene mesh. *Biomaterials* **35**, 8585-8595, doi:10.1016/j.biomaterials.2014.06.057 (2014).
342 Chan, D. *et al.* Polyacrylamide-based hydrogel coatings improve biocompatibility of implanted pump devices. *J Biomed Mater Res A* **111**, 910-920, doi:10.1002/jbm.a.37521 (2023).
343 Veiga, A. S. & Schneider, J. P. Antimicrobial hydrogels for the treatment of infection. *Biopolymers* **100**, 637-644, doi:10.1002/bip.22412 (2013).
344 Gockler, T. *et al.* Tuning Superfast Curing Thiol-Norbornene-Functionalized Gelatin Hydrogels for 3D Bioprinting. *Adv Healthc Mater* **10**, e2100206, doi:https://doi.org/10.1002/adhm.202100206 (2021).
345 Wüthrich, K. *NMR of proteins and nucleic acids*. (John Wiley & Sons, Inc., 1988).
346 Cayot, P. & Tainturier, G. The quantification of protein amino groups by the trinitrobenzenesulfonic acid method: a reexamination. *Analytical biochemistry* **249**, 184-200, doi:https://doi.org/10.1006/abio.1997.2161 (1997).
347 Ramshaw, J. A. M. & Glattauer, V. in *Biophysical and Chemical Properties of Collagen Biophysical Applications* (2019).
348 Holmes, R. *et al.* Thiol-Ene Photo-Click Collagen-PEG Hydrogels: Impact of Water-Soluble Photoinitiators on Cell Viability, Gelation Kinetics and Rheological Properties. *Polymers (Basel)* **9**, doi:https://doi.org/10.3390/polym9060226 (2017).
349 Klotz, I. M. & Elfbaum, S. G. Activated acryl compunds as intermedicates in the thiolation of proteins. *Biochimica et biophysica acta* **86**, 100-105, doi:https://doi.org/10.1016/0304-4165(64)90163-1 (1964).
350 Yamauchi, K., Takeuchi, N., Kurimoto, A. & Tanabe, T. Films of collagen crosslinked by S–S bonds: preparation and characterization. *Biomaterials* **22**, 855-863, doi:https://doi.org/10.1016/S0142-9612(00)00249-0 (2001).
351 Benesch, R. & Benesch, R. E. J. J. o. t. A. C. S. Formation of Peptide Bonds by Aminolysis of Homocysteine Thiolactones1. **78**, 1597-1599 (1956).
352 Vlierberghe, S. V., Schacht, E. & Dubruel, P. Reversible gelatin-based hydrogels: Finetuning of material properties. *European Polymer Journal* **47**, 1039-1047, doi:https://doi.org/10.1016/j.eurpolymj.2011.02.015 (2011).
353 Wang, J. *et al.* A highly efficient waterborne photoinitiator for visible-light-induced three-dimensional printing of hydrogels. *Chemical Communications* **54**, 920-923, doi:10.1039/C7CC09313F (2018).
354 Lee, M., Rizzo, R., Surman, F. & Zenobi-Wong, M. Guiding Lights: Tissue Bioprinting Using Photoactivated Materials. *Chemical Reviews* **120**, 11027, doi:https://doi.org/10.1021/acs.chemrev.0c00077 (2020).
355 Rajpal, G. & Arvan, P. in *Handbook of Biologically Active Peptides (Second Edition)* (ed Abba J. Kastin) 1721-1729 (Academic Press, 2013).
356 Paul, C., Leser, S. & Oesser, S. Significant Amounts of Functional Collagen Peptides Can Be Incorporated in the Diet While Maintaining Indispensable Amino Acid Balance. *Nutrients* **11**, doi:https://doi.org/10.3390/nu11051079 (2019).
357 Kodali, V. K. & Thorpe, C. Oxidative protein folding and the Quiescin-sulfhydryl oxidase family of flavoproteins. *Antioxid Redox Signal* **13**, 1217-1230, doi:https://doi.org/10.1089/ars.2010.3098 (2010).

358 Trivedi, M. V., Laurence, J. S. & Siahaan, T. J. The role of thiols and disulfides on protein stability. *Curr Protein Pept Sci* **10**, 614-625, doi:https://doi.org/10.2174/138920309789630534 (2009).

359 Fundarò, S. P., Salti, G., Malgapo, D. M. H. & Innocenti, S. The Rheology and Physicochemical Characteristics of Hyaluronic Acid Fillers: Their Clinical Implications. *Int J Mol Sci* **23**, doi:https://doi.org/10.3390/ijms231810518 (2022).

360 Ahumada, M., Jacques, E., Calderon, C. & Martínez-Gómez, F. in *Handbook of Ecomaterials* (eds Leticia Myriam Torres Martínez, Oxana Vasilievna Kharissova, & Boris Ildusovich Kharisov) 3503-3522 (Springer International Publishing, 2019).

361 Mour, M. *et al.* Advances in Porous Biomaterials for Dental and Orthopaedic Applications. *Materials* **3**, 2947-2974, doi:https://doi.org/10.3390/ma3052947 (2010).

362 Nguyen, B. V. *et al.* Biomechanical properties of single chondrocytes and chondrons determined by micromanipulation and finite-element modelling. *J R Soc Interface* **7**, 1723-1733, doi:https://doi.org/10.1098/rsif.2010.0207 (2010).

363 Bell, E., Ivarsson, B. & Merrill, C. Production of a tissue-like structure by contraction of collagen lattices by human fibroblasts of different proliferative potential in vitro. *Proceedings of the National Academy of Sciences* **76**, 1274-1278, doi:https://doi.org/10.1073/pnas.76.3.1274 (1979).

364 Malandain, N. *et al.* Cell-Laden 3D Hydrogels of Type I Collagen Incorporating Bacterial Nanocellulose Fibers. *ACS Appl Bio Mater* **6**, 3638-3647, doi:https://doi.org/10.1021/acsabm.3c00126 (2023).

365 Sakura, S. & Fujimoto, D. Absorption and fluorescence study of tyrosine-derived crosslinking amino acids from collagen. *Photochemistry and Photobiology* **40**, 731-734, doi:https://doi.org/10.1111/j.1751-1097.1984.tb04644.x (1984).

366 Ruoslahti, E. RGD and other recognition sequences for integrins. *Annu Rev Cell Dev Biol* **12**, 697-715, doi:https://doi.org/10.1146/annurev.cellbio.12.1.697 (1996).

367 Greenwood-Goodwin, M. & Heilshorn, S. C. in *Biomimetic Approaches for Biomaterials Development* (ed Prof. João F. Mano) 25-54 (2012).

368 Nahian, A. & Sapra, A. in *StatPearls* (StatPearls Publishing Copyright © 2024, StatPearls Publishing LLC., 2024).

369 Kadajji, V. G. & Betageri, G. V. Water Soluble Polymers for Pharmaceutical Applications. *Polymers* **3**, 1972-2009, doi:https://doi.org/10.3390/polym3041972 (2011).

370 LLC, B. R. Bioprinting: Technologies and Global Markets. (February 2023).

371 Weadock, K., Olson, R. M. & Silver, F. H. Evaluation of Collagen Crosslinking Techniques. *Biomaterials, Medical Devices, and Artificial Organs* **11**, 293-318, doi:https://doi.org/10.3109/10731198309118815 (1983).

372 Fushimi, H. *et al.* Recombinant collagen polypeptide as a versatile bone graft biomaterial. *Communications Materials* **1**, 87, doi:https://doi.org/10.1038/s43246-020-00089-9 (2020).

373 Yamauchi, M. & Sricholpech, M. Lysine post-translational modifications of collagen. *Essays Biochem* **52**, 113-133, doi:10.1042/bse0520113 (2012).

374 Huang, B. J., Hu, J. C. & Athanasiou, K. A. Cell-based tissue engineering strategies used in the clinical repair of articular cartilage. *Biomaterials* **98**, 1-22, doi:https://doi.org/10.1016/j.biomaterials.2016.04.018 (2016).

375 Tkalec, G., Knez, Ž. & Novak, Z. Formation of polysaccharide aerogels in ethanol. *RSC Advances* **5**, 77362-77371, doi:https://doi.org/10.1039/c5ra14140k (2015).

376 Seol, Y.-J., Kang, H.-W., Lee, S. J., Atala, A. & Yoo, J. J. Bioprinting technology and its applications. *European Journal of Cardio-Thoracic Surgery* **46**, 342-348, doi:https://doi.org/10.1093/ejcts/ezu148 (2014).

377 Mills, P. A. S. & Mills, D. K. Reduced Supply in the Organ Donor Market and How 3D Printing Can Address This Shortage: A Critical Inquiry into the Collateral Effects of Driverless Cars. *Applied Sciences* **10** (2020).

378 Ding, Z., Tang, N., Huang, J., Cao, X. & Wu, S. Global hotspots and emerging trends in 3D bioprinting research. *Frontiers in Bioengineering and Biotechnology* **11**, doi:https://doi.org/10.3389/fbioe.2023.1169893 (2023).
379 Axpe, E. & Oyen, M. L. Applications of Alginate-Based Bioinks in 3D Bioprinting. *International Journal of Molecular Sciences* **17**, 1976, doi:https://doi.org/10.3390/ijms17121976 (2016).
380 Lee, J., Lee, S.-H., Kim, B. S., Cho, Y.-S. & Park, Y. Development and Evaluation of Hyaluronic Acid-Based Hybrid Bio-Ink for Tissue Regeneration. *Tissue Engineering and Regenerative Medicine* **15**, 761-769, doi:https://doi.org/10.1007/s13770-018-0144-8 (2018).
381 Diamantides, N. *et al.* Correlating rheological properties and printability of collagen bioinks: the effects of riboflavin photocrosslinking and pH. *Biofabrication* **9**, 034102, doi:https://doi.org/10.1088/1758-5090/aa780f (2017).
382 Chawla, S., Midha, S., Sharma, A. & Ghosh, S. Silk-Based Bioinks for 3D Bioprinting. *Advanced Healthcare Materials* **7**, 1701204, doi:https://doi.org/10.1002/adhm.201701204 (2018).
383 Duarte Campos, D. F. *et al.* The Stiffness and Structure of Three-Dimensional Printed Hydrogels Direct the Differentiation of Mesenchymal Stromal Cells Toward Adipogenic and Osteogenic Lineages. *Tissue Engineering Part A* **21**, 740-756, doi:https://doi.org/10.1089/ten.tea.2014.0231 (2014).
384 Kołodziejska, M., Jankowska, K., Klak, M. & Wszoła, M. Chitosan as an Underrated Polymer in Modern Tissue Engineering. *Nanomaterials* **11** (2021).
385 Cernencu, A. I. & Ioniţă, M. The current state of the art in gellan-based printing inks in tissue engineering. *Carbohydrate Polymers* **309**, 120676, doi:https://doi.org/10.1016/j.carbpol.2023.120676 (2023).
386 Ahlfeld, T. *et al.* Methylcellulose – a versatile printing material that enables biofabrication of tissue equivalents with high shape fidelity. *Biomaterials Science* **8**, 2102-2110, doi:https://doi.org/10.1039/D0BM00027B (2020).
387 Urciuolo, A. *et al.* Intravital three-dimensional bioprinting. *Nat Biomed Eng* **4**, 901-915, doi:https://doi.org/10.1038/s41551-020-0568-z (2020).
388 Bishop, E. S. *et al.* 3-D bioprinting technologies in tissue engineering and regenerative medicine: Current and future trends. *Genes & Diseases* **4**, 185-195, doi:https://doi.org/10.1016/j.gendis.2017.10.002 (2017).
389 Yang, E. *et al.* Bio-Based Polymers for 3D Printing of Bioscaffolds. *Polymer Reviews* **58**, 668-687, doi:https://doi.org/10.1080/15583724.2018.1484761 (2018).
390 Alm, J. J., Qian, H. & Le Blanc, K. in *Tissue Engineering (Second Edition)* (eds Clemens A. Van Blitterswijk & Jan De Boer) 427-469 (Academic Press, 2014).
391 Kelly, S. T. & Zydney, A. L. Effects of intermolecular thiol–disulfide interchange reactions on bsa fouling during microfiltration. *Biotechnology and Bioengineering* **44**, 972-982, doi:https://doi.org/10.1002/bit.260440814 (1994).
392 Bradford, M. M. A rapid and sensitive method for the quantitation of microgram quantities of protein utilizing the principle of protein-dye binding. *Analytical biochemistry* **72**, 248-254, doi:https://doi.org/10.1016/0003-2697(76)90527-3 (1976).
393 Walker, J. M. in *Basic Protein and Peptide Protocols* (ed John M. Walker) 5-8 (Humana Press, 1994).
394 Alonso, J. M., Andrade Del Olmo, J., Perez Gonzalez, R. & Saez-Martinez, V. Injectable Hydrogels: From Laboratory to Industrialization. *Polymers (Basel)* **13**, doi:https://doi.org/10.3390/polym13040650 (2021).
395 Li, X. *et al.* 3D Culture of Chondrocytes in Gelatin Hydrogels with Different Stiffness. *Polymers (Basel)* **8**, doi:https://doi.org/10.3390/polym8080269 (2016).